HYDRODYNAMICS AND OXYGEN MODELING OF THE STOCKTON DEEP WATER SHIP CHANNEL

S. Geoffrey Schladow, UC Davis

and

Stephen Monismith, Stanford University

Feb 25, 2009

Final report for CALFED ERP-02D-P51

This report is for the purposes of enhancing and furthering the California Bay-Delta Authority's Environmental Research program.

In addition to the Final Report authors, the following individuals and organizations made substantive contributions to the research that is described in this report:
Laura Doyle (formerly DiPalermo) and William Fleenor, UC Davis
Jim Hench, Derek Fong and Nick Nidzieko, Stanford University
Peter Smith, United States Geological Survey
Francisco Rueda, University of Granada, Spain
Jordan Clark, UC Santa Barbara
David Ho, Paul Schmieder and Peter Schlosser, Columbia University

Executive Summary

The principal objectives of this study were to understand how hydrodynamic and biogeochemical processes interact to produce reductions in dissolved oxygen concentrations in the Stockton Deep Water Ship Channel (DWSC) and to produce a three-dimensional hydrodynamic and coupled water quality model that could be used to examine these interactions. To address these objectives, an ambitious program of field experimentation and numerical model development was undertaken. The collaboration included UC Davis, Stanford University, the US Geological Survey, the University of Granada (Spain), UC Santa Barbara and the Lamont-Doherty Earth Observatory at Columbia University. The individual program elements were the subject of individual reports that were submitted and subsequently accepted by CBDA. This final report primarily collates these individual reports and the peer-reviewed publications that stemmed from them, into a single final report.

The purpose of the field experiments was to understand the circulation, stratification, and dissolved oxygen characteristics of the DWSC, and to provide information for the calibration and validation of a three-dimensional hydrodynamic and water quality model for the DWSC. The data were collected during two experiments: one in August 2004 and the second during August 2005. August was chosen for the experiments because it is the time of year when the most extreme low DO events have occurred in the past. Each experiment consisted of a 3-5 week deployment of acoustic Doppler current profilers (ADCPs) and thermistor mooring arrays. In addition to the long-term deployments, each experiment included two thirty-hour intensive studies, spaced one week apart in order to sample during different tidal regimes. During the intensive experiments, three sets of data were collected. One dataset was from a fixed platform within the DWSC. A second data set was from transects along the San Joaquin River and DWSC. A third data set was from a Self Contained Autonomous MicroProfiler (SCAMP) to study vertical mixing rates.

During the 2005 experiment (the second experiment), a supplemental experiment was conducted, wherein the inert tracer sulfur hexafluoride (SF6) was released upstream of the DWSC, and for a period of approximately 1 week, the cloud of tracer was tracked using in-situ measurements.

The temperature observations showed that a balance of advection, dispersion and surface forcing determines sub-tidal temperature variations in the Deep Water Ship Channel (DWSC), the tidal portion of the San Joaquin River. Notably, dispersion appeared to play a significant role, such that temperatures were elevated in the middle of the DWSC relative to both upstream riverine and

downstream estuarine temperatures. The thermal energy balance suggested a longitudinal dispersion coefficient, $K \approx 1000$ m^2 s^{-1}, a value far in excess of what might be expected from existing descriptions of shear flow dispersion in rivers and estuaries, i.e. $K \approx 100$ m^2 s^{-1} or less. Dispersion in the DWSC appears to result from a combination of how water parcels navigate the array of junctions and how flows in different connected channels are phased. In effect, this combination of processes may be considered to be a form of tidal pumping.

By contrast, the SF6 study yielded a lower estimate of diffusivity. On August 14, 2005, ca. 1.6 mol of SF_6 was injected in the SJR, 13 km upstream from the DWSC. The tracer entered the DWSC within one day, and was mapped for 8 consecutive days following the injection. From the change in SF_6 distribution with time, the longitudinal dispersion was determined to be 32.7 m^2 s^{-1} and net advection was 1.75 km day^{-1} under the conditions observed during the study. The reason for this difference in dispersion can in part be attributed to the SF6 experiment largely occurring in the more riverine, upper part of the study area, whereas the temperature measurements were occurring in the more branching lower part of the study area. It is clear from these results that the impact of the branching nature of the delta on transport and dispersion is not fully understood.

The impacts of geometry and flow on the low DO are inversely correlated, as the net velocity decreases when the channel area increases stepping from the SJR into the DWSC. Based simply on the advection calculated here in this study, the residence time for water in the DWSC is 7.7 days. The observed low DO concentrations suggest that this residence time associated with a flow of 34.5 m^3 sec^{-1} is too large, and that the BOD has ample time to decrease oxygen concentrations.

A major aspect of this project was the application of the 3D finite difference circulation code, SI3D to the DWSC. SI3D solves the governing equations for three-dimensional hydrostatic fluid motions including the behavior of the free surface and density variations associated with salinity and temperature variations on a rectangular Cartesian grid.

The domain encompassed in our model of the DWSC extended from the San Joaquin River near French Camp Slough to just downstream of Turner Cut. The horizontal resolution of the grid was 20 m and the vertical resolution was 1 m. Bathymetry was derived from the USGS bathymetry database. Flows in this domain were driven by prescribed free surface elevations at the open boundaries, creating both tidal and mean flows. These surface elevations were derived from archived

DSM2 model runs. Surface heat exchanges were computed from meteorological data obtained from the Port of Stockton using standard meteorological formulae that derive fluxes from simpler measurements like wind speed.

In Phase One of the modeling, a barotropic version was utilized. The model was calibrated for conditions existing in the summer of 2000. A straightforward comparison of results from this exercise to flows measured at the USGS flow station at Stockton showed an acceptable level of agreement between model and observations, although this calibration exercise revealed the importance of appropriately choosing a value of the horizontal eddy viscosity. Subject to stability constraints, this parameter should be chosen to be as small as possible to best represent the operant physics.

SI3D was then used to model tidal currents observed in 2004, albeit omitting density variations (the barotropic model). Decomposing both modeled and observed currents and elevations into harmonic constituents, i.e. representing both as a sum of variations at tidal frequencies, revealed an important aspect of the model set up that should be considered in future limited area modeling exercises: In order to drive sufficient flows, it appears that free-surface elevation variations computed by DSM2 are larger than what is observed. This resulted in an over-prediction of tidal currents in the DWSC. This suggested that a simple reduction in DSM2 derived elevations during calibration may suffice to get accurate tidal current predictions in the DWSC.

Phase one of the modeling showed the value of a 3D model for practical modeling of flows in the Delta. A physical resolution of ca. 10m in the horizontal and 1m in the vertical can be successfully run on current desktop workstations. It appears that the coupling of DSM2 to a 3D model is straightforward, although it may be necessary in future to consider modifying DSM2 outputs so that they better match observations.

In Phase two of the modeling, the hydrodynamic model was amended to allow for the modeling of baroclinic processes and allow for a water quality model to be run concurrently with the hydrodynamic model. The improved model, SI3DWQ, also used a three-dimensional to two-dimensional mapping structure to decrease the memory requirements of the model. The increased efficiency has improved the ability to use smaller grid sizes. The water quality model includes the transport of water quality constituents as well as source-sink terms for each constituent that take

into account all the major biogeochemical processes. The transport of all water quality constituents is solved using the same two-level, semi-implicit scheme using operator splitting developed for scalar transport in SI3D. SI3DWQ includes the following state variables: arbitrary constituent (used as a conservative tracer), dissolved oxygen, nitrogen species, phosphorus species, organic matter and phytoplankton.

The model SI3DWQ showed promising results, and development and adaptation of the water quality portion of the model suggested that with further model enhancements and improved boundary conditions, a predictive, three-dimensional representation of water quality in the Stockton Deep Water Ship Channel is readily attainable. Some limitation of the current model included the assignment of water temperature boundary conditions and attenuation coefficients. It was obvious from initial model simulations that a constant attenuation coefficient for the entire system was not representative. The model should be updated to allow this constituent to vary over the domain. In addition, assuming well-mixed boundary conditions and a constant initial vertical water temperature are not accurate estimates for this system. Another important improvement to the model would be the assignment of water surface heights at the boundaries. The current model uses DSM2 output to provide boundary conditions. Being able to use the output from another community-supported modeling effort was valuable; however, in this case, DSM2 does not seem to be as accurate as necessary for the section of river under study. With the relatively small model domain, errors introduced at the boundary dominate the entire domain.

Without an accurate model of the hydrodynamics, modeling the water quality will be nearly impossible. There are two ways to improve this downfall. The first would be to extend the model boundaries to locations much further from the section of river of interest. This will decouple the dependence of the area of interest on the boundaries, but would require much more computing power and the further development of the grid. The second would be to move away from the DSM2-derived boundary conditions and derive input from another source. All of these improvements were beyond the scope of this project.

Based on our work, we make the following recommendations:

1. Any circulation modeling that is done for the Delta should use state of the art turbulence closures.

2. To capture the full range of spatial scales important to flows in the Delta, hydrodynamic modeling of the Delta should be done using an unstructured grid model, a nested grid model, or other such numerical device that allows for the efficient resolution of small scale features.

3. The accuracy of hydrodynamic models of the Delta should be assessed using quantitative metrics.

4. Additional meteorological stations must be added to the existing monitoring network operated by the project agencies to allow for model forcing.

Acknowledgements

This work was supported by CALFED Ecosystem Restoration grant ERP-02D-P51. The authors gratefully acknowledge the contributions made by our collaborators listed on Page ii of this report in compiling the individual reports that form the basis of this Final Report. We also acknowledge th assistance with field work provided by a number of students and staff from UC Davis (Eu Gene Chung, David Jassby, Todd Steissberg, Goloka Sahoo, Josh Mantell, Bill Sluis, Daret Kehlet) and from Stanford (Kristen Davis, Sarah Giddings, Nick Nidzieko, Johanna Rosman). The field work was also made possible by the able seamanship of Jay Cuetara and John Yokimizu of the USGS.

We acknowledge the vital role played by those charged with administering this project. Specifically we would like to thank Ellen MacDonald and Diana Cummings at the UC Davis Watershed Sciences Center who provided the bulk of the administrative support and who coordinated with their counterparts at all the partner institutions. Finally, we sincerely thank Leann Androvich for her insistence and her patience.

TABLE OF CONTENTS

1. Introduction

The principal objectives of this study were to understand how hydrodynamic and biogeochemical processes interact to produce reductions in dissolved oxygen concentrations in the Stockton Deep Water Ship Channel (DWSC) and to produce a three-dimensional hydrodynamic and coupled water quality model that could be used to examine these interactions. Our fundamental conceptual model was that thermal stratification forms in the DWSC because mixing due to winds and mean flows is not sufficient to overcome the stratifying effects of surface heating or to adequately flush the channel. The presence of a step change in bottom elevation at the eastern end of the DWSC may also directly contribute to a low flushing rate in the ship channel. As a result, particulate BOD input to the DWSC as well as organic matter produced locally via photosynthesis, are provided with the conditions needed to settle to the sediment where they decompose, leading to the development of low oxygen concentrations near the sediment-water interface when surface oxygen exchange is insufficient to overcome the dissolved oxygen deficits in the lower layer.

To address these objectives, we undertook an ambitious program of field experimentation and numerical model development. The individual program elements were the subject of individual reports that were submitted and subsequently accepted by CBDA. These individual reports constitute the individual Sections of this Final Report. In addition, Appendices are included containing two peer-reviewed papers that have thus far been produced from this research project.

Sections 2 and 3 relate to Task 2 of the contract. Section 2 is a description of the originally proposed field measurement program and the results derived from it. Section 3 provides the results of field work conducted as part of an Amendment to the original contract. Appendix I and II are peer-reviewed publications related to each of these efforts.

Sections 4, 5 and 6 relate to Task 3 of the contract, the development of the 3-D numerical model. Section 4 provides a description of the initial hydrodynamic model and its application to flows in the SDWSC. An improved version of the hydrodynamic model, capable of handling thermal stratification, and with a coupled water quality model, is presented in Section 5. Section 6 contains the User's Manual for the model.

2. Hydrodynamic and Water Quality Data from the Stockton Deep Water Ship Channel: August 2004 and August 2005

The following Report was completed in May 2006, and describes the field operations associated with this study. All raw data collected over the course of the last two years are available through the UC Davis ftp server. The voluminous nature of these time series data make it unwieldy to display it in tabulated form. For more information, contact Geoffrey Schladow at gschladow@ucdavis.edu

Appendix I to the main report contains a peer-reviewed paper that was derived from these materials.

Hydrodynamic and Water Quality Data from the Stockton Deep Water Ship Channel: August 2004 and August 2005.

Jim Hench[2], William Fleenor[1], Laura DiPalermo[1], Nicholas Nidzieko[2], Stephen Monismith[2] and Geoffrey Schladow[1]

1

Environmental Dynamics Laboratory, University of California, Davis

[2] Environmental Fluid Mechanics Laboratory, Stanford University

May 2006

Introduction

During August 2004 and August 2005, data were collected in the Stockton Deep Water Ship Channel (DWSC) by researchers from University of California at Davis, Stanford University and the United States Geological Survey (USGS). The purpose of the field experiment was to understand the circulation, stratification, and dissolved oxygen characteristics of the DWSC, and to provide information for the calibration and validation of a three-dimensional hydrodynamic and water quality model for the Stockton DWSC in order to investigate the causes and possible solutions for the low dissolved oxygen (DO) problems in the channel.

The data were collected during two experiments: one in August 2004 and the second during August 2005. August was chosen for the experiments because it is the time of year when the most extreme low DO events have occurred in the past. Each experiment consisted of a 3-5 week deployment of acoustic Doppler current profilers (ADCPs) and thermistor mooring array. In addition to the long-term deployments, each experiment consisted of two thirty-hour intensive studies, spaced one week apart in order to sample during different tidal regimes. During the experiments, three sets of data were collected. The experiments were based from a 47-ft houseboat anchored just off the main channel (see Fig. 1). The houseboat was placed in the area historically known to have the worst oxygen deficit, and it served two purposes. First, it provided a platform for shipboard CTD casts, ADCP profiles and physical water sampling and filtering. Second, it permitted small transecting boats to operate continuously by providing supplies and crew changes within the study area. In addition to the houseboat, two small boats were used for transecting the San Joaquin River and DWSC. These boats were equipped with an ADCP and a CTD with a DO sensor to collect data throughout the area affected by low DO. The third data collection element was done with a Self Contained Autonomous MicroProfiler (SCAMP) to study vertical mixing rates. The SCAMP collected turbulent microstructure profiles in the center of the channel next to the houseboat.

Description of Equipment:

RDI Acoustic Doppler Current Profilers

The instruments used in the month long moorings were bottom-mounted upward-looking 600 or 1200 kHz ADCPs. Each ADCP had either a self-contained or external pressure sensor to measure water level.

Thermistors

The moorings each had at least eight fast response (<0.5 s) thermistors, and were a mixture of RBR, OEI, and Sea-Bird models. The thermistors were deployed in vertical chains to measure vertical temperature gradients and thus stratification. All thermistors were calibrated before deployment.

SeaBird Conductivity-Temperature-Depth Profilers.

The experiments utilized three different SeaBird CTDs. The CTD located on the houseboat was an SBE-25. This instrument has the following sensors: temperature, pressure, conductivity, pH, dissolved oxygen, transmissivity, PAR, fluorescence and optical back scatter. The CTD used on the USGS R/V Holly Day had the following sensors: temperature, pressure, conductivity, dissolved oxygen, light transmissivity, chlorophyll fluorescence and optical backscatter. The CTD used to collect data at the junction had the following sensors: temperature, pressure, conductivity, dissolved oxygen.

SCAMP

Turbulent microstructure profiles were collected using a SCAMP (PME, Inc.) profiler. The casts were done every ca. 20 minutes in 2004 and every 10 minutes in 2005 during the 30-hr intensive experiments. The SCAMP was deployed in upward-mode where the instrument was lowered with a releasable weight, and profiled upward after a preset time delay. This mode permitted high resolution measurements in the near surface portion of the water column, where stratification was greatest. In 2004, the SCAMP was fitted with a pair of FP07 thermistors. In 2005, the instrument was upgraded to included fast-C, OBS, and fluorescence sensors.

Specifics of experiments and sample data.

August 2004

During August 2004, five ADCP and thermistor strings were deployed at the M1-M5 as shown in Fig. 1. The moorings were in the water from August 2, 2004 until September 2, 2004.. The

mooring at M2, which is in the location closest to the historical DO minimum region was selected for more intensive measurement: 21 thermistors were deployed at 0.5 meter intervals and the ADCP was upgraded to 2GB of memory and configured to measure turbulent Reynolds stresses for the duration of the experiment.

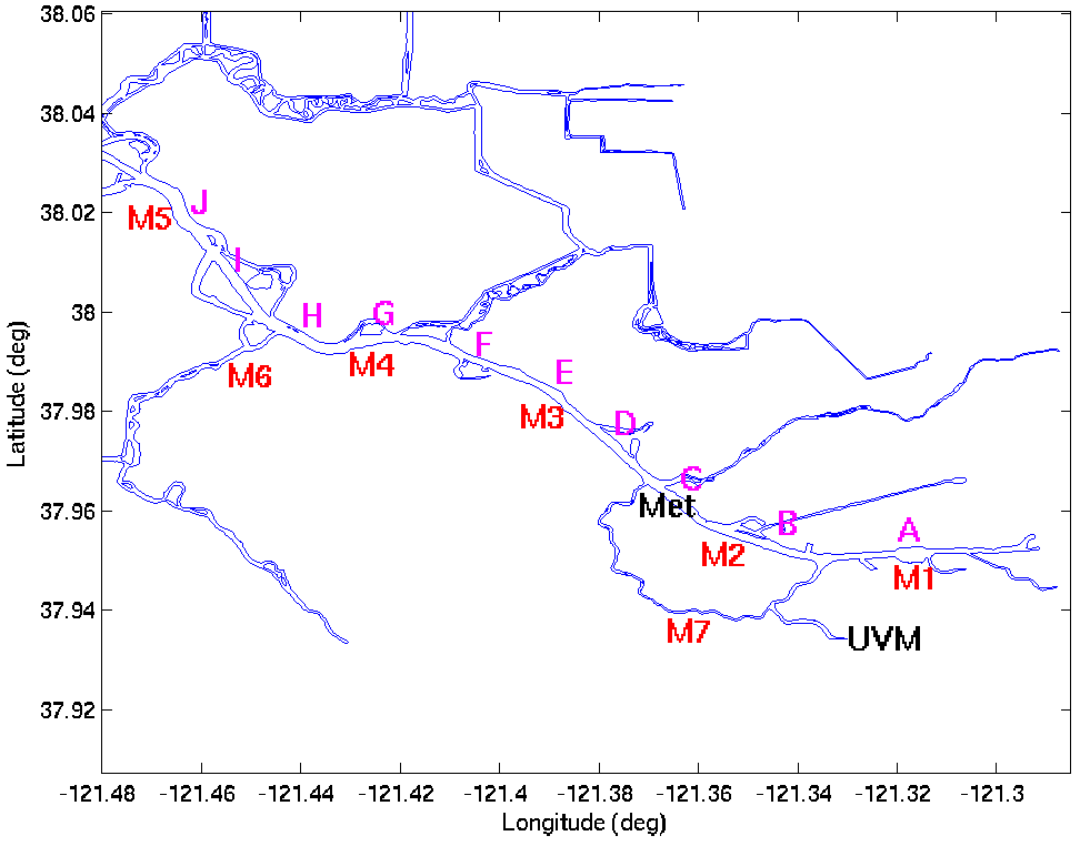

Figure 1: Map of study area and location of field measurements for August 2004. M1 through M5 are locations of ACDP-thermistor string moorings. M6 is the location of an ADCP mooring in Turner Cut to be used for model boundary conditions. M7 is the location of an H-ADCP and pressure sensor to be used for model verifications. Stations A through J are CTD-DO cast locations used during the two cruises. Met is the meteorological and long term CTD-Do mooring. UVM is the long-term USGS gauging station.

A total of 66 instruments were deployed and all were successfully recovered.

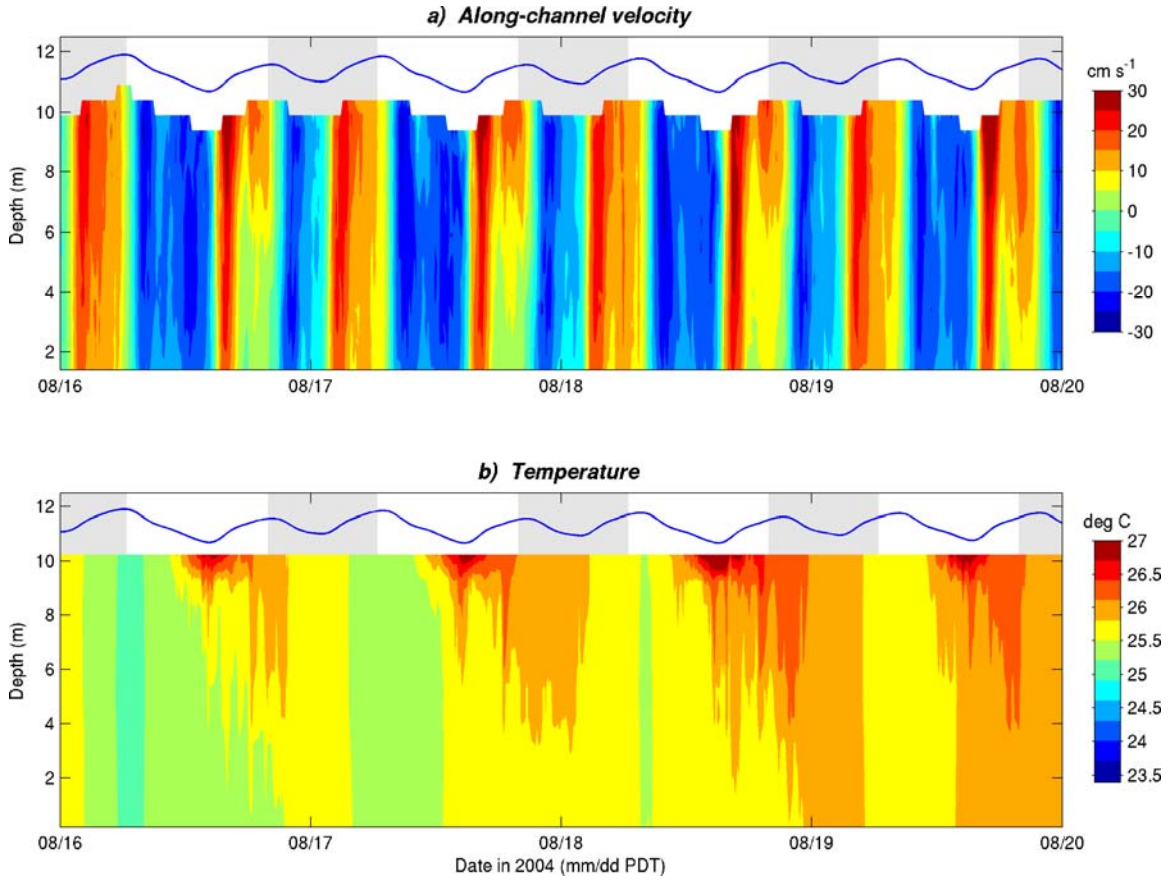

Figure 1 Excerpt from time-series of a) along-channel velocity and b) temperature taken at mooring station M3. Positive velocity is upstream (warm colors) and negative is downstream (cool colors). Blue line indicates observed water level. Grey shading indicates day-night cycle.

The intensive studies took place on August 8-9 (neap tide) and August 16-17, 2004 (spring tide). Water samples for the 2004 experiments were only analyzed for the nitrogen species, but not the phosphorus species. During the 2004 experiments, the PAR sensor on the SBE-25, located on the house boat, was not working properly, and those data should be disregarded. In addition, during the first experiment of 2004, the first 3 hours of SBE-25 data was lost, and during the second experiment, an instrument malfunction caused all but the first eight hours of data to be compromised.

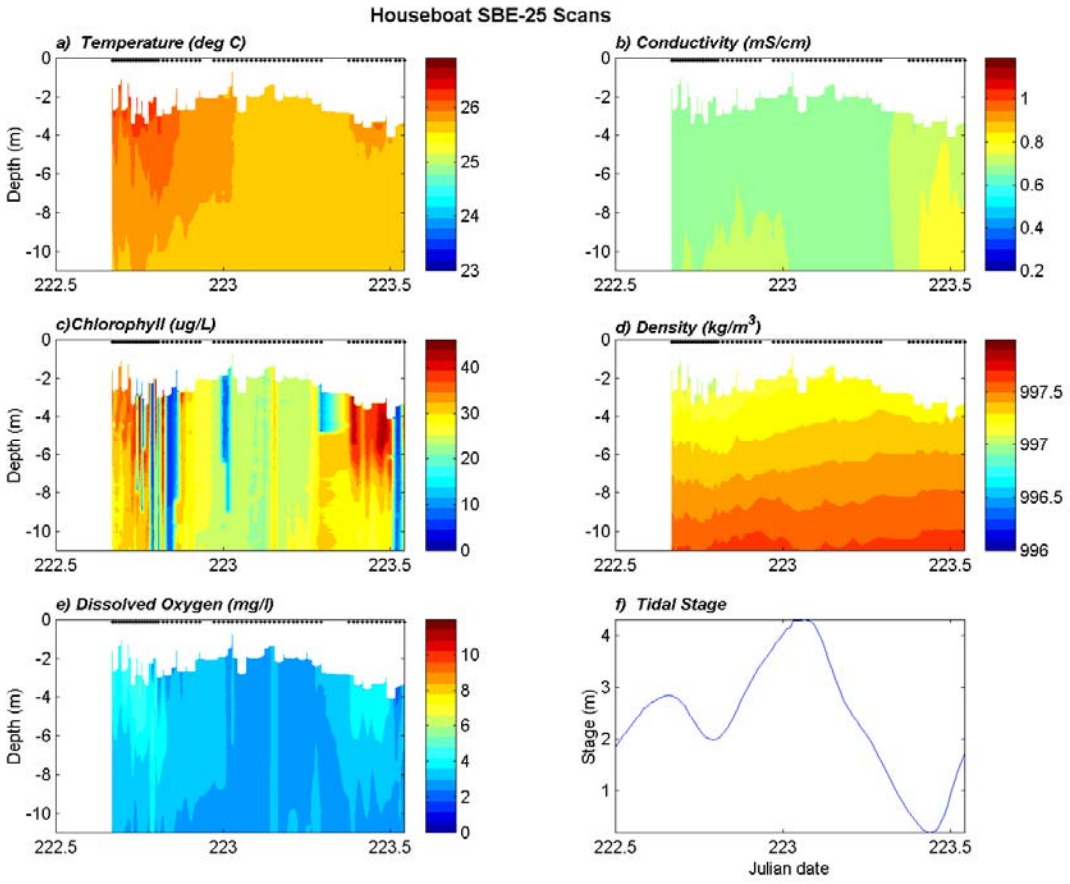

Figure 3: Time-series contour plots of a) temperature b) conductivity c) chlorophyll d) density e) dissolved oxygen and f) tidal stage at the houseboat (M2 in figure 1) August 8-9, 2004.

On the August 8-9 cruise, two small boats were used for transecting. One boat visited sites A-D in Figure 1 and the other boat visited E-J. The Sea-Bird 19plus was dropped at the upstream locations and the SBE-19 was dropped at the downstream locations. The two instruments are not compatible for some constituents, including dissolved oxygen and fluorescence. For this reason, during the second thirty-hour study, the SBE-19 plus was used at all locations. In addition, after looking at some of the data from the August 8-9 data, it was decided that it would be beneficial to carefully study the junction. The second boat transected the region where the San Joaquin River enters the Deep Water Ship Channel. This boat was equipped with a shipboard ADCP and the SBE-19 which was towed continuously 2-m below the surface. Finally, a third small boat was dedicated on each cruise to collecting SCAMP data. The following figures present excerpts of the data collected on the transecting boats and the SCAMP data.

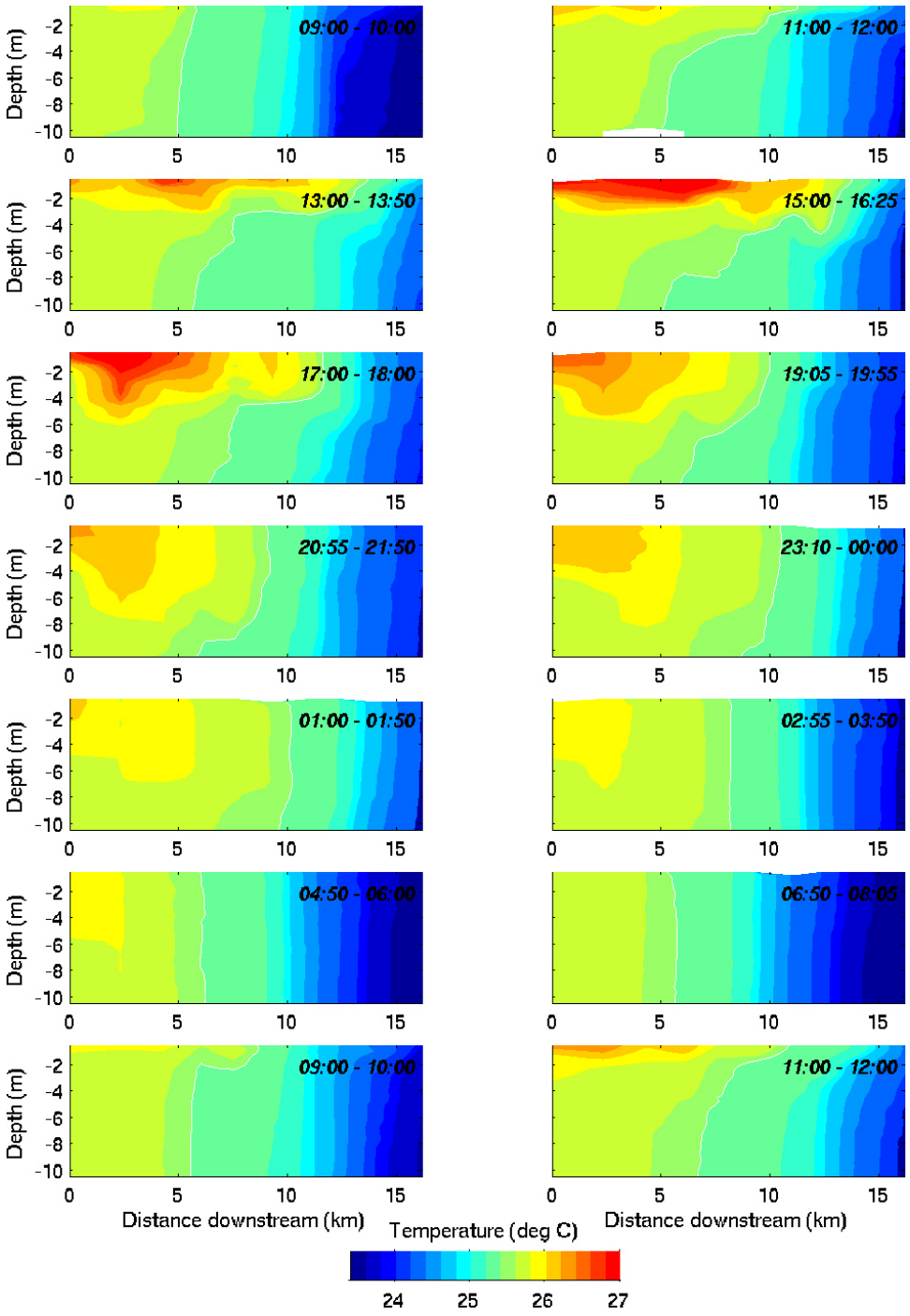

Figure 4: Longitudinal temperature sections taken during 16-17 August 2004 cruise. Distance downstream is relative to the turning basin at the Port of Stockton (at station M1).

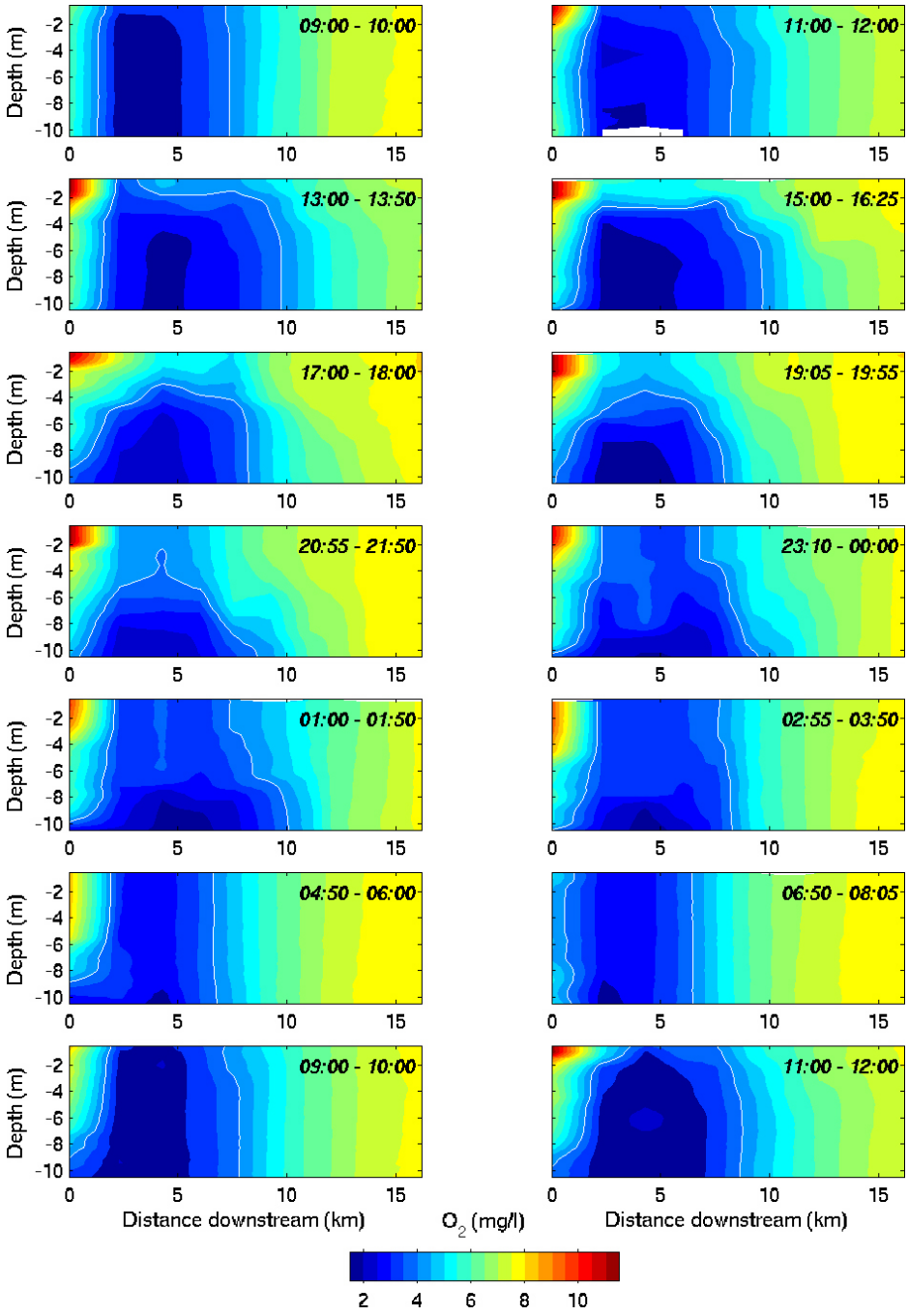

Figure 5: Longitudinal dissolved oxygen sections taken during 16-17 August 2004 cruise. Distance downstream is relative to the turning basin at the Port of Stockton (at station M1).

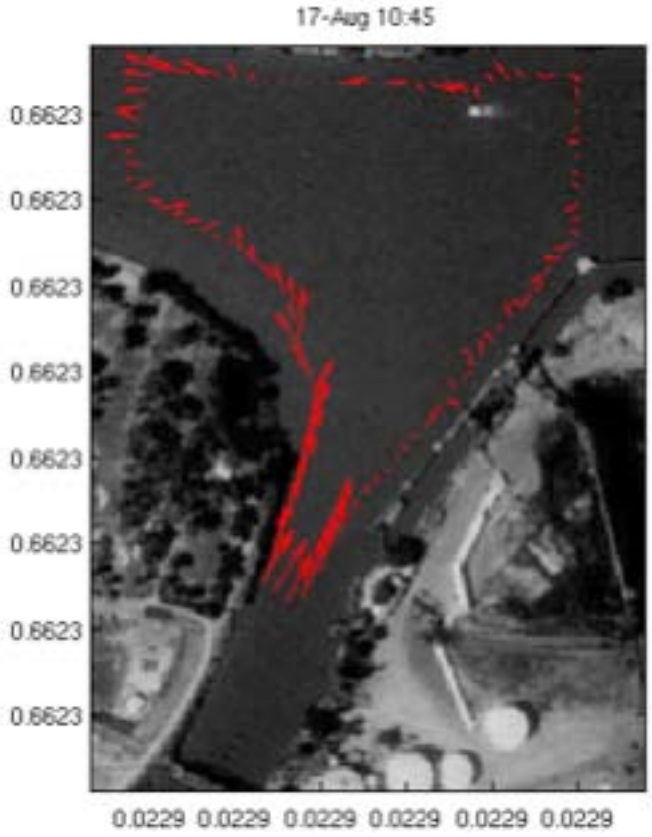

Figure 6: Example of shipboard ADCP data collected along a repeated transect at the mouth of the San Joaquin River at Channel Point (where the SJR meets the Deep Water Shipping Channel).

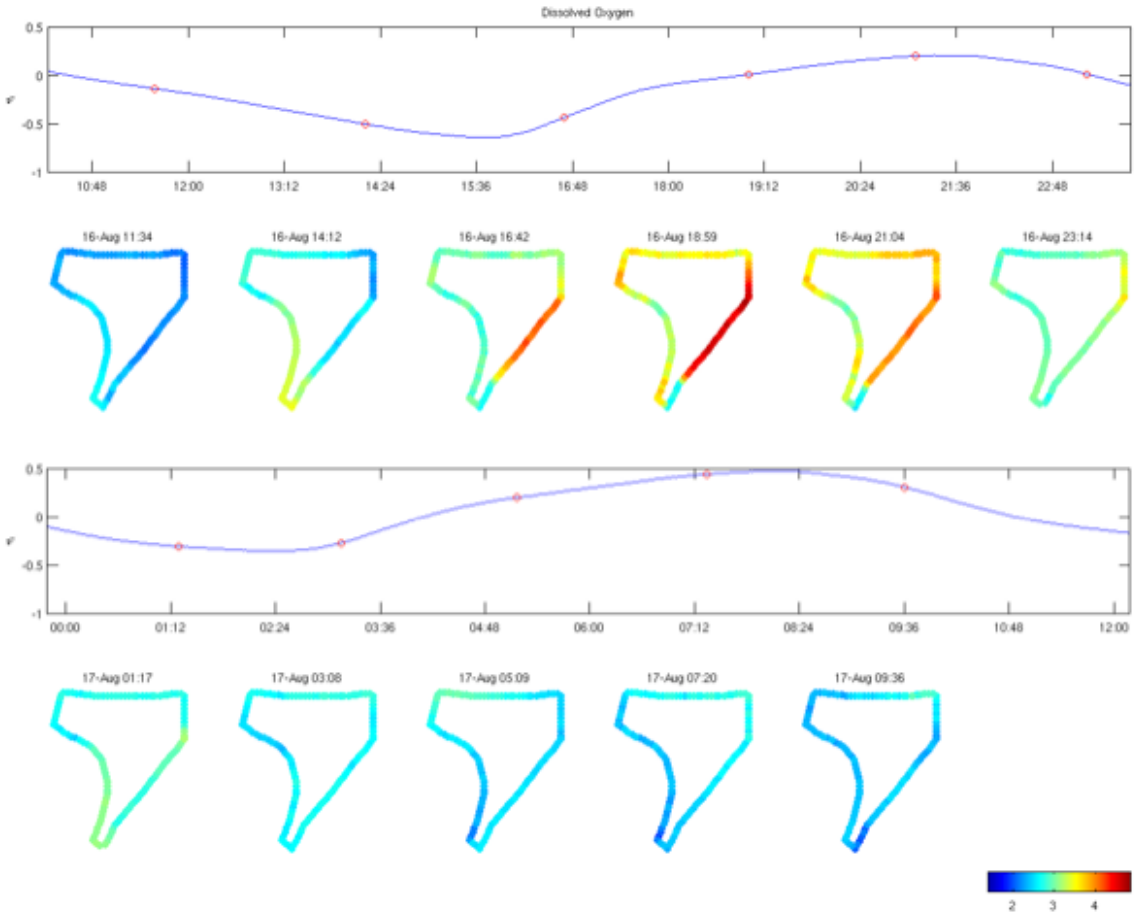

Figure 7: Example of shipboard dissolved oxygen data collected along a repeated transect at the mouth of the San Joaquin River at Channel Point (where the SJR meets the Deep Water Shipping Channel). Data were collected with a continuously sampling CTD/DO sensor set 2 m below the surface.

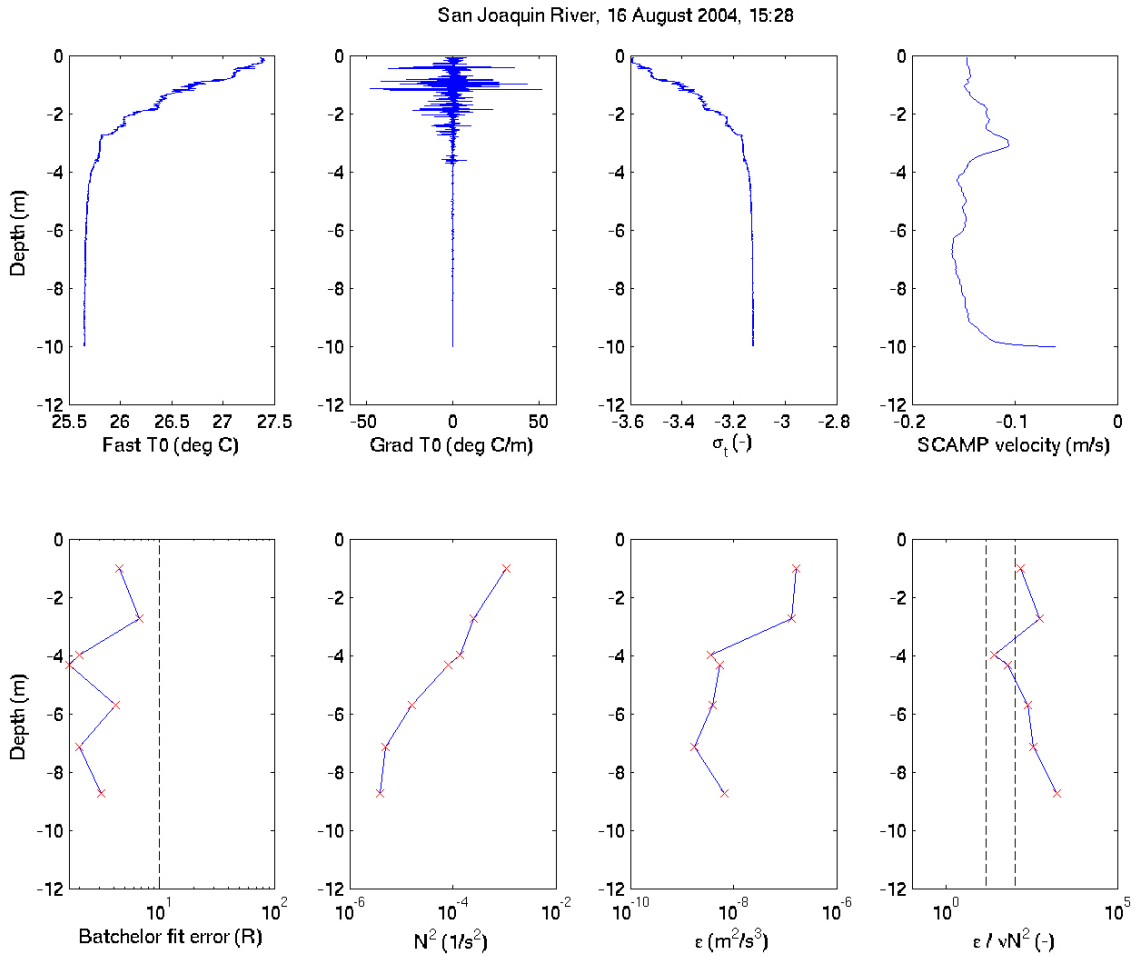

Figure 8: Example microstructure profile. Each profile was screened for quality control and trimmed at the surface and bottom. The data were segmented and for each segment a Batchelor-spectra estimate of the turbulent dissipation rate was computed. A second quality control was conducted for each segment. The buoyancy frequency for each segment was a then calculated, with good segments permitting calculation of buoyancy Reynolds numbers.

August 2005

After interpreting the data from August 2004, the experiment layout for 2005 was modified. As shown in the following map, there were less ADCP and thermistor chains deployed for the month, one was located at the downstream boundary condition (M5 in Figure 9a), another in the river, upstream of the junction (M-1 in Figure 9a) and the third was at the location of the most critical DO problem (M2 in Figure 9a). A final thermistor string was placed near the junction (M0 in Figure 9a).

The moorings were deployed on August 2-3, 2005 and recovered on August 24, 2005. These data are still being quality checked.

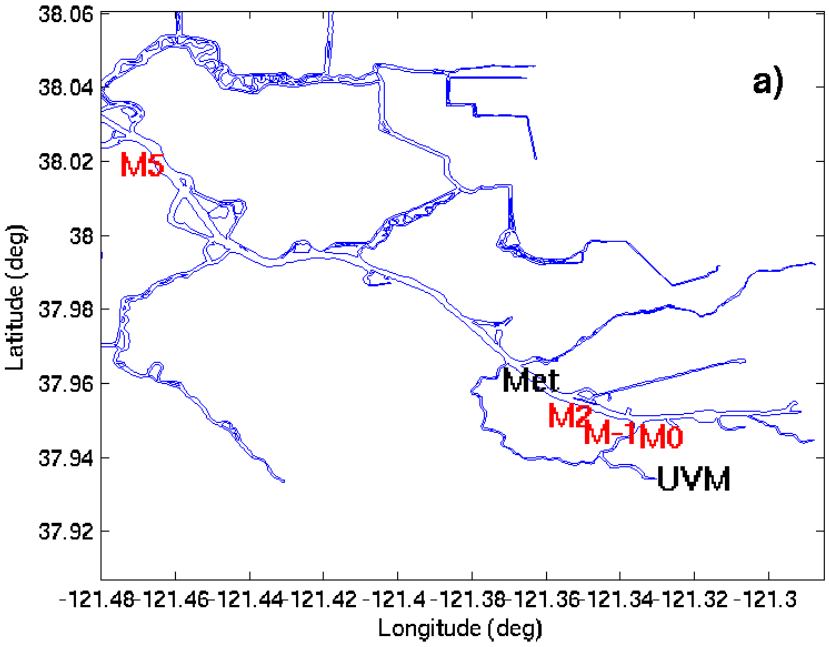

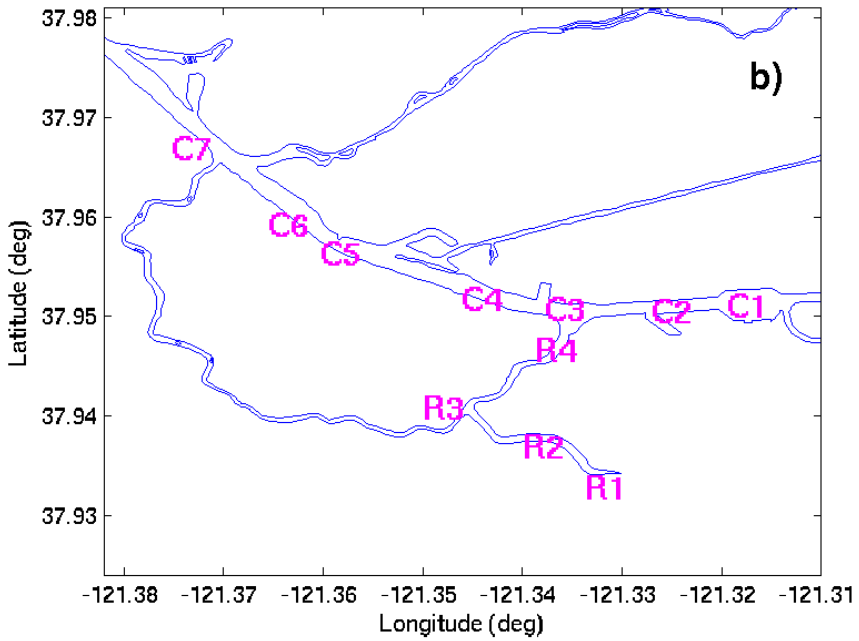

Figure 9: Map of study area and location of field measurements for August 2005. a) shows the locations of moorings. M1, M2 and M5 are the locations of the ADCP and thermistor chains and M0 is the location of the thermistor string only. b) shows the locations of the CTD-DO cast locations used during the two cruises.

The concentrated studies occurred on August 16-17 (spring tide) and August 23-24 (neap tide). The houseboat was located at the same location during 2005. The water samples collected at the house boat during 2005, in addition to being analyzed for the nitrogen species, were also analyzed for phosphorus and total suspended solids.

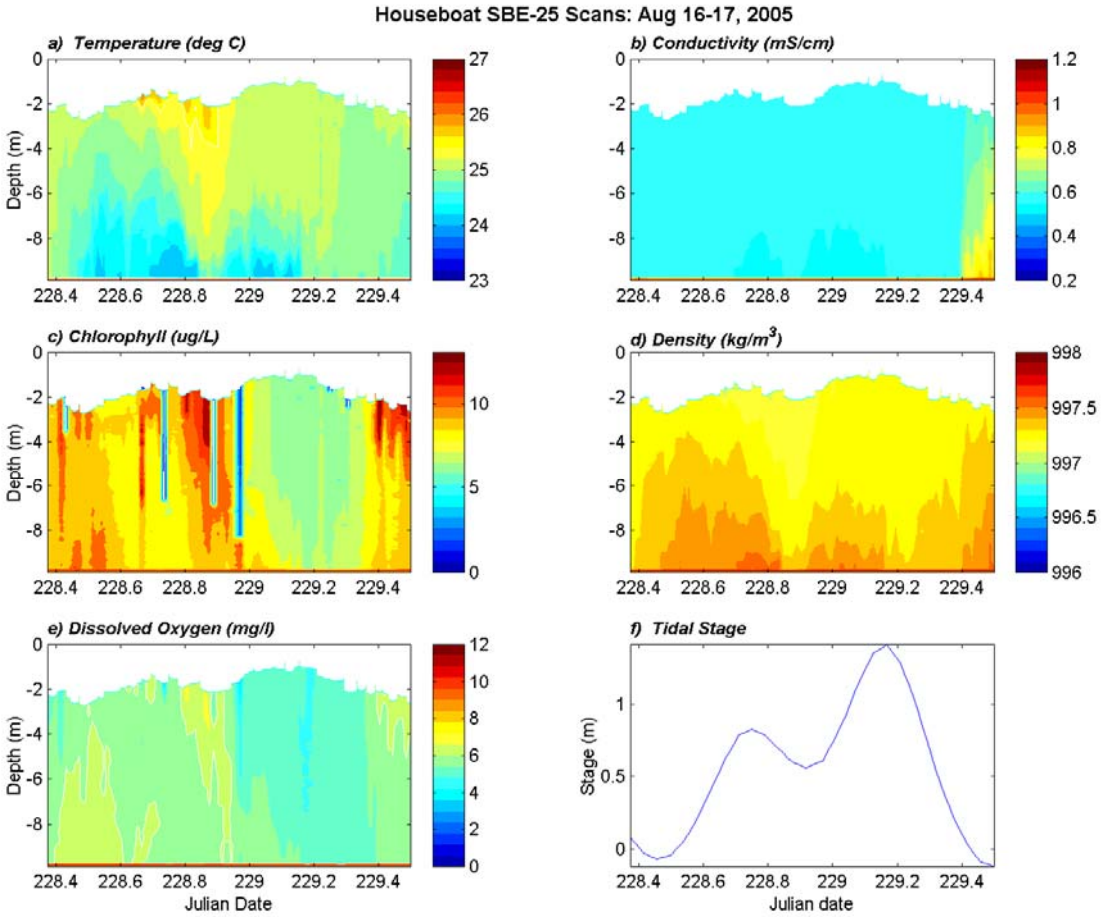

Figure 10: Time-series contour plots of a) temperature b) conductivity c) chlorophyll d) density e) dissolved oxygen and f) tidal stage at the houseboat (M2 in figure 1) August 16-17, 2005. In figure 10b, a spike in the conductivity is noted toward the end of the experiment. This spike was noticed in the SBE25, as well as the SBE 19 plus data.

The locations of the transecting boat also changed during 2005. More locations in the river were visited, and fewer locations in the DWSC were visited, as seen in Figure 9b. The longitudinal transects began upstream of the Stockton wastewater treatment plant and down to near Buckley's cove, on the main shipping channel. Transects were run every 2-hrs, stopping at 11 stations. The continuous ADCP/CTD transects at the junction were modified for the August 2005 experiments. The ADCP was upgraded from a 600 kHz to a 1200 kHz working in a fast-ping mode for increased accuracy. The data from this boat is still being checked for accuracy. The SCAMP measurements were increased in 2005, with upward casts being collected in the same location as 2004, but every 10 minutes. The following figures present excerpts of the data collected on the transecting boats and the SCAMP data.

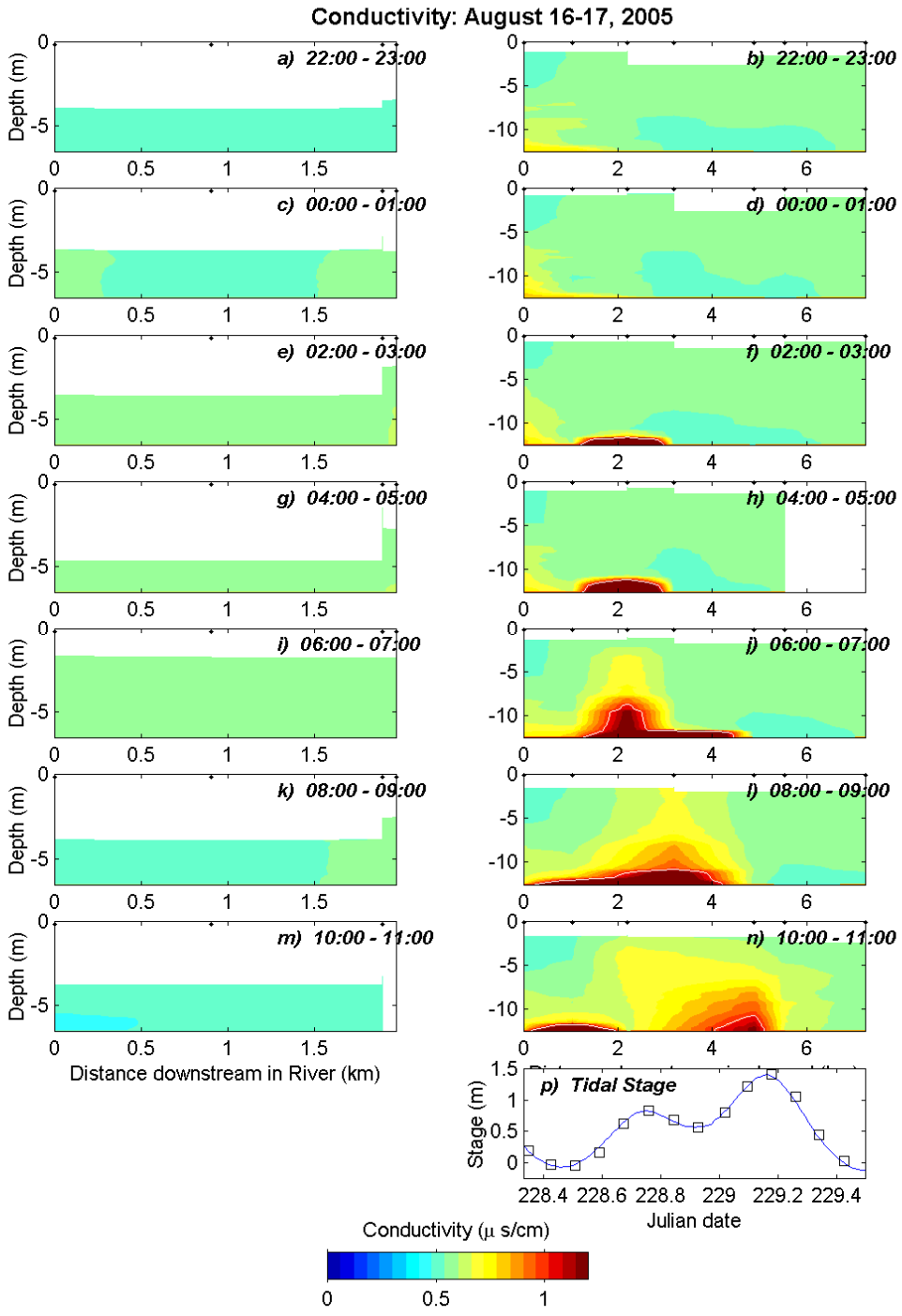

Figure 11: Longitudinal conductivity sections taken during 16-17 August 2005 cruise. Distance downstream in the river (left hand side plots) is relative to the UVM located at Garwood (station R1) and distance downstream in the ship channel (right hand side) is relative to the turning basin at the Port of Stockton (at station M1).

This figure presents the conductivity data for the second half of the experiment. Note the conductivity spike that occurs in the ship channel beginning at 2:00am. The source of this spike is still under investigation.

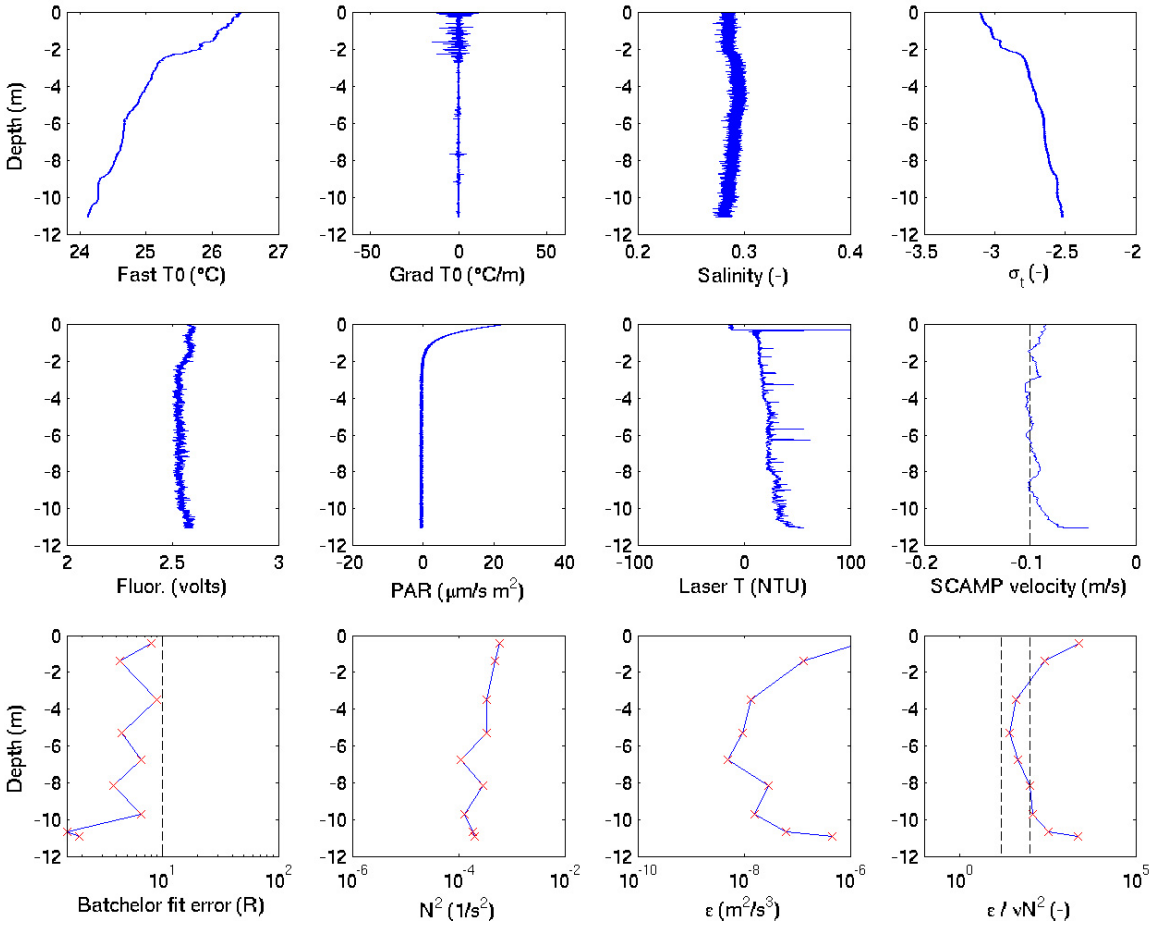

Figure 12: SCAMP microstructure profile data collect on the San Joaquin River at 15:30 on 16 August 2005. Note the sharp change in water mass and turbulence properties at 2 m depth.

Data Availability

All raw data collected over the course of the last two years are available through the UC Davis ftp server. The voluminous nature of these time series data make it unwieldy to display it in tabulated form. For more information, contact Laura DiPalermo via e-mail: ladipalermo@ucdavis.edu or telephone: 530-754-6433.

3. Stockton Deep Water Channel Tracer Experiment

The Report contained in the following pages describes the field operations associated with a supplemental study using the inert tracer, sulfur hexafluoride to track water movement through the SDWSC. Appendix II to the main report includes the peer-reviewed paper that was developed from this effort..

Stockton Deep Water Channel Tracer Experiment

David T. Ho[1], Paul J. Schmieder[1], and Jordan F. Clark[2]

[1]Lamont Doherty Earth Observatory, Columbia University, Palisades NY

[2]Department of Earth Science, University of California, Santa Barbara, CA

Objectives

The objectives of the Stockton Deep Water Channel (SDWC) tracer experiment were to determine the longitudinal dispersion coefficient, tracer residence time, and the net down stream advection using the sulfur hexafluoride (SF_6) tracer method developed by Clark et al. (1996) and Ho et al. (2002). The study was conducted during a period of intensive field measurements as part of the larger project of S. Monismith, G. Schladow, and P. Smith, "Hydrodynamics and oxygen modeling of the Stockton Deep Water Ship Channel."

Methods

For 9 days starting on August 14, 2005, the SF_6 tracer study was conducted within the SDWC and the San Joaquin River. On August 14 (Day 0), approximately 1.6 mol (240 gr) of SF_6 were injected over a period of 10 minutes at an average depth of 3.3 m into the San Joaquin River, 13 km upstream of the confluence between the river and the SDWC. The tracer was injected at slack before ebb tide.

SF_6 samples were analyzed using an automated, high-resolution, measurement system that continuously measured SF_6 concentration in the water at 1 minute intervals (Ho et al., 2002; Caplow et al, 2004). This system included a membrane contactor (Liqui-Cel) to extract gasses from the water sample, dual analytical columns to separate SF_6 from other gases, and a gas chromatograph (GC) with an electron capture detector (ECD) to measure SF_6. Calibration of the system was determined using a gas standard (146 pptv) prepared and certified by Scott-Marrin, Inc. (Riverside, CA). For

this experiment, modifications were made to the original system to use a peristaltic pump in place of the submersible pump.

On subsequent days following the tracer release, Days 1-8, surveys were conducted in the SDWC and the San Joaquin River to define the structure of the tracer patch. Surveys continued until background SF_6 concentrations were observed. Transects were also repeated each day. During the repeated surveys on Days 5, 6, and 8, a CTD sonde was lowered every 1 km to establish the temperature and salinity gradients with depth. Also, water samples from depth were pumped through the continuous system and collected as discrete samples to define vertical SF_6 and DO concentration gradients.

While sampling, the gas stripping efficiency of the membrane contactor decreases due to particles (<40 microns in size) clogging the contactor pores, and water flow rates vary since the flow is controlled manually. Final data calibrations account for the variability of these parameters, and SF_6 concentrations are presented in femto (10^{-15}) moles per liter of water (fmol L^{-1}).

SF_6 data from the SDWC study were corrected for tidal movement in order to obtain a synoptic distribution. SF_6 data from each day were corrected to the time of slack before ebb tide (SBE) at the location of an ADCP (Acoustic Doppler Current Profiler), 14 km downstream of the confluence between the SDWC and the San Joaquin River. The tidal correction follows the methods of Ho et al., (2002):

where x_0 and t_0 are the measurement distance (river kilometer; rkm) and time, respectively, and $x(t)$ is the corrected distance at SBE at time t. v_{max} is the maximum ebb velocity observed at the ADCP location during each day of the study. The tidal period, P, was determined based on the amount time elapsed between consecutive SBE cycles. x_{ref} and t_{ref} refer to the location and time of the SBE reference conditions, respectively. a is the upstream propagation velocity of the tidal wave, and the value for each day was determined from the time difference of low tide between two ADCP's separated by 12 km. a and v_{max} were both assumed to be constant as a function of distance along the SDWC.

SF_6 mass inventories for each day were obtained by combination measured SF_6 concentrations with volumes of the SDWC. Volumes for the portions of the SDWC sampled during the study were determined using electronic NOAA navigational charts in ArcGIS. As the volumes of side channels and embayments are less than the volume of the main channel, these are excluded from the inventory calculations.

Results

The SF_6 concentration data obtained from the repeated daily transects are presented in Figures 1 and 2. In this study, distances along the channel are designated by river kilometers (RKM), and decrease downstream of the ship turning basin in the SDWC. RKM 19 marks the confluence of the San Joaquin River and the SDWC.

In Figure 1, transects are plotted for Days 1 – 8, following the tracer release. In Figure 2, longitudinal SF_6 profiles are presented from the SDWC for Days 2 - 8. Tracer tagged waters entered the SDWC 1 day following the tracer injection. SF_6 concentrations remained high in the upper reaches of the SDWC throughout the survey. This region coincides with the boat turning basin and is upstream of the confluence of the San Joaquin River and the SDWC. The persistent elevated SF_6 concentrations indicate that the residence times for waters in the boat turning basin are greater than the residence times of water further downstream in the SDWC. Based on the migration of peak tracer concentration, the average advection over the investigation was 1.2 km day^{-1}.

Based on the decay of the SF_6 mass inventory, the e-folding residence time for a volatile substance in the SDWC below the confluence of the San Joaquin River is ~6 days. The dispersion coefficient is determined by the change in moment method, which fits a Gaussian curve through the longitudinal profiles and then measures the change in variance over time. The dispersion coefficient is 56.9 m^2 sec^{-1} in the DWSC under the environmental conditions during the study.

A manuscript, which discusses these results in more detail, is currently being prepared. We anticipate submitting it during the summer.

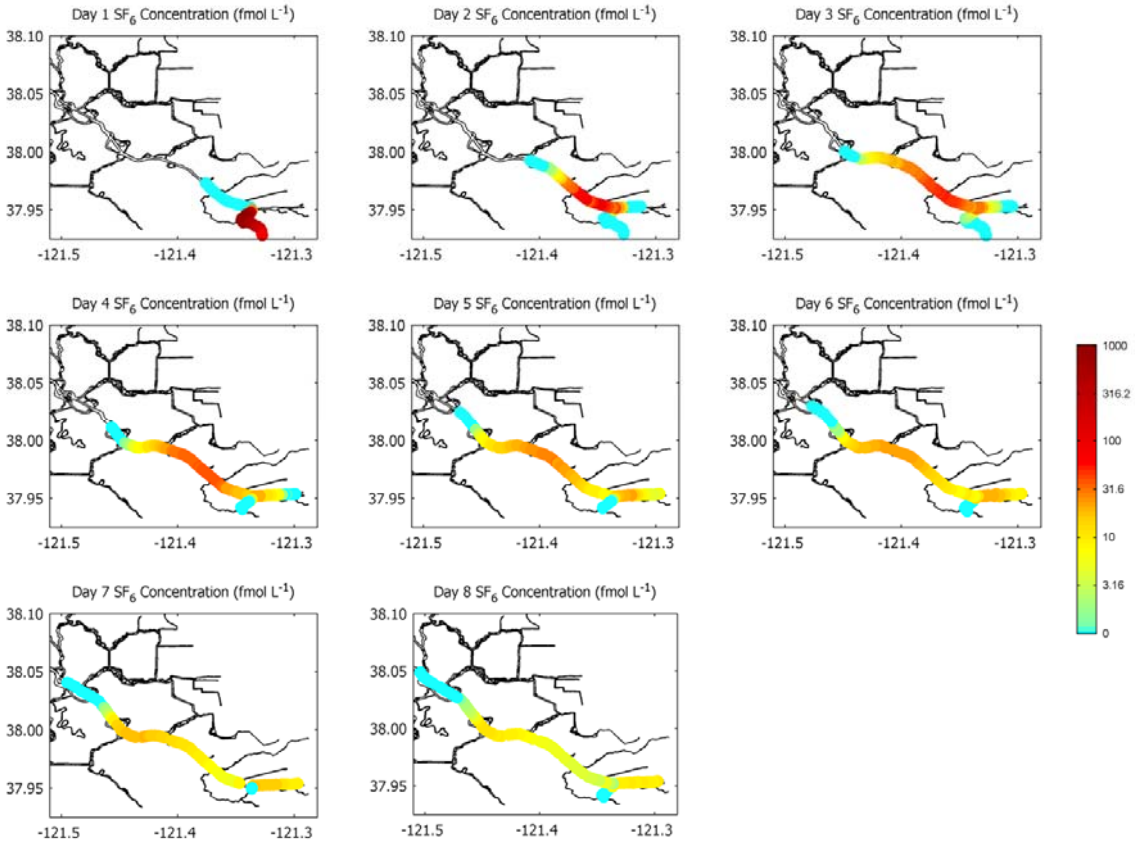

Figure 1: Daily SF_6 concentration data in the San Joaquin River and the SDWC. Concentrations are presented in fmol L^{-1}.

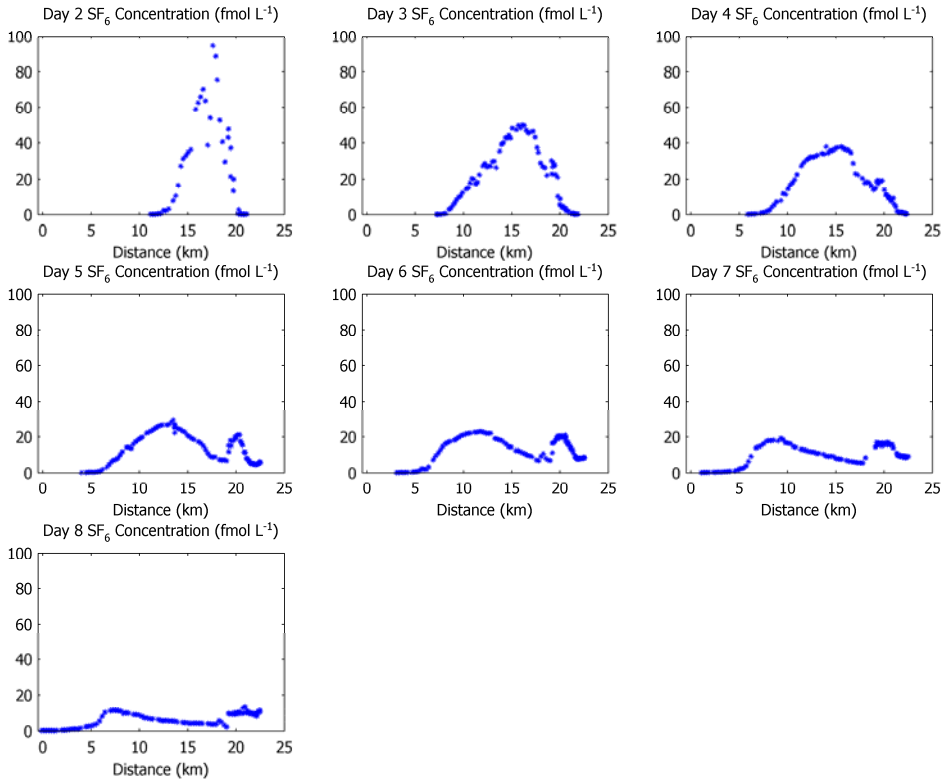

Figure 2: Daily SF_6 longitudinal profiles in the SDWC. Concentrations are presented in fmol L^{-1}. RKM 19 marks the confluence of the San Joaquin River and the SDWC. Upstream of this location is the ship turning basin.

References

Caplow, T., Schlosser, P., Ho, D. T., and Enriquez, R. C. (2004). "Effect of tides on solute flushing from a strait: Imaging flow and transport in the East River with SF_6." *Environ. Sci. Technol.*, 38(17), 4562-4571.

Clark, J. F., Schlosser, P., Stute, M. and Simpson, H. J. (1996) "SF_6-^{3}He tracer release experiment: A new method of determining longitudinal dispersion coefficients in large rivers." *Environ. Sci. Technol.*, 30(5), 1527-1532.

Ho, D. T., Schlosser, P., and Caplow, T. (2002). "Determination of Longitudinal Dispersion Coefficient and Net Advection in the Tidal Hudson River with a Large-Scale, High Resolution SF_6 Tracer Release Experiment." *Environ. Sci. Technol.*, 36(15), 3234 -3241.

Appendix 1: Stockton Deep Water Channel Data

GPS Time (EDT)	Lat	Long	DO (mg L^{-1})	Temp (°C)	RKM	Corrected RKM	SF_6 (fmol L^{-1})
150805-143538	37.97633	-121.38031	5.0	25.5	14.2	18.0	5.0
150805-143650	37.97595	-121.37957	5.0	25.4	14.3	18.1	0.1
150805-143802	37.97595	-121.37959	5.1	25.5	14.3	18.1	0.1
150805-143915	37.97532	-121.37934	5.1	25.5	14.3	18.1	0.0
150805-145734	37.97301	-121.37614	5.2	25.8	14.7	18.4	0.1
150805-145845	37.97275	-121.37538	4.9	25.9	14.8	18.5	0.1
150805-145957	37.97180	-121.37483	5.2	25.9	14.9	18.6	0.1
150805-150110	37.97021	-121.37328	5.2	25.9	15.1	18.8	0.0
150805-150221	37.96860	-121.37180	5.3	25.9	15.3	19.0	0.1
150805-150333	37.96705	-121.37017	5.2	25.8	15.5	19.2	0.1
150805-150445	37.96568	-121.36844	5.4	25.8	15.8	19.5	0.1
150805-150556	37.96412	-121.36688	5.3	25.9	16.0	19.7	0.0
150805-150818	37.96141	-121.36323	5.4	25.8	16.4	20.1	0.1
150805-150931	37.95994	-121.36129	5.7	25.8	16.7	20.4	0.0
150805-151042	37.95873	-121.35916	5.4	25.7	16.9	20.6	0.0
150805-151154	37.95767	-121.35684	5.5	25.6	17.1	20.8	0.0
150805-151305	37.95676	-121.35446	5.8	25.6	17.4	21.1	0.0
150805-151418	37.95584	-121.35201	6.1	25.7	17.6	21.3	0.1
150805-151528	37.95502	-121.34964	5.9	25.6	17.8	21.5	0.0
150805-151641	37.95443	-121.34727	6.2	25.6	18.0	21.8	0.0
150805-151902	37.95306	-121.34264	6.3	25.5	18.5	22.2	0.0
150805-152014	37.95249	-121.33983	6.1	25.5	18.7	22.5	0.0
150805-152126	37.95194	-121.33704	6.1	25.9	19.0	22.7	0.2
150805-152238	37.95008	-121.33610	6.6	25.0	19.1	22.9	24.9
150805-152349	37.94804	-121.33725	7.0	24.4			408.8
150805-152503	37.94673	-121.33950	7.1	24.3			694.1
150805-152614	37.94580	-121.34133	7.1	24.3			851.1
150805-152726	37.94536	-121.34145	7.1	24.4			812.6
150805-154048	37.94809	-121.33716	6.8	24.7			358.7
150805-154200	37.94796	-121.33723	7.0	24.7			354.6
150805-154311	37.94708	-121.33851	7.0	24.6			538.5
150805-154423	37.94594	-121.34087	7.1	24.5			763.1

150805-154535	37.94408	-121.34242	7.1	24.4			1020.2
150805-154647	37.94293	-121.34485	7.2	24.4			1010.2
150805-154758	37.94115	-121.34516	7.2	24.3			1032.3
150805-154910	37.93933	-121.34355	7.2	24.3			845.1
150805-155133	37.93906	-121.33809	7.6	24.4			599.3
150805-155243	37.93829	-121.33563	7.3	24.3			484.6
150805-155356	37.93641	-121.33408	7.4	24.3			432.4
150805-155508	37.93553	-121.33152	7.5	24.4			307.1
150805-155620	37.93437	-121.32918	7.6	24.5			253.7
150805-155731	37.93235	-121.32806	7.4	24.2			221.8
150805-155843	37.93015	-121.32788	7.5	24.2			157.3
150805-155955	37.92805	-121.32717	7.5	24.2			78.3
150805-160217	37.92447	-121.32413	7.7	24.1			56.0
150805-160330	37.92250	-121.32289	7.8	24.1			26.7
150805-160442	37.92101	-121.32088	7.7	24.1			25.0
150805-160553	37.92040	-121.31966	7.7	24.1			15.9
150805-160705	37.92027	-121.31948	7.8	24.1			19.6
150805-160817	37.92012	-121.31930	7.7	24.1			18.9
150805-160929	37.92000	-121.31914	7.7	24.1			15.2
150805-161041	37.91992	-121.31906	7.6	24.0			10.5
150805-161304	37.91986	-121.31891	7.6	24.1			8.9
150805-161416	37.91985	-121.31889	7.7	24.0			9.8
150805-161526	37.91864	-121.32018	7.7	24.1			7.8
150805-161639	37.91687	-121.32148	7.7	24.0			6.6
150805-161750	37.91506	-121.32267	7.7	24.1			5.1
150805-161902	37.91340	-121.32399	7.7	24.1			4.5
150805-162012	37.91142	-121.32454	7.8	24.1			3.7
150805-162126	37.90937	-121.32501	7.7	24.0			3.1
150805-162346	37.90572	-121.32344	7.7	24.0			2.8
150805-162458	37.90404	-121.32449	7.6	24.0			2.1
150805-162610	37.90232	-121.32583	7.8	24.0			1.9
150805-162723	37.90023	-121.32607	7.7	24.0			2.0
150805-162833	37.89831	-121.32682	7.7	24.0			1.8
150805-162945	37.89643	-121.32785	7.9	24.1			2.0
150805-163056	37.89470	-121.32886	7.7	24.0			1.9
150805-163210	37.89524	-121.32837	7.6	24.1			2.3
150805-163431	37.89531	-121.32832	7.7	24.2			2.0
150805-163543	37.89534	-121.32830	7.6	24.2			2.1

160805-115727	37.95882	-121.35829	5.2	25.1			51.7
160805-115839	37.95882	-121.35826	5.2	25.0			44.3
160805-115950	37.95883	-121.35826	5.1	24.9			63.3
160805-120102	37.95884	-121.35825	5.2	24.9			60.6
160805-120213	37.95884	-121.35825	5.2	24.9			68.1
160805-120324	37.95884	-121.35822	5.2	24.9			73.6
160805-125559	37.91550	-121.32194	7.1	23.5			7.9
160805-125712	37.91606	-121.32151	7.1	23.5			1.6
160805-125822	37.91640	-121.32151	7.1	23.5			0.7
160805-125934	37.91540	-121.32233	7.1	23.4			1.0
160805-133031	37.91253	-121.32415	6.7	23.4			0.3
160805-133143	37.91424	-121.32372	6.7	23.5			0.6
160805-133255	37.91469	-121.32314	6.8	23.6			0.5
160805-133406	37.91607	-121.32164	6.9	23.6			0.6
160805-133518	37.91846	-121.32017	6.7	23.6			0.6
160805-133630	37.92060	-121.31978	6.7	23.6			0.8
160805-133741	37.92228	-121.32247	6.7	23.4			0.9
160805-133853	37.92461	-121.32408	6.7	23.6			0.8
160805-134115	37.92894	-121.32769	6.4	23.5			0.8
160805-134227	37.93152	-121.32764	6.5	23.6			0.9
160805-134338	37.93394	-121.32880	6.4	23.5			0.6
160805-134450	37.93544	-121.33135	6.8	23.5			0.7
160805-134601	37.93651	-121.33424	6.6	23.5			0.6
160805-134713	37.93854	-121.33623	6.6	23.6			0.8
160805-134824	37.93912	-121.33926	6.4	23.6			0.5
160805-134937	37.93900	-121.34261	6.8	23.6			0.7
160805-135200	37.94279	-121.34490	6.5	23.8			0.8
160805-135312	37.94424	-121.34225	6.4	23.8			0.8
160805-135424	37.94635	-121.34038	6.8	23.8			0.6
160805-135536	37.94762	-121.33755	6.7	23.7			0.7
160805-135647	37.94981	-121.33582	5.9	24.5			10.6
160805-135911	37.95198	-121.33150	8.1	25.6	19.5	23.2	37.3
160805-140035	37.95230	-121.32813	8.8	25.6	19.8	23.5	20.0
160805-140304	37.95267	-121.32208	10.8	25.7	20.3	24.0	2.7
160805-140417	37.95273	-121.31902	10.2	25.8	20.6	24.3	0.4
160805-140529	37.95280	-121.31598	9.9	25.9	20.8	24.5	0.1
160805-140640	37.95300	-121.31309	10.0	26.0	21.1	24.8	0.2
160805-140752	37.95316	-121.31312	10.3	25.9	21.1	24.8	0.1

160805-140904	37.95310	-121.31618	9.5	25.9	20.8	24.6	0.2
160805-141016	37.95294	-121.31932	10.2	25.8	20.5	24.3	0.0
160805-141128	37.95276	-121.32243	8.7	25.8	20.3	24.1	0.3
160805-141351	37.95215	-121.32855	7.9	25.6	19.7	23.7	13.4
160805-141504	37.95191	-121.33171	7.0	25.6	19.5	23.4	21.4
160805-141614	37.95183	-121.33483	6.2	25.0	19.2	23.2	43.0
160805-141727	37.95233	-121.33807	6.0	24.7	18.9	23.0	29.7
160805-141839	37.95296	-121.34113	6.2	24.9	18.6	22.7	40.6
160805-141951	37.95368	-121.34419	6.2	25.0	18.3	22.5	52.7
160805-142102	37.95462	-121.34707	6.2	25.1	18.1	22.2	75.6
160805-142214	37.95505	-121.34855	6.1	25.3	17.9	22.1	88.6
160805-142438	37.95599	-121.35179	6.1	25.4	17.6	21.8	94.6
160805-142550	37.95692	-121.35462	5.4	25.7	17.3	21.6	54.0
160805-142703	37.95792	-121.35742	5.4	25.5	17.1	21.3	38.8
160805-142815	37.95908	-121.35952	5.7	25.5	16.8	21.1	63.6
160805-142926	37.96059	-121.36160	5.5	25.5	16.6	20.9	70.3
160805-143038	37.96222	-121.36365	5.4	25.5	16.3	20.7	65.9
160805-143150	37.96384	-121.36565	5.4	25.5	16.1	20.4	62.6
160805-143302	37.96556	-121.36756	4.6	25.8	15.8	20.2	58.9
160805-143525	37.96891	-121.37148	5.0	25.6	15.3	19.7	36.4
160805-143638	37.97061	-121.37356	5.2	25.7	15.1	19.4	34.9
160805-143748	37.97230	-121.37545	5.2	25.7	14.8	19.2	33.0
160805-143900	37.97399	-121.37747	5.2	25.6	14.5	18.9	31.5
160805-144012	37.97568	-121.37956	5.2	25.7	14.3	18.6	27.3
160805-144125	37.97747	-121.38153	5.0	25.6	14.0	18.4	16.5
160805-144237	37.97923	-121.38351	5.0	25.7	13.8	18.1	10.6
160805-144349	37.98101	-121.38550	4.9	25.7	13.5	17.8	7.8
160805-144611	37.98405	-121.38909	4.7	25.7	13.0	17.3	3.2
160805-144723	37.98576	-121.39147	4.7	25.7	12.8	17.1	2.1
160805-144833	37.98700	-121.39410	4.3	25.8	12.5	16.8	2.1
160805-144946	37.98811	-121.39701	4.4	25.8	12.2	16.5	0.6
160805-145057	37.98911	-121.39975	4.3	25.8	11.9	16.2	0.3
160805-145209	37.99031	-121.40247	4.2	25.8	11.7	15.9	0.2
160805-145320	37.99132	-121.40521	4.1	25.7	11.4	15.6	0.1
160805-145432	37.99253	-121.40793	4.0	25.7	11.1	15.3	0.1
160805-150632	37.99404	-121.41036	4.5	26.0	10.9	14.9	0.1
160805-150744	37.99397	-121.41021	4.6	26.1	10.9	14.9	0.1
160805-150855	37.99389	-121.40999	4.7	26.2	10.9	15.0	0.2

160805-151007	37.99379	-121.40977	4.4	26.3	10.9	15.0	0.1
160805-151118	37.99349	-121.40962	4.4	26.1	10.9	15.0	0.1
160805-151231	37.99325	-121.40940	4.2	26.1	11.0	15.0	0.1
160805-151342	37.99308	-121.40924	3.9	26.0	11.0	15.0	0.1
160805-151454	37.99250	-121.40832	3.8	25.7	11.1	15.1	0.1
160805-151715	37.99077	-121.40451	4.0	25.7	11.5	15.5	0.2
160805-151828	37.98995	-121.40240	4.1	25.8	11.7	15.8	0.2
160805-151938	37.98922	-121.40033	4.0	25.7	11.9	16.0	0.1
160805-152051	37.98846	-121.39813	4.1	25.7	12.1	16.2	0.2
160805-152201	37.98780	-121.39596	4.0	25.8	12.3	16.4	0.2
160805-152313	37.98687	-121.39383	4.1	25.9	12.5	16.6	0.2
160805-152426	37.98576	-121.39175	4.2	25.9	12.7	16.9	0.7
160805-152538	37.98461	-121.38971	4.3	25.8	13.0	17.1	3.1
160805-152801	37.98182	-121.38651	4.1	26.0	13.4	17.6	1.6
160805-152913	37.98040	-121.38483	4.5	26.0	13.6	17.8	2.3
160805-153025	37.97892	-121.38330	4.6	26.0	13.8	18.0	6.2
160805-153137	37.97754	-121.38178	4.9	26.1	14.0	18.2	9.5
160805-153248	37.97620	-121.38018	4.8	26.0	14.2	18.4	18.1
160805-153400	37.97482	-121.37851	4.8	26.0	14.4	18.7	25.9
160805-153513	37.97352	-121.37686	4.9	26.1	14.6	18.9	35.2
160805-153625	37.97207	-121.37529	5.0	26.1	14.8	19.1	44.9
160805-153848	37.97043	-121.37353	5.0	26.2	15.1	19.3	97.1
160805-154000	37.97022	-121.37329	4.0	26.3	15.1	19.4	134.8
160805-155229	37.96846	-121.37136	5.5	26.2	15.4	19.5	30.0
160805-155342	37.96826	-121.37120	5.5	26.2	15.4	19.6	28.1
160805-155451	37.96763	-121.37039	5.4	26.1	15.5	19.6	37.7
160805-155605	37.96615	-121.36890	5.6	26.2	15.7	19.9	37.8
160805-155716	37.96485	-121.36731	5.5	26.4	15.9	20.1	42.4
160805-155828	37.96355	-121.36567	5.3	26.4	16.1	20.3	33.9
160805-155940	37.96225	-121.36398	5.9	26.3	16.3	20.5	41.4
160805-160052	37.96088	-121.36240	6.0	26.3	16.5	20.7	50.3
160805-160315	37.95874	-121.35866	5.6	25.9	16.9	21.2	55.7
160805-160427	37.95805	-121.35666	5.8	25.9	17.1	21.3	50.0
160805-160538	37.95737	-121.35458	6.0	26.0	17.3	21.6	62.0
160805-160650	37.95676	-121.35298	6.3	26.2	17.5	21.7	58.0
170805-110905	37.95811	-121.35869	5.2	24.6	17.0	15.2	53.7
170805-111017	37.95882	-121.35825	5.2	24.6	17.0	15.2	54.6
170805-111129	37.95837	-121.35835	5.1	24.6	17.0	15.2	55.8

170805-111240	37.95859	-121.35828	5.2	24.7	17.0	15.3	54.4
170805-111350	37.95876	-121.35829	5.2	24.7	17.0	15.3	56.9
170805-111501	37.95854	-121.35825	5.2	24.7	17.0	15.3	55.6
170805-111612	37.95867	-121.35827	5.3	24.7	17.0	15.4	57.8
170805-111723	37.95875	-121.35828	5.3	24.7	17.0	15.4	49.7
170805-111942	37.95878	-121.35826	5.3	24.7	17.0	15.5	56.3
170805-112054	37.95882	-121.35826	5.2	24.7	17.0	15.5	50.2
170805-112205	37.95884	-121.35843	5.3	24.8	16.9	15.5	54.6
170805-112316	37.95817	-121.35883	5.3	24.8	16.9	15.6	55.1
170805-112428	37.95728	-121.35622	5.5	24.7	17.2	15.8	57.9
170805-112539	37.95628	-121.35335	5.4	24.7	17.5	16.1	64.5
170805-112649	37.95553	-121.35032	5.8	24.7	17.7	16.4	57.9
170805-112759	37.95469	-121.34727	5.9	24.6	18.0	16.7	50.1
170805-113021	37.95302	-121.34119	6.0	24.6	18.6	17.3	39.3
170805-113132	37.95227	-121.33816	5.9	24.5	18.9	17.6	34.1
170805-113242	37.95069	-121.33605	5.9	24.3	19.1	17.8	36.0
170805-113353	37.94866	-121.33688	6.2	24.0			21.7
170805-113504	37.94702	-121.33872	6.2	23.9			15.4
170805-113615	37.94587	-121.34105	6.5	23.8			10.1
170805-113724	37.94406	-121.34254	6.5	23.7			7.2
170805-113836	37.94296	-121.34494	6.5	23.8			4.7
170805-114056	37.93952	-121.34355	6.9	23.7			2.2
170805-114207	37.93914	-121.34104	6.8	23.7			1.5
170805-114318	37.93896	-121.33828	6.8	23.7			1.3
170805-114429	37.93819	-121.33580	6.9	23.8			1.0
170805-114540	37.93637	-121.33406	6.9	23.6			0.9
170805-114651	37.93553	-121.33170	6.9	23.7			0.6
170805-114802	37.93453	-121.32940	7.0	23.8			0.6
170805-114911	37.93259	-121.32829	7.0	23.8			0.6
170805-115133	37.92840	-121.32752	6.3	23.7			0.6
170805-115243	37.92797	-121.32715	7.4	23.5			0.6
170805-115355	37.93013	-121.32782	7.4	23.5			0.4
170805-115506	37.93289	-121.32822	7.3	23.4			0.4
170805-115617	37.93490	-121.32981	7.4	23.4			0.4
170805-115728	37.93563	-121.33233	7.3	23.4			0.5
170805-115840	37.93681	-121.33443	7.2	23.4			0.5
170805-115949	37.93849	-121.33586	7.3	23.5			0.5
170805-120211	37.93890	-121.34088	7.5	23.6			0.7

170805-120322	37.93923	-121.34347	7.4	23.5			0.8
170805-120432	37.94098	-121.34484	7.5	23.6			0.9
170805-120543	37.94269	-121.34504	7.4	23.6			1.4
170805-120654	37.94364	-121.34283	7.3	23.6			1.6
170805-120804	37.94540	-121.34138	7.3	23.7			2.3
170805-120915	37.94670	-121.33936	7.3	23.8			2.9
170805-121026	37.94809	-121.33729	7.1	23.8			4.1
170805-121247	37.95065	-121.33549	6.3	24.6	19.2	19.1	22.9
170805-121357	37.95129	-121.33421	6.0	24.8	19.3	19.2	27.0
170805-121509	37.95190	-121.33155	7.1	25.1	19.5	19.4	27.7
170805-121621	37.95228	-121.32830	8.6	25.1	19.7	19.7	21.2
170805-121731	37.95252	-121.32506	10.2	25.2	20.0	20.0	8.8
170805-121843	37.95263	-121.32179	11.3	25.4	20.3	20.3	4.6
170805-121953	37.95263	-121.31865	12.3	25.6	20.6	20.6	3.4
170805-122104	37.95279	-121.31556	11.6	25.7	20.9	20.9	1.8
170805-122324	37.95323	-121.30997	12.2	26.0	21.4	21.4	0.5
170805-122436	37.95336	-121.30802	12.7	26.1	21.5	21.6	0.4
170805-122548	37.95335	-121.30601	12.9	26.1	21.7	21.8	0.2
170805-122659	37.95314	-121.30470	13.0	26.2	21.8	21.9	0.3
170805-122811	37.95311	-121.30670	12.9	26.1	21.7	21.8	0.3
170805-122921	37.95315	-121.30860	12.3	26.0	21.5	21.7	0.2
170805-123032	37.95314	-121.31063	12.0	25.8	21.3	21.6	0.5
170805-123143	37.95316	-121.31300	10.8	25.8	21.1	21.4	0.6
170805-123404	37.95300	-121.31801	10.9	25.6	20.6	21.1	2.0
170805-123515	37.95289	-121.32051	10.5	25.4	20.4	20.9	3.5
170805-123625	37.95271	-121.32297	9.9	25.3	20.2	20.8	4.0
170805-123736	37.95240	-121.32545	8.2	25.2	20.0	20.6	5.5
170805-123847	37.95228	-121.32795	7.4	25.2	19.8	20.5	10.2
170805-123959	37.95214	-121.33048	6.8	25.2	19.6	20.3	22.6
170805-124111	37.95215	-121.33304	6.0	25.0	19.3	20.1	29.2
170805-124222	37.95186	-121.33554	5.8	24.5	19.1	20.0	30.4
170805-124443	37.95290	-121.34046	5.8	24.5	18.7	19.6	22.2
170805-124555	37.95352	-121.34289	5.8	24.4	18.4	19.5	26.5
170805-124705	37.95421	-121.34525	5.8	24.5	18.2	19.3	27.0
170805-124816	37.95487	-121.34768	5.8	24.7	18.0	19.1	29.0
170805-124927	37.95568	-121.35000	5.7	24.8	17.8	19.0	34.9
170805-125038	37.95610	-121.35150	5.8	24.8	17.6	18.9	37.5
170805-125147	37.95677	-121.35366	5.7	24.9	17.4	18.7	43.2

170805-125259	37.95756	-121.35586	5.6	24.9	17.2	18.6	46.4
170805-125520	37.95887	-121.35900	5.6	25.0	16.9	18.4	45.8
170805-125630	37.96001	-121.36059	5.7	24.9	16.7	18.2	45.5
170805-125742	37.96133	-121.36219	5.2	24.9	16.5	18.1	47.0
170805-125854	37.96268	-121.36382	5.2	24.9	16.3	17.9	49.7
170805-130004	37.96399	-121.36541	5.4	25.0	16.1	17.8	50.0
170805-130115	37.96527	-121.36706	5.3	25.0	15.9	17.6	48.3
170805-130228	37.96656	-121.36879	4.9	25.0	15.7	17.5	49.7
170805-130338	37.96782	-121.37040	5.1	25.0	15.5	17.3	47.4
170805-130600	37.97040	-121.37370	5.1	25.0	15.1	17.0	48.2
170805-130712	37.97158	-121.37513	5.1	25.0	14.9	16.9	42.7
170805-130824	37.97297	-121.37612	5.0	25.0	14.7	16.8	44.2
170805-130933	37.97424	-121.37750	5.0	25.0	14.5	16.6	42.6
170805-131045	37.97549	-121.37907	4.9	25.0	14.3	16.5	43.0
170805-131156	37.97678	-121.38052	4.8	25.0	14.1	16.3	40.2
170805-131307	37.97808	-121.38199	4.6	25.0	13.9	16.2	39.2
170805-131417	37.97936	-121.38348	4.3	25.1	13.8	16.0	35.5
170805-131639	37.98192	-121.38639	4.5	25.0	13.4	15.8	26.5
170805-131749	37.98318	-121.38782	4.6	25.1	13.2	15.6	30.0
170805-131900	37.98443	-121.38933	4.4	25.0	13.0	15.5	29.9
170805-132011	37.98547	-121.39101	4.4	25.0	12.8	15.3	27.3
170805-132120	37.98640	-121.39281	4.3	25.0	12.6	15.2	27.4
170805-132232	37.98727	-121.39476	4.3	24.9	12.4	15.0	26.8
170805-132344	37.98812	-121.39679	4.2	24.9	12.2	14.9	28.7
170805-132454	37.98891	-121.39879	4.3	25.0	12.0	14.7	27.5
170805-132714	37.99030	-121.40275	4.2	25.0	11.6	14.4	22.5
170805-132825	37.99110	-121.40472	4.0	25.2	11.4	14.3	18.2
170805-132935	37.99185	-121.40663	4.2	25.1	11.3	14.1	17.3
170805-133046	37.99250	-121.40866	4.3	25.1	11.1	14.0	20.1
170805-133157	37.99321	-121.41070	4.3	25.2	10.9	13.8	20.4
170805-133308	37.99381	-121.41277	4.3	25.4	10.7	13.7	17.9
170805-133420	37.99431	-121.41494	4.2	25.3	10.5	13.5	15.2
170805-133531	37.99480	-121.41707	4.2	25.4	10.3	13.3	14.4
170805-133752	37.99529	-121.42146	4.1	25.4	9.9	13.0	12.3
170805-133903	37.99521	-121.42366	4.1	25.5	9.7	12.8	10.3
170805-134014	37.99490	-121.42583	4.0	25.5	9.5	12.7	9.7
170805-134124	37.99463	-121.42798	4.1	25.6	9.3	12.5	8.3
170805-134237	37.99429	-121.43019	4.0	25.5	9.1	12.3	6.5

170805-134347	37.99402	-121.43236	3.9	25.4	8.9	12.2	5.1
170805-134459	37.99393	-121.43458	3.9	25.4	8.7	12.0	3.6
170805-134609	37.99435	-121.43668	4.0	25.5	8.5	11.9	2.8
170805-134829	37.99577	-121.44064	3.9	25.4	8.1	11.5	0.6
170805-134941	37.99659	-121.44255	3.9	25.5	7.9	11.4	0.3
170805-135053	37.99753	-121.44442	3.9	25.5	7.7	11.2	0.2
170805-135203	37.99861	-121.44606	3.9	25.5	7.5	11.0	0.1
170805-135314	37.99978	-121.44766	3.9	25.5	7.4	10.9	0.1
170805-135426	38.00053	-121.44880	4.0	25.7	7.2	10.8	0.1
170805-145345	38.00705	-121.45430	4.1	26.0	6.3	10.6	0.0
170805-145455	38.00583	-121.45335	4.0	26.0	6.5	10.7	0.0
170805-145605	38.00462	-121.45239	4.2	26.1	6.7	10.9	0.0
170805-145717	38.00343	-121.45131	4.1	26.0	6.8	11.1	0.0
170805-145828	38.00221	-121.45038	4.2	26.1	7.0	11.3	0.2
170805-145938	38.00102	-121.44943	4.2	26.1	7.1	11.4	0.5
170805-150048	37.99993	-121.44828	4.1	26.0	7.3	11.6	1.6
170805-150159	37.99876	-121.44664	3.9	25.7	7.5	11.8	1.9
170805-150419	37.99600	-121.44164	4.1	25.8	8.0	12.4	4.8
170805-150529	37.99476	-121.43898	4.2	26.0	8.3	12.6	7.8
170805-150640	37.99380	-121.43614	4.3	25.9	8.6	12.9	9.9
170805-150751	37.99375	-121.43303	4.3	25.8	8.8	13.2	13.7
170805-150901	37.99413	-121.42998	4.2	25.7	9.1	13.5	14.6
170805-151012	37.99451	-121.42687	4.3	25.9	9.4	13.8	15.4
170805-151124	37.99470	-121.42488	4.5	26.1	9.6	14.0	14.4
170805-151235	37.99525	-121.42333	4.4	25.9	9.7	14.1	13.6
170805-151455	37.99520	-121.42014	4.5	26.1	10.0	14.4	17.0
170805-151606	37.99569	-121.41853	4.4	26.0	10.1	14.6	16.7
170805-151716	37.99496	-121.41734	4.4	25.8	10.3	14.7	20.2
170805-151827	37.99519	-121.41595	4.6	26.1	10.4	14.8	18.1
170805-151939	37.99480	-121.41488	4.3	25.8	10.5	14.9	18.5
170805-152049	37.99479	-121.41335	4.6	25.8	10.6	15.0	17.3
170805-152200	37.99354	-121.41231	4.8	26.0	10.7	15.2	16.1
170805-152311	37.99382	-121.41072	4.4	26.1	10.8	15.3	14.2
170805-152531	37.99190	-121.40834	4.8	26.2	11.1	15.6	27.1
170805-152642	37.99084	-121.40582	4.8	26.1	11.4	15.9	31.1
170805-152752	37.99040	-121.40294	4.6	26.0	11.6	16.1	36.1
170805-152903	37.98958	-121.40004	4.6	26.0	11.9	16.4	44.5
170805-153015	37.98873	-121.39754	4.4	25.8	12.1	16.6	40.8

170805-153124	37.98846	-121.39760	4.8	26.5	12.1	16.6	35.7
170805-153235	37.98841	-121.39769	4.9	26.4	12.1	16.6	36.7
170805-153347	37.98839	-121.39777	4.6	26.0	12.1	16.6	39.5
170805-153608	37.98838	-121.39779	4.9	26.3	12.1	16.6	37.9
170805-153719	37.98839	-121.39774	4.9	26.3	12.1	16.6	39.4
170805-153829	37.98841	-121.39768	4.8	26.3	12.1	16.6	37.3
170805-153941	37.98844	-121.39763	4.5	26.2	12.1	16.6	36.7
170805-154050	37.98844	-121.39759	4.5	26.2	12.1	16.6	36.1
170805-154203	37.98844	-121.39753	4.5	26.2	12.1	16.6	36.9
170805-154313	37.98844	-121.39746	4.5	26.3	12.1	16.6	35.9
170805-154424	37.98844	-121.39739	4.5	26.3	12.2	16.7	32.7
170805-154645	37.98707	-121.39464	5.2	26.2	12.4	16.9	36.9
170805-154756	37.98592	-121.39184	4.9	25.8	12.7	17.2	48.5
170805-154907	37.98436	-121.38940	5.1	26.2	13.0	17.5	50.1
170805-155017	37.98247	-121.38734	5.2	26.1	13.3	17.8	50.7
170805-155128	37.98102	-121.38603	5.4	26.3	13.5	18.0	53.6
170805-155239	37.98023	-121.38478	5.6	26.6	13.6	18.1	54.1
170805-155350	37.97957	-121.38363	5.6	26.5	13.7	18.3	52.2
170805-155502	37.97857	-121.38313	5.6	26.4	13.8	18.4	52.6
170805-155723	37.97653	-121.38055	5.6	27.0	14.2	18.7	57.2
170805-155834	37.97632	-121.38031	5.7	26.9	14.2	18.7	54.3
170805-155944	37.97627	-121.38021	5.7	26.8	14.2	18.7	54.6
170805-160055	37.97620	-121.38014	5.7	26.9	14.2	18.7	54.0
170805-160207	37.97608	-121.38008	5.8	26.9	14.2	18.7	54.6
170805-160318	37.97596	-121.38003	5.8	27.0	14.2	18.7	48.9
170805-160427	37.97585	-121.37998	5.8	27.0	14.2	18.7	53.9
170805-160539	37.97573	-121.37994	5.8	26.9	14.2	18.8	56.1
170805-160800	37.97572	-121.37859	5.4	26.5	14.4	18.9	56.2
170805-160910	37.97455	-121.37851	5.9	26.9	14.4	18.9	53.5
170805-161021	37.97432	-121.37713	5.4	26.5	14.6	19.0	56.6
170805-161131	37.97328	-121.37679	6.0	26.9	14.6	19.1	53.1
170805-161244	37.97282	-121.37552	5.5	26.7	14.8	19.3	55.6
170805-161354	37.97194	-121.37504	5.9	27.0	14.9	19.3	51.1
170805-161505	37.97122	-121.37405	5.4	26.7	15.0	19.5	55.3
170805-161616	37.97035	-121.37337	6.0	27.0	15.1	19.6	50.4
170805-161837	37.96869	-121.37184	5.7	26.8	15.3	19.8	51.1
170805-161949	37.96809	-121.37059	6.3	26.9	15.4	19.9	49.7
170805-162059	37.96714	-121.36994	5.4	26.5	15.5	20.0	55.0

170805-162211	37.96651	-121.36885	5.4	27.0	15.7	20.1	47.8
170805-162322	37.96590	-121.36786	4.8	26.4	15.8	20.2	35.1
170805-162433	37.96486	-121.36748	5.7	26.9	15.9	20.3	37.4
170805-162542	37.96449	-121.36612	6.6	26.6	16.0	20.5	48.4
170805-162654	37.96338	-121.36555	6.9	27.0	16.1	20.6	56.4
170805-162915	37.96258	-121.36456	7.1	27.6	16.2	20.7	55.2
170805-163026	37.96244	-121.36438	7.2	27.5	16.3	20.7	55.8
170805-163137	37.96227	-121.36416	7.2	27.5	16.3	20.7	56.7
170805-163249	37.96212	-121.36396	7.4	27.5	16.3	20.7	55.1
170805-163358	37.96198	-121.36378	7.3	27.4	16.3	20.7	57.1
170805-163509	37.96182	-121.36358	7.3	27.2	16.4	20.8	58.1
170805-163619	37.96167	-121.36338	7.3	27.2	16.4	20.8	58.8
170805-163730	37.96153	-121.36315	7.3	27.1	16.4	20.8	57.9
170805-163952	37.96072	-121.36209	7.4	26.7	16.6	20.9	56.6
170805-164104	37.95990	-121.36105	7.7	27.1	16.7	21.0	54.5
170805-164214	37.95934	-121.35989	7.9	27.0	16.8	21.1	53.7
170805-164325	37.95814	-121.35915	8.4	27.3	16.9	21.3	50.6
170805-164436	37.95835	-121.35724	7.8	26.7	17.1	21.4	52.1
170805-164546	37.95701	-121.35649	8.3	27.1	17.2	21.5	51.0
170805-164657	37.95741	-121.35479	8.5	27.0	17.3	21.6	47.3
170805-164809	37.95610	-121.35373	8.0	27.6	17.4	21.8	49.5
170805-165031	37.95556	-121.35073	7.6	27.5	17.7	22.0	43.5
170805-165142	37.95550	-121.34929	8.1	26.8	17.8	22.1	41.1
170805-165252	37.95463	-121.34827	8.6	27.2	18.0	22.2	35.3
170805-165403	37.95491	-121.34672	8.9	26.7	18.1	22.3	32.0
170805-165514	37.95381	-121.34564	9.2	26.7	18.2	22.5	31.5
170805-165625	37.95381	-121.34420	9.1	26.6	18.3	22.6	23.1
170805-165737	37.95307	-121.34263	8.5	25.9	18.5	22.7	22.5
170805-165848	37.95248	-121.33946	8.8	26.3	18.8	23.0	18.8
180805-111719	37.99844	-121.41066	3.8	24.3			10.0
180805-111831	37.99842	-121.41066	3.8	24.3			10.1
180805-112201	37.99842	-121.41066	3.7	24.3			10.8
180805-112312	37.99843	-121.41065	3.7	24.3			10.4
180805-112422	37.99842	-121.41066	3.7	24.3			10.0
180805-112533	37.99842	-121.41067	3.7	24.2			9.0
180805-112644	37.99858	-121.41180	3.7	24.2			10.0
180805-112757	37.99861	-121.41506	3.6	24.3			10.2
180805-112906	37.99784	-121.41805	3.5	24.3			9.7

180805-113016	37.99616	-121.42063	3.7	24.7			9.8
180805-113237	37.99449	-121.42645	3.7	24.7	9.4	8.9	7.0
180805-113349	37.99373	-121.43037	3.7	24.7	9.1	8.6	4.6
180805-113501	37.99341	-121.43385	3.7	24.6	8.8	8.4	3.8
180805-113612	37.99378	-121.43723	3.7	24.6	8.5	8.1	3.4
180805-113724	37.99493	-121.44041	3.7	24.6	8.2	7.9	2.2
180805-113834	37.99645	-121.44317	3.8	24.5	7.9	7.6	1.3
180805-113947	37.99813	-121.44594	3.9	24.4	7.6	7.4	0.9
180805-114057	38.00009	-121.44821	4.0	24.4	7.3	7.1	0.6
180805-114319	38.00456	-121.45205	4.4	24.2	6.7	6.6	0.4
180805-114430	38.00687	-121.45385	4.7	24.1	6.4	6.4	0.3
180805-114540	38.00915	-121.45562	4.8	24.1	6.1	6.2	0.1
180805-114651	38.01114	-121.45679	5.0	24.3	5.9	6.0	0.1
180805-114802	38.00953	-121.45558	4.8	24.5	6.1	6.2	0.1
180805-114913	38.00775	-121.45425	4.5	24.7	6.3	6.5	0.2
180805-115024	38.00595	-121.45291	4.3	24.7	6.5	6.7	0.3
180805-115134	38.00418	-121.45161	4.1	24.8	6.8	7.0	0.5
180805-115354	38.00069	-121.44879	3.8	24.9	7.2	7.5	0.8
180805-115507	37.99901	-121.44707	3.8	24.9	7.4	7.7	1.0
180805-115616	37.99764	-121.44516	3.7	25.0	7.7	7.9	1.3
180805-115727	37.99643	-121.44298	3.7	25.0	7.9	8.2	1.8
180805-115838	37.99546	-121.44061	3.7	25.0	8.1	8.5	2.4
180805-115948	37.99475	-121.43814	3.6	25.0	8.4	8.7	4.2
180805-120059	37.99392	-121.43571	3.7	25.0	8.6	9.0	5.3
180805-120211	37.99362	-121.43306	3.7	24.9	8.9	9.2	7.1
180805-120431	37.99420	-121.42784	3.7	24.9	9.3	9.7	7.9
180805-120542	37.99473	-121.42519	3.6	24.9	9.6	10.0	11.8
180805-120653	37.99509	-121.42252	3.7	25.0	9.8	10.2	11.4
180805-120805	37.99521	-121.41983	3.7	24.9	10.0	10.5	14.5
180805-120915	37.99493	-121.41726	3.7	24.9	10.3	10.7	16.7
180805-121026	37.99427	-121.41474	3.7	25.0	10.5	11.0	17.9
180805-121137	37.99339	-121.41230	3.7	25.0	10.7	11.2	19.7
180805-121248	37.99261	-121.40979	3.8	24.9	11.0	11.5	22.6
180805-121509	37.99091	-121.40491	3.9	25.0	11.4	12.0	27.5
180805-121620	37.99001	-121.40250	3.9	25.0	11.7	12.2	29.2
180805-121732	37.98909	-121.40005	3.9	24.9	11.9	12.5	30.5
180805-121843	37.98823	-121.39764	3.9	24.9	12.1	12.7	31.4
180805-121954	37.98734	-121.39520	3.9	24.8	12.4	13.0	32.4

180805-122105	37.98623	-121.39292	3.9	24.9	12.6	13.2	32.2
180805-122215	37.98498	-121.39081	4.0	24.9	12.8	13.5	32.6
180805-122326	37.98357	-121.38883	4.1	25.0	13.1	13.7	33.4
180805-122547	37.98054	-121.38532	4.0	24.9	13.5	14.2	34.2
180805-122700	37.97897	-121.38349	4.1	24.9	13.8	14.4	34.1
180805-122812	37.97732	-121.38182	4.2	24.9	14.0	14.7	38.0
180805-122922	37.97591	-121.38033	4.2	24.8	14.2	14.9	34.6
180805-123031	37.97462	-121.37874	4.3	24.9	14.4	15.1	35.9
180805-123144	37.97314	-121.37680	4.4	24.9	14.6	15.4	35.9
180805-123254	37.97163	-121.37502	4.5	24.9	14.9	15.6	36.9
180805-123405	37.97008	-121.37319	4.5	24.9	15.1	15.8	37.4
180805-123626	37.96685	-121.36978	4.6	24.9	15.6	16.3	37.8
180805-123737	37.96539	-121.36780	4.8	24.9	15.8	16.6	36.9
180805-123849	37.96379	-121.36586	4.9	24.9	16.1	16.8	36.4
180805-124000	37.96221	-121.36397	4.7	25.0	16.3	17.1	35.9
180805-124111	37.96059	-121.36214	5.2	25.0	16.6	17.3	34.7
180805-124222	37.95927	-121.36005	5.4	24.9	16.8	17.6	28.8
180805-124333	37.95829	-121.35769	5.9	25.0	17.0	17.8	23.2
180805-124445	37.95733	-121.35518	5.8	25.0	17.3	18.1	22.5
180805-124704	37.95557	-121.35031	5.9	24.9	17.7	18.6	20.5
180805-124816	37.95478	-121.34770	5.7	24.8	18.0	18.8	17.9
180805-124927	37.95401	-121.34514	5.7	24.8	18.2	19.1	18.6
180805-125037	37.95334	-121.34255	5.8	24.8	18.5	19.3	17.9
180805-125147	37.95286	-121.33996	5.7	24.7	18.7	19.5	16.0
180805-125259	37.95246	-121.33793	5.6	24.6	18.9	19.7	14.0
180805-125410	37.95216	-121.33539	6.3	25.0	19.1	20.0	14.8
180805-125521	37.95191	-121.33276	6.4	24.9	19.4	20.2	17.5
180805-125742	37.95235	-121.32757	7.1	25.0	19.8	20.7	19.3
180805-125852	37.95256	-121.32501	9.7	25.2	20.0	20.9	14.0
180805-130003	37.95276	-121.32242	9.9	25.4	20.3	21.2	11.1
180805-130114	37.95273	-121.31978	10.4	25.6	20.5	21.4	10.0
180805-130226	37.95284	-121.31710	9.2	25.6	20.7	21.6	8.7
180805-130336	37.95291	-121.31452	9.6	25.6	21.0	21.9	9.2
180805-130447	37.95312	-121.31192	10.4	25.8	21.2	22.1	4.4
180805-130819	37.95333	-121.30655	12.8	26.1	21.7	22.6	1.2
180805-130930	37.95338	-121.30502	13.9	26.2	21.8	22.8	1.0
180805-131042	37.95334	-121.30344	13.5	26.3	21.9	22.9	1.0
180805-131153	37.95334	-121.30188	13.8	26.3	22.1	23.1	0.6

180805-131303	37.95356	-121.30037	12.6	26.5	22.2	23.2	0.5
180805-131414	37.95377	-121.29887	11.5	26.4	22.3	23.4	0.4
180805-131524	37.95343	-121.29982	11.1	26.3	22.3	23.4	0.4
180805-131636	37.95337	-121.30149	12.9	26.4	22.1	23.3	0.6
180805-131856	37.95328	-121.30473	14.0	26.2	21.8	23.1	1.0
180805-132006	37.95331	-121.30643	11.7	26.1	21.7	23.0	1.1
180805-132117	37.95329	-121.30817	12.2	25.8	21.5	22.9	1.1
180805-132229	37.95314	-121.31029	11.0	25.7	21.3	22.8	1.9
180805-132340	37.95317	-121.31355	9.7	25.5	21.0	22.6	5.9
180805-132451	37.95309	-121.31679	10.7	25.8	20.7	22.3	7.3
180805-132600	37.95293	-121.31991	11.1	25.5	20.5	22.1	9.2
180805-132712	37.95273	-121.32316	10.3	25.3	20.2	21.9	11.0
180805-132932	37.95228	-121.32952	7.7	25.1	19.6	21.5	18.7
180805-133043	37.95207	-121.33274	6.9	25.1	19.4	21.3	19.4
180805-133153	37.95081	-121.33495	5.8	24.9	19.2	21.2	18.8
180805-133304	37.94917	-121.33639	6.6	24.2			8.6
180805-133415	37.94788	-121.33747	6.5	24.2			2.0
180805-133526	37.94694	-121.33905	6.5	24.2			0.9
180805-133637	37.94613	-121.34078	6.5	24.2			0.6
180805-133748	37.94540	-121.34155	6.5	24.3			0.6
180805-134008	37.94361	-121.34342	6.6	24.2			0.4
180805-134119	37.94305	-121.34468	6.7	24.2			0.4
180805-134229	37.94244	-121.34569	6.7	24.3			0.3
180805-134341	37.94140	-121.34537	6.7	24.2			0.3
180805-134452	37.94053	-121.34453	6.6	24.2			0.3
180805-134603	37.94061	-121.34459	6.6	24.2			0.2
180805-134715	37.94082	-121.34484	6.2	24.2			0.2
180805-134826	37.94109	-121.34496	6.5	24.1			0.3
180805-135047	37.94474	-121.34192	6.4	24.1			0.4
180805-135158	37.94672	-121.33946	6.6	24.1			0.3
180805-135307	37.94840	-121.33701	6.5	24.2			0.6
180805-135419	37.95077	-121.33591	6.4	24.6	19.1	21.8	11.1
180805-135530	37.95219	-121.33835	6.3	24.7	18.9	21.6	10.6
180805-135641	37.95267	-121.34149	6.3	24.7	18.6	21.4	15.9
180805-135751	37.95353	-121.34411	6.4	25.3	18.3	21.2	16.6
180805-135902	37.95365	-121.34446	6.4	25.2	18.3	21.2	16.1
180805-140123	37.95518	-121.34914	6.3	25.2	17.9	20.9	17.8
180805-140234	37.95599	-121.35212	6.3	25.2	17.6	20.7	19.3

180805-140345	37.95721	-121.35503	5.9	25.5	17.3	20.4	22.9
180805-140457	37.95835	-121.35809	5.9	25.3	17.0	20.2	33.1
180805-140608	37.96002	-121.36049	5.9	25.1	16.7	20.0	34.0
180805-140720	37.96131	-121.36125	6.0	25.2	16.6	19.9	29.7
180805-140829	37.96090	-121.36289	6.5	25.3	16.5	19.8	26.2
180805-140941	37.96228	-121.36269	6.2	25.2	16.4	19.8	26.6
180805-141202	37.96340	-121.36446	5.9	25.2	16.2	19.7	25.8
180805-141313	37.96338	-121.36586	6.4	25.3	16.1	19.6	27.2
180805-141424	37.96452	-121.36607	6.3	25.4	16.0	19.5	27.8
180805-141534	37.96457	-121.36726	6.2	25.4	15.9	19.5	30.7
180805-141645	37.96577	-121.36737	6.3	25.5	15.8	19.4	31.4
180805-141756	37.96580	-121.36875	6.1	25.5	15.7	19.4	36.0
180805-141906	37.96700	-121.36884	5.2	25.5	15.6	19.3	36.3
180805-142018	37.96690	-121.37052	5.3	25.6	15.5	19.2	38.5
180805-142238	37.96863	-121.37145	5.4	25.3	15.3	19.1	38.5
180805-142349	37.96956	-121.37201	5.2	25.4	15.2	19.1	41.0
180805-142500	37.96979	-121.37287	5.5	25.5	15.2	19.0	38.4
180805-142611	37.96987	-121.37332	5.7	25.5	15.1	19.0	38.5
180805-142721	37.97037	-121.37371	5.7	25.6	15.1	19.0	39.0
180805-142833	37.97053	-121.37389	5.9	25.8	15.0	19.0	38.2
180805-142943	37.97061	-121.37405	5.8	25.7	15.0	19.0	38.7
180805-143055	37.97064	-121.37418	5.8	25.6	15.0	19.0	39.6
180805-143315	37.97070	-121.37399	5.6	25.4	15.0	19.0	40.4
180805-143426	37.97069	-121.37403	5.7	25.6	15.0	19.1	38.9
180805-143538	37.97069	-121.37407	5.8	25.9	15.0	19.1	38.8
180805-143649	37.97077	-121.37409	5.6	25.7	15.0	19.1	37.0
180805-143800	37.97136	-121.37395	5.0	25.4	15.0	19.1	40.7
180805-143911	37.97170	-121.37460	5.6	25.6	14.9	19.1	37.8
180805-144022	37.97229	-121.37542	5.2	25.3	14.8	19.0	41.2
180805-144133	37.97313	-121.37589	5.8	25.6	14.7	18.9	36.8
180805-144352	37.97464	-121.37720	5.5	25.4	14.5	18.8	39.8
180805-144505	37.97457	-121.37869	5.4	25.4	14.4	18.7	41.1
180805-144614	37.97590	-121.37869	5.3	25.5	14.3	18.7	40.6
180805-144726	37.97603	-121.38021	5.6	25.6	14.2	18.6	40.0
180805-144836	37.97718	-121.38045	5.2	25.8	14.1	18.5	41.0
180805-144947	37.97756	-121.38153	5.4	25.6	14.0	18.4	41.9
180805-145058	37.97837	-121.38223	5.0	25.5	13.9	18.3	44.2
180805-145209	37.97874	-121.38359	5.4	25.6	13.8	18.2	41.4

180805-145429	37.98075	-121.38501	5.2	25.7	13.6	18.0	43.6
180805-145541	37.98099	-121.38651	5.5	25.7	13.4	17.9	40.2
180805-145652	37.98239	-121.38670	5.3	25.6	13.3	17.9	37.6
180805-145804	37.98281	-121.38807	5.2	25.6	13.2	17.7	41.1
180805-145913	37.98429	-121.38811	4.4	25.4	13.1	17.7	41.0
180805-150024	37.98421	-121.38978	5.2	25.7	13.0	17.6	37.8
180805-150136	37.98561	-121.39035	5.3	25.6	12.8	17.5	40.4
180805-150246	37.98560	-121.39186	5.0	25.4	12.7	17.4	40.8
180805-150508	37.98709	-121.39399	4.7	25.4	12.5	17.2	42.2
180805-150619	37.98721	-121.39540	5.0	25.6	12.4	17.1	40.8
180805-150729	37.98810	-121.39629	4.4	25.4	12.3	17.0	42.7
180805-150840	37.98880	-121.39718	4.6	25.5	12.2	16.9	41.2
180805-150951	37.98830	-121.39871	4.9	25.7	12.1	16.8	40.8
180805-151102	37.98855	-121.39940	4.8	25.7	12.0	16.7	39.3
180805-151214	37.98889	-121.40012	4.9	25.7	11.9	16.7	39.9
180805-151324	37.98967	-121.40101	4.6	25.6	11.8	16.6	42.0
180805-151544	37.99041	-121.40321	4.7	25.8	11.6	16.4	41.0
180805-151809	37.99116	-121.40535	4.7	25.9	11.4	16.2	39.0
180805-151916	37.99126	-121.40643	4.6	25.7	11.3	16.1	39.4
180805-152027	37.99194	-121.40727	4.6	25.8	11.2	16.0	39.8
180805-152138	37.99192	-121.40846	4.6	25.8	11.1	16.0	35.0
180805-152250	37.99297	-121.40927	4.2	25.6	11.0	15.8	36.3
180805-152401	37.99403	-121.41018	4.5	25.6	10.9	15.7	29.0
180805-152624	37.99697	-121.41036	5.4	25.9			4.5
180805-152733	37.99786	-121.40923	5.5	25.9			3.4
180805-152845	37.99883	-121.40793	5.6	26.1			3.1
180805-152956	38.00001	-121.40687	5.7	26.1			2.6
180805-153107	38.00119	-121.40588	5.6	26.0			2.4
180805-153218	38.00241	-121.40494	5.5	26.1			2.5
180805-153329	38.00362	-121.40394	5.1	26.1			3.1
180805-153439	38.00467	-121.40273	5.9	26.4			2.8
180805-153701	38.00603	-121.39955	5.8	26.3			1.6
180805-153811	38.00661	-121.39793	5.9	26.4			0.9
180805-153922	38.00725	-121.39641	5.9	26.5			0.6
180805-154033	38.00800	-121.39486	5.7	26.3			0.6
180805-154144	38.00869	-121.39330	5.6	26.5			0.3
180805-154254	38.00909	-121.39287	5.8	26.3			0.4
180805-154405	38.00804	-121.39516	5.6	26.3			0.4

180805-154517	38.00703	-121.39731	5.8	26.2			0.4
180805-154737	38.00489	-121.40274	5.7	26.2			1.5
180805-154849	38.00289	-121.40470	5.5	26.1			2.4
180805-154958	38.00086	-121.40633	5.7	26.2			2.3
180805-155109	37.99883	-121.40796	5.3	26.1			3.1
180805-200000	0.00000	0.00000	11.1	25.7			3.7
190805-112635	37.99843	-121.41066	4.0	23.6			15.6
190805-112747	37.99842	-121.41065	4.0	23.6			15.2
190805-113020	37.99842	-121.41067	3.9	23.6			15.1
190805-113132	37.99842	-121.41067	3.9	23.7			14.9
190805-113243	37.99842	-121.41067	3.9	23.7			14.8
190805-113354	37.99843	-121.41067	3.9	23.6			14.4
190805-113503	37.99842	-121.41066	3.9	23.6			14.1
190805-113615	37.99845	-121.41101	3.9	23.5			14.3
190805-113725	37.99866	-121.41363	3.9	23.6			16.1
190805-113837	37.99849	-121.41667	3.8	23.7			15.8
190805-114057	37.99563	-121.42175	3.9	24.2	9.8	9.4	16.1
190805-114208	37.99484	-121.42466	3.9	24.2	9.6	9.2	15.2
190805-114320	37.99436	-121.42759	3.9	24.2	9.3	9.0	13.3
190805-114431	37.99393	-121.43049	3.9	24.1	9.1	8.8	12.6
190805-114542	37.99368	-121.43345	4.0	24.2	8.8	8.6	12.1
190805-114654	37.99378	-121.43649	3.9	24.0	8.6	8.4	11.3
190805-114805	37.99472	-121.43912	3.9	24.0	8.3	8.2	9.4
190805-114914	37.99578	-121.44166	4.0	24.0	8.0	8.0	7.9
190805-115136	37.99871	-121.44639	4.2	23.8	7.5	7.5	5.7
190805-115247	38.00046	-121.44845	4.4	23.7	7.3	7.3	4.8
190805-115357	38.00236	-121.45038	4.5	23.7	7.0	7.1	3.5
190805-115508	38.00442	-121.45205	4.7	23.6	6.7	6.9	2.3
190805-115619	38.00648	-121.45375	4.9	23.5	6.4	6.6	1.8
190805-115730	38.00861	-121.45543	5.2	23.4	6.1	6.4	1.2
190805-115841	38.01079	-121.45703	5.4	23.3	5.9	6.2	0.8
190805-115952	38.01291	-121.45875	5.7	23.1	5.6	5.9	0.6
190805-120213	38.01705	-121.46190	5.8	23.0	5.0	5.5	0.4
190805-120324	38.01900	-121.46360	5.9	22.9	4.8	5.3	0.3
190805-120435	38.02091	-121.46497	6.2	22.8	4.5	5.1	0.2
190805-120547	38.02290	-121.46621	6.1	22.7	4.3	4.9	0.1
190805-120658	38.02456	-121.46792	6.1	22.6	4.1	4.7	0.1
190805-120808	38.02580	-121.46996	6.2	22.9	3.8	4.5	0.1

190805-120919	38.02605	-121.46976	6.3	23.2	3.8	4.6	0.1
190805-121030	38.02495	-121.46824	6.2	23.4	4.0	4.8	0.1
190805-121246	38.02176	-121.46492	6.0	23.6	4.5	5.3	0.2
190805-121402	38.01979	-121.46350	5.8	23.8	4.7	5.5	0.4
190805-121512	38.01806	-121.46208	5.9	23.9	5.0	5.8	0.3
190805-121623	38.01624	-121.46055	5.8	23.9	5.2	6.1	0.3
190805-121735	38.01436	-121.45908	5.6	24.1	5.5	6.3	0.4
190805-121846	38.01251	-121.45762	5.3	24.2	5.7	6.6	0.6
190805-121955	38.01067	-121.45622	5.1	24.4	5.9	6.8	0.9
190805-122107	38.00881	-121.45469	4.8	24.5	6.2	7.1	1.9
190805-122328	38.00532	-121.45211	4.4	24.6	6.6	7.6	3.2
190805-122438	38.00352	-121.45096	4.2	24.7	6.9	7.8	4.5
190805-122550	38.00176	-121.44957	4.1	24.8	7.1	8.1	6.0
190805-122701	38.00012	-121.44799	4.1	24.8	7.3	8.3	7.1
190805-122811	37.99845	-121.44658	4.1	24.8	7.5	8.5	7.4
190805-122922	37.99725	-121.44439	4.0	24.9	7.8	8.8	8.1
190805-123033	37.99609	-121.44217	3.9	24.9	8.0	9.0	10.0
190805-123145	37.99489	-121.43990	3.9	24.9	8.2	9.3	11.8
190805-123404	37.99347	-121.43507	4.0	24.6	8.7	9.7	14.2
190805-123515	37.99326	-121.43244	4.0	24.5	8.9	10.0	14.3
190805-123627	37.99364	-121.42976	4.0	24.5	9.2	10.2	13.6
190805-123738	37.99438	-121.42727	4.0	24.4	9.4	10.5	15.9
190805-123848	37.99483	-121.42472	4.0	24.4	9.6	10.7	17.2
190805-123959	37.99532	-121.42214	4.0	24.6	9.8	10.9	18.2
190805-124110	37.99545	-121.41948	4.0	24.8	10.1	11.2	19.0
190805-124221	37.99491	-121.41698	4.0	24.8	10.3	11.4	19.9
190805-124442	37.99348	-121.41209	4.1	24.8	10.8	11.9	22.1
190805-124553	37.99267	-121.40959	4.1	24.8	11.0	12.1	22.7
190805-124705	37.99191	-121.40705	4.1	24.8	11.2	12.4	23.3
190805-124816	37.99096	-121.40469	4.1	24.8	11.5	12.6	24.1
190805-124926	37.98997	-121.40240	4.1	24.9	11.7	12.9	25.0
190805-125039	37.98922	-121.39987	4.0	24.9	11.9	13.1	25.8
190805-125147	37.98840	-121.39756	4.1	24.9	12.1	13.3	26.2
190805-125259	37.98754	-121.39516	4.0	24.9	12.4	13.6	26.7
190805-125520	37.98514	-121.39096	4.1	24.9	12.8	14.0	26.6
190805-125630	37.98375	-121.38906	4.0	24.9	13.1	14.3	26.8
190805-125743	37.98214	-121.38730	4.1	24.9	13.3	14.5	28.1
190805-125853	37.98069	-121.38570	4.1	24.8	13.5	14.7	29.4

190805-130004	37.97983	-121.38427	4.0	24.6	13.7	14.9	27.0
190805-130115	37.97966	-121.38427	4.1	24.7	13.7	14.9	25.7
190805-130227	37.97964	-121.38431	4.2	24.7	13.7	15.0	25.1
190805-130336	37.97962	-121.38429	4.2	24.7	13.7	15.0	22.3
190805-130557	37.97725	-121.38163	4.3	24.8	14.0	15.4	24.5
190805-130709	37.97568	-121.37980	4.5	24.8	14.3	15.6	24.1
190805-130819	37.97411	-121.37799	4.5	24.9	14.5	15.9	23.1
190805-130930	37.97248	-121.37631	4.5	24.9	14.7	16.1	22.7
190805-131042	37.97103	-121.37436	4.7	24.9	15.0	16.3	20.8
190805-131153	37.96956	-121.37253	4.7	24.9	15.2	16.6	20.1
190805-131304	37.96804	-121.37080	4.9	24.9	15.4	16.8	19.0
190805-131415	37.96639	-121.36911	5.0	24.9	15.7	17.0	18.4
190805-131635	37.96321	-121.36558	5.0	24.9	16.1	17.5	17.3
190805-131746	37.96171	-121.36361	5.1	24.9	16.4	17.7	16.3
190805-131858	37.96015	-121.36164	5.2	24.8	16.6	18.0	14.9
190805-132010	37.95882	-121.35944	5.5	24.7	16.9	18.2	12.9
190805-132120	37.95767	-121.35716	5.7	24.7	17.1	18.4	10.8
190805-132230	37.95678	-121.35472	5.8	24.6	17.3	18.7	9.2
190805-132342	37.95592	-121.35217	6.1	24.5	17.6	18.9	8.8
190805-132454	37.95518	-121.34955	6.1	24.6	17.8	19.2	8.9
190805-132714	37.95361	-121.34448	6.1	24.5	18.3	19.6	7.5
190805-132825	37.95289	-121.34188	6.2	24.6	18.5	19.9	7.1
190805-132936	37.95208	-121.33933	6.0	24.4	18.8	20.1	7.4
190805-133047	37.95193	-121.33673	6.0	24.4	19.0	20.3	6.9
190805-133157	37.95183	-121.33398	6.3	24.7	19.3	20.5	11.8
190805-133308	37.95207	-121.33119	6.3	24.8	19.5	20.8	15.0
190805-133418	37.95229	-121.32845	6.3	24.8	19.7	21.0	17.9
190805-133529	37.95251	-121.32571	6.5	24.7	20.0	21.2	19.1
190805-133750	37.95268	-121.32027	9.1	25.0	20.5	21.7	17.7
190805-133901	37.95271	-121.31751	10.3	25.2	20.7	21.9	15.3
190805-134013	37.95281	-121.31469	10.4	25.3	20.9	22.2	11.6
190805-134125	37.95312	-121.31193	11.6	25.5	21.2	22.4	7.8
190805-134234	37.95326	-121.30970	11.9	25.5	21.4	22.6	6.5
190805-134345	37.95330	-121.30779	13.1	25.9	21.6	22.8	5.4
190805-134457	37.95329	-121.30587	13.1	25.9	21.7	22.9	5.0
190805-134609	37.95329	-121.30395	13.2	25.8	21.9	23.1	5.1
190805-134830	37.95338	-121.30023	13.9	25.9	22.2	23.4	4.9
190805-134940	37.95369	-121.29844	12.9	25.9	22.4	23.6	5.2

190805-135051	37.95385	-121.29668	12.1	25.8	22.5	23.7	5.8
190805-135202	37.95386	-121.29786	13.5	26.0	22.4	23.7	6.2
190805-135313	37.95354	-121.29965	14.0	26.0	22.3	23.6	5.2
190805-135424	37.95319	-121.30142	14.7	25.9	22.1	23.5	4.8
190805-135535	37.95304	-121.30322	15.6	26.0	22.0	23.4	4.5
190805-135646	37.95323	-121.30495	14.9	25.8	21.8	23.3	5.0
190805-135906	37.95319	-121.30845	13.8	25.5	21.5	23.1	5.3
190805-140018	37.95315	-121.31034	13.5	25.5	21.3	23.0	6.5
190805-140130	37.95320	-121.31304	11.9	25.4	21.1	22.9	8.3
190805-140241	37.95306	-121.31587	10.6	25.2	20.8	22.7	11.6
190805-140352	37.95311	-121.31862	9.6	25.2	20.6	22.5	16.4
190805-140503	37.95277	-121.32109	8.0	25.0	20.4	22.4	21.1
190805-140613	37.95269	-121.32376	7.8	24.9	20.1	22.2	21.0
190805-140724	37.95259	-121.32652	8.0	25.0	19.9	22.0	20.1
190805-140943	37.95219	-121.33187	7.1	24.9	19.4	21.7	17.9
190805-141100	37.95137	-121.33455	7.0	24.9	19.2	21.6	15.1
190805-141207	37.94973	-121.33586	7.3	24.0			10.3
190805-141318	37.94836	-121.33704	7.4	23.9			1.7
190805-141429	37.94723	-121.33838	7.6	23.9			0.4
190805-141539	37.94657	-121.34016	7.4	23.9			0.3
190805-141651	37.94540	-121.34140	7.6	23.9			0.2
190805-141802	37.94412	-121.34239	8.0	23.9			0.1
190805-142023	37.94315	-121.34410	7.7	23.9			0.1
190805-142134	37.94258	-121.34539	7.8	23.9			0.1
190805-142245	37.94160	-121.34559	7.9	24.0			0.2
190805-142355	37.94167	-121.34566	7.7	23.9			0.1
190805-142507	37.94152	-121.34574	7.8	23.9			0.2
190805-142618	37.94158	-121.34567	7.6	23.8			0.1
190805-142729	37.94175	-121.34565	7.7	23.8			0.1
190805-142840	37.94202	-121.34573	7.4	23.8			0.1
190805-143101	37.94251	-121.34552	7.3	23.9			0.2
190805-143212	37.94273	-121.34520	7.2	24.0			0.2
190805-143322	37.94285	-121.34474	7.3	24.0			0.1
190805-143435	37.94307	-121.34422	7.4	23.9			0.1
190805-143544	37.94316	-121.34377	7.4	23.9			0.1
190805-143654	37.94343	-121.34326	7.4	23.9			0.1
190805-143805	37.94355	-121.34287	7.3	23.9			0.1
190805-143916	37.94363	-121.34254	7.4	23.9			0.2

190805-144137	37.94498	-121.34159	7.2	23.9			0.1
190805-144247	37.94567	-121.34138	7.2	23.9			0.1
190805-144358	37.94598	-121.34117	7.0	23.9			0.1
190805-144509	37.94612	-121.34105	6.8	24.0			0.1
190805-144620	37.94656	-121.34001	6.6	23.9			0.1
190805-144731	37.94761	-121.33780	6.7	23.9			0.2
190805-144841	37.94941	-121.33631	6.3	23.9			0.1
190805-144952	37.95133	-121.33590	6.3	24.4	19.1	22.5	5.3
190805-145214	37.95245	-121.33911	6.8	24.3	18.8	22.3	5.9
190805-145325	37.95296	-121.34064	6.9	24.3	18.6	22.2	5.5
190805-145435	37.95336	-121.34212	7.0	24.4	18.5	22.1	5.5
190805-145548	37.95361	-121.34297	6.8	24.6	18.4	22.0	5.7
190805-145658	37.95412	-121.34489	6.9	24.7	18.2	21.9	7.1
190805-145809	37.95475	-121.34704	6.7	24.8	18.0	21.7	7.7
190805-145919	37.95479	-121.34743	6.7	24.7	18.0	21.7	7.4
190805-150030	37.95481	-121.34748	6.7	24.7	18.0	21.8	7.4
190805-154804	37.95432	-121.34663	7.3	25.1	18.1	22.7	6.4
190805-154915	37.95425	-121.34658	7.4	25.2	18.1	22.7	6.5
190805-155027	37.95419	-121.34655	7.2	25.2	18.1	22.7	5.6
190805-155138	37.95517	-121.34782	7.0	25.0	18.0	22.6	6.9
190805-155248	37.95581	-121.35081	7.0	25.0	17.7	22.4	7.5
190805-155401	37.95676	-121.35395	7.3	25.2	17.4	22.1	7.6
190805-155510	37.95782	-121.35689	7.2	25.5	17.1	21.9	13.3
190805-155620	37.95807	-121.35776	6.9	25.5	17.0	21.8	13.5
190805-155842	37.95766	-121.35778	7.0	25.7	17.1	21.8	13.3
190805-155953	37.95780	-121.35769	6.9	25.7	17.1	21.9	13.7
190805-160105	37.95781	-121.35763	7.1	25.6	17.1	21.9	13.1
190805-160216	37.95869	-121.35905	6.9	25.4	16.9	21.7	12.2
190805-160326	37.96015	-121.36097	6.8	25.3	16.7	21.5	12.7
190805-160437	37.96195	-121.36317	6.5	25.3	16.4	21.3	12.2
190805-160549	37.96384	-121.36533	6.8	25.5	16.1	21.0	12.4
190805-160700	37.96413	-121.36576	6.7	25.5	16.1	21.0	11.6
190805-160921	37.96395	-121.36563	6.5	25.4	16.1	21.0	11.8
190805-161032	37.96393	-121.36556	6.7	25.4	16.1	21.0	10.4
190805-161143	37.96511	-121.36725	6.8	25.4	15.9	20.8	11.0
190805-161253	37.96659	-121.36890	5.7	25.3	15.7	20.6	16.5
190805-161404	37.96811	-121.37094	6.0	25.2	15.4	20.4	18.1
190805-161515	37.96991	-121.37317	4.9	25.1	15.1	20.1	155.1

190805-170931	37.96889	-121.37198	6.2	26.1	15.3	20.2	18.5
190805-171042	37.96881	-121.37180	5.9	25.9	15.3	20.2	18.4
190805-171152	37.96972	-121.37303	6.0	25.8	15.2	20.1	21.3
190805-171303	37.97090	-121.37441	5.8	25.8	15.0	19.9	20.6
190805-171414	37.97186	-121.37556	5.9	25.6	14.8	19.7	17.8
190805-171526	37.97310	-121.37673	5.9	25.5	14.7	19.5	19.0
190805-171636	37.97508	-121.37852	6.0	25.5	14.4	19.2	16.8
190805-171748	37.97697	-121.38074	5.9	25.5	14.1	18.9	21.6
190805-172008	37.97853	-121.38253	5.8	25.5	13.9	18.6	18.2
190805-172119	37.97839	-121.38242	5.9	25.6	13.9	18.6	19.6
190805-172229	37.97824	-121.38228	6.0	25.6	13.9	18.6	19.1
190805-172340	37.97813	-121.38215	6.0	25.6	13.9	18.6	20.0
190805-172451	37.97801	-121.38204	6.0	25.5	13.9	18.6	18.2
190805-172601	37.97849	-121.38243	5.4	25.4	13.9	18.6	21.9
190805-172712	37.98012	-121.38424	5.6	25.5	13.7	18.3	21.0
190805-172823	37.98192	-121.38634	5.3	25.7	13.4	18.0	23.5
190805-173044	37.98422	-121.38857	5.2	25.5	13.1	17.6	24.6
190805-173155	37.98410	-121.38837	5.1	25.5	13.1	17.6	26.4
190805-173306	37.98398	-121.38826	5.6	25.6	13.1	17.6	22.8
190805-173416	37.98367	-121.38824	5.6	25.6	13.1	17.6	22.2
190805-173527	37.98356	-121.38803	5.6	25.6	13.1	17.6	22.0
190805-173638	37.98344	-121.38779	5.5	25.7	13.2	17.6	22.2
190805-173749	37.98333	-121.38753	5.5	25.6	13.2	17.6	22.9
190805-173900	37.98415	-121.38854	5.5	25.5	13.1	17.5	23.2
190805-174121	37.98684	-121.39305	5.4	25.8	12.6	16.9	26.5
190805-174232	37.98803	-121.39562	5.2	25.6	12.3	16.6	27.9
190805-174343	37.98889	-121.39849	5.3	25.5	12.0	16.2	25.8
190805-174455	37.98885	-121.39912	5.4	25.6	12.0	16.2	24.8
190805-174604	37.98871	-121.39893	5.4	25.6	12.0	16.2	24.6
190805-174715	37.98858	-121.39873	5.3	25.6	12.0	16.2	25.5
190805-174826	37.98846	-121.39849	5.2	25.5	12.1	16.2	25.6
190805-174937	37.98834	-121.39826	5.2	25.6	12.1	16.2	26.0
190805-175158	37.98815	-121.39769	5.3	25.6	12.1	16.2	26.7
190805-175309	37.98828	-121.39747	5.3	25.5	12.2	16.2	25.2
190805-175421	37.98818	-121.39726	5.3	25.6	12.2	16.2	24.5
190805-175532	37.98806	-121.39699	5.4	25.7	12.2	16.2	24.1
190805-175642	37.98793	-121.39670	5.3	25.6	12.2	16.2	24.4
190805-175755	37.98787	-121.39639	5.3	25.6	12.3	16.3	24.7

190805-175904	37.98780	-121.39612	5.3	25.6	12.3	16.3	24.6
190805-180014	37.98774	-121.39578	5.3	25.6	12.3	16.3	25.3
190805-180236	37.98819	-121.39706	4.9	25.3	12.2	16.1	28.3
190805-180347	37.98919	-121.39962	5.0	25.5	11.9	15.8	27.7
190805-180457	37.99000	-121.40227	4.9	25.4	11.7	15.5	26.7
190805-180609	37.99107	-121.40495	5.0	25.4	11.4	15.1	26.6
190805-180719	37.99232	-121.40743	5.0	25.5	11.2	14.8	30.2
190805-180830	37.99269	-121.40912	4.9	25.6	11.0	14.6	27.5
190805-180941	37.99244	-121.40896	5.0	25.7	11.0	14.6	26.3
190805-181051	37.99222	-121.40861	5.0	25.7	11.1	14.6	26.9
190805-181313	37.99186	-121.40802	5.1	25.8	11.2	14.7	26.8
190805-181424	37.99166	-121.40766	5.1	25.8	11.2	14.7	26.1
190805-181535	37.99144	-121.40743	4.9	25.7	11.2	14.7	24.1
190805-181646	37.99226	-121.40856	5.0	25.5	11.1	14.5	28.5
190805-181756	37.99354	-121.41083	4.9	25.5	10.8	14.2	27.4
190805-181909	37.99444	-121.41353	5.2	25.6	10.6	13.9	24.1
190805-182019	37.99509	-121.41631	5.2	25.7	10.3	13.6	23.1
190805-182130	37.99551	-121.41919	5.3	25.7	10.1	13.2	19.0
190805-182350	37.99535	-121.41918	5.4	25.7	10.1	13.2	24.0
190805-182501	37.99529	-121.41875	5.4	25.8	10.1	13.2	23.2
190805-182611	37.99523	-121.41859	5.2	25.7	10.1	13.2	29.9
190805-182723	37.99536	-121.42112	4.9	25.6	9.9	12.9	26.4
190805-182835	37.99505	-121.42393	5.1	25.7	9.7	12.6	26.0
190805-182945	37.99469	-121.42671	4.7	25.5	9.4	12.2	28.2
190805-183055	37.99434	-121.42945	4.5	25.4	9.2	11.9	27.7
190805-183205	37.99384	-121.43139	4.7	25.6	9.0	11.7	23.3
190805-183429	37.99363	-121.43080	4.7	25.6	9.1	11.7	21.4
190805-183539	37.99349	-121.43078	4.9	25.7	9.1	11.7	23.7
190805-183650	37.99339	-121.43366	4.9	25.7	8.8	11.4	22.9
190805-183801	37.99391	-121.43640	5.2	25.8	8.6	11.0	20.4
190805-183911	37.99495	-121.43886	5.0	25.7	8.3	10.7	19.1
190805-184024	37.99609	-121.44139	5.0	25.7	8.0	10.4	18.0
190805-184135	37.99634	-121.44202	5.0	25.7	8.0	10.3	18.0
190805-184244	37.99607	-121.44157	5.0	25.8	8.0	10.3	17.5
190805-184505	37.99649	-121.44232	4.7	25.6	8.0	10.1	19.6
190805-184616	37.99793	-121.44457	4.9	25.7	7.7	9.8	17.7
190805-184727	37.99921	-121.44698	5.1	25.6	7.4	9.5	16.2
190805-184837	38.00087	-121.44885	5.1	25.6	7.2	9.1	17.5

190805-184948	38.00236	-121.45006	4.8	25.5	7.0	8.9	16.2
190805-185059	38.00266	-121.45006	4.9	25.5	7.0	8.8	16.2
190805-185209	38.00214	-121.45033	4.9	25.6	7.0	8.8	16.3
190805-185320	38.00182	-121.45022	5.0	25.7	7.0	8.8	18.1
190805-185542	38.00155	-121.45020	4.9	25.5	7.0	8.8	15.2
190805-185652	38.00362	-121.45105	5.0	25.4	6.8	8.5	14.4
190805-185805	38.00573	-121.45255	4.8	25.3	6.6	8.1	13.2
190805-185915	38.00770	-121.45405	4.8	25.2	6.3	7.8	12.0
190805-190026	38.00980	-121.45537	4.8	25.2	6.1	7.5	12.4
190805-190137	38.01052	-121.45617	5.0	25.3	6.0	7.3	9.8
190805-190247	38.01035	-121.45587	4.9	25.3	6.0	7.3	9.4
190805-190359	38.01018	-121.45560	4.9	25.3	6.0	7.3	9.5
190805-190619	38.00966	-121.45540	4.9	25.3	6.1	7.4	9.7
190805-190731	38.00942	-121.45512	4.8	25.3	6.1	7.4	9.9
190805-190840	38.00919	-121.45489	4.9	25.3	6.1	7.4	10.6
190805-190952	38.00897	-121.45462	4.8	25.3	6.2	7.4	10.4
190805-191103	38.00874	-121.45438	4.8	25.3	6.2	7.4	10.6
190805-191214	38.00856	-121.45411	4.9	25.3	6.3	7.4	10.8
190805-191325	38.00838	-121.45383	4.8	25.3	6.3	7.5	10.5
190805-191436	38.00814	-121.45371	5.0	25.4	6.3	7.5	10.0
190805-191659	38.00750	-121.45369	5.0	25.4	6.4	7.5	10.1
190805-191809	38.00726	-121.45339	5.0	25.4	6.4	7.5	10.4
190805-191920	38.00707	-121.45312	5.0	25.3	6.4	7.5	10.4
190805-192031	38.00688	-121.45288	5.1	25.4	6.5	7.5	10.6
190805-192141	38.00670	-121.45267	5.0	25.5	6.5	7.5	9.7
190805-192252	38.00697	-121.45288	5.0	25.3	6.5	7.5	10.3
190805-192403	38.00877	-121.45484	5.1	25.1	6.2	7.1	9.0
190805-192513	38.01050	-121.45625	5.0	25.1	5.9	6.8	7.1
190805-192735	38.01331	-121.45863	5.3	25.1	5.6	6.3	4.5
190805-192846	38.01544	-121.45991	5.5	25.0	5.3	5.9	3.4
190805-192957	38.01762	-121.46106	5.5	25.0	5.1	5.6	3.4
190805-193109	38.01769	-121.46216	5.5	24.8	5.0	5.5	2.2
190805-193219	38.01747	-121.46184	5.6	24.9	5.0	5.5	1.9
190805-193330	38.01726	-121.46144	5.5	24.9	5.1	5.6	1.8
190805-193442	38.01700	-121.46108	5.6	25.0	5.1	5.6	2.0
190805-193553	38.01566	-121.45979	5.4	25.0	5.3	5.8	2.6
190805-193813	38.01078	-121.45688	5.2	25.1	5.9	6.5	3.9
190805-193923	38.00837	-121.45507	4.9	25.1	6.2	6.8	5.8

190805-194034	38.00608	-121.45305	4.9	25.2	6.5	7.2	7.8
190805-194145	38.00361	-121.45135	4.9	25.3	6.8	7.5	9.5
190805-194257	38.00099	-121.44972	4.9	25.3	7.1	7.9	10.2
190805-194408	37.99905	-121.44737	4.9	25.3	7.4	8.2	11.8
190805-194519	37.99738	-121.44461	4.8	25.3	7.7	8.6	12.4
190805-194631	37.99624	-121.44205	4.9	25.4	8.0	8.8	14.5
190805-194850	37.99354	-121.43659	5.0	25.3	8.6	9.5	11.6
190805-195001	37.99355	-121.43324	4.6	25.3	8.8	9.8	16.4
190805-195111	37.99383	-121.42986	5.0	25.5	9.1	10.1	17.1
190805-195224	37.99451	-121.42651	5.0	25.5	9.4	10.5	17.4
190805-195334	37.99503	-121.42314	5.0	25.6	9.7	10.8	19.6
190805-195445	37.99636	-121.42034	4.7	25.5			21.8
190805-195556	37.99806	-121.41772	4.7	25.4			22.1
190805-195707	37.99868	-121.41446	4.6	25.3			24.3
200805-105004	37.99853	-121.41053	4.2	24.2			20.4
200805-105115	37.99852	-121.41053	4.2	24.2			20.1
200805-105226	37.99852	-121.41053	4.2	24.2			13.2
200805-105337	37.99851	-121.41054	4.1	24.2			21.7
200805-105449	37.99849	-121.41055	4.1	24.2			19.9
200805-105601	37.99849	-121.41054	4.1	24.2			20.5
200805-105712	37.99850	-121.41054	4.1	24.2			19.8
200805-105822	37.99849	-121.41055	4.0	24.2			20.5
200805-110046	37.99849	-121.41056	4.1	24.2			20.0
200805-110156	37.99849	-121.41057	4.0	24.2			20.3
200805-110306	37.99850	-121.41056	4.0	24.2			20.3
200805-110418	37.99846	-121.41065	4.0	24.0			18.8
200805-110528	37.99863	-121.41164	4.1	23.8			19.8
200805-110639	37.99870	-121.41432	4.1	23.8			20.7
200805-110750	37.99847	-121.41702	4.1	24.0			20.1
200805-110901	37.99711	-121.41922	4.0	23.9			20.4
200805-111122	37.99515	-121.42395	4.2	24.1	9.7	11.0	17.2
200805-111233	37.99469	-121.42665	4.2	24.0	9.4	10.7	16.9
200805-111342	37.99431	-121.42929	4.2	24.1	9.2	10.5	16.6
200805-111455	37.99381	-121.43204	4.1	24.0	8.9	10.2	16.5
200805-111605	37.99369	-121.43475	4.2	23.9	8.7	10.0	15.9
200805-111716	37.99434	-121.43732	4.3	23.9	8.5	9.8	14.0
200805-111827	37.99530	-121.43976	4.3	23.8	8.2	9.5	13.0
200805-111938	37.99647	-121.44204	4.4	23.7	8.0	9.3	11.5

200805-112159	37.99864	-121.44646	4.6	23.6	7.5	8.8	6.6
200805-112310	38.00038	-121.44850	4.9	23.4	7.3	8.5	6.7
200805-112420	38.00265	-121.45021	5.3	23.2	7.0	8.2	3.8
200805-112531	38.00491	-121.45202	5.5	23.1	6.7	7.9	2.3
200805-112642	38.00717	-121.45376	5.5	23.1	6.4	7.6	2.0
200805-112753	38.00946	-121.45545	5.7	22.9	6.1	7.3	2.9
200805-112903	38.01168	-121.45713	5.9	22.8	5.8	7.0	1.3
200805-113016	38.01354	-121.45880	6.0	22.7	5.5	6.7	0.9
200805-113236	38.01802	-121.46158	6.1	22.6	5.0	6.2	0.5
200805-113346	38.02009	-121.46366	6.1	22.5	4.7	5.8	0.4
200805-113457	38.02242	-121.46523	6.2	22.5	4.4	5.5	0.4
200805-113608	38.02436	-121.46742	6.3	22.4	4.1	5.2	0.3
200805-113719	38.02603	-121.46992	6.3	22.3	3.8	4.9	0.2
200805-113829	38.02775	-121.47231	6.3	22.3	3.5	4.6	0.2
200805-113940	38.02915	-121.47478	6.3	22.3	3.3	4.3	0.3
200805-114051	38.03069	-121.47735	6.4	22.3	3.0	4.0	0.2
200805-114313	38.03272	-121.48138	6.4	22.8	2.6	3.6	0.2
200805-114423	38.03140	-121.47924	6.4	22.9	2.8	3.9	0.1
200805-114534	38.03017	-121.47695	6.4	23.0	3.0	4.2	0.1
200805-114645	38.02881	-121.47476	6.3	23.0	3.3	4.5	0.2
200805-114755	38.02746	-121.47262	6.3	23.1	3.5	4.8	0.2
200805-114906	38.02637	-121.47029	6.3	23.1	3.8	5.1	0.2
200805-115017	38.02492	-121.46824	6.3	23.2	4.0	5.5	0.2
200805-115127	38.02349	-121.46632	6.2	23.2	4.2	5.8	0.3
200805-115349	38.01987	-121.46343	6.1	23.4	4.7	6.4	0.3
200805-115501	38.01815	-121.46176	6.1	23.5	5.0	6.7	0.5
200805-115611	38.01634	-121.46032	5.9	23.6	5.2	7.0	0.7
200805-115722	38.01440	-121.45915	5.6	23.8	5.4	7.3	1.3
200805-115833	38.01245	-121.45789	5.7	23.8	5.7	7.6	2.3
200805-115945	38.01066	-121.45649	5.6	23.9	5.9	7.9	1.9
200805-120054	38.00875	-121.45525	5.3	24.1	6.1	8.2	2.0
200805-120206	38.00706	-121.45367	5.2	24.2	6.4	8.5	3.3
200805-120427	38.00327	-121.45090	4.6	24.3	6.9	9.2	7.3
200805-120537	38.00145	-121.44943	4.5	24.4	7.1	9.5	9.5
200805-120648	37.99969	-121.44779	4.4	24.5	7.4	9.8	10.9
200805-120759	37.99812	-121.44586	4.3	24.6	7.6	10.1	12.7
200805-120911	37.99688	-121.44350	4.3	24.6	7.8	10.4	14.7
200805-121021	37.99571	-121.44116	4.2	24.6	8.1	10.7	16.0

200805-121132	37.99433	-121.43894	4.2	24.6	8.3	11.0	16.8
200805-121243	37.99363	-121.43633	4.3	24.4	8.6	11.3	17.4
200805-121506	37.99353	-121.43102	4.3	24.2	9.0	11.9	18.1
200805-121616	37.99419	-121.42835	4.3	24.3	9.3	12.2	18.9
200805-121727	37.99470	-121.42572	4.2	24.3	9.5	12.5	19.7
200805-121838	37.99517	-121.42308	4.2	24.5	9.7	12.8	20.6
200805-121948	37.99521	-121.42038	4.2	24.4	10.0	13.1	20.9
200805-122101	37.99507	-121.41770	4.2	24.5	10.2	13.4	21.7
200805-122211	37.99446	-121.41510	4.2	24.6	10.5	13.7	21.7
200805-122320	37.99353	-121.41277	4.2	24.6	10.7	14.0	22.2
200805-122542	37.99187	-121.40774	4.3	24.7	11.2	14.6	22.6
200805-122653	37.99105	-121.40542	4.2	24.7	11.4	14.9	22.5
200805-122803	37.99003	-121.40317	4.2	24.7	11.6	15.2	23.0
200805-122915	37.98913	-121.40069	4.2	24.6	11.9	15.5	23.0
200805-123026	37.98832	-121.39817	4.2	24.6	12.1	15.8	22.6
200805-123135	37.98748	-121.39566	4.3	24.6	12.3	16.1	22.0
200805-123247	37.98638	-121.39317	4.3	24.7	12.6	16.4	22.0
200805-123358	37.98514	-121.39094	4.2	24.6	12.8	16.7	22.0
200805-123618	37.98219	-121.38750	4.4	24.6	13.3	17.2	19.1
200805-123730	37.98058	-121.38564	4.4	24.7	13.5	17.5	18.7
200805-123841	37.97901	-121.38376	4.4	24.6	13.8	17.8	18.3
200805-123952	37.97742	-121.38185	4.4	24.7	14.0	18.1	17.8
200805-124103	37.97578	-121.37997	4.6	24.7	14.2	18.4	16.7
200805-124213	37.97416	-121.37814	4.6	24.7	14.5	18.7	15.8
200805-124326	37.97261	-121.37636	4.7	24.7	14.7	18.9	14.5
200805-124435	37.97109	-121.37470	4.7	24.7	14.9	19.2	14.4
200805-124657	37.96802	-121.37099	4.9	24.7	15.4	19.8	12.4
200805-124808	37.96634	-121.36931	4.9	24.7	15.6	20.0	12.3
200805-124918	37.96479	-121.36747	5.0	24.7	15.9	20.3	11.9
200805-125029	37.96324	-121.36557	5.2	24.7	16.1	20.6	11.1
200805-125140	37.96166	-121.36366	5.1	24.7	16.4	20.9	10.7
200805-125250	37.96015	-121.36171	5.4	24.6	16.6	21.2	9.9
200805-125402	37.95882	-121.35977	5.4	24.6	16.8	21.4	9.5
200805-125512	37.95784	-121.35730	5.6	24.6	17.1	21.7	9.1
200805-125733	37.95614	-121.35229	5.9	24.6	17.6	22.3	7.1
200805-125844	37.95541	-121.34970	6.0	24.5	17.8	22.5	6.9
200805-125954	37.95464	-121.34721	6.1	24.6	18.0	22.8	9.2
200805-130105	37.95389	-121.34465	6.0	24.5	18.3	23.1	10.8

200805-130216	37.95324	-121.34202	6.0	24.4	18.5	23.3	8.2
200805-130327	37.95241	-121.33947	5.9	24.3	18.8	23.6	7.2
200805-130437	37.95203	-121.33707	5.8	24.3	19.0	23.8	7.0
200805-130550	37.95194	-121.33424	6.9	24.7	19.2	24.1	11.3
200805-130810	37.95214	-121.32880	6.9	24.8	19.7	24.7	19.0
200805-130920	37.95230	-121.32647	6.8	24.8	19.9	24.9	18.9
200805-131031	37.95247	-121.32395	6.6	24.7	20.1	25.1	20.7
200805-131141	37.95261	-121.32128	6.7	24.6	20.4	25.4	20.1
200805-131250	37.95265	-121.31863	8.6	24.8	20.6	25.6	17.5
200805-131404	37.95278	-121.31579	8.4	25.1	20.8	25.9	17.0
200805-131515	37.95296	-121.31313	9.8	25.1	21.1	26.1	14.9
200805-131626	37.95315	-121.31056	10.0	25.1	21.3	26.4	12.6
200805-131847	37.95325	-121.30669	13.5	25.6	21.7	26.7	8.9
200805-131958	37.95313	-121.30478	13.6	25.7	21.8	26.9	8.1
200805-132109	37.95308	-121.30285	13.0	25.7	22.0	27.1	8.2
200805-132219	37.95324	-121.30097	13.5	25.8	22.2	27.3	7.9
200805-132331	37.95356	-121.29905	12.8	25.9	22.3	27.4	8.2
200805-132442	37.95392	-121.29719	12.0	25.8	22.5	27.6	8.8
200805-132553	37.95407	-121.29660	13.0	25.8	22.5	27.7	8.3
200805-132703	37.95399	-121.29839	13.6	26.0	22.4	27.5	8.2
200805-132924	37.95308	-121.30159	13.6	25.8	22.1	27.3	8.2
200805-133035	37.95305	-121.30307	14.4	25.7	22.0	27.1	7.9
200805-133145	37.95329	-121.30447	14.8	25.6	21.8	27.0	7.8
200805-133258	37.95334	-121.30614	15.1	25.6	21.7	26.9	8.0
200805-133407	37.95337	-121.30770	13.6	25.3	21.6	26.7	9.0
200805-133518	37.95337	-121.30928	11.5	25.1	21.4	26.6	10.9
200805-133630	37.95342	-121.31098	10.5	25.1	21.3	26.5	12.6
200805-133741	37.95309	-121.31267	10.5	25.1	21.1	26.3	13.4
200805-134001	37.95179	-121.31548	10.1	25.0	20.9	26.1	15.1
200805-134112	37.95277	-121.31664	10.2	24.9	20.8	26.0	16.0
200805-134223	37.95370	-121.31797	7.8	25.0	20.6	25.8	19.3
200805-134335	37.95363	-121.31843	7.2	25.0	20.6	25.8	20.9
200805-134444	37.95265	-121.31897	7.3	24.9	20.6	25.8	20.9
200805-134555	37.95208	-121.31988	7.4	24.7	20.5	25.7	19.6
200805-134707	37.95289	-121.32115	7.1	24.9	20.4	25.6	19.9
200805-134818	37.95267	-121.32257	6.9	24.9	20.2	25.5	20.0
200805-135038	37.95275	-121.32540	7.4	25.0	20.0	25.2	20.1
200805-135150	37.95210	-121.32690	7.5	24.8	19.9	25.1	20.4

200805-135302	37.95246	-121.32844	7.5	24.9	19.7	25.0	20.4
200805-135411	37.95206	-121.32969	7.3	24.9	19.6	24.9	19.3
200805-135522	37.95206	-121.33116	7.7	24.7	19.5	24.8	17.6
200805-135634	37.95220	-121.33262	7.5	24.8	19.4	24.6	16.7
200805-135745	37.95147	-121.33456	7.8	24.8	19.2	24.5	16.4
200805-135856	37.94994	-121.33598	7.1	23.8			11.3
200805-140117	37.94700	-121.33872	7.3	23.5			0.7
200805-140228	37.94593	-121.34104	7.4	23.6			0.4
200805-140338	37.94411	-121.34237	7.5	23.6			0.3
200805-140451	37.94303	-121.34469	7.5	23.6			0.2
200805-140603	37.94150	-121.34548	7.3	23.6			0.2
200805-140714	37.93971	-121.34391	7.4	23.6			0.1
200805-140824	37.93905	-121.34340	7.0	23.6			0.1
200805-140935	37.93914	-121.34335	7.4	23.5			0.1
200805-141153	37.94008	-121.34374	7.6	23.5			0.2
200805-141306	37.94044	-121.34415	7.5	23.5			0.1
200805-141416	37.94092	-121.34470	7.7	23.5			0.1
200805-141527	37.94257	-121.34523	7.5	23.5			0.1
200805-141638	37.94356	-121.34309	7.3	23.5			0.1
200805-141749	37.94591	-121.34112	7.2	23.5			0.3
200805-141859	37.94727	-121.33805	7.2	23.5			0.3
200805-142010	37.94959	-121.33614	6.7	24.4			1.0
200805-142232	37.95202	-121.33114	7.0	24.7	19.5	24.8	17.6
200805-142342	37.95227	-121.32801	6.4	24.7	19.8	25.0	18.1
200805-142453	37.95255	-121.32473	6.7	25.0	20.1	25.3	18.6
200805-142605	37.95261	-121.32143	6.9	25.0	20.4	25.6	20.4
200805-145940	37.95177	-121.31694	10.3	25.3	20.8	25.7	15.4
200805-150050	37.95195	-121.31763	7.1	25.2	20.7	25.6	21.8
200805-150203	37.95293	-121.32050	7.1	25.1	20.4	25.3	20.8
200805-150313	37.95291	-121.32367	7.7	25.3	20.1	25.0	20.2
200805-150424	37.95266	-121.32694	7.3	25.2	19.9	24.8	20.8
200805-150535	37.95216	-121.32981	7.4	25.1	19.6	24.5	20.0
200805-150647	37.95208	-121.33305	7.5	25.2	19.3	24.2	21.7
200805-150758	37.95197	-121.33517	7.2	25.1	19.1	24.1	18.1
200805-151018	37.95179	-121.33503	7.7	25.4	19.2	24.0	17.2
200805-151128	37.95169	-121.33497	7.6	25.4	19.2	24.0	17.3
200805-151240	37.95159	-121.33494	7.5	25.3	19.2	24.0	17.4
200805-151352	37.95144	-121.33491	7.7	25.3	19.2	24.0	16.5

200805-151501	37.95128	-121.33500	7.8	25.2	19.2	24.0	14.4
200805-151611	37.95176	-121.33679	7.0	24.5	19.0	23.8	13.4
200805-151724	37.95267	-121.34164	6.8	24.6	18.6	23.4	10.3
200805-151835	37.95338	-121.34310	6.8	24.6	18.4	23.3	7.7
200805-152055	37.95524	-121.34603	6.9	24.7	18.1	22.9	8.7
200805-152206	37.95604	-121.34749	7.1	24.8	17.9	22.8	7.9
200805-152317	37.95594	-121.34896	7.2	24.9	17.8	22.7	7.9
200805-152427	37.95585	-121.35042	7.2	25.0	17.7	22.5	8.0
200805-152538	37.95581	-121.35189	7.3	25.0	17.6	22.4	8.0
200805-152649	37.95578	-121.35335	6.8	25.0	17.5	22.3	7.0
200805-152801	37.95643	-121.35482	6.5	25.0	17.3	22.1	8.7
200805-152910	37.95736	-121.35628	6.7	24.8	17.2	22.0	10.6
200805-153132	37.95813	-121.35921	6.6	24.8	16.9	21.7	10.3
200805-153242	37.95943	-121.36067	6.7	24.9	16.7	21.5	8.8
200805-153353	37.96115	-121.36214	6.5	24.8	16.5	21.3	8.2
200805-153504	37.96293	-121.36360	6.4	24.8	16.3	21.1	9.2
200805-160937	37.96332	-121.36653	6.3	25.1	16.0	20.2	7.1
200805-161049	37.96362	-121.36799	6.2	25.0	15.9	20.1	8.2
200805-161200	37.96522	-121.36946	6.0	25.2	15.7	19.9	8.2
200805-161311	37.96702	-121.37092	5.5	25.0	15.5	19.7	10.8
200805-161423	37.96890	-121.37239	5.8	25.1	15.2	19.4	10.2
200805-161533	37.97085	-121.37385	5.7	25.2	15.0	19.2	9.3
200805-161643	37.97277	-121.37532	5.6	25.1	14.8	19.0	11.0
200805-161755	37.97424	-121.37678	5.5	25.1	14.6	18.8	10.5
200805-162016	37.97457	-121.37971	5.8	25.2	14.3	18.5	9.5
200805-162127	37.97457	-121.38117	5.8	25.2	14.2	18.4	9.7
200805-162239	37.97458	-121.38264	5.8	25.2	14.1	18.2	9.4
200805-162350	37.97459	-121.38410	5.8	25.2	14.0	18.1	9.7
200805-162501	37.97453	-121.38557	5.7	25.1	13.9	18.0	10.1
200805-162612	37.97602	-121.38703	5.7	25.1	13.6	17.7	9.6
200805-162723	37.97780	-121.38849	5.5	25.1	13.4	17.5	10.5
200805-162833	37.97983	-121.38996	5.1	25.2	13.2	17.3	13.4
200805-163056	37.98333	-121.39289	5.3	25.1	12.8	16.8	14.5
200805-163207	37.98445	-121.39435	5.5	25.2	12.6	16.7	12.5
200805-163318	37.98443	-121.39582	5.5	25.3	12.5	16.5	12.1
200805-163428	37.98447	-121.39728	5.5	25.3	12.4	16.4	11.9
200805-163539	37.98445	-121.39874	5.5	25.2	12.3	16.3	10.7
200805-163651	37.98560	-121.40021	5.5	25.1	12.1	16.1	11.4

200805-163802	37.98688	-121.40167	5.1	25.0	11.9	15.9	12.3
200805-163913	37.98819	-121.40314	5.0	25.2	11.7	15.7	14.7
200805-164132	37.99007	-121.40607	5.0	25.1	11.4	15.4	15.4
200805-164243	37.99114	-121.40753	4.8	25.1	11.2	15.2	18.3
200805-164354	37.99103	-121.40899	5.1	25.2	11.1	15.1	15.6
200805-164505	37.99103	-121.41046	5.1	25.3	11.0	14.9	13.0
200805-164615	37.99111	-121.41192	5.0	25.3	10.9	14.8	13.8
200805-164726	37.99200	-121.41339	4.9	25.2	10.7	14.6	15.4
200805-164837	37.99318	-121.41485	5.1	25.3	10.5	14.4	16.4
200805-164948	37.99395	-121.41632	5.0	25.1	10.4	14.3	15.0
200805-165209	37.99551	-121.41924	4.8	25.2	10.1	13.9	19.0
200805-165320	37.99548	-121.42071	4.9	25.3	10.0	13.8	17.7
200805-165431	37.99554	-121.42217	5.0	25.3	9.8	13.6	14.8
200805-165542	37.99554	-121.42364	5.1	25.3	9.7	13.5	15.5
200805-165652	37.99545	-121.42510	4.9	25.3	9.5	13.3	17.1
200805-165804	37.99517	-121.42657	5.0	25.3	9.4	13.2	18.8
200805-165915	37.99486	-121.42803	4.8	25.2	9.3	13.0	18.2
200805-170026	37.99448	-121.42949	5.0	25.3	9.1	12.9	18.3
200805-180031	37.99330	-121.43389	5.0	25.6	8.8	11.2	19.4
200805-180141	37.99359	-121.43535	4.8	25.4	8.7	11.1	20.9
200805-180252	37.99400	-121.43682	4.8	25.5	8.5	10.9	21.2
200805-180403	37.99460	-121.43828	4.8	25.4	8.4	10.7	21.1
200805-180514	37.99579	-121.43974	4.8	25.5	8.2	10.5	22.0
200805-180626	37.99705	-121.44121	4.9	25.6	8.0	10.4	21.7
200805-180737	37.99862	-121.44267	4.8	25.5	7.8	10.1	22.4
200805-180847	38.00021	-121.44414	5.0	25.6	7.6	9.9	20.8
200805-181108	38.00259	-121.44707	4.9	25.4	7.2	9.5	21.1
200805-181218	38.00244	-121.44853	5.0	25.5	7.1	9.4	20.8
200805-181329	38.00222	-121.44999	5.0	25.5	7.0	9.3	21.4
200805-181440	38.00345	-121.45146	5.0	25.5	6.8	9.1	21.2
200805-181552	38.00561	-121.45292	5.1	25.5	6.5	8.8	21.8
200805-181703	38.00771	-121.45439	5.2	25.5	6.3	8.5	21.5
200805-181814	38.00955	-121.45585	5.1	25.4	6.0	8.3	16.3
200805-181925	38.01137	-121.45732	5.2	25.5	5.8	8.0	15.4
200805-182146	38.01501	-121.46024	4.8	25.3	5.3	7.5	18.1
200805-182257	38.01526	-121.46171	4.7	25.3	5.2	7.3	18.5
200805-182409	38.01503	-121.46317	4.8	25.3	5.1	7.2	17.4
200805-182519	38.01481	-121.46464	4.7	25.2	5.0	7.1	17.5

200805-182630	38.01462	-121.46610	4.7	25.3	4.9	7.0	16.5
200805-182741	38.01472	-121.46757	4.8	25.2	4.7	6.8	16.2
200805-182852	38.01671	-121.46903	5.0	25.2	4.5	6.5	14.8
200805-183002	38.01832	-121.47049	5.1	25.3	4.3	6.3	13.9
200805-183224	38.02234	-121.47342	5.0	25.1	3.8	5.8	13.2
200805-183334	38.02398	-121.47489	5.4	25.1	3.6	5.6	11.8
200805-183447	38.02552	-121.47635	5.3	25.2	3.4	5.4	12.0
200805-183557	38.02662	-121.47782	5.3	25.2	3.2	5.2	11.5
200805-183708	38.02763	-121.47928	5.6	25.2	3.0	5.0	8.2
200805-183819	38.02876	-121.48074	5.6	25.1	2.8	4.8	8.1
200805-183931	38.03010	-121.48221	5.9	24.9	2.7	4.6	7.0
200805-184041	38.03142	-121.48367	5.7	24.8	2.5	4.4	4.4
200805-184300	38.03100	-121.48660	5.6	24.7	2.3	4.1	4.3
200805-184412	38.03077	-121.48807	5.8	24.8	2.2	4.0	3.9
200805-184523	38.03215	-121.48953	6.1	24.5	2.0	3.8	3.2
200805-184633	38.03347	-121.49099	6.2	24.4	1.8	3.6	2.0
200805-184744	38.03493	-121.49246	6.2	24.3	1.6	3.4	1.4
200805-184855	38.03591	-121.49392	6.6	24.1	1.4	3.2	0.9
200805-185007	38.03710	-121.49539	6.6	24.0	1.3	3.0	0.6
200805-185118	38.03834	-121.49685	6.5	23.9	1.1	2.8	0.4
200805-185336	38.04076	-121.49978	6.5	23.8	0.7	2.4	0.3
200805-185448	38.04208	-121.50124	6.7	23.9	0.5	2.2	0.4
200805-185558	38.04299	-121.50271	6.6	23.9	0.4	2.0	0.3
200805-185709	38.04438	-121.50417	6.7	23.9	0.1	1.8	0.3
200805-185819	38.04602	-121.50564	6.7	23.9	-0.1	1.5	0.2
200805-185931	38.04757	-121.50710	6.8	23.9	-0.3	1.3	0.2
200805-190040	38.04854	-121.50857	6.8	23.9	-0.5	1.1	0.2
200805-190151	38.04836	-121.51003	6.8	23.9	-0.6	1.0	0.1
200805-190413	38.04749	-121.51296	6.7	23.8	-0.8	0.7	0.2
200805-190524	38.04655	-121.51442	6.7	23.7	-0.8	0.7	0.2
200805-190636	38.04420	-121.51589	6.6	23.7	-0.8	0.6	0.2
200805-190746	38.04243	-121.49784	6.6	23.7	0.8	2.1	0.2
200805-190856	38.04069	-121.49484	6.6	23.7	1.1	2.4	0.3
200805-191008	38.03900	-121.49171	6.6	23.8	1.4	2.7	0.2
200805-191118	38.03707	-121.48913	6.6	23.9	1.7	3.0	0.3
200805-191229	38.03556	-121.48669	6.5	24.0	2.0	3.2	0.6
200805-191450	38.03258	-121.48133	6.4	24.0	2.6	3.7	0.7
200805-191600	38.03109	-121.47843	6.3	24.1	2.9	4.0	1.0

200805-191711	38.02937	-121.47562	6.1	24.2	3.2	4.3	1.1
200805-191822	38.02784	-121.47294	6.0	24.6	3.5	4.5	2.4
200805-191933	38.02620	-121.47056	6.1	24.6	3.8	4.8	3.1
200805-192044	38.02445	-121.46784	5.7	24.7	4.1	5.0	3.9
200805-192154	38.02208	-121.46608	5.3	24.7	4.4	5.3	5.0
200805-192305	38.01961	-121.46437	5.1	24.8	4.7	5.6	8.1
200805-192528	38.01511	-121.46056	5.2	25.0	5.3	6.1	10.7
200805-192638	38.01281	-121.45866	5.1	25.1	5.6	6.4	11.8
200805-194521	37.99394	-121.42939	5.0		9.2	9.5	21.0
200805-194632	37.99451	-121.42607	5.0		9.5	9.8	20.8
200805-194741	37.99496	-121.42271	5.0	25.5	9.8	10.1	20.2
200805-194853	37.99661	-121.42007	4.7	25.5			20.3
200805-195004	37.99789	-121.41796	4.7	25.4			19.1
200805-195115	37.99869	-121.41558	4.8	25.2			17.8
200805-195225	37.99875	-121.41297	4.9	25.2			17.4
200805-195336	37.99862	-121.41040	5.0	25.3			16.2
200805-195557	38.00035	-121.40642	5.2	25.7			15.9
200805-195708	38.00270	-121.40459	5.2	25.7			15.5
200805-195819	38.00480	-121.40246	5.2	25.5			15.3
200805-195930	38.00579	-121.40012	5.4	25.6			13.4
210805-114038	37.99841	-121.41066	4.4	23.8			16.1
210805-114148	37.99841	-121.41065	4.4	23.9			16.1
210805-114300	37.99839	-121.41067	4.3	23.8			15.6
210805-114410	37.99866	-121.41151	4.4	24.0			16.3
210805-114523	37.99849	-121.41025	4.3	24.0			16.3
210805-114632	37.99838	-121.41029	4.4	23.8			16.0
210805-114744	37.99844	-121.41099	4.3	23.9			16.1
210805-114855	37.99865	-121.41090	4.4	23.9			15.9
210805-115115	37.99849	-121.41010	4.3	23.9			15.8
210805-115225	37.99842	-121.41018	4.3	23.8			16.2
210805-115336	37.99849	-121.41052	4.3	23.8			15.3
210805-115447	37.99848	-121.41061	4.3	23.9			15.4
210805-115558	37.99850	-121.41057	4.2	23.7			14.0
210805-115709	37.99873	-121.41275	4.3	23.8			15.6
210805-115821	37.99860	-121.41624	4.4	24.0			16.4
210805-115932	37.99718	-121.41914	4.3	23.9			17.4
210805-120153	37.99502	-121.42522	4.5	24.2	9.5	10.7	17.5
210805-120304	37.99433	-121.42847	4.5	24.2	9.2	10.3	17.7

210805-120414	37.99391	-121.43175	4.5	24.2	9.0	10.0	17.3
210805-120525	37.99372	-121.43508	4.5	24.0	8.7	9.7	17.5
210805-120636	37.99444	-121.43828	4.5	23.9	8.4	9.4	16.2
210805-120747	37.99564	-121.44126	4.6	23.8	8.1	9.0	15.2
210805-120858	37.99708	-121.44407	4.5	23.8	7.8	8.7	13.8
210805-121008	37.99878	-121.44649	4.7	23.7	7.5	8.4	14.2
210805-121228	38.00274	-121.45033	5.0	23.6	7.0	7.8	10.3
210805-121339	38.00502	-121.45203	5.3	23.4	6.7	7.4	7.8
210805-121450	38.00726	-121.45370	5.2	23.4	6.4	7.1	6.5
210805-121601	38.00938	-121.45551	5.8	23.1	6.1	6.8	5.6
210805-121711	38.01155	-121.45730	5.9	23.0	5.8	6.4	3.5
210805-121823	38.01387	-121.45894	6.1	22.8	5.5	6.1	2.4
210805-121934	38.01619	-121.46051	6.1	22.8	5.2	5.8	1.9
210805-122045	38.01846	-121.46217	6.2	22.7	4.9	5.5	1.6
210805-122305	38.02287	-121.46564	6.3	22.6	4.3	4.8	1.4
210805-122417	38.02464	-121.46813	6.3	22.6	4.0	4.4	0.8
210805-122530	38.02633	-121.47075	6.3	22.6	3.7	4.1	0.6
210805-122640	38.02797	-121.47327	6.3	22.5	3.5	3.8	0.5
210805-122752	38.02960	-121.47569	6.4	22.5	3.2	3.5	0.4
210805-122901	38.03115	-121.47805	6.3	22.4	2.9	3.2	0.5
210805-123014	38.03275	-121.48072	6.4	22.4	2.6	2.8	0.4
210805-123124	38.03429	-121.48333	6.4	22.3	2.3	2.5	0.4
210805-123345	38.03722	-121.48875	6.6	22.2	1.8	1.8	0.3
210805-123455	38.03876	-121.49144	6.5	22.2	1.5	1.5	0.2
210805-123606	38.04032	-121.49413	6.6	22.1	1.2	1.1	0.2
210805-123717	38.04185	-121.49661	6.7	22.4	0.9	0.8	0.1
210805-123826	38.04074	-121.49509	6.6	22.6	1.1	1.1	0.1
210805-123940	38.03943	-121.49252	6.5	22.7	1.3	1.4	0.2
210805-124052	38.03812	-121.49006	6.6	22.7	1.6	1.8	0.2
210805-124203	38.03675	-121.48769	6.5	22.8	1.9	2.2	0.3
210805-124423	38.03371	-121.48347	6.4	23.0	2.4	2.8	0.3
210805-124533	38.03259	-121.48183	6.5	23.0	2.5	3.1	0.2
210805-124644	38.03156	-121.47970	6.5	23.0	2.8	3.4	0.4
210805-124755	38.03022	-121.47722	6.4	23.1	3.0	3.8	0.4
210805-124906	38.02884	-121.47480	6.4	23.2	3.3	4.1	0.5
210805-125017	38.02752	-121.47235	6.4	23.2	3.5	4.5	0.6
210805-125128	38.02620	-121.47021	6.5	23.2	3.8	4.8	0.6
210805-125238	38.02483	-121.46787	6.4	23.3	4.0	5.2	0.8

210805-125459	38.02085	-121.46487	6.2	23.4	4.5	5.9	1.1
210805-125609	38.01893	-121.46335	6.2	23.5	4.8	6.2	1.4
210805-125720	38.01691	-121.46168	6.0	23.6	5.1	6.6	2.3
210805-125832	38.01517	-121.46061	5.9	23.6	5.3	6.9	2.3
210805-125942	38.01380	-121.45962	5.8	23.7	5.4	7.1	2.8
210805-130053	38.01175	-121.45797	5.7	24.0	5.7	7.5	3.9
210805-130204	38.00997	-121.45656	5.3	24.2	6.0	7.8	6.4
210805-130316	38.00797	-121.45497	5.0	24.4	6.2	8.2	9.3
210805-130536	38.00406	-121.45184	4.9	24.6	6.7	8.9	13.9
210805-130647	38.00211	-121.45026	4.9	24.6	7.0	9.2	14.6
210805-130759	38.00001	-121.44879	4.8	24.6	7.3	9.6	15.1
210805-130910	37.99849	-121.44658	4.7	24.6	7.5	9.9	16.1
210805-131022	37.99721	-121.44413	4.6	24.7	7.8	10.3	17.5
210805-131132	37.99578	-121.44183	4.6	24.7	8.0	10.6	17.9
210805-131245	37.99461	-121.43921	4.7	24.6	8.3	11.0	17.8
210805-131355	37.99372	-121.43650	4.7	24.6	8.6	11.3	18.1
210805-131616	37.99382	-121.43071	4.7	24.5	9.1	12.0	17.8
210805-131727	37.99446	-121.42786	4.7	24.5	9.3	12.3	19.3
210805-131837	37.99490	-121.42514	4.6	24.5	9.6	12.7	18.4
210805-131948	37.99507	-121.42270	4.6	24.5	9.8	13.0	16.6
210805-132101	37.99515	-121.41978	4.7	24.6	10.0	13.3	16.5
210805-132211	37.99479	-121.41678	4.6	24.6	10.3	13.7	16.2
210805-132322	37.99398	-121.41390	4.7	24.7	10.6	14.0	14.7
210805-132433	37.99315	-121.41111	4.8	24.7	10.8	14.3	14.2
210805-132653	37.99109	-121.40561	4.8	24.7	11.4	15.0	13.2
210805-132803	37.99004	-121.40291	4.7	24.7	11.6	15.4	12.8
210805-132915	37.98910	-121.40004	4.7	24.6	11.9	15.7	12.4
210805-133027	37.98826	-121.39713	4.8	24.7	12.2	16.1	12.0
210805-133139	37.98709	-121.39442	4.7	24.7	12.5	16.4	11.7
210805-133249	37.98581	-121.39198	4.7	24.7	12.7	16.7	11.7
210805-133400	37.98432	-121.38964	4.7	24.6	13.0	17.1	10.9
210805-133511	37.98253	-121.38776	4.8	24.7	13.2	17.4	10.8
210805-133731	37.97920	-121.38390	5.0	24.7	13.7	18.0	10.4
210805-133844	37.97745	-121.38187	5.0	24.7	14.0	18.3	9.4
210805-133953	37.97562	-121.37990	5.0	24.7	14.3	18.6	9.2
210805-134104	37.97369	-121.37780	5.0	24.7	14.5	19.0	9.5
210805-134215	37.97182	-121.37562	5.1	24.7	14.8	19.3	9.0
210805-134328	37.97040	-121.37387	5.3	24.6	15.0	19.6	8.0

210805-134438	37.96861	-121.37181	5.5	24.7	15.3	19.9	7.8
210805-134549	37.96666	-121.36990	5.6	24.7	15.6	20.2	7.6
210805-134809	37.96325	-121.36563	5.7	24.7	16.1	20.9	7.0
210805-134919	37.96148	-121.36348	5.8	24.6	16.4	21.2	6.4
210805-135030	37.95970	-121.36125	6.0	24.6	16.7	21.5	6.2
210805-135142	37.95817	-121.35870	6.2	24.6	17.0	21.8	6.0
210805-135252	37.95725	-121.35596	6.5	24.6	17.2	22.1	5.7
210805-135404	37.95619	-121.35297	6.7	24.5	17.5	22.4	5.6
210805-135516	37.95520	-121.34999	6.6	24.5	17.8	22.8	5.5
210805-135627	37.95425	-121.34700	6.3	24.6	18.1	23.1	8.4
210805-141215	37.95228	-121.33544	7.0	24.8	19.1	24.3	14.4
210805-141325	37.95194	-121.33352	7.2	25.0	19.3	24.5	15.4
210805-141437	37.95216	-121.33030	6.9	25.0	19.6	24.8	16.3
210805-141548	37.95237	-121.32716	6.7	25.0	19.8	25.1	16.7
210805-141659	37.95251	-121.32405	7.1	25.0	20.1	25.4	16.4
210805-141811	37.95264	-121.32089	7.0	25.0	20.4	25.6	17.0
210805-141922	37.95266	-121.31776	7.8	25.1	20.7	25.9	15.8
210805-142033	37.95278	-121.31465	10.9	25.5	20.9	26.2	13.9
210805-142254	37.95324	-121.30948	13.4	25.8	21.4	26.6	9.6
210805-142404	37.95328	-121.30761	14.0	26.0	21.6	26.8	9.6
210805-142515	37.95320	-121.30576	14.8	26.2	21.7	27.0	9.5
210805-142625	37.95314	-121.30393	14.6	26.2	21.9	27.1	9.3
210805-142737	37.95310	-121.30206	14.6	26.2	22.1	27.3	9.2
210805-142848	37.95340	-121.30029	16.7	26.4	22.2	27.4	8.4
210805-142959	37.95376	-121.29860	15.5	26.4	22.4	27.6	9.1
210805-143110	37.95388	-121.29688	15.2	26.4	22.5	27.7	9.1
210805-143331	37.95369	-121.29916	17.3	26.5	22.3	27.5	9.0
210805-143442	37.95338	-121.30076	15.0	26.3	22.2	27.4	9.2
210805-143551	37.95317	-121.30232	15.7	26.3	22.0	27.3	9.3
210805-143703	37.95323	-121.30397	16.0	26.3	21.9	27.1	8.8
210805-143814	37.95333	-121.30557	15.3	26.2	21.7	27.0	9.6
210805-143924	37.95333	-121.30718	14.9	26.1	21.6	26.8	9.5
210805-144036	37.95330	-121.30885	13.2	25.7	21.5	26.7	10.3
210805-144147	37.95327	-121.31066	12.5	25.6	21.3	26.5	11.0
210805-144407	37.95304	-121.31544	8.1	25.3	20.9	26.1	15.7
210805-144519	37.95284	-121.31862	7.4	25.2	20.6	25.9	15.7
210805-144630	37.95276	-121.32179	7.8	25.2	20.3	25.6	15.6
210805-144741	37.95270	-121.32496	7.9	25.3	20.0	25.3	15.6

210805-144851	37.95246	-121.32811	8.2	25.3	19.8	25.1	15.1
210805-145002	37.95228	-121.33130	8.1	25.2	19.5	24.8	16.3
210805-145113	37.95154	-121.33429	7.4	25.0	19.2	24.6	17.1
210805-145224	37.94996	-121.33599	8.1	24.2			12.0
210805-145446	37.94913	-121.33644	8.0	24.1			0.4
210805-145556	37.94934	-121.33636	8.1	24.1			0.2
210805-145707	37.94958	-121.33633	8.0	24.1			0.3
210805-145818	37.94983	-121.33629	7.8	24.1			0.2
210805-145929	37.94998	-121.33624	8.2	24.1			0.2
210805-150040	37.95011	-121.33616	7.9	24.3	19.1	24.5	0.2
210805-150151	37.95024	-121.33607	7.6	24.3	19.1	24.5	2.9
210805-150302	37.95018	-121.33603	7.6	24.4	19.1	24.5	5.0
210805-161948	37.95248	-121.33946	6.9	24.6	18.8	23.3	6.0
210805-162101	37.95292	-121.34156	7.0	24.6	18.6	23.1	6.0
210805-162210	37.95349	-121.34372	7.2	24.8	18.4	22.9	5.9
210805-162321	37.95419	-121.34573	7.2	25.0	18.2	22.7	6.1
210805-162432	37.95489	-121.34775	7.1	25.0	18.0	22.6	5.9
210805-162542	37.95562	-121.34971	7.0	25.1	17.8	22.4	5.9
210805-162653	37.95625	-121.35176	6.8	25.0	17.6	22.2	6.6
210805-162804	37.95687	-121.35385	6.6	25.4	17.4	22.0	7.2
210805-163025	37.95840	-121.35780	6.6	25.1	17.0	21.6	7.3
210805-163135	37.95927	-121.35964	6.6	25.2	16.8	21.4	6.8
210805-163246	37.96060	-121.36096	6.5	25.1	16.6	21.2	6.7
210805-163357	37.96189	-121.36232	6.5	25.0	16.5	21.1	6.2
210805-163508	37.96289	-121.36398	6.3	24.8	16.3	20.9	5.7
210805-163619	37.96406	-121.36562	6.2	24.7	16.1	20.7	5.8
210805-163730	37.96528	-121.36720	6.1	24.8	15.9	20.5	6.2
210805-163840	37.96651	-121.36872	5.4	24.9	15.7	20.3	7.4
210805-164101	37.96908	-121.37168	5.9	25.0	15.3	19.9	7.1
210805-164212	37.97041	-121.37320	5.9	24.9	15.1	19.7	6.7
210805-164324	37.97159	-121.37446	5.9	25.1	14.9	19.5	6.9
210805-164435	37.97272	-121.37577	5.8	25.1	14.8	19.3	7.0
210805-164547	37.97390	-121.37697	5.8	25.0	14.6	19.2	7.2
210805-164658	37.97503	-121.37825	5.8	25.1	14.4	19.0	7.1
210805-164808	37.97609	-121.37960	5.8	25.1	14.3	18.8	7.1
210805-164921	37.97727	-121.38092	5.6	25.1	14.1	18.7	7.2
210805-165140	37.97942	-121.38360	5.5	25.0	13.7	18.3	8.0
210805-165251	37.98071	-121.38500	5.5	25.0	13.6	18.1	8.0

210805-165403	37.98196	-121.38646	5.4	25.0	13.4	17.9	8.2
210805-165514	37.98329	-121.38771	5.0	25.1	13.2	17.7	8.8
210805-165625	37.98450	-121.38891	5.2	25.0	13.0	17.6	9.7
210805-165735	37.98548	-121.39052	5.4	25.0	12.8	17.4	8.6
210805-165847	37.98647	-121.39220	5.4	25.1	12.7	17.2	8.8
210805-165958	37.98734	-121.39393	5.2	25.2	12.5	17.0	9.1
210805-170218	37.98850	-121.39684	5.0	25.2	12.2	16.7	9.6
210805-170329	37.98898	-121.39786	5.0	25.1	12.1	16.6	9.8
210805-170441	37.98937	-121.39973	5.1	25.0	11.9	16.4	9.5
210805-170550	37.98993	-121.40152	5.2	25.1	11.8	16.2	9.1
210805-170701	37.99064	-121.40330	5.1	25.1	11.6	16.1	9.2
210805-170811	37.99123	-121.40509	5.0	25.0	11.4	15.9	9.5
210805-170923	37.99191	-121.40693	5.1	25.2	11.2	15.7	10.2
210805-171034	37.99258	-121.40868	4.9	25.1	11.1	15.5	11.4
210805-171255	37.99402	-121.41213	5.2	25.2	10.7	15.2	10.1
210805-171405	37.99464	-121.41390	4.9	25.1	10.6	15.0	10.3
210805-171516	37.99513	-121.41581	4.9	25.1	10.4	14.8	11.0
210805-171627	37.99538	-121.41783	4.9	25.1	10.2	14.6	10.6
210805-171737	37.99557	-121.41983	5.0	25.2	10.0	14.4	11.5
210805-171850	37.99670	-121.41985	5.4	25.2			9.6
210805-174340	38.00138	-121.40551	6.1	25.8			3.5
210805-174453	38.00255	-121.40473	6.1	25.9			3.4
210805-174602	38.00371	-121.40386	6.7	25.8			3.0
210805-174714	38.00469	-121.40250	6.8	25.9			3.2
210805-174824	38.00549	-121.40069	6.5	25.9			3.3
210805-174935	38.00628	-121.39846	6.7	26.0			2.3
210805-175048	38.00716	-121.39659	6.8	26.0			2.1
210805-175158	38.00794	-121.39458	6.7	26.2			2.2
210805-175418	38.00967	-121.39070	6.7	26.3			2.1
210805-175529	38.01063	-121.38884	6.6	26.2			1.8
210805-175640	38.01152	-121.38690	6.5	26.2			1.8
210805-175750	38.01239	-121.38493	6.7	26.3			1.7
210805-175903	38.01360	-121.38401	6.6	26.2			1.5
210805-180014	38.01521	-121.38519	6.9	26.0			2.8
210805-180124	38.01685	-121.38639	7.3	26.1			3.5
210805-180235	38.01870	-121.38678	7.4	26.0			3.7
210805-180457	38.02206	-121.38823	7.5	25.6			3.0
210805-180607	38.02313	-121.39018	7.8	25.8			1.8

210805-180720	38.02412	-121.39215	7.6	25.8			0.7
210805-180830	38.02489	-121.39414	7.9	25.7			0.3
210805-180941	38.02582	-121.39614	8.0	25.7			0.2
210805-181053	38.02663	-121.39825	7.8	25.6			0.2
210805-181202	38.02758	-121.40011	7.9	25.6			0.1
210805-181313	38.02874	-121.40181	8.0	25.8			0.0
210805-200041	38.00701	-121.39722	5.5	25.6			12.7
210805-200151	38.00817	-121.39419	6.0	25.8			10.1
210805-200302	38.00948	-121.39131	6.2	25.9			6.6
210805-200413	38.01069	-121.38859	6.2	25.9			4.6
210805-200634	38.01276	-121.38313	6.4	26.3			3.5
210805-200747	38.01460	-121.38454	7.1	26.0			4.2
210805-200858	38.01649	-121.38640	7.1	26.0			2.3
210805-201008	38.01878	-121.38704	7.1	26.0			0.9
210805-201119	38.02083	-121.38705	7.2	25.9			0.6
210805-201230	38.02251	-121.38905	7.2	25.9			0.4
210805-201332	38.02350	-121.39126	7.3	25.6			0.0
210805-201526	38.02204	-121.38936	7.2	25.6			0.1
220805-111659	38.04552	-121.41905	6.5	23.1			0.1
220805-111810	38.04551	-121.41906	6.5	23.2			0.1
220805-111921	38.04553	-121.41907	6.5	23.2			0.1
220805-112034	38.04552	-121.41915	6.6	23.3			0.0
220805-112144	38.04516	-121.41949	6.6	23.3			0.0
220805-112255	38.04450	-121.41984	6.6	23.3			0.1
220805-112404	38.04403	-121.42026	6.6	23.3			0.1
220805-112517	38.04335	-121.42108	6.5	23.3			0.0
220805-112736	38.04214	-121.41873	6.6	23.2			0.1
220805-112847	38.04234	-121.41701	6.7	23.3			0.1
220805-112958	38.04162	-121.41432	6.6	23.3			0.1
220805-113109	38.04113	-121.41087	6.7	23.3			0.0
220805-113221	38.04162	-121.40739	6.7	23.4			0.1
220805-113332	38.04105	-121.40499	6.8	23.5			0.0
220805-113443	38.03846	-121.40469	6.7	23.5			0.0
220805-113553	38.03588	-121.40499	6.8	23.4			0.0
220805-113814	38.03079	-121.40368	6.8	23.5			0.0
220805-113925	38.02842	-121.40218	6.8	23.5			0.0
220805-114034	38.02687	-121.39967	6.8	23.6			0.1
220805-114147	38.02541	-121.39671	6.7	23.7			0.1

220805-114257	38.02411	-121.39382	6.6	23.8			0.1
220805-114408	38.02322	-121.39176	6.6	23.8			0.1
220805-114520	38.02198	-121.38904	6.6	23.9			0.1
220805-114631	38.02005	-121.38735	6.6	23.9			0.1
220805-114853	38.01520	-121.38578	6.3	24.0			0.6
220805-115005	38.01302	-121.38450	5.6	23.8			1.4
220805-115115	38.01174	-121.38730	5.1	23.8			4.4
220805-115226	38.01038	-121.39021	5.1	23.8			6.0
220805-115337	38.00905	-121.39318	5.1	23.9			6.7
220805-115448	38.00771	-121.39616	5.1	23.9			7.3
220805-115558	38.00646	-121.39915	5.0	23.9			9.7
220805-115709	38.00562	-121.40114	5.0	24.0			6.9
220805-115932	38.00312	-121.40441	5.1	24.0			7.5
220805-120042	38.00066	-121.40626	5.1	24.0			7.9
220805-120155	37.99864	-121.40878	5.0	23.9			9.2
220805-120305	37.99858	-121.41028	4.8	23.9			9.8
220805-120414	37.99857	-121.41150	4.9	23.9			9.4
220805-120526	37.99855	-121.41131	4.9	23.9			9.0
220805-120637	37.99858	-121.41108	4.9	24.0			9.2
220805-120748	37.99849	-121.41062	4.9	24.0			8.8
220805-122751	37.99872	-121.41536	5.0	24.0			7.1
220805-122902	37.99765	-121.41853	5.1	24.1			8.3
220805-123014	37.99589	-121.42134	5.2	24.2			8.7
220805-123125	37.99513	-121.42468	5.2	24.2	9.6	10.4	9.4
220805-123235	37.99456	-121.42809	5.2	24.2	9.3	10.0	9.9
220805-123348	37.99403	-121.43167	5.2	24.2	9.0	9.7	10.2
220805-123457	37.99390	-121.43507	5.2	24.0	8.7	9.3	10.6
220805-123608	37.99482	-121.43833	5.2	24.0	8.4	9.0	10.6
220805-123829	37.99763	-121.44424	5.4	23.9	7.7	8.3	10.4
220805-123940	37.99919	-121.44707	5.5	23.8	7.4	7.9	10.1
220805-124052	38.00135	-121.44920	5.6	23.8	7.1	7.6	9.3
220805-124203	38.00369	-121.45095	5.7	23.6	6.8	7.3	8.6
220805-124314	38.00595	-121.45283	6.1	23.5	6.5	6.9	6.9
220805-124425	38.00827	-121.45475	6.3	23.4	6.2	6.5	5.3
220805-124537	38.01068	-121.45657	6.5	23.3	5.9	6.2	4.5
220805-124648	38.01299	-121.45851	6.5	23.2	5.6	5.8	4.0
220805-124908	38.01779	-121.46168	6.6	23.1	5.0	5.1	2.6
220805-125020	38.01942	-121.46290	6.6	23.1	4.8	4.9	2.6

220805-125137	38.02205	-121.46482	6.7	23.0	4.5	4.5	2.5
220805-125241	38.02395	-121.46670	6.9	22.9	4.2	4.2	2.0
220805-125354	38.02599	-121.46929	6.9	22.8	3.9	3.8	1.5
220805-125505	38.02779	-121.47204	6.9	22.8	3.6	3.5	1.3
220805-125615	38.02939	-121.47487	6.9	22.7	3.3	3.1	1.1
220805-125726	38.03103	-121.47771	7.0	22.7	2.9	2.7	0.9
220805-125947	38.03416	-121.48336	7.3	22.5	2.3	2.0	0.5
220805-130059	38.03592	-121.48610	7.2	22.4	2.0	1.7	0.4
220805-130209	38.03752	-121.48895	7.1	22.4	1.7	1.3	0.4
220805-130320	38.03921	-121.49177	7.2	22.4	1.4	0.9	0.3
220805-130431	38.04077	-121.49470	7.3	22.3	1.1	0.6	0.3
220805-130541	38.04239	-121.49756	7.3	22.3	0.8	0.2	0.2
220805-130654	38.04452	-121.50002	7.3	22.3	0.5	-0.2	0.1
220805-130804	38.04653	-121.50219	7.1	22.3	0.2	-0.5	0.2
220805-131426	38.04861	-121.50401	7.5	22.6	-0.1	-0.7	0.2
220805-131539	38.04882	-121.50385	7.4	22.6	-0.1	-0.7	0.1
220805-131648	38.04685	-121.50274	7.4	22.7	0.1	-0.4	0.2
220805-131759	38.04474	-121.50131	7.4	22.7	0.4	0.0	0.2
220805-131911	38.04310	-121.49901	7.4	22.8	0.6	0.3	0.2
220805-132022	38.04143	-121.49688	7.4	22.9	0.9	0.7	0.2
220805-132132	38.04011	-121.49439	7.4	22.9	1.2	1.1	0.1
220805-132243	38.03868	-121.49196	7.4	22.9	1.4	1.5	0.2
220805-132503	38.03598	-121.48708	7.2	23.1	2.0	2.2	0.3
220805-132614	38.03455	-121.48453	7.2	23.2	2.2	2.6	0.5
220805-132725	38.03297	-121.48204	7.2	23.3	2.5	3.0	0.5
220805-132836	38.03140	-121.47950	7.0	23.3	2.8	3.4	0.9
220805-132948	38.02981	-121.47692	7.1	23.3	3.1	3.8	1.0
220805-133057	38.02839	-121.47437	7.0	23.4	3.3	4.1	1.1
220805-133209	38.02685	-121.47175	7.0	23.4	3.6	4.6	1.1
220805-133320	38.02541	-121.46914	6.9	23.6	3.9	4.9	1.5
220805-133541	38.02152	-121.46543	6.8	23.8	4.4	5.7	2.3
220805-133652	38.01928	-121.46402	6.7	23.8	4.7	6.1	2.5
220805-133803	38.01716	-121.46232	6.7	23.8	5.0	6.5	2.7
220805-133913	38.01499	-121.46063	6.5	23.8	5.3	6.9	3.2
220805-134024	38.01281	-121.45882	6.5	24.2	5.6	7.3	3.8
220805-134135	38.01064	-121.45705	6.2	24.4	5.9	7.7	5.3
220805-134245	38.00849	-121.45547	5.6	24.6	6.1	8.1	7.9
220805-134356	38.00638	-121.45372	5.7	24.7	6.4	8.5	10.2

220805-134616	38.00218	-121.45050	5.5	24.7	7.0	9.2	11.1
220805-134726	38.00007	-121.44885	5.4	24.6	7.2	9.6	11.3
220805-134838	37.99838	-121.44644	5.5	24.7	7.5	10.0	11.2
220805-134949	37.99678	-121.44399	5.4	24.7	7.8	10.4	11.1
220805-135101	37.99561	-121.44124	5.4	24.7	8.1	10.7	10.8
220805-135210	37.99415	-121.43876	5.5	24.7	8.4	11.1	9.5
220805-135323	37.99364	-121.43619	5.4	24.7	8.6	11.4	10.1
220805-135434	37.99334	-121.43304	5.4	24.6	8.9	11.8	9.7
220805-135654	37.99437	-121.42692	5.4	24.6	9.4	12.5	9.1
220805-135805	37.99482	-121.42378	5.5	24.7	9.7	12.9	8.9
220805-135917	37.99506	-121.42053	5.4	24.6	10.0	13.3	8.7
220805-140028	37.99491	-121.41732	5.5	24.6	10.3	13.7	8.0
220805-140139	37.99416	-121.41430	5.7	24.8	10.5	14.0	7.2
220805-140250	37.99300	-121.41140	5.6	24.7	10.8	14.4	7.1
220805-140402	37.99198	-121.40834	5.7	24.8	11.1	14.8	6.7
220805-140511	37.99078	-121.40554	5.8	24.8	11.4	15.2	6.6
220805-140732	37.98885	-121.39966	5.9	24.7	12.0	15.9	6.2
220805-140843	37.98780	-121.39672	5.8	24.6	12.2	16.2	5.7
220805-140954	37.98691	-121.39422	5.8	24.6	12.5	16.6	5.5
220805-141104	37.98544	-121.39168	5.7	24.6	12.8	16.9	5.7
220805-141217	37.98372	-121.38912	6.0	24.7	13.1	17.3	5.5
220805-141328	37.98188	-121.38699	6.0	24.8	13.3	17.6	5.4
220805-141438	37.97997	-121.38484	6.2	24.7	13.6	18.0	5.4
220805-141550	37.97808	-121.38254	6.3	24.7	13.9	18.4	4.9
220805-141810	37.97422	-121.37838	6.4	24.7	14.5	19.0	4.6
220805-141921	37.97245	-121.37607	6.6	24.7	14.7	19.4	4.5
220805-142032	37.97052	-121.37389	6.8	24.6	15.0	19.7	4.3
220805-142143	37.96859	-121.37171	7.0	24.7	15.3	20.1	4.2
220805-142254	37.96663	-121.36949	7.0	24.7	15.6	20.4	4.2
220805-142405	37.96466	-121.36722	7.0	24.7	15.9	20.8	4.2
220805-142517	37.96282	-121.36479	7.1	24.7	16.2	21.1	4.2
220805-142627	37.96091	-121.36259	7.2	24.7	16.5	21.5	4.1
220805-142848	37.95761	-121.35736	7.6	24.7	17.1	22.2	3.9
220805-142959	37.95647	-121.35428	7.9	24.7	17.4	22.5	3.8
220805-143110	37.95551	-121.35116	7.9	24.6	17.7	22.8	3.5
220805-143221	37.95469	-121.34813	7.6	24.7	18.0	23.2	3.7
220805-143332	37.95383	-121.34516	7.5	24.7	18.2	23.5	5.6
220805-143442	37.95300	-121.34223	7.8	24.2	18.5	23.8	4.8

220805-143553	37.95240	-121.33920	7.7	24.0	18.8	24.1	3.2
220805-143704	37.95215	-121.33609	7.5	24.3	19.1	24.4	2.2
220805-143926	37.95221	-121.32967	7.3	25.1	19.6	25.0	9.4
220805-144036	37.95240	-121.32660	8.0	25.1	19.9	25.3	9.1
220805-144147	37.95254	-121.32388	8.0	25.0	20.1	25.5	9.8
220805-144258	37.95259	-121.32115	7.6	25.0	20.4	25.8	10.5
220805-144408	37.95246	-121.31856	8.3	25.0	20.6	26.0	9.6
220805-144522	37.95278	-121.31578	13.6	25.7	20.8	26.3	9.7
220805-144631	37.95305	-121.31317	14.7	25.8	21.1	26.5	10.8
220805-144743	37.95321	-121.31053	15.6	25.7	21.3	26.7	10.1
220805-145002	37.95328	-121.30678	17.5	26.2	21.6	27.1	9.2
220805-145113	37.95329	-121.30484	19.7	26.5	21.8	27.2	8.9
220805-145224	37.95325	-121.30291	18.1	26.5	22.0	27.4	9.1
220805-145335	37.95332	-121.30098	17.2	26.2	22.2	27.6	8.1
220805-145445	37.95363	-121.29913	15.0	26.2	22.3	27.7	10.0
220805-145558	37.95392	-121.29721	14.7	26.2	22.5	27.9	10.5
220805-145709	37.95397	-121.29756	14.1	26.1	22.4	27.9	11.2
220805-145819	37.95366	-121.29937	16.6	26.2	22.3	27.7	10.8
220805-150041	37.95336	-121.30304	19.3	26.5	22.0	27.4	9.4
220805-150151	37.95342	-121.30488	18.0	26.3	21.8	27.3	9.8
220805-150303	37.95334	-121.30678	16.6	26.2	21.6	27.1	9.6
220805-150414	37.95331	-121.30851	15.1	25.7	21.5	27.0	10.1
220805-150524	37.95324	-121.31019	15.6	25.9	21.3	26.8	9.6
220805-150634	37.95330	-121.31179	14.1	25.7	21.2	26.7	10.8
220805-150747	37.95334	-121.31437	12.7	25.7	21.0	26.5	13.4
220805-150857	37.95326	-121.31670	10.4	25.5	20.7	26.3	12.7
220805-151118	37.95294	-121.32147	8.7	25.3	20.3	25.9	9.5
220805-151228	37.95266	-121.32423	8.6	25.2	20.1	25.6	9.9
220805-151339	37.95239	-121.32696	7.8	25.0	19.9	25.4	10.1
220805-151450	37.95221	-121.32970	8.0	25.2	19.6	25.2	9.2
220805-151600	37.95208	-121.33238	7.9	25.1	19.4	25.0	9.4
220805-151711	37.95125	-121.33469	8.2	25.0	19.2	24.8	9.5
220805-151822	37.94948	-121.33624	8.5	23.9			5.9
220805-151933	37.94890	-121.33672	8.7	23.7			1.5
220805-152154	37.94641	-121.34031	8.9	23.6			0.2
220805-152305	37.94463	-121.34187	9.0	23.6			0.1
220805-152416	37.94328	-121.34389	9.0	23.6			0.1
220805-152528	37.94183	-121.34564	9.3	23.5			0.1

220805-152639	37.94037	-121.34435	9.2	23.6			0.0
220805-152748	37.94139	-121.34534	8.4	23.6			0.1
220805-152900	37.94314	-121.34393	8.4	23.6			0.1
220805-153011	37.94525	-121.34154	8.6	23.6			0.1
220805-153231	37.94910	-121.33648	8.3	24.1			0.1
220805-153341	37.95028	-121.33559	8.0	24.8	19.2	24.8	4.0
220805-153454	37.95156	-121.33494	7.6	24.6	19.2	24.8	5.1
220805-153604	37.95226	-121.33385	7.7	25.0	19.2	24.8	8.1
220805-153715	37.95161	-121.33262	7.8	25.2	19.4	24.9	9.1
220805-153815	37.95225	-121.33193	8.2	25.4	19.4	25.0	8.6
220805-153938	37.95233	-121.33061	8.4	25.5	19.5	25.1	8.8
220805-154026	37.95215	-121.32980	8.1	25.3	19.6	25.2	9.1
220805-154307	37.95194	-121.32680	7.7	25.1	19.9	25.4	9.5
220805-154419	37.95240	-121.32578	9.1	25.6	20.0	25.5	8.7
220805-154530	37.95266	-121.32456	7.7	25.1	20.1	25.6	9.9
220805-154641	37.95268	-121.32330	8.0	25.2	20.2	25.7	9.4
220805-154752	37.95276	-121.32206	7.8	25.1	20.3	25.7	9.6
220805-154902	37.95230	-121.32084	8.4	25.2	20.4	25.9	9.5
220805-155014	37.95320	-121.31994	8.5	25.3	20.5	25.9	9.2
220805-155125	37.95204	-121.31870	9.9	25.7	20.6	26.0	9.1
220805-155345	37.95332	-121.31759	11.5	25.6	20.7	26.0	10.5
220805-155457	37.95284	-121.31709	13.7	26.0	20.7	26.1	10.7
220805-155607	37.95168	-121.31647	14.6	26.2	20.8	26.2	10.7
220805-155718	37.95294	-121.31626	12.2	25.9	20.8	26.1	10.8
220805-155829	37.95369	-121.31587	12.4	26.0	20.8	26.1	10.8
220805-155940	37.95222	-121.31542	16.1	26.4	20.9	26.2	9.9
220805-160050	37.95289	-121.31483	13.9	26.1	20.9	26.2	10.0
220805-160202	37.95263	-121.31390	14.2	26.1	21.0	26.3	10.4
220805-160424	37.95313	-121.31163	16.6	26.4	21.2	26.4	9.7
220805-160533	37.95320	-121.31047	16.2	26.3	21.3	26.5	9.8
220805-160644	37.95322	-121.31096	15.2	26.2	21.3	26.5	9.4
220805-160756	37.95316	-121.31293	13.9	26.1	21.1	26.3	10.2
220805-160907	37.95307	-121.31490	12.6	26.0	20.9	26.1	10.7
220805-161018	37.95287	-121.31645	12.4	25.8	20.8	26.0	11.4
220805-161129	37.95309	-121.31735	12.3	25.9	20.7	25.9	11.3
220805-161240	37.95276	-121.31779	11.7	25.7	20.7	25.9	11.9
220805-170042	37.95287	-121.31861	9.3	26.2	20.6	25.0	10.3
220805-170153	37.95293	-121.32107	8.8	25.9	20.4	24.8	10.2

220805-170304	37.95275	-121.32442	8.5	26.1	20.1	24.6	9.6
220805-170415	37.95250	-121.32780	8.2	26.2	19.8	24.3	9.4
220805-170525	37.95219	-121.33110	8.0	26.0	19.5	24.0	10.9
220805-170636	37.95200	-121.33443	7.4	25.7	19.2	23.8	10.5
220805-170747	37.95195	-121.33482	7.2	25.5	19.2	23.7	9.7
220805-170858	37.95190	-121.33473	7.2	25.5	19.2	23.7	9.7
220805-171119	37.95194	-121.33544	8.0	24.5	19.1	23.6	8.4
220805-171230	37.95263	-121.33861	8.3	24.6	18.8	23.3	3.6
220805-171342	37.95331	-121.34192	8.4	25.0	18.5	23.1	3.2
220805-171453	37.95407	-121.34454	8.5	25.0	18.3	22.8	2.4
220805-171602	37.95431	-121.34569	8.7	25.3	18.2	22.7	1.9
220805-171714	37.95497	-121.34808	8.9	25.6	18.0	22.5	2.4
220805-171825	37.95576	-121.35036	9.2	25.6	17.7	22.3	2.9
220805-171936	37.95654	-121.35265	8.8	25.9	17.5	22.1	3.5
220805-172156	37.95815	-121.35702	9.3	26.2	17.1	21.7	4.7
220805-172307	37.95857	-121.35822	9.4	26.0	17.0	21.5	4.2
220805-172418	37.95841	-121.35862	9.2	25.8	17.0	21.5	3.9
220805-172530	37.95833	-121.35866	8.9	25.5	17.0	21.5	3.8
220805-172639	37.95829	-121.35864	9.0	25.6	17.0	21.5	3.5
220805-172749	37.95823	-121.35858	9.1	25.8	17.0	21.4	3.4
220805-172902	37.95943	-121.36011	8.7	25.8	16.8	21.3	3.7
220805-173013	37.96132	-121.36230	8.7	25.7	16.5	21.0	3.7
220805-173234	37.96510	-121.36686	7.7	25.9	15.9	20.4	3.8
220805-173345	37.96704	-121.36912	6.3	25.7	15.6	20.2	4.7
220805-173455	37.96901	-121.37128	7.6	25.8	15.3	19.9	4.7
220805-173606	37.97092	-121.37359	7.5	25.8	15.0	19.6	5.1
220805-173717	37.97118	-121.37409	7.8	25.8	15.0	19.5	4.6
220805-173828	37.97109	-121.37407	7.6	25.8	15.0	19.5	4.8
220805-173938	37.97104	-121.37407	7.7	25.7	15.0	19.5	4.6
220805-174050	37.97096	-121.37405	7.6	25.8	15.0	19.5	6.5
220805-174310	37.97358	-121.37673	7.7	25.6	14.6	19.1	3.9
220805-174421	37.97557	-121.37885	5.9	25.7	14.3	18.8	26.5
220805-181443	37.97946	-121.38350	7.3	25.7	13.7	17.7	4.0
220805-181553	37.98061	-121.38499	7.1	25.6	13.6	17.5	3.5
220805-181704	37.98202	-121.38660	6.9	25.9	13.4	17.3	4.5
220805-181815	37.98397	-121.38888	7.1	25.8	13.1	17.0	4.9
220805-181926	37.98581	-121.39134	6.7	25.6	12.8	16.7	5.2
220805-182037	37.98671	-121.39309	6.7	25.6	12.6	16.5	5.0

220805-182147	37.98655	-121.39330	7.0	25.8	12.6	16.5	4.6
220805-182258	37.98647	-121.39329	7.1	25.8	12.6	16.4	4.9
220805-182519	37.98645	-121.39310	7.0	25.8	12.6	16.4	3.7
220805-182630	37.98697	-121.39392	6.4	25.8	12.5	16.3	4.0
220805-182741	37.98829	-121.39659	6.5	25.6	12.2	16.0	3.7
220805-182852	37.98934	-121.39964	7.0	25.9	11.9	15.7	4.5
220805-183003	37.99032	-121.40270	7.1	25.9	11.6	15.5	4.1
220805-183113	37.99148	-121.40563	6.3	25.9	11.4	15.2	4.8
220805-183224	37.99258	-121.40854	6.8	25.9	11.1	14.9	5.0
220805-183336	37.99371	-121.41158	5.9	25.6	10.8	14.6	6.5
220805-183558	37.99465	-121.41448	6.2	25.8	10.5	14.3	5.3
220805-183710	37.99459	-121.41442	6.4	25.9	10.5	14.3	5.2
220805-183820	37.99449	-121.41440	6.6	26.0	10.5	14.3	4.0
220805-183930	37.99518	-121.41679	6.4	25.8	10.3	14.0	4.7
220805-184042	37.99557	-121.42003	6.3	26.1	10.0	13.7	5.1
220805-184153	37.99529	-121.42325	6.4	25.9	9.7	13.5	5.6
220805-184304	37.99477	-121.42645	6.1	25.9	9.4	13.2	5.6
220805-184415	37.99429	-121.42963	6.6	26.1	9.1	12.9	5.9
220805-184635	37.99419	-121.43590	6.3	26.1	8.6	12.3	7.1
220805-184747	37.99494	-121.43889	6.1	25.9	8.3	12.0	8.5
220805-193512	37.99567	-121.44051	6.3	26.3	8.1	10.8	7.4
220805-193624	37.99697	-121.44304	5.9	26.1	7.9	10.5	8.8
220805-193733	37.99833	-121.44541	6.1	26.1	7.6	10.2	8.7
220805-193845	37.99995	-121.44763	6.3	26.2	7.3	9.9	8.6
220805-193956	38.00178	-121.44955	6.5	26.3	7.1	9.7	8.3
220805-194108	38.00373	-121.45112	6.3	26.2	6.8	9.4	8.6
220805-194218	38.00578	-121.45254	6.4	26.2	6.6	9.1	9.0
220805-194329	38.00782	-121.45408	6.3	26.1	6.3	8.9	11.1
220805-194549	38.01170	-121.45715	6.6	26.2	5.8	8.3	9.6
220805-194700	38.01374	-121.45865	6.1	25.8	5.5	8.1	9.9
220805-201930	38.00817	-121.45376	6.1	25.6	6.3	8.0	8.2
220805-202042	38.00570	-121.45255	6.4	25.7	6.6	8.2	8.0
220805-202154	38.00297	-121.45104	6.3	25.6	6.9	8.5	8.1
220805-202305	38.00042	-121.44921	6.3	25.6	7.2	8.7	7.9
220805-202415	37.99825	-121.44690	6.4	25.7	7.5	9.0	7.8
220805-202526	37.99655	-121.44392	6.8	25.9	7.8	9.3	7.4
220805-202637	37.99507	-121.44084	6.8	26.0	8.1	9.5	7.5
220805-202749	37.99374	-121.43758	6.4	25.9	8.5	9.8	7.5

220805-203009	37.99374	-121.43048	5.9	25.6	9.1	10.3	7.0
220805-203120	37.99440	-121.42692	5.9	25.7	9.4	10.6	6.7
220805-203229	37.99493	-121.42342	6.0	25.8	9.7	10.9	6.4
220805-203341	37.99636	-121.42032	5.7	25.6			5.6
220805-203451	37.99802	-121.41772	5.6	25.4			5.4
220805-203604	37.99872	-121.41449	5.6	25.3			5.2
220805-203713	37.99860	-121.41129	5.7	25.3			5.0
220805-203825	37.99862	-121.40805	5.9	25.8			5.0
220805-204035	38.00257	-121.40475	5.9	25.9			3.9
220805-204159	38.00497	-121.40216	5.9	25.7			3.8
220805-204308	38.00605	-121.39924	6.0	25.7			3.4
220805-204419	38.00724	-121.39626	6.2	25.9			3.2
220805-204530	38.00846	-121.39347	6.5	26.0			2.1
220805-204641	38.00977	-121.39070	6.5	26.1			2.5
220805-204752	38.01091	-121.38796	6.8	26.5			1.5
220805-204903	38.01215	-121.38577	6.5	26.4			1.8
220805-205122	38.01586	-121.38592	8.3	26.7			1.2
220805-205233	38.01817	-121.38680	8.2	26.5			0.9
220805-205511	38.02249	-121.38957	8.0	26.2			0.2
220805-205622	38.02382	-121.39207	8.2	26.0			0.1

4. An Application of the Si3D Hydrodynamics Model to the Stockton Deep Water Ship Channel: Physics and Model Application

The following section contains the final report describing the initial application of the Si3D model to the Stockton Deep Water Ship Channel. At the time the report was completed, the model only represented barotropic forcing, viz., the effects of tides on water motion. The impact that vertical stratification had on water motions (the baroclinic forcing) was developed at a later stage in the project.

AN APPLICATION OF THE SI3D HYDRODYNAMICS MODEL TO THE STOCKTON DEEP WATER SHIP CHANNEL: PHYSICS AND MODEL APPLICATION

Stephen Monismith and Jim Hench, Stanford University

Peter Smith, USGS

William Fleenor, Laura Doyle, and S. Geoffrey Schladow, UC Davis

May 2008

Report for CALFED ERP-02D-P51

Executive Summary

This report describes the physics and three-dimensional modeling of the Stockton Deepwater Ship Channel (DWSC) in summer. Besides tides, the physical processes that we find are important reflect the importance of temperature stratification. Like a lake, the DWSC is heated by the sun, cooled by evaporation, and mixed by the wind at the surface as well being mixed from underneath by turbulence produced at the bottom by tidal flows. While the top-bottom temperature difference is generally less than 3 deg C, this amount of stratification significantly alters turbulent mixing of momentum and thus changes the vertical distribution of currents from what would be expected for a homogeneous water body. For example, during two field experiments (August 2004 and 2005), we observed vertically sheared flows, similar to gravitational circulation, although with upstream flow at the surface, i.e. in the sense opposite to usual estuarine circulation. By implication, stratification also alters the vertical transport of dissolved substances like dissolved oxygen. However, unlike lakes, even at the height of summer, the DWSC appears to stratify and de-stratify every day. The implication for the biogeochemistry/water quality of the DWSC remains to be clarified.

At the scale of the Delta, the overall spatial gradients in depth-averaged temperature reflect a balance between surface heat fluxes, downstream advection and dispersion. Notably, dispersion plays a significant role such that temperatures are elevated in the middle of the DWSC relative to both upstream riverine and downstream estuarine temperatures. The thermal energy balance inherent to this model suggests a longitudinal dispersion coefficient, $K_x \approx 1000$ m^2 s^{-1}, a value far in excess of what might be expected from existing descriptions of shear flow dispersion in rivers and estuaries, i.e. 100 m^2 s^{-1} or less (Fischer et al 1979). Dispersion in the DWSC appears to result from a combination of how water parcels navigate the array of junctions and how flows in different connected channels are phased. Although given that multiple channels are involved also means that the dispersion may also have similarities to the chaotic dispersion model of Ridderinkhof and Zimmerman (1992). Indeed scale dependence should be expected since particle clouds that remain in a given channel only experience the kind of shear flow dispersion described by (7) whereas as particle clouds that span a significant portion of the Delta effectively feel the dispersive effects of a number of channel junctions leading (hypothetically) to the large dispersion coefficients we infer from our simple model and from observations.

A major aspect of this project was the application of the USGS 3D finite difference circulation code, SI3D to the DWSC. SI3D solves the governing equations for three-dimensional hydrostatic fluid

motions including the behavior of the free surface and density variations associated with salinity and temperature variations on a rectangular Cartesian grid. The version of SI3D that we used included modifications by Dr. Francisco Rueda to include the effects of surface heating and cooling. This version of SI3D had been previously used by Rueda to successfully model flows and temperature variability in Lake Tahoe.

The domain included in our model of the DWSC extended from the San Joaquin River near French Camp Slough to just downstream of Turner Cut. The horizontal resolution of the grid was 20 m and the vertical resolution was 1 m. Bathymetry was derived from the USGS bathymetry database. Flows in this domain were driven by prescribed free surface elevations at the open boundaries, creating both tidal and mean flows. These surface elevations were derived from archived DSM2 model runs. Surface heat exchanges were computed from meteorological data obtained from the Port of Stockton using standard meteorological formulae that derive fluxes from simpler measurements like wind speed.

The DWSC model was first calibrated for conditions existing in the summer of 2000. A straightforward comparison of results from this exercise to flows measured at the USGS flow station at Stockton showed an acceptable level of agreement between model and observations, although this calibration exercise revealed the importance of appropriately choosing a value of the horizontal eddy viscosity. Subject to stability constraints, this parameter should be chosen to be as small as possible to best represent the operant physics.

The second application of SI3D was to model tidal currents observed in 2004, albeit omitting density variations. This is referred to as the barotropic model since it omits baroclinic pressure gradients associated with density variations. Decomposing both modeled and observed currents and elevations into harmonic constituents, i.e. representing both as a sum of variations at tidal frequencies, revealed an important aspect of the model set up that is worth considering in future limited area modeling exercises: In order to drive sufficient flows, it appears that free-surface elevation variations computed by DSM2 are larger than what is observed. This results in an over-prediction of tidal currents in the DWSC. Although we did not do so, this does suggest that a simple reduction in DSM2 derived elevations during calibration may suffice to get accurate tidal current predictions in the DWSC.

The third application of SI3D was one that included temperature variations and baroclinic pressure gradients, i.e. the full simulation of the DWSC. Unfortunately, despite substantial effort, including attempts to simplify the geometry, we were not able to obtain a working baroclinic model of the

DWSC. Instead, the computed flows invariably developed instabilities after a few tidal cycles. We were unable to determine the source of these instabilities.

In summary, the modeling activities supported by this project showed the value and the limitations of a limited domain 3D model for practical modeling of flows in the Delta. On the good side, a physical resolution of ca. 10m in the horizontal and 1m in the vertical can be successfully run on current desktop workstations. It appears that the coupling of DSM2 to a 3D model is straightforward, although it may be necessary in future to consider modifying DSM2 outputs so that they better match observations. A more problematic issue for our modeling was the simple fact that we were never able to get the baroclinic version of SI3D to produce a stable calculation. This is disappointing because the observations make clear that baroclinic processes, notably the effects of diurnal stratification on turbulence, can have a dramatic effect on flow structure, and thus potentially on water quality. Perhaps the most important conclusion from this modeling exercise is that it is essential to support complex models with high-quality, well-designed observations.

Finally, based on our work, we make the following recommendations:

5. Any circulation modeling that is done for the Delta should use state of the art turbulence closures.
6. To capture the full range of spatial scales important to flows in the Delta, hydrodynamic modeling of the Delta should be done using an unstructured grid model.
7. The accuracy of hydrodynamic models of the Delta should be assessed using quantitative metrics.
8. If it is of interest to predict temperatures in the Delta, additional meteorological stations be added to the existing monitoring network operated by the project agencies.

Finally, it does appear that circulation models can be used to good effect in managing the Delta and to understand its functioning. Thus, we encourage their further use, especially the development and application of fully 3D models like SI3D since the physics of interest is ultimately three dimensional

Acknowledgements

This work was supported by CALFED Ecosystem Restoration grant ERP-02D-P51. The authors gratefully acknowledge the help with field work provided by a number of students and staff from Stanford (Kristen Davis, Sarah Giddings, Nick Nidzieko, Johanna Rosman,) and from Davis (Eu Gene Chung, David Jassby, Todd Steissberg, Goloka Sahoo, Josh Mantell). The field work was also made possible by the able seamanship of Jay Cuetara and John Yokimizu of the USGS. Dr.

Francisco Rueda provided considerable assistance in trying to implement SI3D for the Stockton Deep Water Ship Channel.

Introduction and background

The principal objective of this study was to understand how hydrodynamic and biogeochemical processes interact to produce reductions in dissolved oxygen concentrations in the Stockton Deep Water Ship Channel (DWSC – figure 1). Our fundamental conceptual model is that thermal stratification forms in the DWSC because mixing due to winds and mean flows is not sufficient to overcome the stratifying effects of surface heating or to adequately flush the channel. The presence of a step change in bottom elevation at the eastern end of the DWSC may also directly contribute to a low flushing rate in the ship channel. As a result, particulate BOD input to the DWSC as well as organic matter produced locally via photosynthesis, are provided with the conditions needed to settle to the sediment where they decompose, leading to the development of low oxygen concentrations near the sediment-water interface when surface oxygen exchange is insufficient to overcome the dissolved oxygen deficits in the lower layer. The process may be further exacerbated by enhanced rates of phosphorus release under anoxic conditions, which in turn will stimulate algal growth. These three physical factors – the lack of flushing, the thermal stratification and the unusual bathymetry of the system – interacting with the biological and chemical drivers of the system, combine to produce the severe water quality conditions that have been observed.

Our view of the system is based on the synthesis given in Lee and Lee-Jones (2000) who in discussing historical data for the DWSC, cite the following factors as contributing to reduced DO in the DWSC:

(1) increased residence time due to decreases in flow velocity that accompanied increases in depth due to dredging – presumably this reflects an increase in the amount of microbial degradation of organic materials that enter the DWSC from upstream;

(2) a decrease in the amount of surface re-aeration per unit volume , another effect of increased depth;

(3) decreased production of DO per unit volume by photosynthesis, again an effect of increases in flow depth, presumably without any change in photic depth.

Most importantly, these bio-geochemical processes may vary with depth. For example in the presence of thermal stratification oxygen that enters the water column via surface gas transfer as well as oxygen produced in the photic zone via photosynthesis may not be mixed vertically to the deeper parts of the water column. Phytoplankton biomass might increase in the presence of stratification when otherwise benthic grazers like *corbicula fluminae* might be able to suppress phytoplankton blooms. Conversely, sediment-water column interactions will be limited to the bottom mixed layer if

stratification forms. We hypothesize that vertical structure and stratification dynamics are central to understanding the functioning of the DWSC. Consequently, to have predictive value, any model of the DWSC, not only must correctly resolve key chemical processes related to oxygen dynamics, but must also resolve the stratification dynamics operant in the DWSC.

Given the central role hydrodynamics plays in DWSC oxygen dynamics, our field program and computations were designed to quantify the relationship between stratification dynamics and physical forcing, i.e., solar heating and tidal and mean currents. Our working hypothesis is that stratification in the DWSC forms when currents and hence bottom-produced turbulence, are weak, and that stratification breaks down when currents are strong. Since flows in the DWSC are due to both river flow and tides, "strong" currents may be the result of spring tides or of large through-flows on the San Joaquin River. It is possible that most of the time mixing is just sufficient for the system to remain well mixed, such that under low flow conditions, or during periods of particularly strong heating, the system becomes stratified, thus, as discussed above, significantly affecting the various processes that determine DO levels. Thus, our first objective is to develop a predictive relationship between stratification and physical conditions using a combination of a 3D, i.e, vertically resolved, hydrodynamic model and detailed field observations.

Secondly, given the complex hydrodynamics of the Delta, and the possibility of various modifications to these flows, i.e., the construction of an operable tide gate in Old River, it is important to be know how the DWSC is affected by overall Delta hydrodynamics. Moreover a 3D model with adequate resolution of the DWSC will be too computationally expensive to cover the entire Delta. Hence our second objective is to link a 1-D model of the Delta, most likely the community model DSM2, so as to provide appropriate forcing of our 3D model.

The rest of this report is organized as follows: We start (§2) by discussing the salient features of the field observational program carried out in August 2004 and August 2005, highlighting important physics that it was intended to model. These observations have already been reported in a data report previously submitted to CALFED (citation). Next (§3), we describe the basic structure of SI3D. Note that details of the numerical methods used can be found in Smith (2006) as well as in Rueda (2001). We also describe the grid used for subsequent modeling, the way in which boundary conditions were supplied to the model, and the initial calibration of the model to tides and mean flows for the year 2000. In §4 we discuss the application of the calibrated model minus the effects of density variations to modeling tidal flows observed in August 2004 during our first field experiment. In order to calculate effects of thermal stratification on transport and mixing, we derived estimates

of surface heat fluxes using meteorological data obtained from CIMIS and from the Port of Stockton (§5). A comparison of calculated heat fluxes with observed changes in heat content for both 2004 and 2005 shows the importance of dispersion in determining local temperatures in the DWSC. In §6 we discuss the effects of including density variations (buoyancy effects on stratification and baroclinic pressure gradients) in SI3D modeling of the DWSC domain. Unfortunately, this modeling effort was not successful in that we were not able to obtain stable model runs even when the model domain was simplified to be little more than a box. We argue that this is a result of the short length of the domain. We finish by summarizing our results and by offering suggestion for further work, most notably highlighting the importance of the need for a relatively large domain in order to model stratification effects in the DWSC.

Figure 1.1 Stockton Deep Water Ship Channel and environs

2. Overview of observations: Physical processes operant in the DWSC in summer

2.1 Overview of observations

A detailed discussion of the field observations is given in our field data report[1]. We deployed several ADCPs and thermistor chains in the DWSC in August 2004 and August 2005. The stations where these instruments were placed in shown in figure 2.1.

2.2 Thermal variability

To help understand both model dynamics and observations of the temperature field, we also obtained from the CDEC data server, other available temperature records in the San Joaquin River for the periods of the two field experiments. After some adjustments to account for inter-calibration errors (esp. in the 2005 Stanford-Davis moorings), we were able to fit our observations into the large-scale thermal behavior of the San Joaquin River. We have plotted these in color below for both 2004 and 2005 (figures 2.2 and 2.3), with the x axis in each image representing time and the y axis showing stations, arrayed with downstream (Antioch) at the top of the figure and upstream (Vernalis) at the bottom.

Both 2004 and 2005 show significant diurnal temperature variations as well as longer period variations that may either be associated with changes in meteorological forcing (esp. the latter half of 2005 which was a period of significant cooling) or in spring-neap variations in upstream (negative) heat flux due to tidal dispersion. Interestingly, the 2004 data show 2 different temperature patterns, one in which the temperatures monotonically increase up into the river and one in which the DWSC near Stockton (i.e. near RRI) is the warmest part of the San Joaquin. The 2005 data only show the latter pattern, a likely effect of larger flows in August 2005 than in August 2004. In any event, both 2004 and 2005 show the importance of heat fluxes from both the Bay and from the San Joaquin River in setting temperatures in the DWSC. For example, at a tidally averaged flow of 20 m^3/s (600 cfs), the 3 deg C drop in temperature between M0 and M5 is equivalent to ca. 100 W/m^2 surface heat flux, i.e., is comparable to significant rates of heating or cooling due to synoptic weather variability.

In addition to the importance of estimating surface fluxes correctly, the implications of these observations for modeling are two-fold:

1. The model must have approximately the correct mean flow at the upstream boundary to cool or heat the DWSC domain at the proper rate advectively.
2. The model must correctly represent tidal (shear-flow) dispersion in order to correctly cool the DWSC from the downstream end.

2.3 Barotropic flows

The observed barotropic velocities at the M2 mooring are compared to the flow measured by the USGS UVM at the Garwood bridge (the UVM station closest to the DWSC) in figure 2.4a and 2.4b. While these time comparisons look "good", it is worth looking more closely at the match As a basis for examining the quality of the fit of numerical modeling and our observations, we show a scatter plot of the 2004 UVM/M2 data in figure 2.5.

Besides comparison of the tidal variability, it is useful to look at a comparison of the low-pass M2 and UVM flows. As seen in figure 2.6, while the overall patterns are similar, there are significant differences, both in mean and variation, between low-pass filtered flows seen by the ADCP and by the UVM. These differences are likely due to the placement of the ADCP at M2 on the side of the channel (to avoid shipping) and the fact that at M2, the subtidal flow has considerable vertical structure (see §2.5) and thus may also vary significantly across the channel. Thus, the conversion between ADCP velocity and flow, i.e., the rating curve, may not be describable by a simple linear relation. This is important to bear in mind when comparing ADCP data and model results since if the model does not properly resolve the vertical and horizontal structure of the mean flow, its match to observations should be comparable to that seen in figure 2.6.

2.4 Effects of stratification on turbulence

Diurnally varying thermal stratification is a persistent feature of the DWSC in summer (Fig. 2.8). During both field experiments we carried out two 30 hour long measurement programs using a SCAMP (Self Contained Autonomous Microstructure Profiler) to measure profiles of thermal microstructure (Carter and Imberger 1986). By fitting local spectra to small-scale (ca. 1mm vertical resolution) temperature variations, the rate of turbulent kinetic energy (TKE) dissipation, ε, can be inferred. Often used to represent how energetic turbulence is locally, ε plays a critical role in the

theory of turbulent stratified flows. As discussed in Shih et al (2004, see also Ivey and Imberger 1992) it has been observed that the value of the parameter

$$A = \frac{\varepsilon}{\nu N^2} \tag{1}$$

determines the extent to which density stratification affects turbulent mixing of momentum and heat, i.e. the eddy viscosities and eddy diffusivities. Here ν is the molecular viscosity and

$$N^2 = -\frac{1}{\rho}\frac{\partial \rho}{\partial z} g \tag{2}$$

is the square of the buoyancy frequency. When $A > 200$, there is little effect of stratification whereas $200 > A > 10$, stratification progressively has more effect, reducing eddy coefficients relative to their value in unstratified flows. When $A < 10$, turbulent mixing is completely suppressed such that heat fluxes are functionally zero while modeling of weak momentum fluxes is complicated by the fact that much of the transfer of momentum is accomplished by internal waves such that eddy viscosities may not be appropriate.

A sample of the data returned by SCAMP is shown in figure 2.9. This profile was taken in the afternoon during the spring tide 30 hour experiment in 2004. Stratification formed by diurnal heating is evident throughout the water column. As seen in the panel labeled "Grad T0" , the small scale temperature gradient, turbulent mixing primarily confined to the upper 2 m or so of the water column, showing the dynamical importance of even a small (3 deg C) amount of stratification.

Figure 2.9 shows time-depth variations of the N^2 and ε while figure 2.10 shows the time-depth variation in *A*, both taken from the neap-tide 30 hour experiment in 2005. It is noteworthy that the region of large temperature gradient (large N^2), i.e., the diurnal thermocline (*sensu* Imberger 1985), descends through the day as wind and cooling generated turbulence in the upper mixed layer (the near-surface region of elevated ε) causes the upper mixed layer to deepen. There is also a region near the bed of bed-generated turbulence, but evidently surface mixing seems to dominate over near-bed mixing. This is important because it means that eddy viscosity formulations parameterized using only bed stresses, even if corrected for stratification, should not give accurate predictions of turbulent mixing. Overall, it is clear that observed diurnal stratification is important to turbulent mixing in the DWSC.

2.5 Vertically variable mean flows

As part of examining/comparing ADCP and USGS UVM data, we also looked at mean flows at our M2 mooring. Plots of the time averaged stream-wise velocity (positive is directed towards the Bay) as functions of depth are shown in figure 2.11, where it can be seen that the similarity of the two profiles is striking. Moreover both profiles are strongly sheared in a way not expected for a homogeneous water column, which should show a monotonic increase in velocity with height. Given that baroclinic pressure gradients are essentially zero in this reach, the shear in these profiles must be due to variations in turbulent shear stress divergence associated with diurnal stratification, with the largest asymmetries occurring near the bottom where the largest mean downstream flows are observed.

When combined with the turbulence microstructure measurements we reported previously, these observations suggest a potential difficulty with the standard application of SI3D to this flow. SI3D nominally uses stratification (Richardson number) corrections to turbulent channel flow eddy viscosities. In the present case, much of the turbulence variation is associated with surface convection, something not readily accounted for in the scheme the USGS version of SI3D uses. Thus to correctly represent shear in the tidal flows, the averaged effect of which is seen above, the model may need to make use of more sophisticated closures like GOTM (General Ocean Turbulence Model) which are more capable of accounting for mixing due to cooling.

2.6 Summary

The data acquired during 2004 and 2005 define the following important features of flow in the DWSC that the circulation model should be designed to represent:

(1) Shear flow dispersion is an important determinant of overall, large-scale temperature variations in the DWSC. It appears that an appropriate value of *K*, the shear flow dispersion coefficient is $O(10^3)$ m^2/s. Given the very large value of *K,* far larger than would be expected based on vertical or lateral shear in the DWSC, it may be important to properly represent the dispersive effects of the junctions in order to predict the overall temperature structure of the Delta.

(2) Local velocity measurements may vary somewhat from values inferred from gauged flows. This may define the limits of calibration accuracy for the model.

(3) The DWSC in summer is (as originally hypothesized) stratified in summer, although the stratification develops and breaks down diurnally.

(4) The observed diurnal stratification modifies vertical mixing in ways that simple eddy viscosity models are not likely to capture. However, diurnal variations in stratification and mixing give rise to a vertically sheared net flow resembling gravitational circulation and that is as strong or stronger than the depth-averaged net subtidal flow, i.e. the flow that can be influenced by reservoir releases.

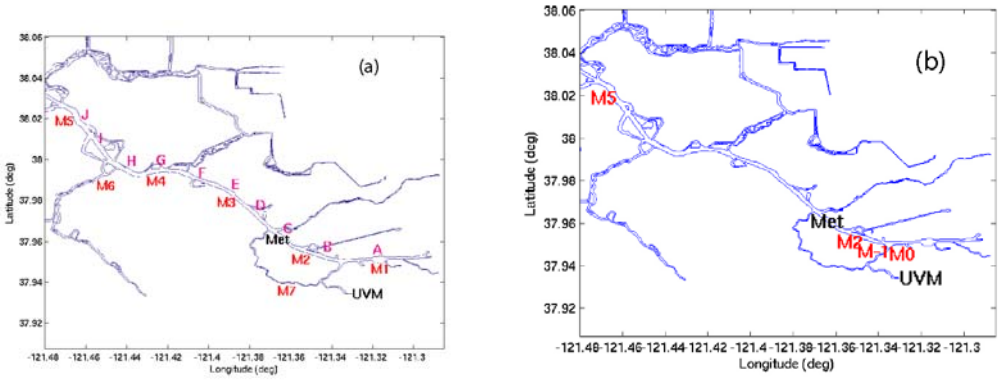

Figure 2.1 Map of study area and location of field measurements for (a) August 2004 and (b) August 2005. The letters in (a) refer to CTD transect stations.

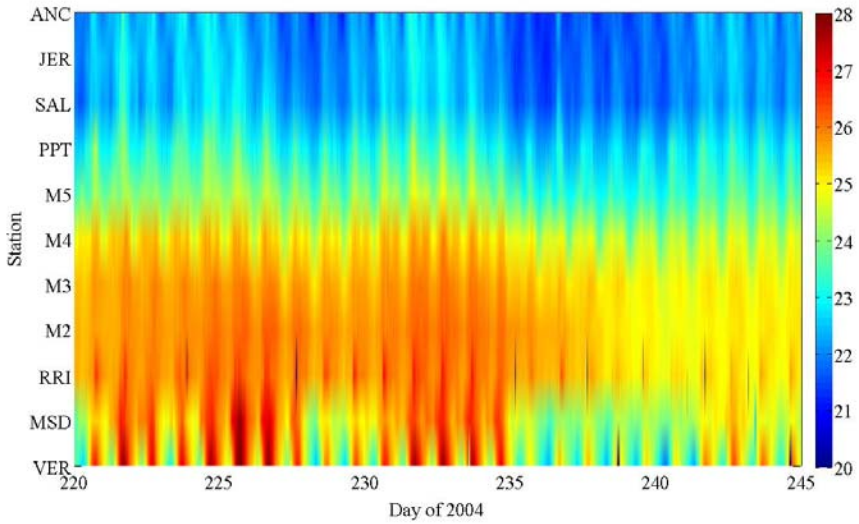

Figure 2.2 San Joaquin River July/Aug 2004: Stations are VERnalis, MoSDale, BranDT bridge, M0, Rough and Ready Island, M1, M2, M5, Prisoners PoinT, San Andreas Landing, JERsey point, and ANtioCh. All temperatures in deg C.

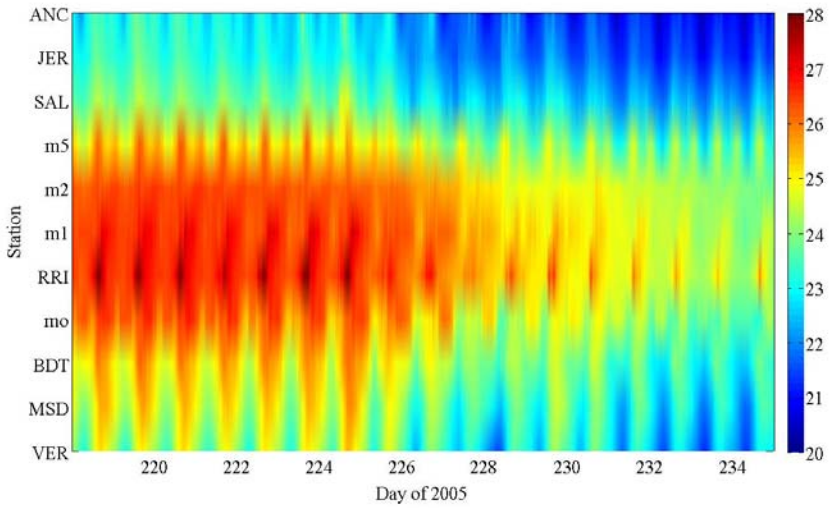

Figure 2.3 Same as figure 2.2 except for July/Aug 2005. Labels as above

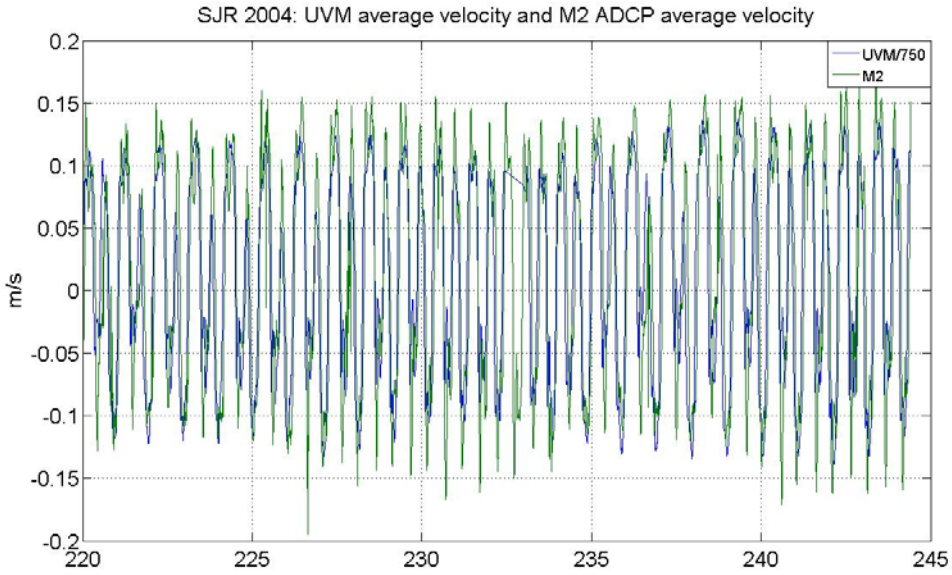

Figure 2.4a Comparison of M2 depth-averaged velocity (multiplied by 750 m^2) and the Garwood UVM for July/August 2004.

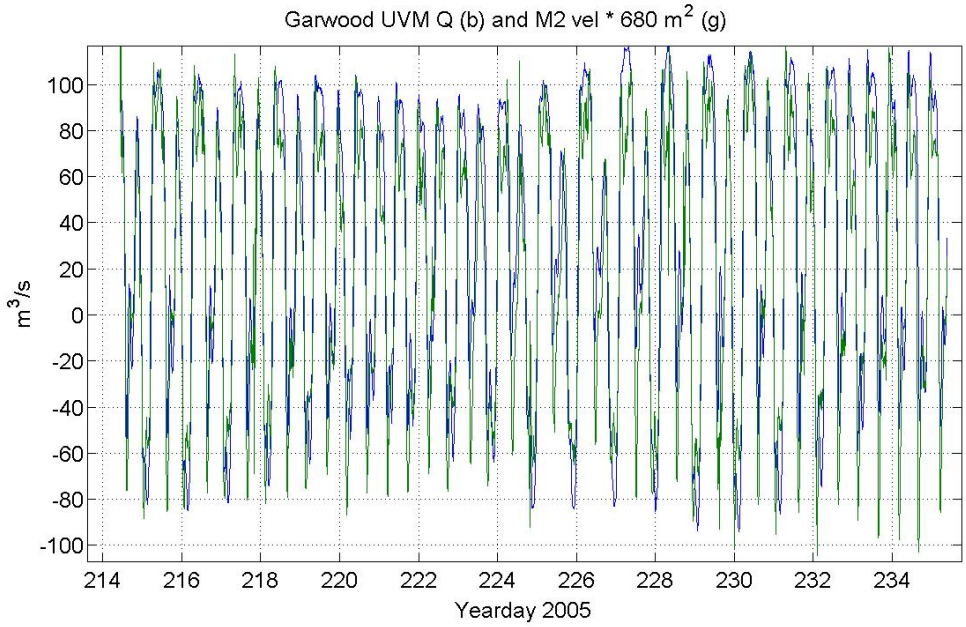

Figure 2.4b Comparison of M2 depth-averaged velocity (multiplied by 750 m^2) and the Garwood UVM for July/August 2005.

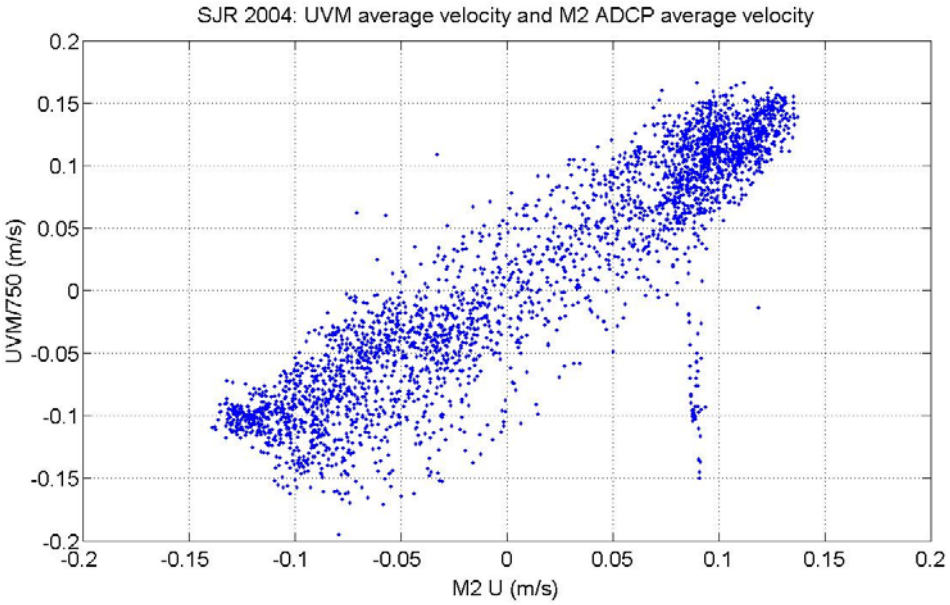

Figure 2.5 Direct comparison of UVM and M2 data for 2004.

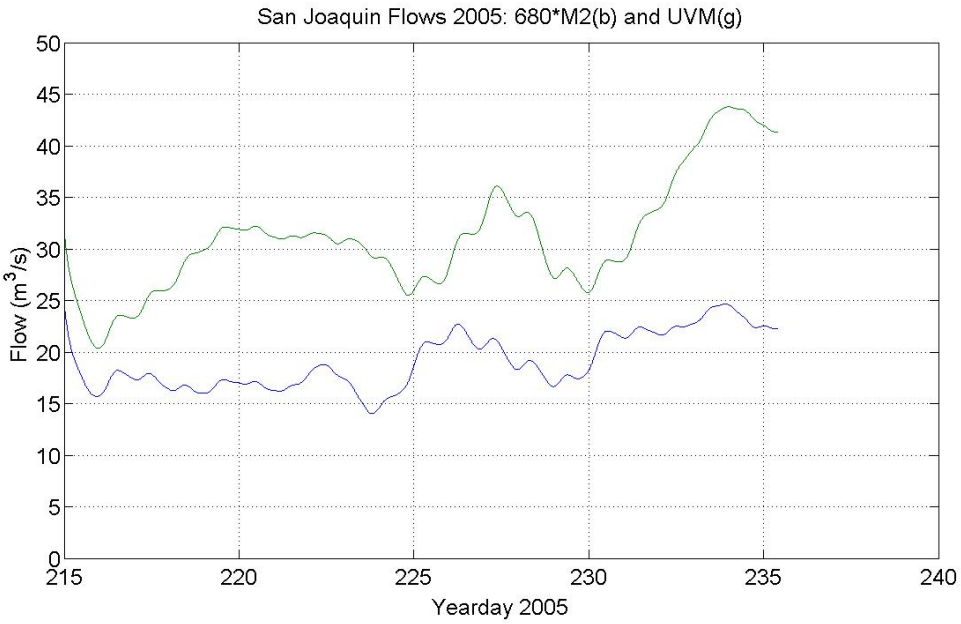

Figure 2.6 Low-pass filtered UVM data and inferred flows and M2.

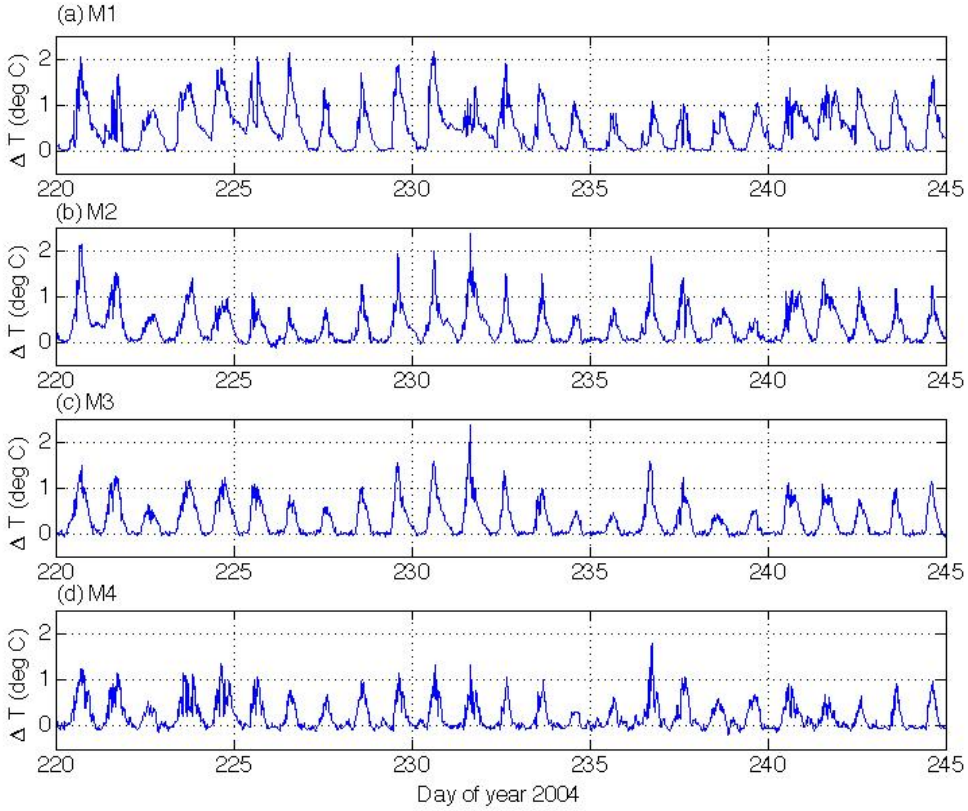

Figure 2.7: Top bottom temperature differences at Stanford/Davis DWSC thermistor chain moorings in 2004.

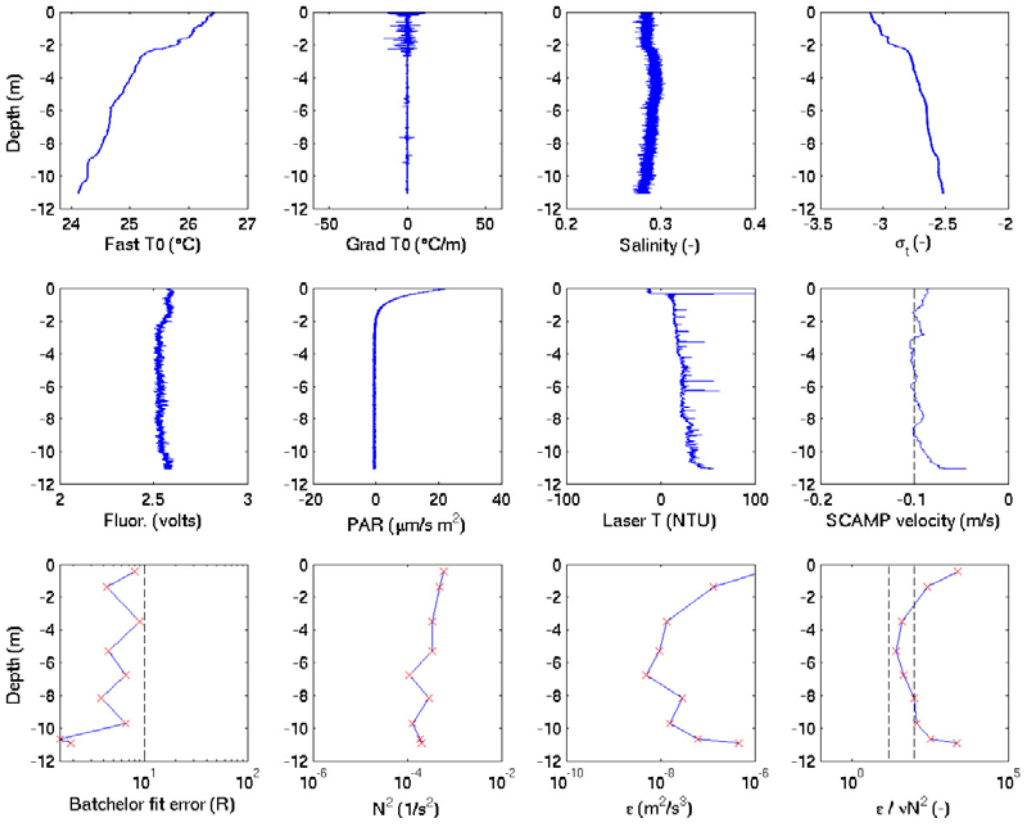

Figure 2.8: SCAMP microstructure profile data collect on the San Joaquin River at 15:30 on 16 August 2005. Note the sharp change in water mass and turbulence properties at 2 m depth.

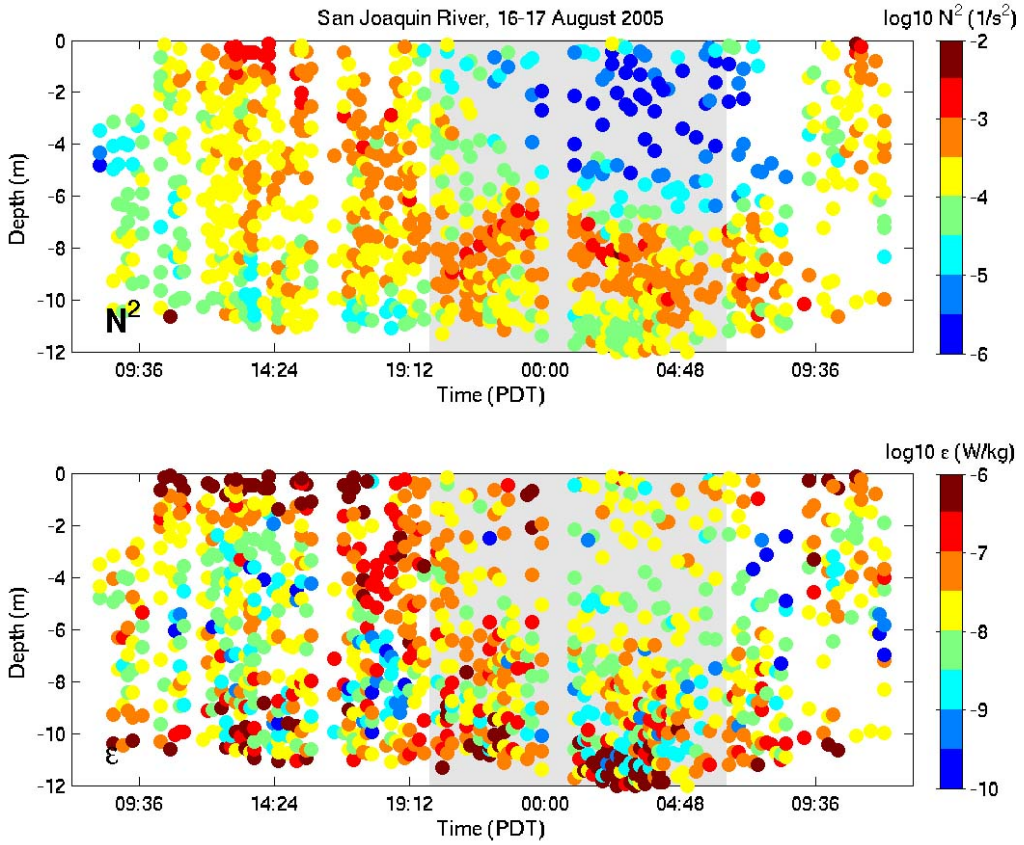

Figure 2.9: Stratification (N^2) and turbulence dissipation (ε) during the spring tide experiment in 2005.

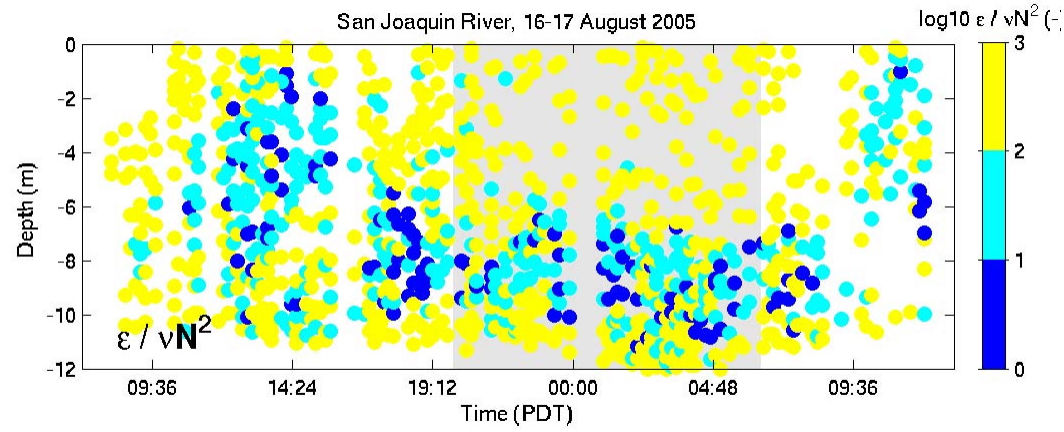

Figure 2.10: Values of A for the spring tide experiment in 2005.

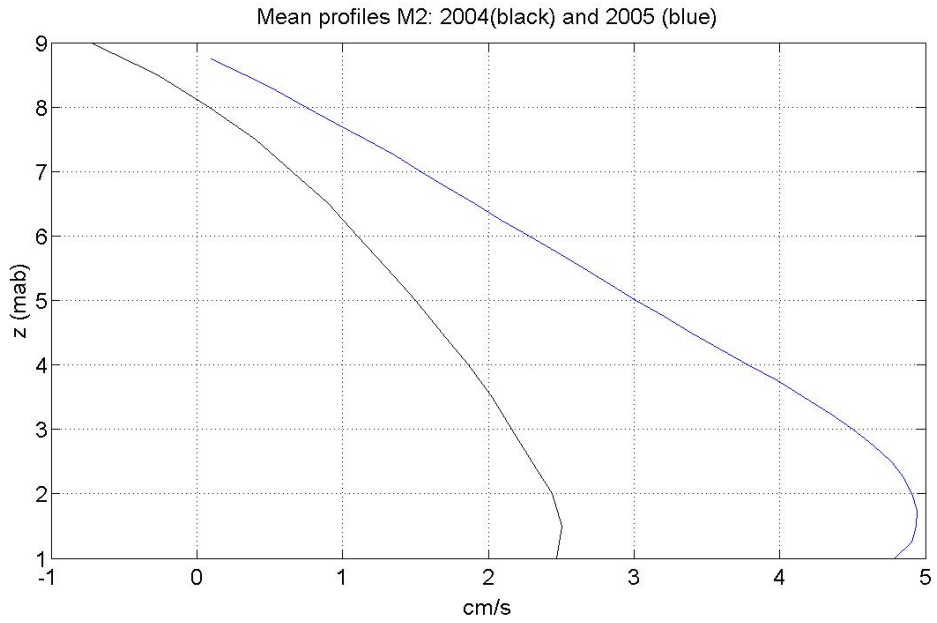

Figure 2.11: Residual flows at M2

3. SI3D: Basic structure, grid development, boundary conditions, and initial calibration[2]

3.1 Overview of the USGS code SI3D

A 3D hydrodynamic model SI3D, developed by Peter Smith of the USGS (Smith 1997, 2006), was applied to calculate flows in the region sketched in figure 2 below. SI3D numerically solves the hydrostatic Reynolds-averaged form of the Navier-Stokes equations, including transport equations for temperature and salinity, and an equation of state relating temperature and salinity to fluid density.

Depending on the version used, SI3D uses two forms of eddy viscosity. The first is a simple proscribed eddy viscosity distribution with a Richardson number based reduction due to stratification (Smith 2006). The second version (Rueda 2001) used eddy viscosities and diffusivities derived from the Mellor-Yamada level 2.5 closure (Blumberg and Mellor 1987).

At its core, SI3D uses a semi-implicit three-level leapfrog-trapezoidal fixed resolution finite difference scheme formulated on a staggered Cartesian grid (Arakawa C-grid) to solve the layered-averaged form of the 3-D shallow water equations (Smith and Larock 1993, Smith 1997, Smith and Larock 1997). The grid system is composed of horizontal layers, and the governing equations are integrated over the height of each layer. The layer integrated volume transport replaces velocity as the dependent variable so that the depth integrated continuity equation is effectively linear. The semi-implicit approach is based on treating the gravity wave and vertical diffusion terms implicitly to avoid time-step limitations due to gravity-wave CFL conditions, and to guarantee stability of the method. All other terms –including advection– are treated explicitly. This approach is similar to that followed in TRIM3D (Casulli and Cheng 1992, Gross et al 1999a,b), and avoids the use of mode splitting to solve the problem posed by a system of equations that supports both fast (barotropic or external) and slow (baroclinic or internal) waves. The leapfrog-trapezoidal algorithm used for time stepping gives second order accuracy both in time and space. The leapfrog scheme is used in the first iteration and is followed by as many trapezoidal steps as desired. The objective of the second iteration is to remove the well-known computational mode associated with the leapfrog discretization (Durran, 1999) and to increase the stability of the code.

---

[2] The modeling described in this section was carried out wholly by Dr. P.E. Smith of the USGS, the original developer of SI3D.

The layer-averaged scalar transport equation used for heat and for scalars is solved using a two-level, semi-implicit scheme that uses operator splitting (Rueda 2001). Only the vertical diffusion in the governing equation is treated implicitly, following the Crank-Nicholson or trapezoidal method. The 1-D advection operators in each of the three Cartesian directions are discretized using flux limiters. The corrected fluxes are constructed with the monotone upstream differencing scheme, the Lax-Wendroff second-order method, and the Van Leer MC limiter. Special care was taken in the design of the temperature transport model to achieve consistency with continuity (Gross 1997) that would guarantee a mass conservative scheme. The method avoids spurious oscillations in the solution that could interfere in the calculations of turbulent transfer coefficients. Those oscillations appear, in particular, in the vicinity of discontinuities and poorly resolved gradients. Such conditions could occur at the end of the Turning Basin in the Stockton Channel, where a sharp step separates the dredged portion from Lake McLeod upstream. As discussed in Rueda (2001) and in §5, radiative heating is computed using the Beer-Lambert law with observationally derived values of the attenuation coefficient while surface heat exchanges are computed using standard bulk parameterizations (see e.g. Kondo 1975).

3.2 Development of a SI3D grid for the DWSC

The goal of the present work was to build a model domain that balanced grid resolution with computational speed and memory availability. Ideally, the model horizontal resolution should match the smallest horizontal flow features expected to develop in the model domain, i.e., approximately 5 to 10 m (or less). On the other hand, as a general principle, the farther away from the area of most interest that the model boundaries can be placed the better. Thus, ideally the model should have a large domain and very fine resolution.

This ideal must be balanced by two concerns: execution speed and memory size. For example, each doubling of the horizontal grid resolution means a factor of 4 increase in memory that is required and a factor of 8 increase in computation time. At present, SI3D does not have memory mapping, i.e. it must allocate memory to all points that are inside a 3D box that encloses the domain of interest. As a result, given 32-bit operating system workstations available at the time of this project, the maximum memory that can be used is approximately 2 Gbytes. Reflecting this memory limitation and a compromise between execution speed and resolution, we chose a grid resolution of 20 m in the horizontal and 1 m in the vertical. The grid was also rotated 34 degrees from North so as to align the gird as much as possible with the main channel. As discussed in Monsen (2000), this

is necessary to minimize reduction in the flow through narrow channels which may only have one or two grid points.

The overall domain was chosen to limit the number of open boundaries as much as possible, although in the Delta this is quite challenging. The overall model domain shown in figure 3.1 has 5 open boundaries, boundaries for which stage or flow and temperatures must be specified. The basic data for the grid was obtained from the USGS and DWR databases and in some shallow areas (e.g. Burns cutoff) from NOAA nautical charts.

3.3 Boundary conditions

The model takes water level (stage) boundary conditions from DSM2 at 4 points: (1) San Joaquin River below Turner Cut (U/S end DSM channel 172) ; (2) Fourteen mile Slough (U/S end DSM channel 312); (3) Turner Cut (D/S end DSM channel 31) and the San Joaquin river below French Camp Slough (U/S end DSM channel 13). These are all shown in Figure 3.2. The datum used for both the bathymetry and the boundary water surface elevations was the National Geodetic Vertical Datum of 1929 (NGVD29). Temperature data was specified on all these open boundaries using measured data.

3.4 Calibration of the model

The model was initially applied to simulate flows and water levels only (no temperature) for September 2 to October 7, 2000 (days 245 to 280). This barotropic case was used to debug the bathymetry and to look at the effects of horizontal diffusion on model calibration.

In general the comparison between SI3D results and data from this period (drawn from the USGS hydrodynamics database) shows that when driven with DSM2 water levels, SI3D tidal predictions are quite similar to those of DSM2 (Fig 3.3-3.5). Subtidal flows are in slightly better agreement with observations (Fig 3.6), although the improvement is minor.

In contrast, including the effects of horizontal mixing of momentum seem to have quite a pronounced effect on the computed fields. In effect, discretizing the momentum equations over a finite-resolution grid should produce Reynolds stress like quantities due to unresolved sub-grid scale eddying motions. These are typically represented in the form (for one velocity component, say U)

$$A_x \frac{\partial^2 U}{\partial x^2} + A_y \frac{\partial^2 U}{\partial y^2}$$

For comparison sake, if A_x and A_y really represented turbulent motions, they would be approximately equal to du_* ; 10^{-2} m^2/s (Fischer et al 1979) for conditions typical of flows in the DWSC.

As seen in figures 3.7 and 3.8, the choice of horizontal mixing coefficients has a large influence on the computed subtidal flow. Not surprisingly, smaller values of A give results closer to observations, since the effect of increased friction due to sidewall drag, what horizontal mixing will ultimately produce, will be to slow down the flow through the DWSC. The fact that further reducing A below 0.1 m^2/s (the physically plausible value) has little effect indicates that other sources of numerical damping of the flow (e.g. the treatment of advective accelerations) effectively are stronger than the damping produced by $A = 0.01$ m^2/s and weaker than $A = 0.1$ m^2/s.

The effects of horizontal mixing also influence spatial structure of the flow as can be seen in Figure 3.9, where it can be seen that the computed flow at the junction of the San Joaquin River and the DWSC is weakened and smeared out by high values of A. Thus, it appears that it is necessary to keep $A \leq 0.1$ m^2/s(at least with the 30 m grid) to best model flows in the DWSC.

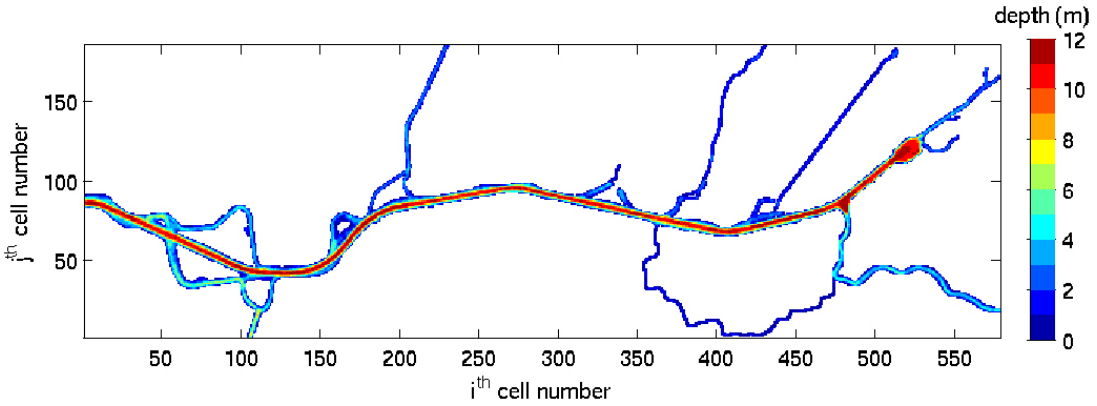

Figure 3.1 SI3D model domain showing bathymetry

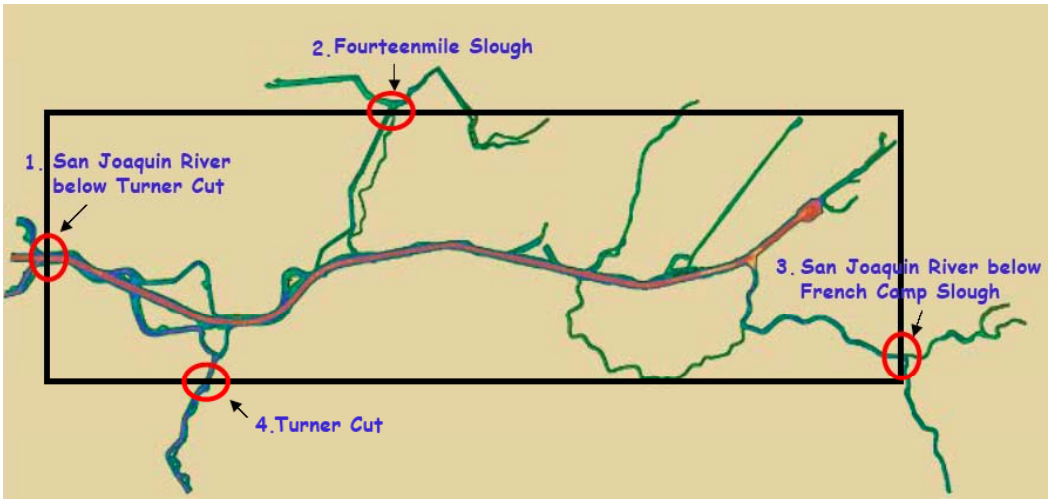

Figure 3.2 Boundary condition locations for SI3D

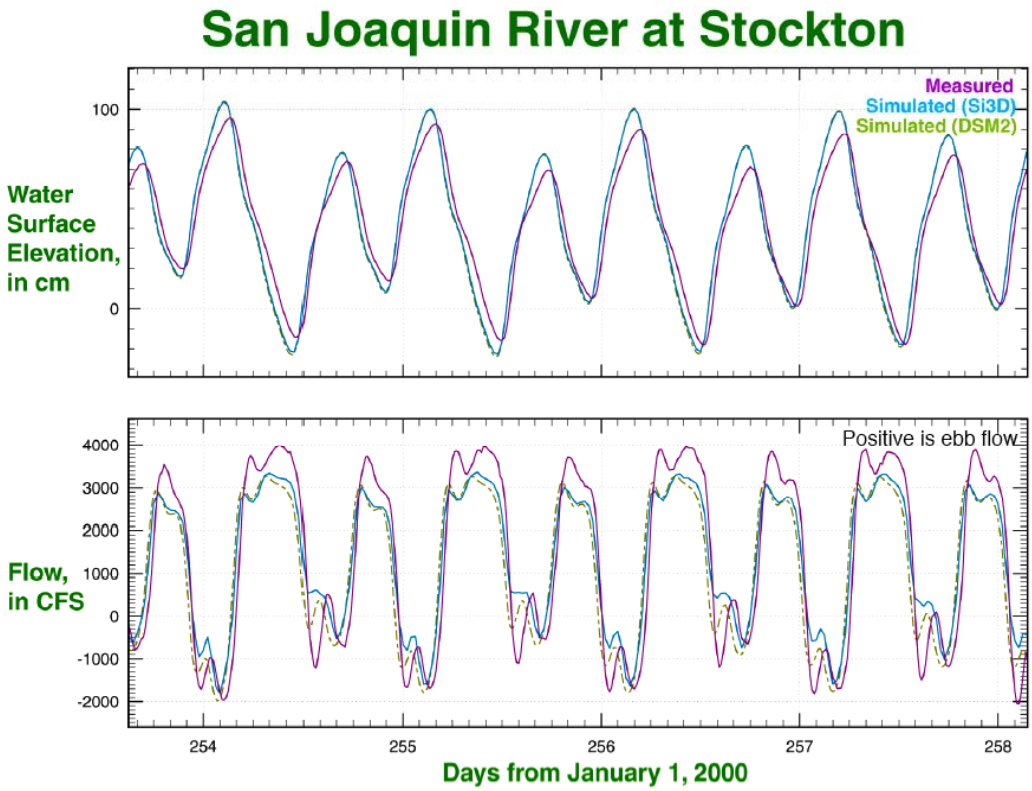

Figure 3.3: Model results for SI3D – water levels and flows in the San Joaquin River at Stockton

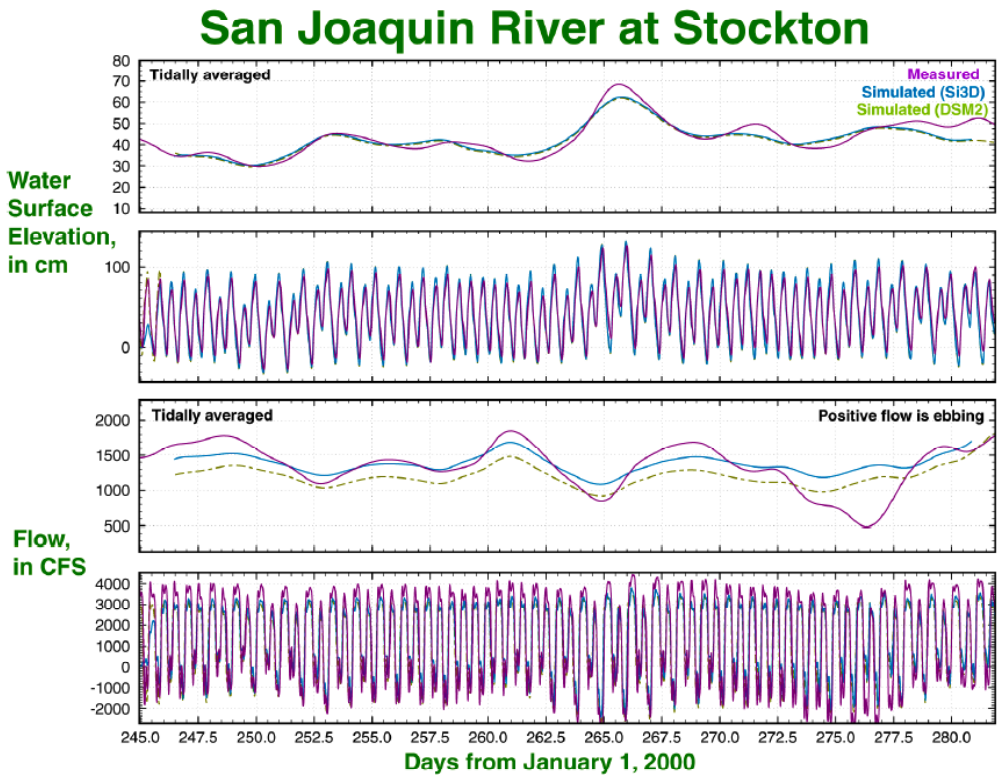

Figure 3.4: Model results for full simulation period

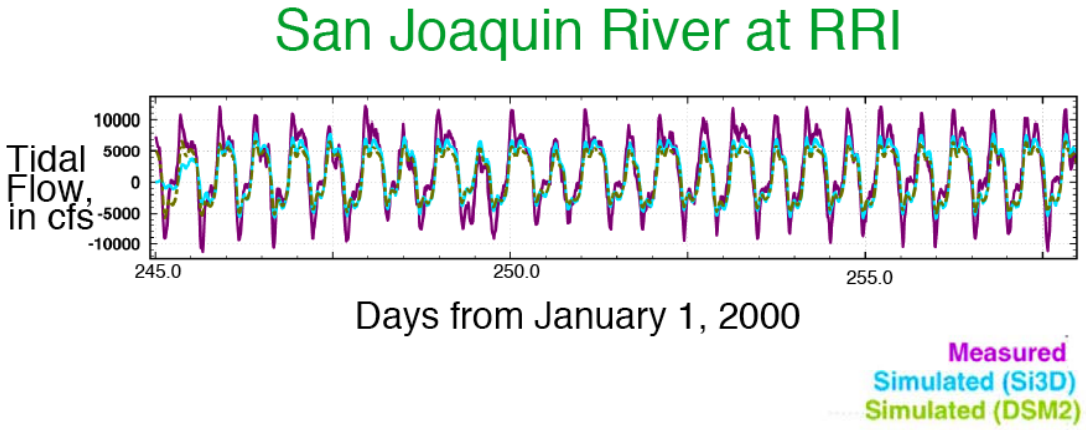

Figure 3.5: Tidal flow comparison at Rough and Ready Island

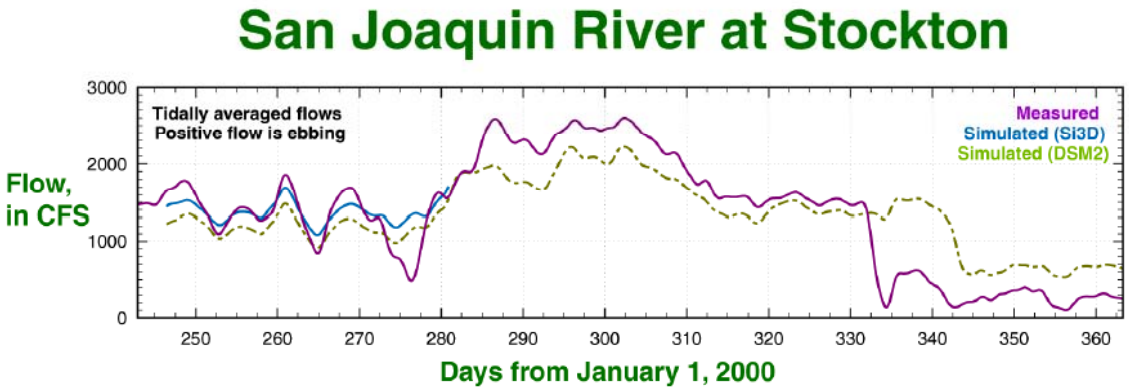

Figure 3.6 Mean flow comparison: model versus observations for flows in the Sand Joaquin River at Stockton

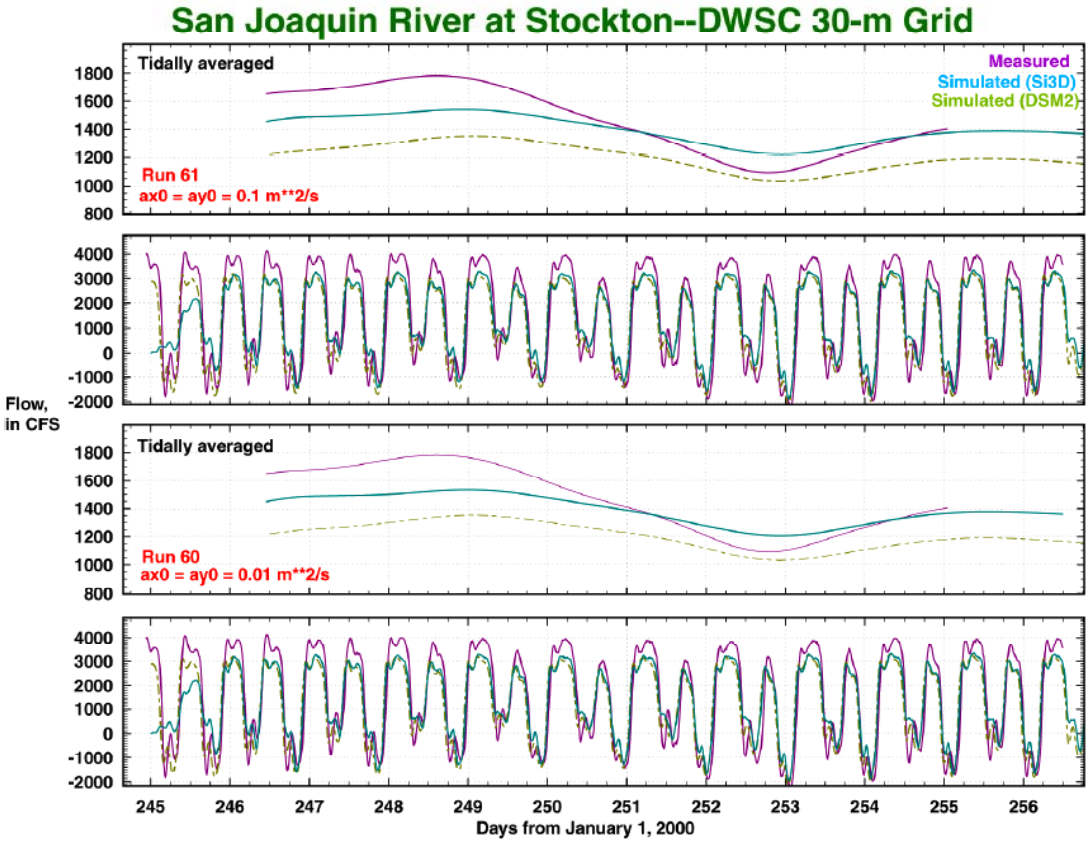

Figure 3.7 Effect of horizontal mixing coefficient on compute flows: A=(0.01,0.1) m^2/s

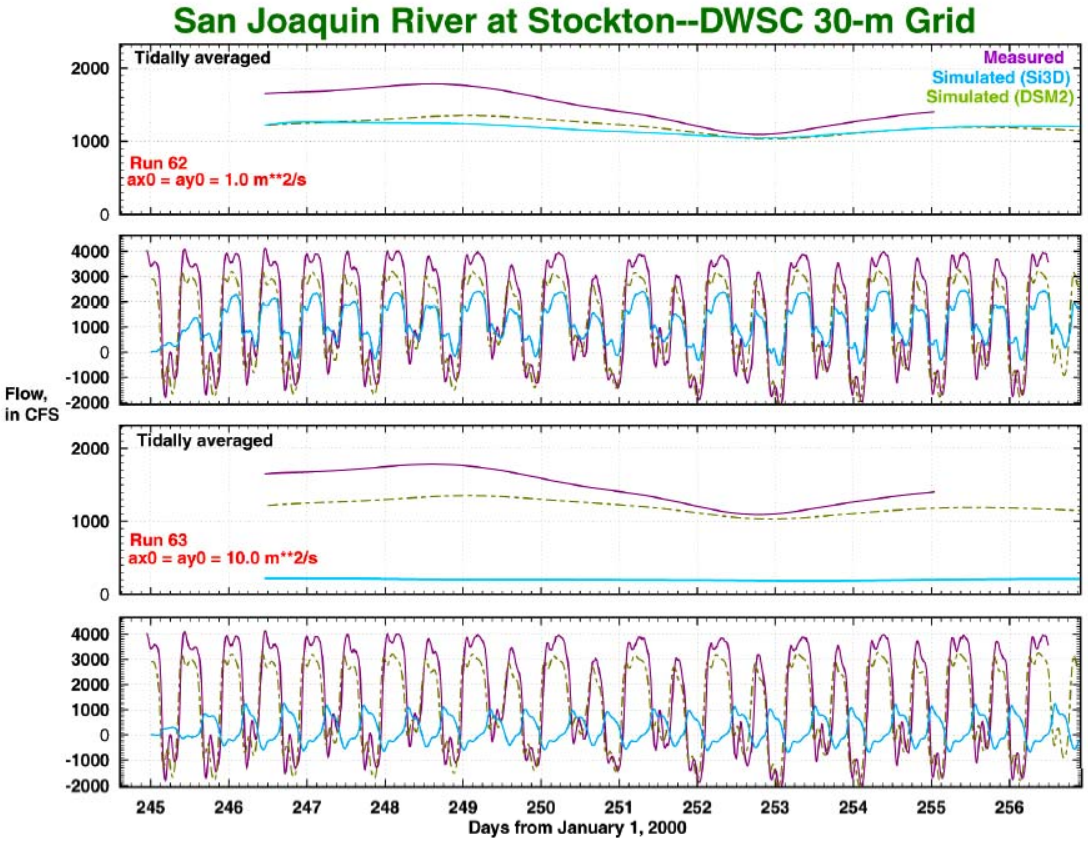

Figure 3.8 Effect of horizontal mixing coefficient on compute flows: A=(1,10) m^2/s

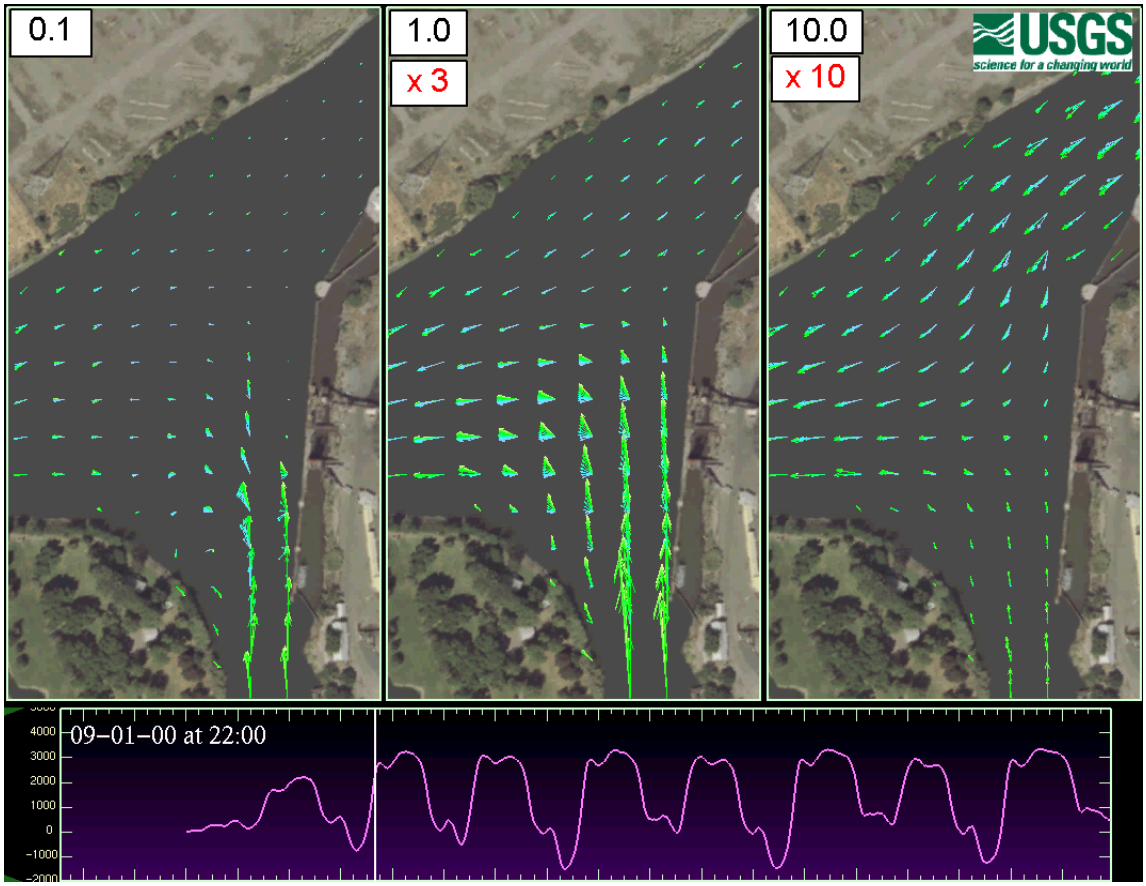

Figure 3.9 Effects of A on flow patterns at junction of San Joaquin River and DWSC – phase of tide (in terms of flow) is given in the bottom panel.

4. Calculation of the 3D Barotropic flow for August 2004

4.1 Model set up

Following initial model development and calibration, we applied SI3D to model the flows in the DWSC for the August 2004 experimental period. Our initial efforts focused on computing flows and water levels as was done for the 2000 runs, i.e. in the absence of stratification and buoyancy effects. As before, the model was driven with water levels on open boundaries derived from DSM2. All of the calculations were done on Apple G5 Macintosh workststations with compilation done using the Absoft Fortran compiler.

4.2 Water level results

Figure 4.1 shows a sample result for water level at various stations throughout the DWSC. Note that this comparison is not a stringent test since the boundaries are reasonably close to all points in the interior and there is little phase difference between the two ends of the channel. Consequently, water levels in the interior of the domain largely reflect the boundary conditions. Rather than just plot one time series on top of another, we also used a scatter plot to examine the correspondence of measured and modeled water surfaces (Figure 4.2). This comparison shows clearly that while the correlations are generally good with $r^2 > 0.87$ for all of the data, a systematic deviation is apparent with the model generally showing higher water levels on the high tides than was observe.

This comparison can also been using harmonic analysis (see e.g. Gross et al 1999a). In this case both observed and modeled elevations and velocities can be decomposed into tidal constituents (see e.g., Emery and Thomson 2004):

$$\zeta = \sum_n A_n \cos\left(\omega_n t + \phi_n\right) \tag{3}$$

where A_n is the amplitude, ω_n is the (known) frequency and ϕ_n is the phase of the nth tidal constituent. Both A_n and ϕ_n are determined by least-squares fitting of the data (or model results) to (3). Generally the most important tidal constituents are M2, S2 K1, and O1, where the first two of these are the principal semi-diurnal components and the latter two are the principal diurnal components. Longer period tides, notably Msf, the fortnightly tide, are possible while in shallow waters like the DWSC, non astronomical periods like M4 (quarter-diurnal) can also arise through non-linear interaction of astronomically-forced tides.

The results of this comparison for water levels in August 2004 are shown in figure 3.3. The comparison of observed and modeled constituents shows that model M2 and K1 amplitudes are

systematically too large, even near the oceanic open boundary, suggesting that the 2004 DSM2 model output used to force SI3D overestimates the semi-diurnal forcing relative to observed values. The fact that DSM2 tides are too high may be attributed to the fact that the 1D model of DSM2 requires stronger pressure gradients, i.e. larger tides, to achieve a given flow. Thus if the calibration of DSM2 was done optimize flows, it might be expected that water levels might differ from reality.

4.3 Comparison of computed and observed flows

Currents also exhibit some differences between observations and model (figure 4.4). While the phasing of currents looks good, the model shows less shear in the water column than is observed. This effect is quite pronounced in the harmonically decomposed velocity profiles (figure 4.5), which show significant differences in both the M2 and K1 velocity profiles. The reason that observed profiles are more sheared in the water column than are modeled ones is not clear, although it is possible that this represents an effect of stratification on vertical mixing of momentum, which would tend to increase water column shear while reducing near-bed currents and hence near-bed shear. Additionally, as expected given that tidal variations in water level are too large, the overall amplitudes of M2 and K1 are also too large.

4.4 Summary

Application of the barotropic version of SI3D, as calibrated for 2000 conditions to the time period of the 2004 field experiment show decent agreement between modeled and observed flows, although significant differences emerge. Notably, because forcing with DSM2 water levels is too strong, water level variations are too large and tidal currents are too strong. Moreover, at least the barotropic version of the model does not properly reflect the real vertical shear observed in the DWSC.

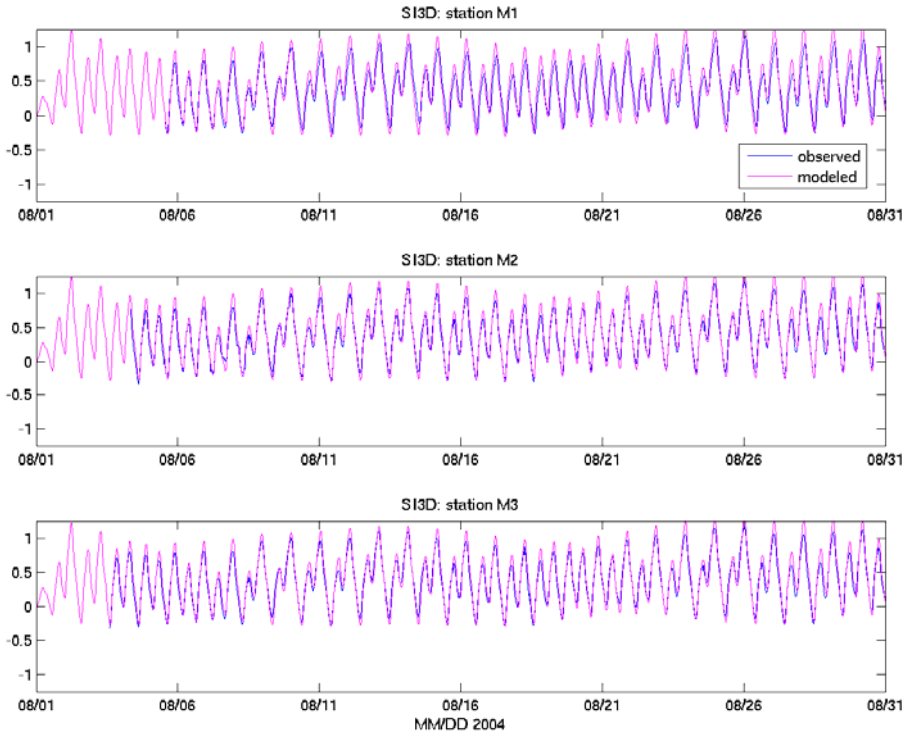

Figure 4.1 Time-series comparison of observed and modeled water levels for August 2004 at selected station in the San Joaquin River.

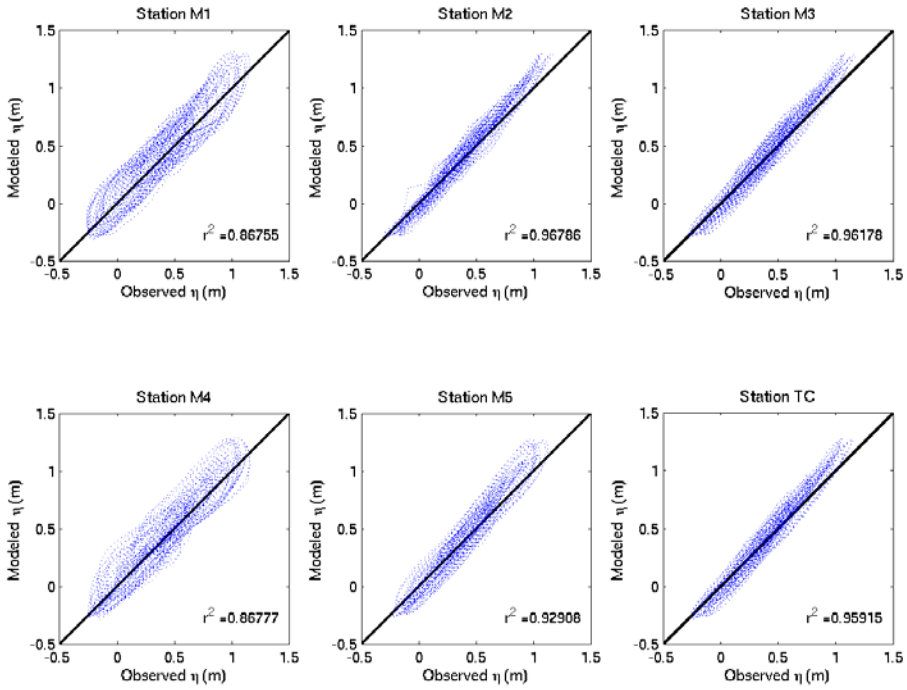

Figure 4.2 Comparison of modeled and observed water levels at selected stations in the San Joaquin River.

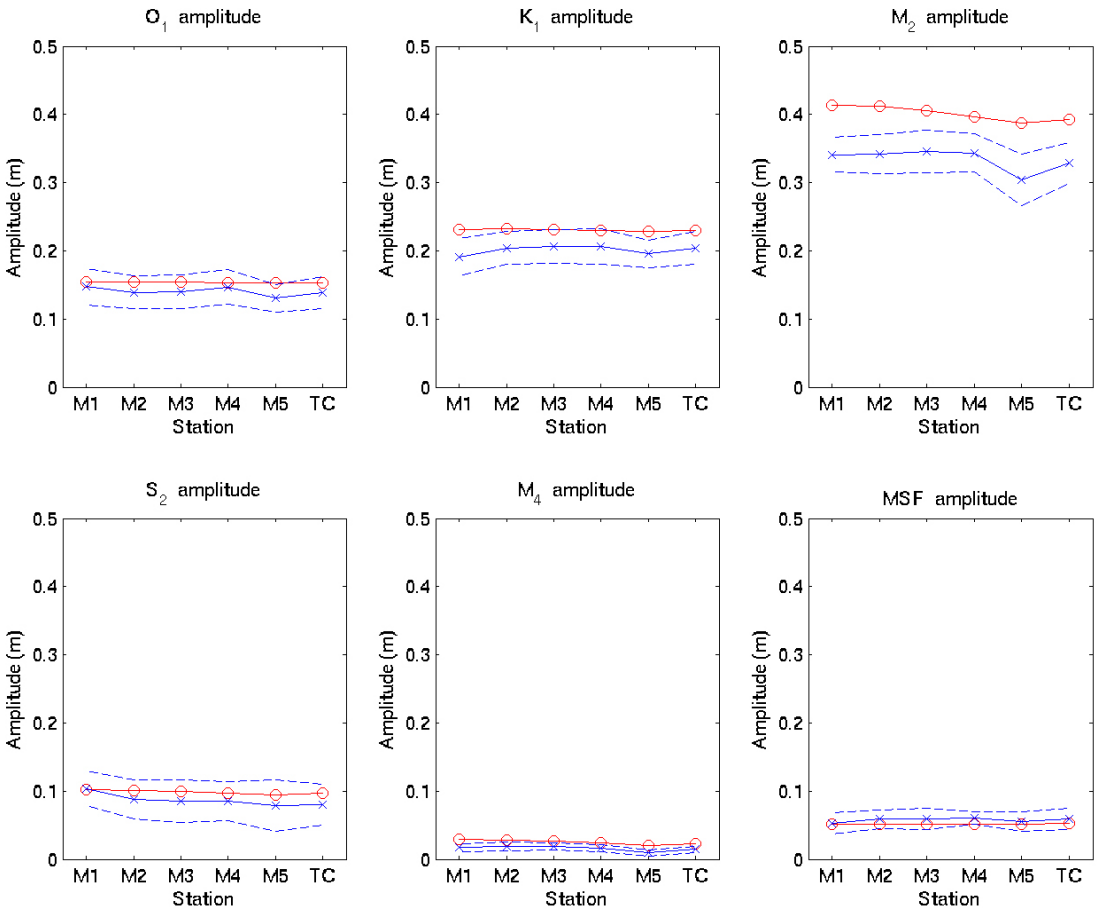

Figure 4.3 Comparison of observed (blue) and modeled (red) water level tidal constituents. Dashed blue lines indicate 95% confidence intervals on observed values.

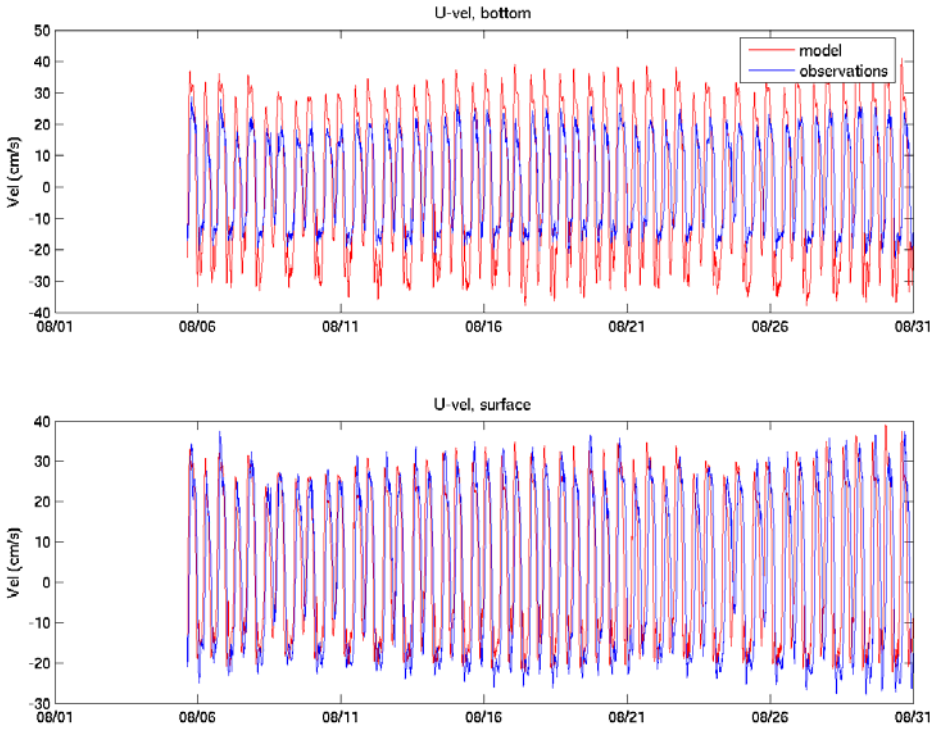

Figure 4.4 Comparison of 2004 observed (blue) and modeled (red) velocities at Station M5, from a barotropic SI3D simulation.

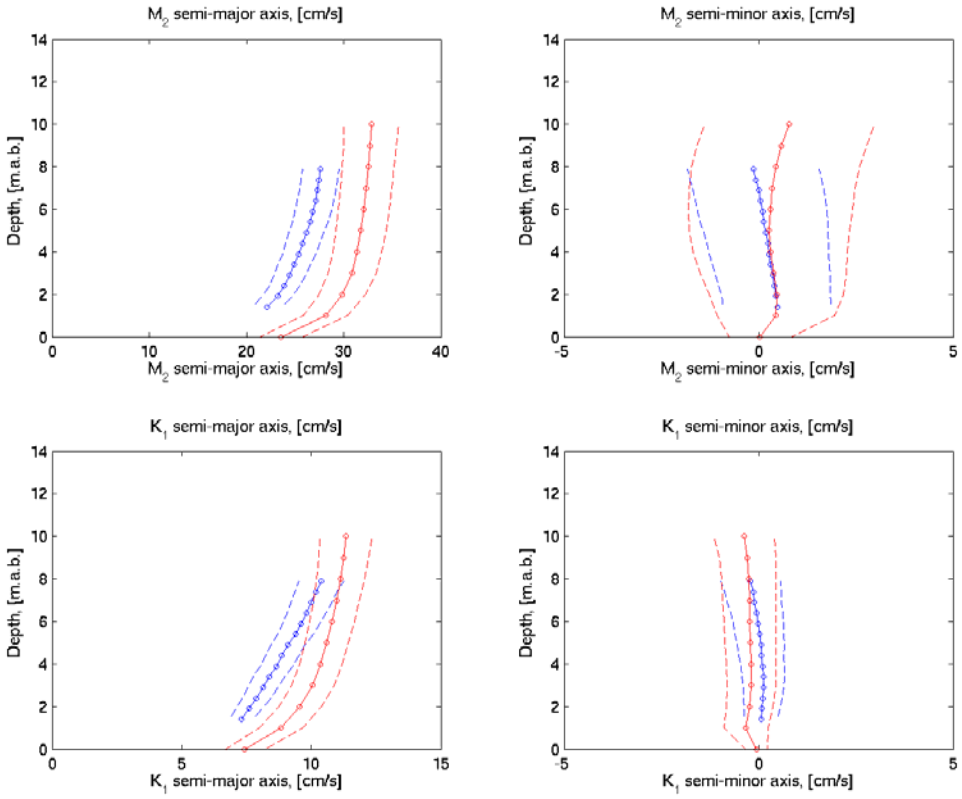

Figure 4.5 Comparison of 2004 observed (blue) and modeled (red) tidal ellipse parameters from harmonic analysis at Station M5.

5. Heat fluxes for temperature modeling

The shortwave radiation Q_{sw} is usually measured directly, although it can be calculated given knowledge of cloud cover. Unlike the other components of the surface heat flux, Q_{sw} penetrates into the water column according to Beer's law:

$$Q_{sw}(z) = Q_{sw}(z)\exp(\beta z) \tag{4}$$

where β^{-1} is the effective extinction depth for light. Often (4) is modified to be the sum of three terms reflecting different extinction lengths for different portions of the visible spectrum.

Q_{lw} is the difference between incoming infrared radiation from the sky and outgoing infrared radiation from the water surface. The standard model for Q_{lw} is:

$$Q_{lw} = 5.23 \times 10^{-8} T_s^4 - 5.18 \times 10^{-13} T_a^6 \left(1 + 0.2C^2\right) \tag{5}$$

where T_s is the water surface temperature, T_a is the atmospheric temperature (measured ideally at 10m above the water surface), and *C* is the fraction of sky covered with clouds. The dependence on clouds is the result of blackbody radiation by water moisture in the atmosphere.

H_l the surface heat loss due to evaporation, is parameterized in terms of air density, ρ_a, latent heat of evaporation, L_w, the wind speed U_{10}, the relative humidity at 10 m, *r*, and the saturation humidity at the water surface temperature, $q_s(T_s)$

$$H_l = \rho_a L_w C_l U_{10} \left(q_s - q(r, T_a)\right) \tag{6}$$

The exchange coefficient $C_l \approx 0.0015$ is an empirical function of fetch and atmospheric stability. In a like fashion, the sensible heat flux is given as

$$H_s = \rho c_p C_s U_{10} \left(T_s - T_a\right) \tag{7}$$

where c_p is the heat capacity of water at constant pressure and $C_s \approx C_l$ is also an empirical constant.

Assuming that Q_{sw} is known, to compute heat fluxes one needs U_{10}, T_a, T_s, *r*, and *C*. In SI3D, all heat fluxes can be specified, or they can be computed using model-computed values of T_s. This latter approach has the advantage of providing negative feedback; if the model gets warmer than observations, the heat losses will be greater than in reality, whereas if the model is tending to be

colder, heat losses will be less. In either case, the model temperature should be driven towards the observed one. This behavior is well known in thermal models of lakes.

To provide the variables needed to compute heat fluxes in the model, meteorological data were obtained from the Port of Stockton (wind speed and direction, air temperature and relative humidity) and for the CIMIS[3] weather station in Manteca (incident shortwave radiation), approximately xx km from our M2 mooring. Combined with our surface temperature data, these sets of meteorological data were used to compute heat fluxes (latent, sensible and net longwave) using the set of Matlab™ routines describe by Palowiscz et al (2001). Because we did not have any data on cloud fraction, i.e. the portion of the sky covered by clouds, we assumed a clear sky ($C = 0$) for all our calculations.

These calculated fluxes for 2004 and 2005 are shown in figure 5.1 and 5.2, where it can be seen that latent heat fluxes make up a significant fraction of the overall thermal energy balance, although an uncertainty in the net longwave radiation due to uncertainty about cloud cover can easily be 10 W/m^2 . To assess the fidelity of this heat flux, we compared the cumulative change in heat content with the change in thermal energy content at the M2 mooring for both 2004 and 2005 (figures 5.3 and 5.4). In both cases, the computed fluxes show net heating whereas the observations in general do not.

The observed and calculated changes in heat content can be reconciled by a two step process: (1) assuming that subtidal variations in heat content that are not accounted for by surface heat fluxes are due to dispersion (Fischer et al 1979), they can be removed by subtracting off the difference in low-pass filtered (4^{th} order Butterworth, f_c=0.5 cpd) heat contents; (2) multiplying the latent heat and sensible heat fluxes by empirical factors the such that the remaining differences do not vary systematically with either latent and sensible heat fluxes shows systematic errors. This latter

[3] CIMIS url

adjustment should account for the fact that the standard bulk formulae parameters, which have been derived from open ocean measurements, may not be accurate for the limited fetches of our system and that the wind and humidity measurements at the Port of Stockton may not fully characterize the true fields of wind speed and humidity over the SJR.

The results of this process are shown in figures 5.3 (2004), 5.4 (2005) and 5.5 (errors for 2005).

Making these adjustments to the heat flux shows a downriver dispersive heat flux in both years of ca. 100 to 200 W/m^2, with the sign of the flux correct for Fickian diffusion-like process. We can check the consistency with known values of shearflow dispersion for estuaries of ca. 10-1000 m^2/s (Fischer et al 1979), by examining an integrated version of the heat conservation equation (see e.g. Edinger et al 1980)

$$A(x)\frac{\partial T}{\partial t} - Q_f \frac{\partial T}{\partial x} = \frac{\partial}{\partial x}\left(K(x)A(x)\frac{\partial T}{\partial x}\right) - \frac{WH}{\rho c_p} \qquad (8)$$

Here A is the cross-sectional area, Q_f is the river flow, T is the temperature, K is the dispersion coefficient, W is the local width, and H is the surface heat flux in watts/m^2. The x axis points upstream and a positive heat flux represents a loss of heat from the water.

If we integrate (8) from $x=x_0$, the downstream end of DWSC where to the upstream end at Vernalis, $x=x_1$ and assume that the surface heat flux is uniform (in the absence of any other data) we find that

$$\int_{x_0}^{x_1} A(x)\frac{\partial T}{\partial t}dx \;;\; (x_1 - x_0)\overline{W}\,\overline{H}\frac{\partial \overline{T}}{\partial t}$$

$$\int_{x_0}^{x_1} -Q_f \frac{\partial T}{\partial x}dx = -Q_f T\Big|_{x_0}^{x_1} = -Q_f\left(T(x_1) - T(x_0)\right)$$

$$\int_{x_0}^{x_1} \frac{\partial}{\partial x}\left(K(x)A(x)\frac{\partial T}{\partial x}\right)dx = K(x)A(x)\frac{\partial T}{\partial x}\Big|_{x_0}^{x_1} \approx -K(x_0)A(x_0)\frac{\partial T}{\partial x}(x_0)$$

$$\int_{x_0}^{x_1} -\frac{WH}{\rho c_p}dx = -(x_1 - x_0)\frac{\overline{W}\overline{H}}{\rho c_p}$$

where overbar quantities are averages between x=x_0 and x=x_1 . Thus,

$$\rho c_p \overline{H}\frac{\partial \overline{T}}{\partial t} + H; \; -\frac{\rho c_p K(x_0)A(x_0)\frac{\partial T}{\partial x}(x_0)}{\overline{W}(x_1 - x_0)} + \rho c_p Q_f \frac{\left(T(x_1) - T(x_0)\right)}{\overline{W}(x_1 - x_0)} \qquad (9)$$

Note that the LHS of (9) is the thermal energy balance calculated minus any correction so that the RHS is the correction, i.e. the RHS = O(100 W/m^2). From figure A6, we have $\partial T/\partial x \approx 0.1$ deg/km at x_0, while $x_1 - x_0 \approx 40$ km, and $T(x_1) - T(x_0) \approx$ 0.7 deg C. For 2004, $Q_f \approx 5$ m^3/s, so the second term on the right is ca. 4 W/m^2. Thus the correction must mostly be due to tidal dispersion at the downstream end, with $K \approx 1000$ m^2/s required to satisfy (9).

This value of K is at the large end of what is typically found for rivers and estuaries (see Fischer et al 1979) and most likely reflects the dispersive effects of the numerous channel junctions and bifurcations along the SJR. Most importantly, we see that subtidal dispersive heat fluxes are comparable to net surface heat exchanges and thus in order for a circulation model be able to predict temperatures in a system like the SJR, it must do a reasonable job at predicting dispersive heat fluxes as well as making use of accurate surface heat fluxes.

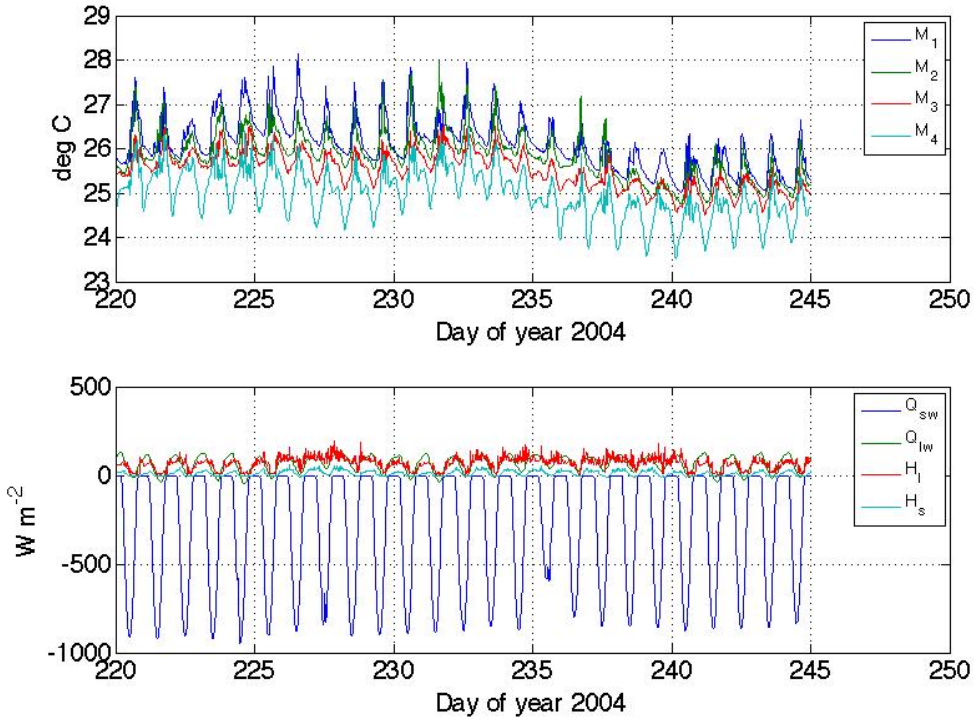

Figure 5.1 Temperatures and heat fluxes for 2004

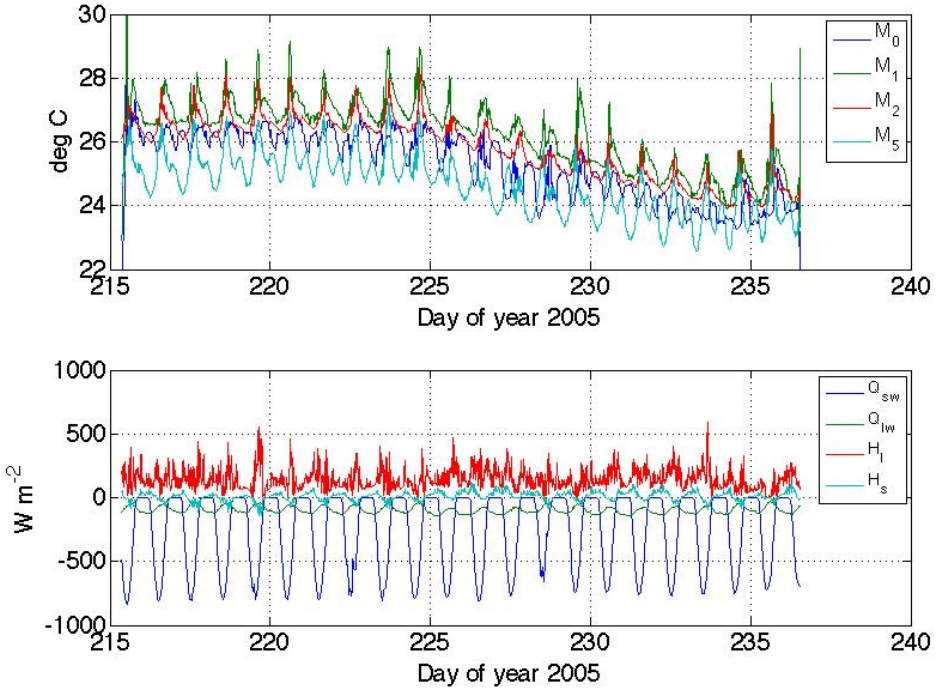

Figure 5.2 Temperatures and heat fluxes for 2005

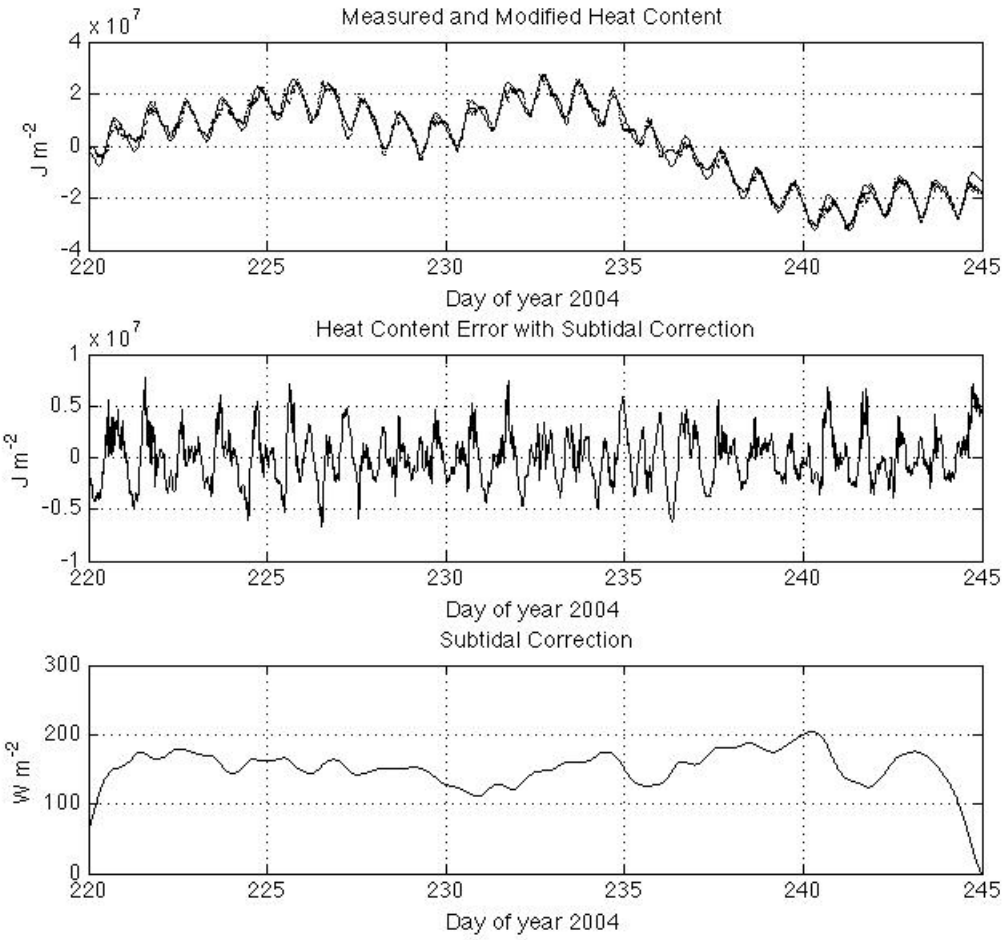

Figure 5.3 Heat content including corrections for 2004

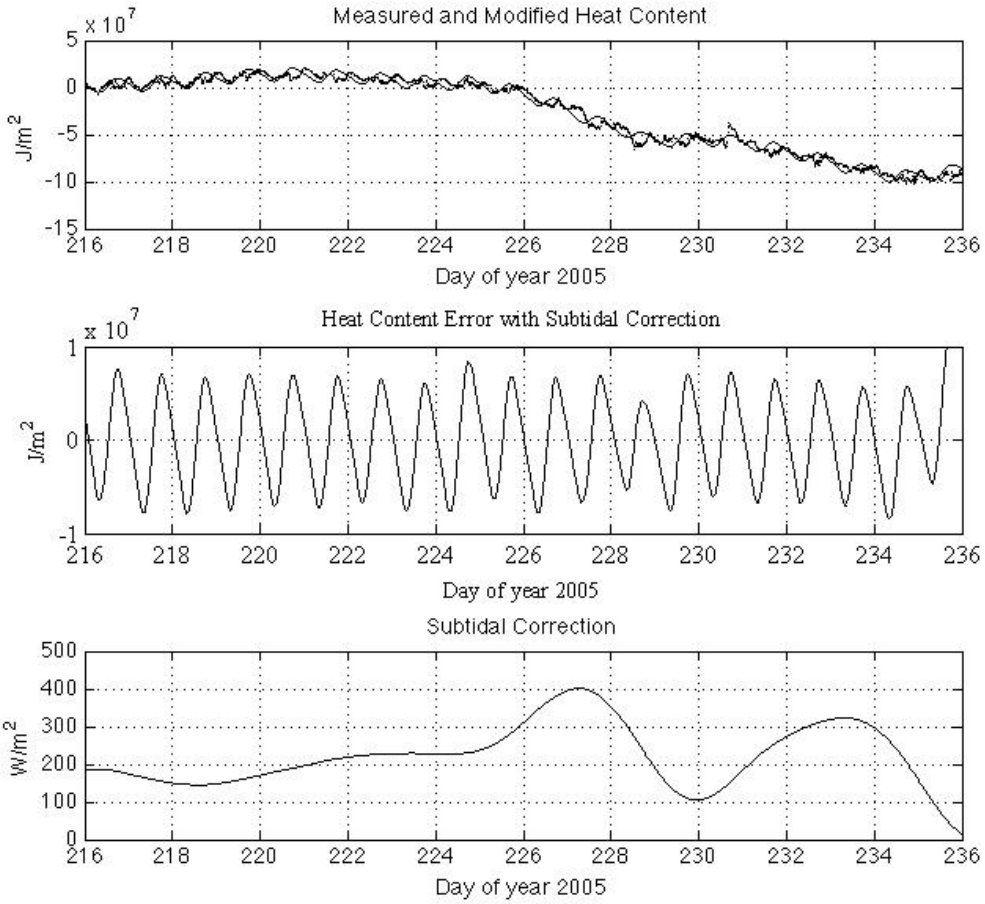

Figure 5.4 Heat content including corrections for 2005

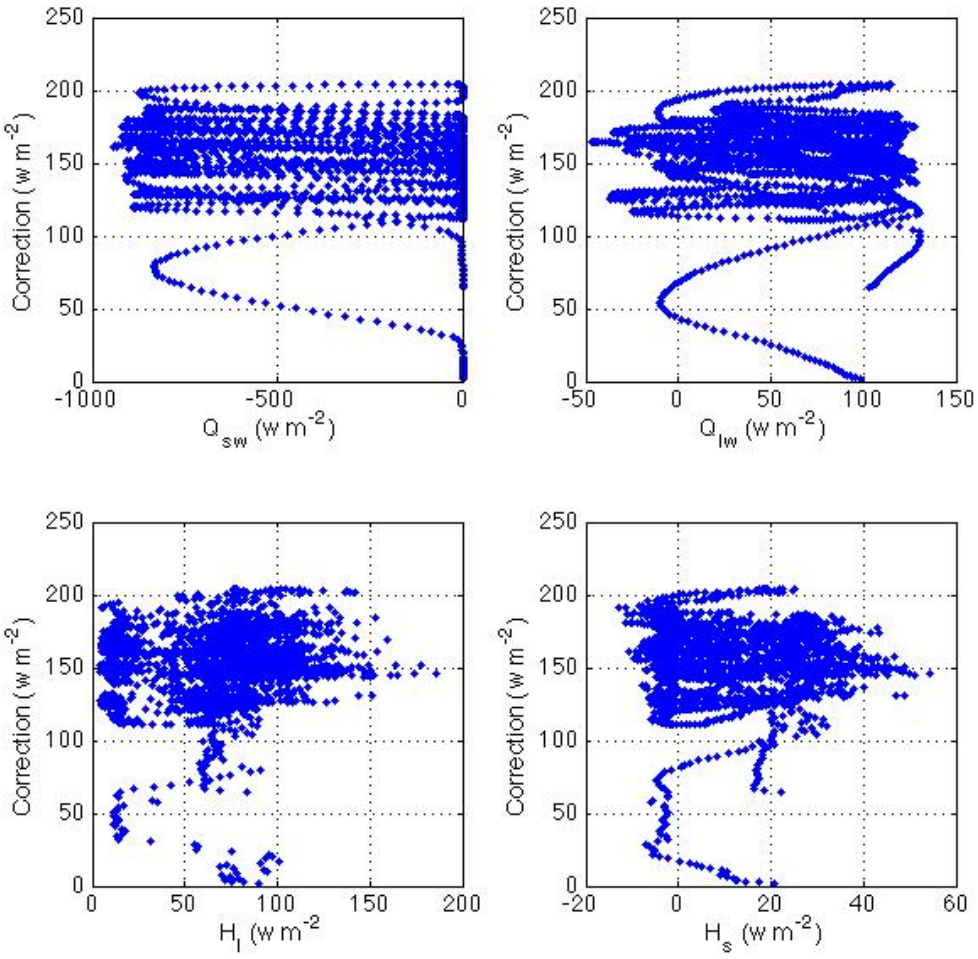

Figure 5.5 Heat flux differences for 2004

6. Calculation of the 3D baroclinic flow

Using the barotropic forcing discussed above (§3 and 4) and the heat fluxes (§5) discussed above, we attempted to run the full set of conditions, i.e. tidal and thermal forcing for 2004. The model used was the extended version of SI3D developed by Dr. Francisco Rueda as part of his PhD at UC Davis (Rueda 2001). This code has been used successfully to model flows in lakes (see e.g. Rueda and Schladow 2003, Rueda et al 2003). Our experience was somewhat different.

Turning on thermal forcing caused the model results to "blow up", i.e. caused the model to become unstable developing unphysical oscillations in computed velocities and temperatures such that no useable results could be achieved with baroclinic forcing. An example of this behavior is shown in figure 5.1, a sample output from one such run. The $2\Delta x$ oscillations seen in the vertical velocity near the end of the run are typical of problems that develop with accurate numerical methods, like the leap-frog trapezoidal SI3D uses when some stability boundary is crossed. We were not able to properly identify the appropriate stability condition.

Once this instability emerged, we tried a number of different strategies to pin down the source of the problem:

Work continued with the 3D circulation model, trying to obtain physically realistic simulations of thermal stratification. Our initial work with the full grid of the San Joaquin River proved unsuccessful, and model runs went quickly unstable. A large number of runs were made to diagnose and correct this problem including:

- runs with advective acceleration terms turned off in selected sections of the 30-m grid
- runs with different compiler flags and optimization levels
- runs with different matrix solvers
- runs with decreased time-step to increase model stability
- runs with different levels of surface heat flux forcing
- run with low-pass filtered surface heat flux forcing, to increase model stability
- runs applying smoothing on the leap-frog step to zeta, velocity, and/or temperature
- runs varying lateral eddy viscosity to increase model stability
- runs with some of the model open boundaries closed to simply the boundary conditions
- runs with zero-gradient open boundary conditions (requiring recoding in main program)
- runs with different vertical mixing schemes including Mellor-Yamada 2.5
- runs with baroclinic pressure gradient terms turned off to increase model stability

- runs with flux limiters to increase model stability
- runs with tides and/or surface wind-stress turned off

None of these runs produced adequate results. Further attempts to diagnose and solve the model stability problems were done using a highly idealized grid of DWSC. A grid was built of a straight channel with same nominal width, length, and depth as the DWSC. Further runs were done on this simplified domain, with marginal success.

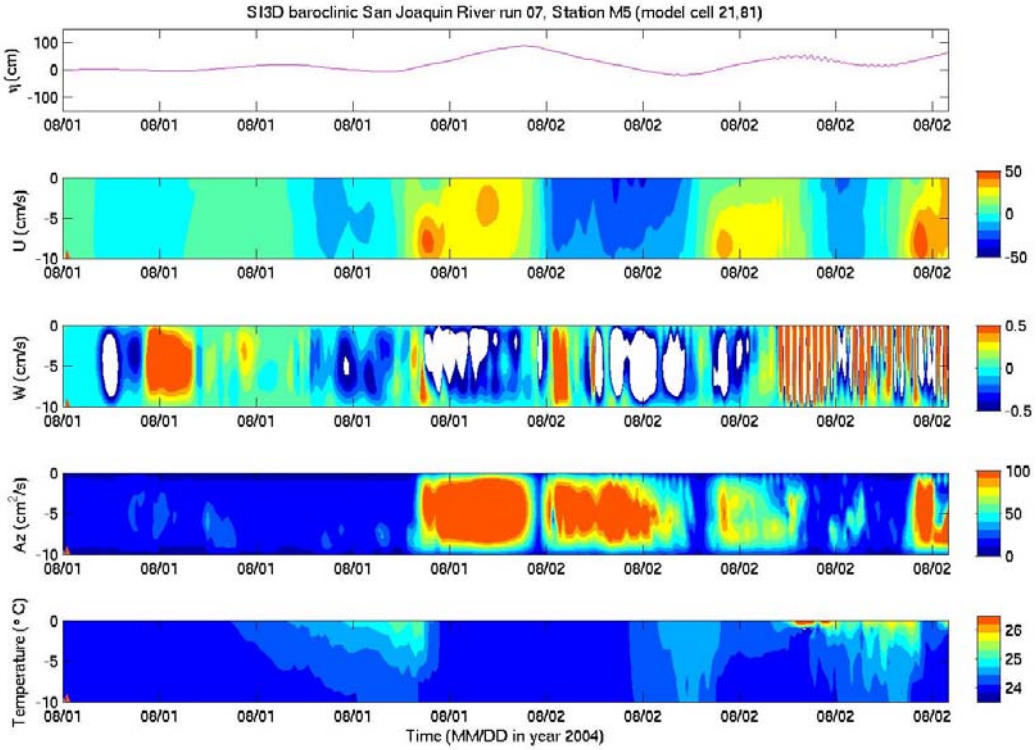

Figure 6.1 SI3D baroclinic model output at station M5 showing model instability.

7. Conclusions and Recommendations

In short, the modeling activities supported by this project showed the value and the limitations of a limited domain 3D model for practical modeling of flows in the Delta. On the good side, a physical resolution of ca. 10m in the horizontal and 1m in the vertical can be successfully run on current desktop workstations. It appears that the coupling of DSM2 to a 3D model is straightforward, although it may be necessary in future to consider modifying DSM2 outputs so that they better match observations. A more problematic issue for our modeling was the simple fact that we were never able to get the baroclinic version of SI3D to produce a stable calculation. This is disappointing because the observations make clear that baroclinic processes, notably the effects of diurnal stratification on turbulence, can have a dramatic effect on flow structure, and thus potentially on water quality. Perhaps the most important conclusion from this modeling exercise is that it is essential to support complex models with high-quality, well-designed observations.

To move forward with understanding the biogeochemical functioning of the DWSC, it is clear that the highest priority is to get a functional baroclinic circulation model. This model must have several characteristics to be accurate:

1. Our observations make clear that the model must use some form of turbulence closure that properly accounts for the effects of stratification on turbulence, i.e. not a simple Munk-Anderson style closure that parametrizes stratification effects solely in terms of the local Richardson number. Given the widespread use of more advanced closures like GOTM[4] in 3D circulation codes, this does not seem to be problematic. Thus we recommend that any circulation modeling that is done for the Delta use state of the art turbulence closures.
2. In the course of the project, it became clear that including a larger domain that stretched farther upstream would have been useful for carrying out the water quality modeling component. Since the version of SI3D that we used in this project did not include memory mapping, limits on memory that could be addressed by the executing code meant that the domain that could be covered at sufficient resolution was effectively limited to the domain covered by the grid shown above. Likewise, given the large range of channel sizes existing in the DWSC, it appears that an unstructured grid code like

[4] General Ocean Turbulence Model – see website

UnTRIM[5] (Casulli and Walters 2000) or SUNTANS[6] (Fringer et al 2006) would be preferable. Indeed, current consulting work by Ed Gross and Mike MacWilliams carried out for the POD workgroup has resulted in a Delta grid for UnTRIM. Likewise, a Stanford-Berkeley consortium recently (April 2008) received funding from the Coastal Conservancy to apply SUNTANS to San Francisco Bay, including a model grid that will extend at least to the confluence of the Sacramento and San Joaquin rivers. Thus we recommend that further hydrodynamic modeling of the Delta be done using an unstructured grid model. Moreover, given the widespread interest in such modeling, we strongly recommend the use of an open-source rather than proprietary code.

3. Assessing model fidelity requires developing formal criteria for assessing errors. One method that we employed to do so was to compare modeled and observed harmonic constants. Other approaches are possible and have been carefully laid out in the literature (see e.g. Warner et al 2005). Thus, we recommend that no results from modeling of the Delta be accepted if the only evaluation is what one might call the "LPG" metric[7].
4. A key aspect of modeling thermal variability in general is to correctly specify heat exchange between the Bay-Delta and the atmosphere. A current limitation to this activity is the lack of meteorological stations, similar to those deployed by CIMIS, over much of the Delta. Thus we recommend that a few key additional meteorological stations be added to the existing monitoring network operated by the project agencies. These stations should be distributed with a view towards capturing the east-west variability in wind, humidity, insolation, and longwave radiation from the sky. Moreover, given uncertainty about the use of the standard bulk flux formulations for the very short

[5] UnTRIM = Unstructured Tidal Residual and Intertidal Mudflat model

[6] SUNTANS – Stanford Unstructured Nonhydrostatic Terrain-following Adaptive Navier-Stokes Simulator

[7] LPG = Looks Pretty Good – this means some form of simple comparison plots, either as overlays or side by side.

fetches that characterize many of the Delta channels, it would be valuable to make direct, eddy-covariance measurements on water vapor flux for typical Delta channels.

5. Temperature measuring instruments maintained by the project agencies can contribute enormously to our ability to understand and model thermal variability in the Delta. We recommend that their calibration be assessed on a more regular basis than is currently done.

Finally, despite the issues listed above, it does appear that circulation models can be used to good effect in managing and understanding the functioning of the Delta. Thus, we encourage their further use, especially the development and application of fully 3D models like SI3D since the physics of interest is ultimately three-dimensional.

Appendix: Dispersion and heating in a tidal river[8]

We focus here on a simple analytical model of subtidal variations in temperature. Consequently, we also assume the heat flux to be constant, or at least not vary diurnally. We also assume that the temperature is, to first order, uniform across the cross-section and thus varies only in the longitudinal direction. Such 1D models have a long history in the theory and modeling of salinity in estuaries (see e.g.). Thus, our starting point is the 1D advection dispersion equation for heat, including surface heating through an imposed surface heat that depends on wind speed, air-water temperature difference etc. (see e.g. Fischer et al 1979) give above as eq (8)

$$A(x)\frac{\partial T}{\partial t} - Q_f \frac{\partial T}{\partial x} = \frac{\partial}{\partial x}\left(K(x)A(x)\frac{\partial T}{\partial x}\right) - \frac{WH}{\rho c_p}$$

For the sake of developing analytical solutions that describe the main features of the temperature distributions reported above, we further neglect time variations, assume that K and A do not depend on x and that the surface heat exchange can be represented by the form

$$\frac{H}{\rho c_p} = -\alpha\left(T_e - T\right) \tag{10}$$

where α is the heat transfer velocity and T_e is the equilibrium temperature in the water, both of which are functions of the given the meteorological conditions and the incident shortwave radiation (Mohseni and Stefan, 1999). With these drastic simplifications (8)becomes

$$-\frac{Q_f}{A}\frac{\partial T}{\partial x} = K\frac{\partial^2 T}{\partial x^2} + \alpha\frac{\left(T_e - T\right)}{D} \tag{11}$$

[8] A version of this appendix was submitted on February 14, 2008 to the journal "Estuaries and Coasts" for possible publication.

where $D = A/W$ is the effective depth. We suppose that the temperature at the riverine and ocean ends of this tidal river are specified. Without loss of generality, these can be assumed to be the same, so that

$$T = T_0 \quad x = 0, L \tag{12}$$

To proceed, we look at the deviation of the temperature from T_0, i.e.

$$T' = T - T_0 \tag{13}$$

and then construct dimensionless variables from the temperature difference $\Delta T = T_e - T_0$:

$$\begin{aligned} T^* &= T'/\Delta T \\ x^* &= x/L \end{aligned} \tag{14}$$

In terms of these dimensionless variables (11) becomes

$$\frac{\partial^2 T^*}{\partial x^{*2}} + \frac{Q_f L}{KA}\frac{\partial T^*}{\partial x^*} = -\frac{\alpha L^2}{KD}\left(1 - T^*\right) \tag{15}$$

or

$$\frac{\partial^2 T^*}{\partial x^{*2}} + P_1\frac{\partial T^*}{\partial x^*} = -P_2\left(1 - T^*\right) \tag{16}$$

The parameter $P_1 = Q_f L/KA$ reflects the relative importance of advection and dispersion; this term will be important when L is comparable to or larger than intrusion length KA/Q_f that plays a fundamental role in salinity intrusion. $P_2 = \alpha L^2/KD$ reflects the relative importance of diffusion to heat exchange. In this case, heat transfer will be important when L is comparable to the diffusion scale $\left(KD/\alpha\right)^{1/2}$.

The solution to (16) given the imposed conditions is easily found to be

$$T^* = 1 + A_+ \exp\left(\lambda_+ x^*\right) + A_- \exp\left(\lambda_- x^*\right) \tag{17}$$

where

$$\lambda_{\pm} = -\frac{P_1}{2} \pm \frac{\sqrt{P_1^2 + 4P_2}}{2}$$

$$A_+ = \frac{-1 + \exp(\lambda_-)}{\exp(\lambda_+)} \left(1 - \frac{\exp(\lambda_-)}{\exp(\lambda_+)}\right)^{-1}$$

$$A_- = -1 - A_+$$

As expected, the nature of the temperature field in the river depends on both advection and heat exchange, i.e., for systems like the San Joaquin River, on both water project operations (which determine flows in summer) and on weather. . The solution given by (17) can easily be modified to choose $T^*(1) = \delta$, i.e. to specify an upstream temperature that is $T_0 + \delta\Delta T$. For this case A_- remains as given above (in terms of A_+) but A_+ becomes

$$A_+ = \frac{\delta - 1 + \exp(\lambda_-)}{\exp(\lambda_+) - \exp(\lambda_-)}$$

In figure A1 to A4, we have plotted sample solutions for different values of P_1 and P_2. The basic behavior that emerges is that for weak flows the temperature approaches the equilibrium temperature, whereas for strong flows, the temperature remains close to that of the boundaries. In all cases, because $T_e > T_0$ the maximum temperature is found in the interior of the domain, exactly as seen in the observations reported in §2. This simple theory shows that as the flow rate drops, upstream diffusion of "coldness" from the downstream boundary becomes increasingly important. For the case with asymmetrical boundary conditions, as the flow (P_1) increases, the maximum temperature in the interior rises as the flow carries heat from the upstream boundary further into the domain.

To apply this theory to the DWSC it is necessary to estimate α, the heat transfer parameter. This can be done using the observations to compute T_e and then to use the observed surface heat transfer, H to

$$\alpha = \frac{H}{\rho c_p \left(T_e - T_s\right)} \tag{18}$$

Calculated values of T_e are shown in figure A5 while values of a plotted as functions of various components of the meteorological forcing are shown in figure A6.

The striking aspect of these plots is how high the equilibrium temperature is above observed water temperatures. From this data we might estimate that $T_e - T_0 \approx 8$ deg C, thus the relative warming of fluid in the DWSC by ca. 3 deg C relative to up and downstream suggests $\left(T/\left(T_e - T_0\right)\right)_{\max} \approx 0.3$. Meanwhile, a typical value of $\alpha \approx 6 \times 10^{-6}$ ms^{-1}. L can be estimated to be ca. 75 km, so that with and $Q_f \approx$ 5 m^{3}s^{-1} (2004), a relatively large value of the dispersion coefficient, i.e. $K_x \approx$ 1000 m^2 s^{-1} is required to produce a temperature variation that roughly matches what was observed in the DWSC (figure A6).

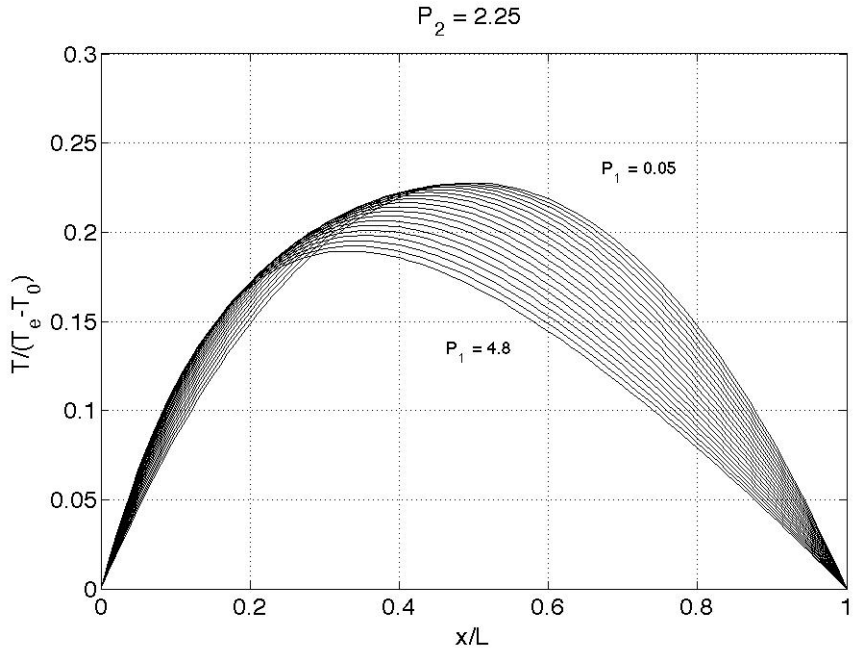

Figure A1 : Solution for symmetrical temperatures; parameters as indicated

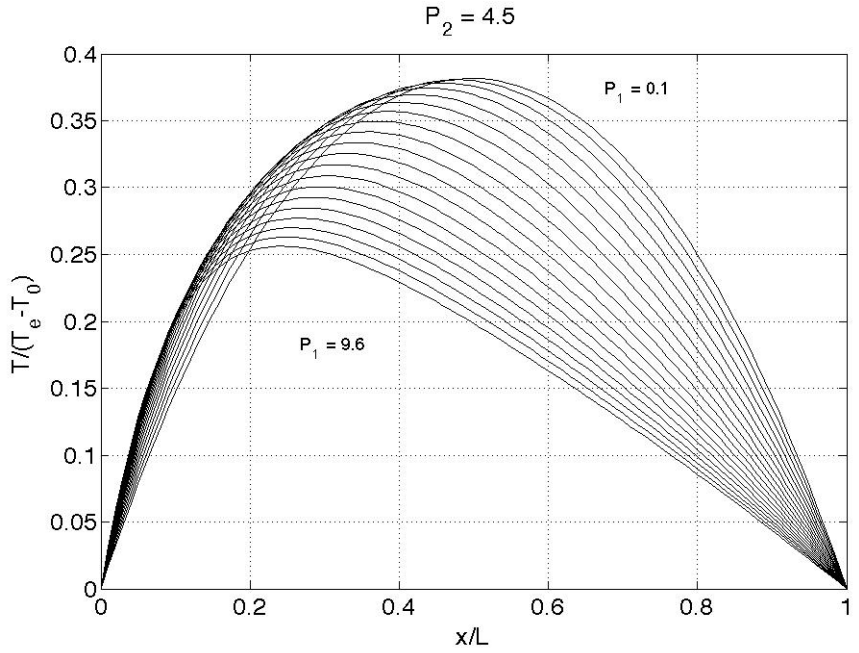

Figure A2 Solution for symmetrical temperatures; parameters as indicated

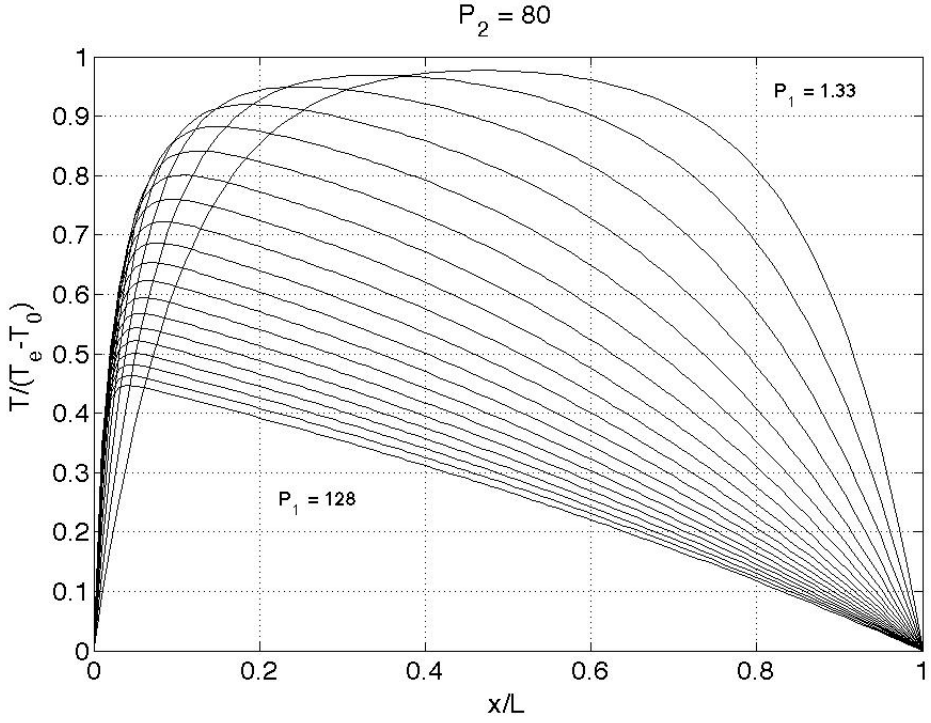

Figure A3: Solution for symmetrical temperatures; parameters as indicated

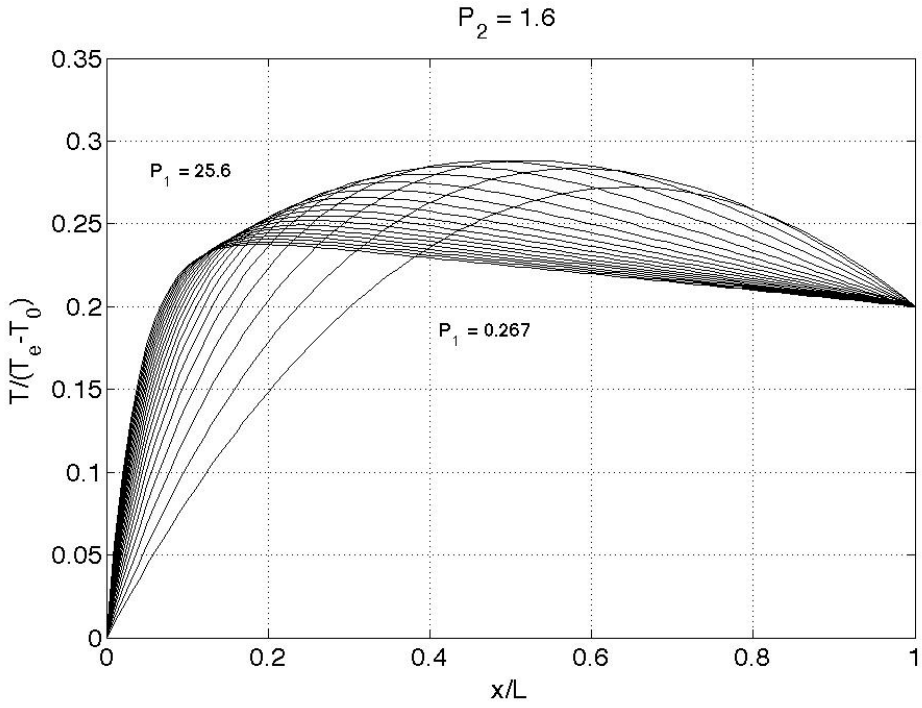

Figure A4: Asymmetrical boundary condition - This one chosen to best match observations

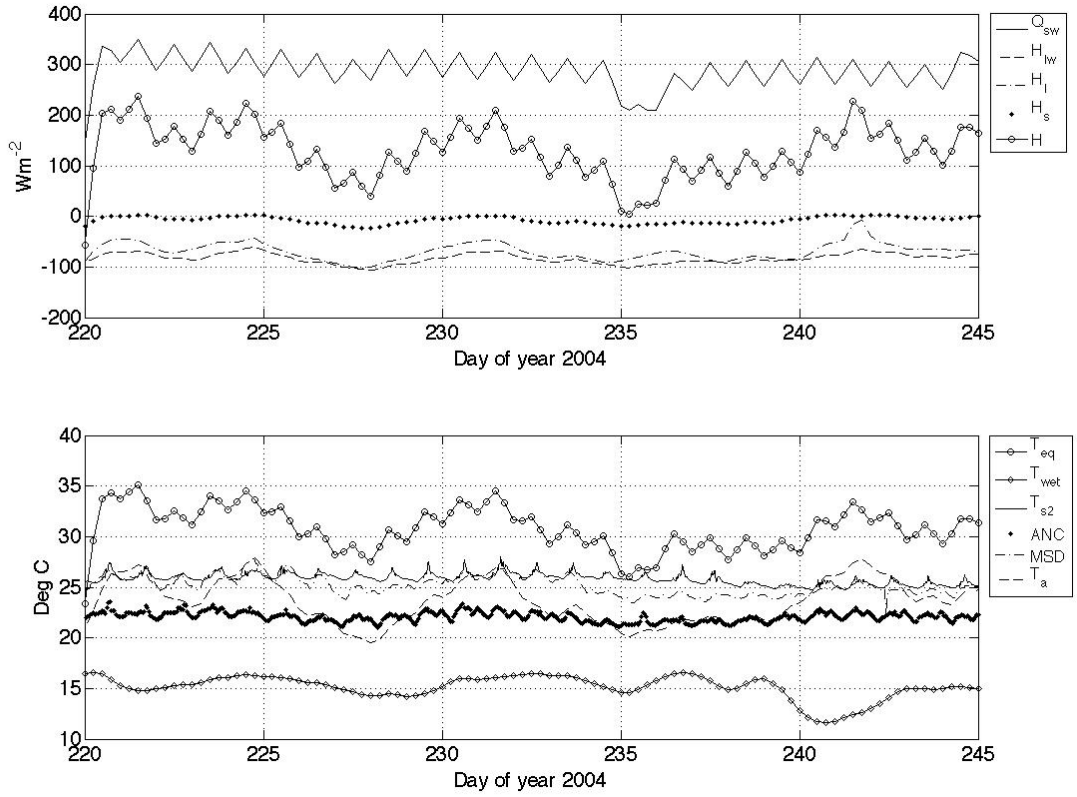

Figure A5: Meteorological forcing, boundary temperatures and T_e calculated for the M2 mooring. All variables reflect conditions observed during the 2004 field experiment.

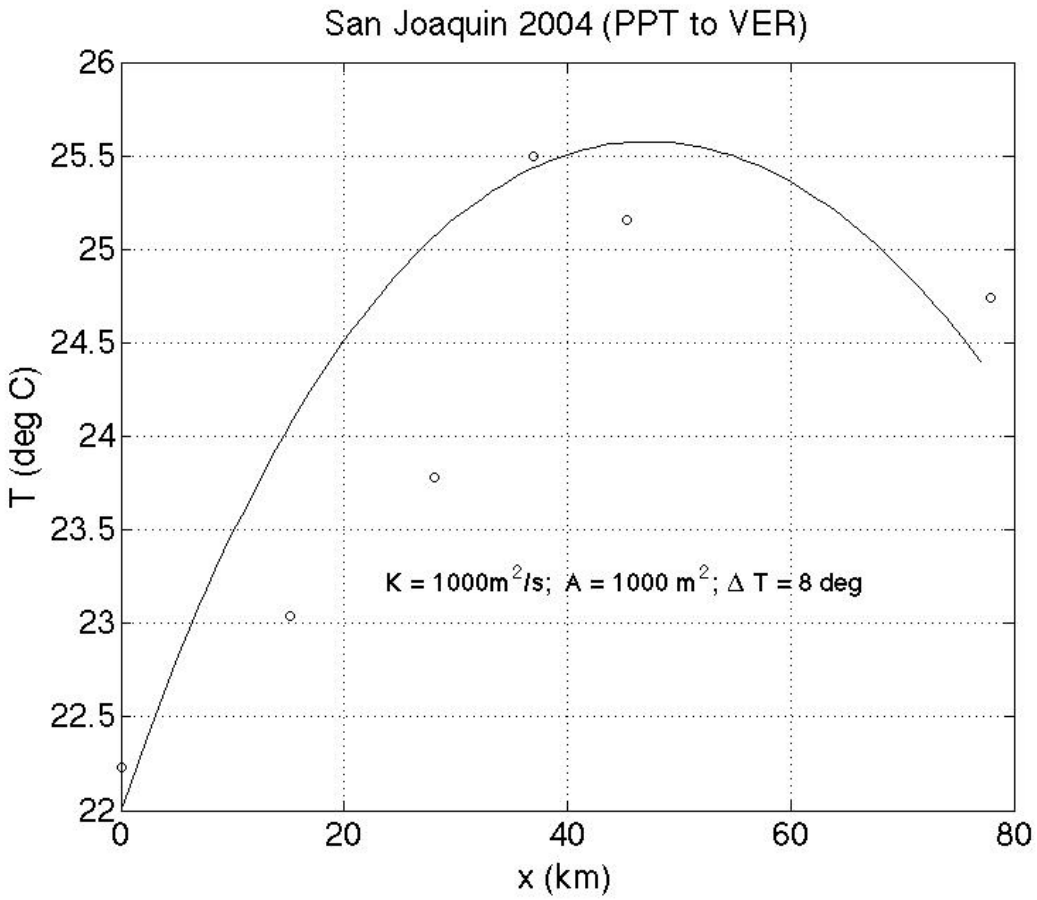

Figure A6: Q = 5 m^3/s, L=75 km, α = 6 x 10^{-6} m/s, K = 1000 m^2/s and A = 1000 m^2. The open symbols represent mean temperatures for the 2004 experiment starting at Prisoners Point and going upstream to Vernalis.

References

Blumberg, A. F., and G. L. Mellor, (1987). "A description of a three-dimensional coastal ocean circulation model," in: *Three-Dimensional Coastal Ocean Models*, S. Heaps, ed., American Geophysical Union, Washington, DC., 1-16.

Carter, G. D., and J. Imberger, (1986). "Vertically rising microstructure profiler," *J. Atmos. Oceanic Technol.*, 3, 462–471.

Casulli, V., and R. T. Cheng, (1992). "Semi-implicit finite difference methods for three-dimensional shallow water flow," *Intern. J. Numerical Methods Fluids*, 15, 629-648.

Casulli, V. and R.A. Walters, (2000). "An unstructured grid, three-dimensional model based on the shallow water equations," *Intern. J. Numerical Methods Fluids*, 32, 331-348.

Durran, D. R., (1999). *Numerical Methods for Wave Equations in Geophysical Fluid Dynamics*, Springer.

Edinger, J.E. , D.K. Brady, and J.C. Geyer ,(1974). *Heat exchange and transport in the environment*, Electric Power Research Institute report 14, 125 pp.

Emery, W.J. and R.E. Thomson, (2004). *Data analysis methods in physical oceanography* (2^{ed}), Elsevier, 638 pp.

Fischer, H.B., E.J. List, R.C.Y. Koh, J. Imberger, and N.H. Brooks, (1979). *Mixing in Inland and Coastal Waters*, Academic Press, 483 pp.

Fringer, O.B., M. Gerritsen, and R. L. Street, (2006). "An unstructured-grid, finite-volume, nonhydrostatic, parallel coastal-ocean simulator", *Ocean Modelling*, 14, 139-278.

Gross, E. S. (1997). *Numerical modeling of hydrodynamics and scalar transport in an estuary*. Ph.D. Dissertation, Stanford University.

Gross, E.S., Koseff, J.R. Koseff, and S.G. Monismith, (1999a). "Evaluation of advective schemes for estuarine salinity simulations," *J. Hyd. Div. ASCE* , 125(1), pp. 32-46.

Gross, E.S., J.R. Koseff, and S.G. Monismith, (1999b). "Three-dimensional salinity simulations in South San Francisco Bay," *J. Hyd. Div. ASCE* , 125(11), pp. 1199-1209.

Lee, G.F. and A. Jones-Lee, (2000). "Synopsis of Issues in Developing the San Joaquin River Deep Water Ship Channel DO TMDL", unpublished report submitted to San Joaquin River DO TMDL Steering Committee and the CVRWQCB, G. Fred Lee & Associates, El Macero, CA.

Mohseni, O. and H.G. Stefan, (1999). "Stream temperature/air temperature relationship: a physical interpretation, " *J. Hydrology*. 218, pp. 128-141.

Pawlowicz, R., B. Beardlsey, S. Lentz, E. Dever, and A. Anis, (2001). "Software simplifies air-sea data estimates," *EOS Trans. Am. Geophys. Union*, 82, 2.

Ridderinkhof, H. and J. T. F. Zimmerman, (1992) "Chaotic stirring in a tidal system," *Science* 258 (5085), 1107-1109.

Rueda, F. J., (2001). *A three-dimensional hydrodynamic and transport model for lake environments*, Ph.D. Dissertation, University of California, Davis.

Rueda, F.J. and Schladow, S.G., (2003). "The internal dynamics of a large polymictic lake. Part II: three-dimensional numerical simulations," *ASCE J. Hyd. Eng.*, 129(2), 92-101.

Rueda, F.J., Schladow, S.G. and Palmarsson, S.O., (2003). "Basin-scale internal wave dynamics during a winter cooling period in a large lake," *J. Geophys. Res.* 108 (C3), 10.1029/2001JC000942.

Smith, P. E., (1997). *A three-dimensional, finite-difference model for estuarine circulation*, Ph.D. Dissertation, University of California, Davis.

Smith, P. E., and B. E. Larock, (1993). "A finite-difference model for 3-D flow in bays and estuaries." *Hydraulic Engineering'93. ASCE Hydraulics Division Conference, July 25-30, 1993*, San Francisco, CA, 2166-2122.

Smith, P. E., and B. E. Larock, (1997). "Semi-implicit, numerical schemes for 3-D flow modeling." *Environmental and Coastal Hydraulics: Protecting the Aquatic Habitat. Theme B. Water for a Changing Global Community. The 27th Congress of the International Association for Hydraulic Research.*, 773-778.

Smith, P.E., (2006). "A semi-implicit, three-dimensional model for estuarine circulation", *USGS Open File Report 2006-1004*, 176 pp.

Warner, J.C., W.R. Geyer, and J. A. Lerczack, (2005). "Numerical modeling of an estuary: A comprehensive skill assessment," *J. Geophys. Res.*, 110(C05001), doi:10.1029/2004JC002691.

5. An Application of the SI3DWQ Hydrodynamics and Water Quality Model to the Stockton Deep Water Ship Channel

The SI3DWQ model is a new, integrated, three-dimensional hydrodynamic and water quality model, developed as part of this project. The hydrodynamic sub-model is the USGS-developed SI3D, with improvements made by Francisco Rueda of University of Granada. Many of these improvements were made subsequent to the initial testing of the hydrodynamic model described in Section 5. The water quality sub-model, which includes thirteen state variables, is totally new. The model domain encompasses the 14-km stretch of river subject to low dissolved oxygen concentrations and simulations from the San Joaquin River below French Camp Slough, to the San Joaquin River below Turner Cut. Model inputs are derived for the four open boundaries from a number of available sources, including data collected for this project during August 2004 (see Section 2) and long-term data sets collected by USGS and DWR in the San Joaquin River and DSM2 model output.

AN APPLICATION OF THE SI3DWQ HYDRODYNAMICS AND WATER QUALITY MODEL TO THE STOCKTON DEEP WATER SHIP CHANNEL

Laura Doyle, William Fleenor and S. Geoffrey Schladow, UC Davis
Stephen Monismith and Jim Hench, Stanford University
Peter Smith, USGS
Francisco Rueda, University of Granada

May 2008

Final report for CALFED ERP-02D-P51

Executive Summary

This report describes the three-dimensional modeling of hydrodynamic and biogeochemical processes in the Stockton Deep Water Ship Channel (DWSC) for August 2004. Since the 1960s, a 14-km stretch of this body of water, located in the freshwater tidal reaches of the San Joaquin River, has experienced low concentrations of dissolved oxygen. The hypothesis for the current investigation, based on past research, is that during summer months, when heat fluxes increase and river flow decreases, thermal stratification forms in the DWSC, causing biogeochemical processes to vary with depth and preventing dissolved oxygen that enters at the surface from mixing to the sediment interface where increased decomposition of organic matter occurs. The objectives of this study were to develop a model that accurately describes the physical and biochemical processes occurring in the channel to test this hypothesis. A second objective was to use the model together with the community-supported DSM2 developed by the Department of Water Resources (DWR) to explore management options to improve conditions in the basin.

A new, integrated, three-dimensional hydrodynamic and water quality model, SI3DWQ, was developed for this project. The hydrodynamic sub-model is the USGS-developed SI3D, with improvements made by Francisco Rueda of University of Granada. The water quality sub-model, which includes thirteen state variables, was added by Laura Doyle of University of California, Davis, as part of this project. The model domain encompasses the 14-km stretch of river subject to low dissolved oxygen concentrations and simulations from the San Joaquin River below French Camp Slough, to the San Joaquin River below Turner Cut. Model inputs are derived for the four open boundaries from a number of available sources, including data collected for this project during August 2004 and long-term data sets collected by USGS and DWR in the San Joaquin River and DSM2 model output. In addition, meteorological data are used to drive the heat flux portion of the model.

Initial model simulations of the complete hydrodynamic model produced very encouraging results. The basic thermal structure observed in the ship channel for August 2004 was reproduced with the model. However, it is unlikely that the differences in velocity, water surface elevation and water temperature can be fully resolved without more accurate boundary conditions, than those that are currently produced by DSM2. Once a more representative set of boundary conditions can be

applied, SI3DWQ can be better calibrated and the entire suite of water quality constituents, beyond the key water quality variable temperature, can be predicted.

Acknowledgements

This work was supported by CALFED Ecosystem Restoration grant ERP-02D-P51. The authors gratefully acknowledge the help with field work provided by a number of students and staff from Stanford (Kristen Davis, Sarah Giddings, Nick Nidzieko, Johanna Rosman) and from Davis (Steve Andrews, David Jassby, Todd Steissberg, Eugene Chung, Mike Barad, Jehan Fugitt, Bill Sluis, Daret Kehlet, Josh Mantell). The field work was also made easy through the experience and assistance lent by Jay Cuetara and John Yokimizu of the USGS.

1. Introduction

1.1 Background

Since the 1960s, a 14-km reach of the Stockton Deep Water Ship Channel (DWSC - Figure 1-1), part of the freshwater tidal reaches of the San Joaquin River, has been subject to critically low concentrations of dissolved oxygen. Researches have conducted numerous studies of the hypoxic conditions and agree that the low oxygen concentrations are the consequence of the complex hydrodynamic and biogeochemical processes in the estuary. In response to the low dissolved oxygen concentrations in the San Joaquin River Basin, the Central Valley Regional Water Quality Control Board of California (CVRWQCB) has imposed a dissolved oxygen total maximum daily load (TMDL) on the basin. The TMDL requires dissolved oxygen concentrations above 5 mg/L during October through June and above 6 mg/L for July through September. The higher concentration in late summer and early fall is in response to the fall run Chinook salmon population. Other TMDL limits are under considerations for the San Joaquin River.

Figure 1-1: The Sacramento-San Joaquin Delta, showing location of Stockton Deep Water Ship Channel.

The low dissolved oxygen problem in the Stockton DWSC has been recognized and studied for many years, and an extensive data set exists. There are considered to be five major factors that contribute to the low dissolved oxygen levels in the ship channel:

1. The morphology of the channel.
2. The load of oxygen demanding substances from the wastewater control facility.
3. The load of oxygen demanding substances from non-point sources upstream.
4. River flow conditions.
5. Environmental conditions, including water temperature and meteorology.

(Bain and Pierce 1968; Lee and Jones-Lee 2000; Lee and Jones-Lee 2003; Lehman *et al.* 2004; Jassby 2005; Jassby and Van Nieuwenhuyse 2005). Jassby (2005) further suggests that the variability in dissolved oxygen is linear in three processes: the residence time in the ship channel, the decomposition of oxygen-demanding materials, and phytoplankton metabolism. Although previous work agrees that the low dissolved oxygen concentrations are a combination of all five of these factors, there is disagreement as to which of these factors has the most influence.

Bain and Pierce (1968) were the first to suggest that the alteration of the natural morphology of the channel had a negative impact on the water quality in the area. The altered morphology increases the residence time of the water and thus allows for further decomposition of plant matter and associated consumption of dissolved oxygen. The Stockton wastewater treatment facility is a point source that contributes nitrogenous biological oxygen demand (NBOD), carbonaceous biological oxygen demand (CBOD) and other nutrients necessary for algal growth in its effluent. This oxygen demand is transported into the DWSC. The algal growth that results from the increased nutrients adds a second source of oxygen demand in the ship channel. In their study of the sources of dissolved oxygen deficits, Lehman *et al.* (2004) show that nitrification of ammonia load from the wastewater facility was the major source of oxygen demand in 2000 and 2001. Lee (2003) suggests that when San Joaquin River flows are low and ammonia concentrations in the wastewater facility are high, the resulting NBOD can account for eighty percent of the oxygen demand in the DWSC. He further suggests that this is exactly the condition that caused the winter hypoxia conditions and fish kills that were observed in the winter of 2003 and 2004. Non-point sources of oxygen demanding substances include detritus (dead and decaying phytoplankton and organic matter) transported from upstream sources, as well as nitrogen and NBOD from upstream.

The flow in the San Joaquin River is heavily managed year round. The flow of the San Joaquin River and its tributaries is highly regulated by reservoir releases and agricultural and other diversions. The management of the flow causes a decrease in the natural flow in March through July and an increase in the natural flow in September through October. In addition, the Central Valley and State Water Projects pumping stations have a large influence on the flow rate through the downstream reaches of the San Joaquin River. When the Head of the Old River Barrier is not in place and the water projects are pumping water, the flow patterns through the South Delta are changed significantly, with more San Joaquin River flow entering the Old River. The decreased flow causes an increase in the residence time in the DWSC, causing oxygen-demanding substances to exert demand for a longer period of time. Jassby (2005) and Lee (2003) agree that flow is the single most important factor that can control dissolved oxygen demands.

1.2 Purpose

The principal objective of this study is to use a three-dimensional numerical model of the DWSC, calibrated using field data collected during seasons with low dissolved oxygen, to understand how

hydrodynamic and biogeochemical processes interact to produce reductions in dissolved oxygen concentrations in the San Joaquin River. The fundamental conceptual model is that thermal stratification forms in the DWSC because mixing due to wind and mean flows is not sufficient to overcome the stratifying effects of surface heating or to adequately flush the channel. The presence of a step change in bottom elevation and channel width at the eastern end of the DWSC may also directly contribute to a low flushing rate in the ship channel. As a result, particulate BOD input to the DWSC as well as organic matter produced locally via photosynthesis, are provided with the conditions conducive to settling to the bottom where they decompose. The condition leads to the development of low oxygen concentrations near the sediment-water interface when surface oxygen exchange is insufficient to overcome the dissolved oxygen deficits in the lower layer. These three physical factors – the lack of flushing, the thermal stratification and the unusual bathymetry of the system – interacting with the biological and chemical drivers of the system, combine to produce the severe water quality conditions that have been observed.

Most importantly, due to thermal stratification, the biogeochemical processes may vary with depth. For example, in the presence of thermal stratification, oxygen that enters the water column via surface gas transfer as well as oxygen produced in the photic zone via photosynthesis may not be vertically mixed to the deeper parts of the water column. Phytoplankton biomass might increase in the presence of stratification when benthic grazers otherwise might be able to suppress phytoplankton blooms. Conversely, sediment-water column interactions will be limited to the bottom mixed layer if stratification forms. It is hypothesized that vertical structure and stratification dynamics are central to understanding the functioning of the DWSC. Consequently, to have predictive value, any model of the DWSC, must not only correctly resolve key chemical processes related to oxygen dynamics, but must also resolve the stratification dynamics operant in the DWSC.

Given the central role hydrodynamics play in DWSC oxygen dynamics, the field data collection program and computations for this project were designed to quantify the relationship between stratification dynamics and physical forcing. The working hypothesis is that stratification in the DWSC forms when currents, and hence bottom-produced turbulence are weak, and that stratification breaks down when currents are strong. Since flows in the DWSC are due to both river flow and tides, "strong" currents may be the result of spring tides and/or large through-flows on the San Joaquin River. It is possible that most of the time mixing is just sufficient for the system to

remain well mixed and that under low flow conditions, or during periods of particularly strong heating, the system becomes stratified, significantly affecting the various processes that determine DO levels. Thus, the first objective is to develop a predictive relationship between stratification and physical conditions using a combination of a 3-D, e.g., vertically resolved, hydrodynamic model and detailed field observations. The second objective is to build upon the representation of the physical processes in the channel and predict the biochemical processes and water quality conditions in the channel.

Lastly, given the complex hydrodynamics of the Delta, and the possibility of various modifications to these flows, e.g., the construction of an operable tide gate in Old River, it is important to know how the DWSC is affected by overall Delta hydrodynamics. A 3-D model with adequate resolution of the DWSC will be too computationally expensive to cover the entire Delta. Hence our second objective is to link a 1-D model of the Delta, most likely the community model DSM2, so as to provide appropriate forcing from the 3-D model.

2. The integrated hydrodynamic and water quality model: SI3DWQ

A new, integrated hydrodynamic and water quality model, SI3DWQ, was developed for this project. For a full description of this model, see Doyle (2007). The model has two main parts: a hydrodynamic model and a water quality model. The hydrodynamic model predicts the circulation of the water due to tides, river flow, wind, and density variations. In order to capture stratification processes, the hydrodynamic model includes a water temperature variable. The hydrodynamic model was based on SI3D, developed by Smith (1997, 2006) and Rueda (2001). The water quality model represents the transport and biogeochemical processes occurring in the water and includes thirteen state variables, including dissolved oxygen, algae and nutrients. The water quality model was added to the hydrodynamic model by Doyle for this project.

2.1 Hydrodynamic Model

The hydrodynamic model used in this study is the three-dimensional, semi-implicit model SI3D, first developed by Peter Smith of the USGS (Smith 1997, 2006) and further developed by Francisco Rueda of the University of Granada, Spain (Rueda, 2001). This model has been used extensively in the San Francisco-San Joaquin Delta system as well as in lakes, reservoirs and other tidal systems (Rueda and Schladow 2003, Rueda et al. 2003, Rueda & Cowen 2005). The model is based on the

continuity equation for incompressible fluids, the Reynolds-averaged form of the Navier-Stokes equations for momentum, the transport equation for temperature and salinity, and an equation of state relating temperature and salinity to fluid density. The governing hydrodynamic equations, subject to appropriate boundary conditions (momentum and heat fluxes), are solved in layer-averaged form using a semi-implicit, three-level, leapfrog-trapezoidal finite-difference scheme on a staggered Cartesian grid. The scalar transport equation is solved using a two-level, semi-implicit scheme that uses operator splitting. Only the vertical diffusion terms are treated implicitly, using the Crank-Nicholson scheme; the 1-D advection operators are discretized with flux-limiter methods. The corrected fluxes are constructed with the monotone upstream differencing scheme, the Lax-Wendroff second-order method, and the Van Leer MC limiter. Turbulent mixing is represented in the 3-D model following level 2.5 Mellor-Yamada hierarchy of turbulence closure models (Kantha and Clayson 1994). Horizontal mixing of momentum is parameterized using a constant mixing coefficient. Horizontal diffusion of scalars is not represented in the model.

The current version of the hydrodynamic model includes improvements added by Rueda at the University of Granada. The improvements allowed the water quality model to be run concurrently with the hydrodynamic model, and allows for the modeling of baroclinic processes. These improvements were not available at the time the results described in Monismith et al. (2008) were produced. The model now uses a three-dimensional to two-dimensional mapping structure to decrease the amount of memory necessary to run the model. The increased efficiency has improved the ability to model smaller grid sizes.

2.2 Water Quality Model

The water quality sub-model was developed and tested during the course of this project. The sub-model is solved within the same model as the hydrodynamic sub-model. The water quality model includes the transport of water quality constituents as well as source-sink terms for each constituent that take into account all biogeochemical processes. The transport of all water quality constituents is solved using the same two-level, semi-implicit scheme using operator splitting developed for scalar transport in SI3D. Only the vertical diffusion terms are treated implicitly, using the Crank-Nicholson scheme. The 1-D advection operators are discretized with flux-limiter methods. The corrected fluxes are constructed with the monotone upstream differencing scheme, the Lax-Wendroff second-order method, and the Van Leer MC limiter. The construction of all source-sink

terms was based on a number of previously tested water quality models, including the publicly available RMA-11 (King 1998) and CE-QUAL-W2 (Chapra 1997). SI3DWQ includes the following state variables: arbitrary constituent (used as a conservative tracer), dissolved oxygen, nitrogen species, phosphorus species, organic matter and phytoplankton.

2.3 Model Configuration

The area of interest for the model is the 14-km stretch of the Stockton DWSC subject to low dissolved oxygen. In order to capture the three-dimensional detail in the reach, ideally, the horizontal resolution should match the smallest horizontal flow features expected to develop in the model domain, i.e., approximately 5 to 10 m (or less). In addition, the boundaries need to be sufficiently far from the area of interest so as not to influence the results. Thus, ideally the model should have a large domain and very fine resolution. However, it is also critical to consider computational limitations. A decrease in grid size will increase computational time. The current model configuration takes all these limitations and idealizations into account. To allow the least interference between the model domain and the area of interest, the model domain runs from the San Joaquin River below French Camp Slough, to the San Joaquin River below Turner Cut. The San Joaquin-Sacramento Delta system contains many channels, but to minimize the open boundaries, only two additional channels are deemed significant and taken as boundaries. The domain includes 579 x 186 grid cells in the horizontal plane, each is 30 m by 30 m, and there are 12 vertical layers, each 1 m. Many of these cells are 'dry', and no computations are completed. Figure 2-2 shows the rotated model domain, denoting wet cells and the location of four open boundaries.

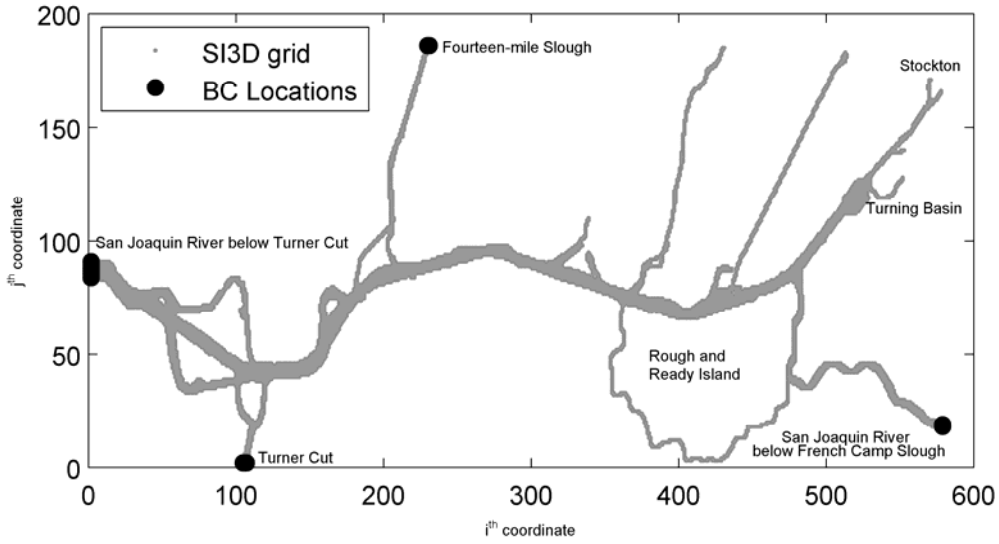

Figure 2-2. Rotated DWSC grid showing locations of open boundaries. The grid was rotated 34 degrees counter clockwise.

In order to comply with the Courant-Fridrichs-Lewey (CFL) condition, and keep the model stable, the time step for the current grid is 20-seconds. The CFL condition is defined as $u\Delta t/\Delta x$ where u is the velocity, Δt is the time step and Δx is the grid size. For stability of the model, the ratio should be less than or equal to one. The model calibration period is August 7, 2004 through August 19, 2004 (Julian Day 220 – Julian Day 232). This period was chosen because of the availability of both boundary condition and calibration data.

3. Model Inputs

As described in the following sections, a number of inputs are necessary to drive the model. At each open boundary inputs are needed for each constituent. As shown in Figure 2-2, there are four open boundaries, the San Joaquin River below Turner Cut, Fourteen-Mile slough, the San Joaquin River below French Camp Slough and Turner Cut. Table 1 summarizes the boundary condition information. The numbering shown below is used by the model and will be referenced throughout this documentation.

Table 1. Boundary Condition numbering for SI3D.

Boundary	Name	Side of domain
1	San Joaquin River below Turner Cut	West
2	Fourteen-mile Slough	North
3	San Joaquin River below French Camp Slough	East
4	Turner Cut	South

In addition to inputs at each of these boundaries, meteorological information is necessary to calculate surface heat fluxes.

3.1 Hydrodynamic Boundary Conditions

The hydrodynamic sub-model in SI3DWQ requires both hydrodynamic and water temperature boundary conditions. The model can accept hydrodynamic boundary conditions in three forms: water surface elevations, surface flow or sub-surface flow. For the application in the Stockton Deep Water Ship Channel, water surface elevation output from DWR's DSM2 model is used as input into the model. Table 2 summarizes the DSM2 locations used as input into SI3D.

Table 2. Boundary Locations and corresponding DSM2 locations.

SI3D Boundary	DSM2 Location
San Joaquin River below Turner Cut	031_6515
Fourteen-mile Slough	312_11385
San Joaquin River below French Camp Slough	013_0
Turner Cut	172_0

The model reads fifteen-minute water surface elevations at each of the open boundaries, and interpolates to the time step modeled. The water surface elevation boundary conditions are shown in Figure 3-3. The first two days of the model show smoothed conditions, this is to provide the model a warm-up period.

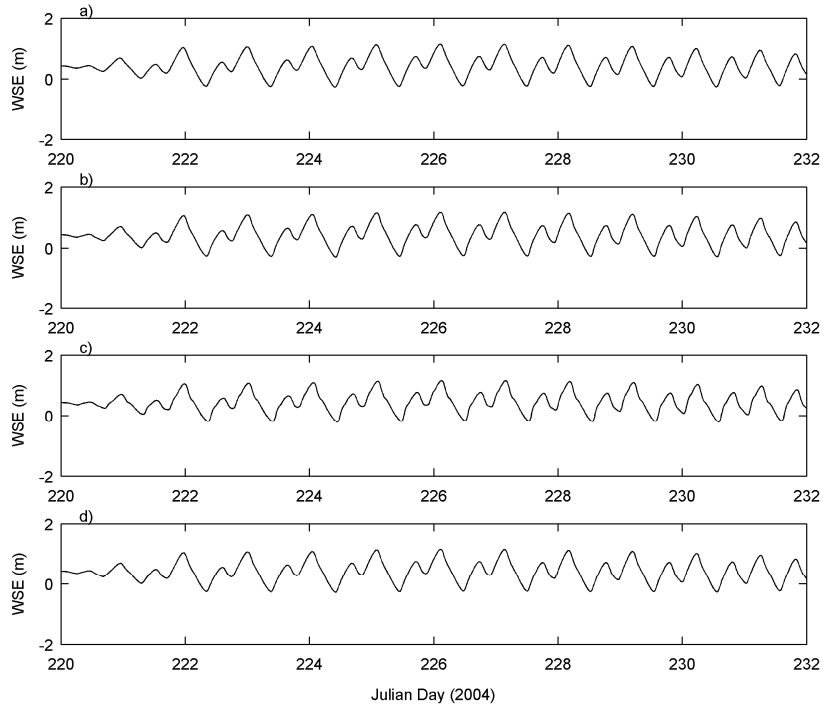

Figure 3-3. Water surface elevation boundary condition for (a) San Joaquin River below Tuner Cut, (b) Fourteen-Mile Slough, (c) San Joaquin River below French Camp Slough and (d) Turner Cut.

The water temperature boundary conditions were constructed from a number of sources. During August of 2004 and 2005, month long extensive studies were conducted in the Stockton Deep Water Ship Channel. The studies consisted of month-long moorings with ADCP and thermistor strings to help gain an understanding of the hydrodynamic processes in the channel. In addition, during the month, two 30-hour experiments were conducted. During the 30-hour experiments, among other measurements, conductivity-temperature-depth profiles were taken with a Sea-Bird (SBE) at eleven locations in the San Joaquin River and Deep Water Ship Channel. Figure 3-4 shows the locations in the model domain where measurements were taken during the experiments. This month long record is supplemented with continuous measurements taken in the San Joaquin River by a number of government agencies, including the Department of Water Resources (DWR) and the United States Geological Service (USGS). Locations of interest include San Joaquin River at Vernalis (VNS), San Joaquin River at Mossdale (MSD), San Joaquin River at Garwood Bridge (2005

only) and Rough and Ready Island (RRI). Figure 3-5 shows monthly average water temperature profiles for the tidal portion of the San Joaquin River, from Antioch to Vernalis as collected by long-term moorings. Additional data were obtained from the City of Stockton. The data from the City were collected a part of NPDES permits and include many physical and chemical constituents. The data were collected at seven locations in the Stockton Deep Water Ship Channel.

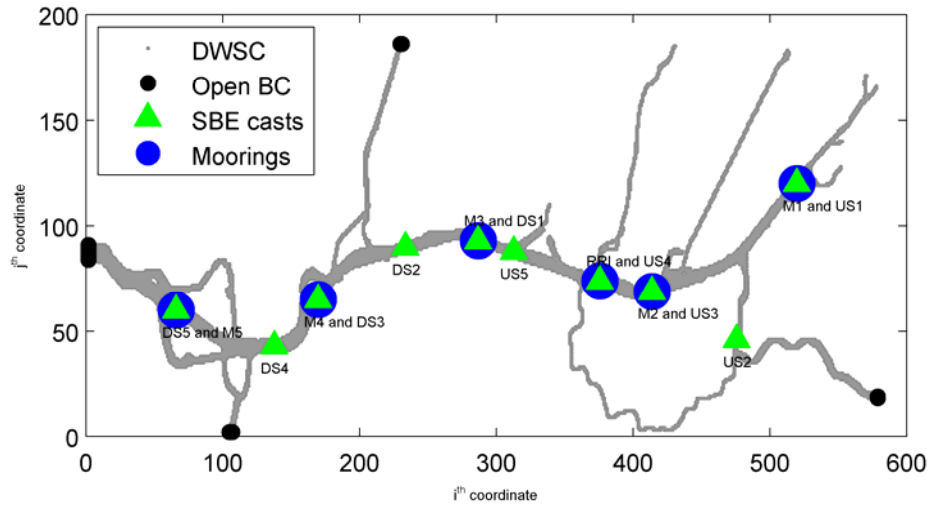

Figure 3-4. DWSC map showing location where field data were collected.

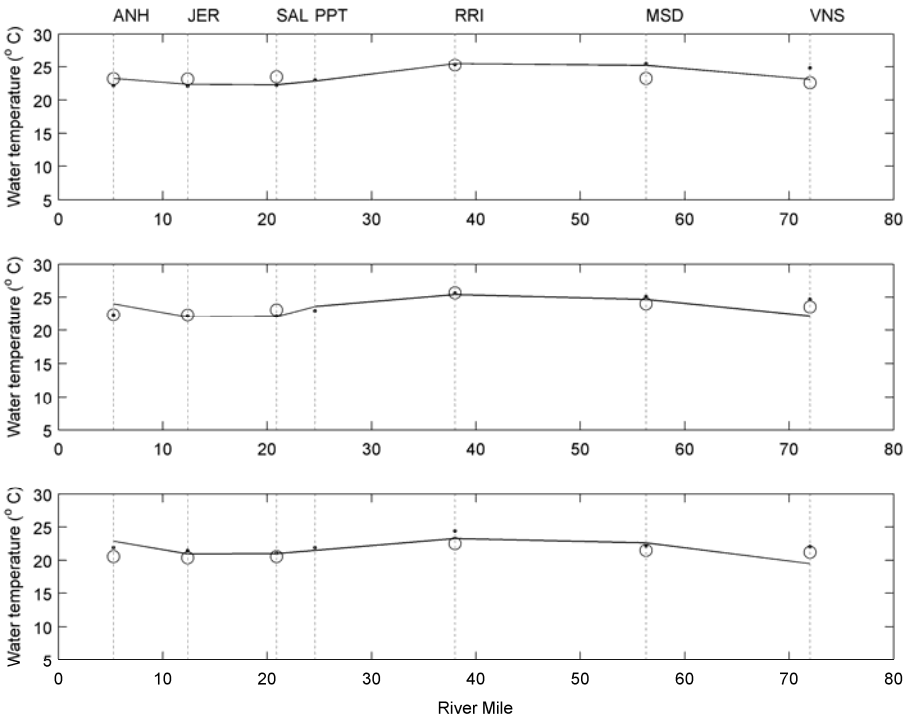

Figure 3-5. Profile of monthly mean water temperature for July (top), August (middle) and September (bottom) in the San Joaquin River. The solid line is the historical average, based on available data from 1984 – 2003, the dots are monthly averages for 2004 and the open circles are monthly averages for 2005. The left side is downstream, and the right side is upstream. The plots show the temperature profile for the portion of the river that is influenced by the tide.

3.1.1 San Joaquin River below Turner Cut Water Temperature Boundary Condition

The month long record of water temperatures recorded at DS5/M5 is used to create a fifteen-minute time series of water temperature at the western boundary. Although this location is not directly on the boundary, the detailed record gives the best estimate for the water temperature at the San Joaquin River below Turner Cut. As seen in Figure 3-5, water temperature decreases in the channel from east to west, as a result of the influence of water from the Sacramento River pulled southward by the export pumps. Therefore, if an improvement is made to the boundary condition, it will be a decrease in water temperature. However, without further data to support the change in temperature from the boundary to M5, the M5 measured water temperature is the best available input. Figure 3-6 shows a contour plot of water temperature at M5 during August 2004. For most of the time period, the water temperature is constant with depth. SI3DWQ assumes a well-mixed

boundary and the surface temperature was chosen as the input for this boundary. Figure 3-7 shows the boundary condition. Similar to the water surface elevation boundary, this boundary is smoothed for the first two days to give the model time to start-up.

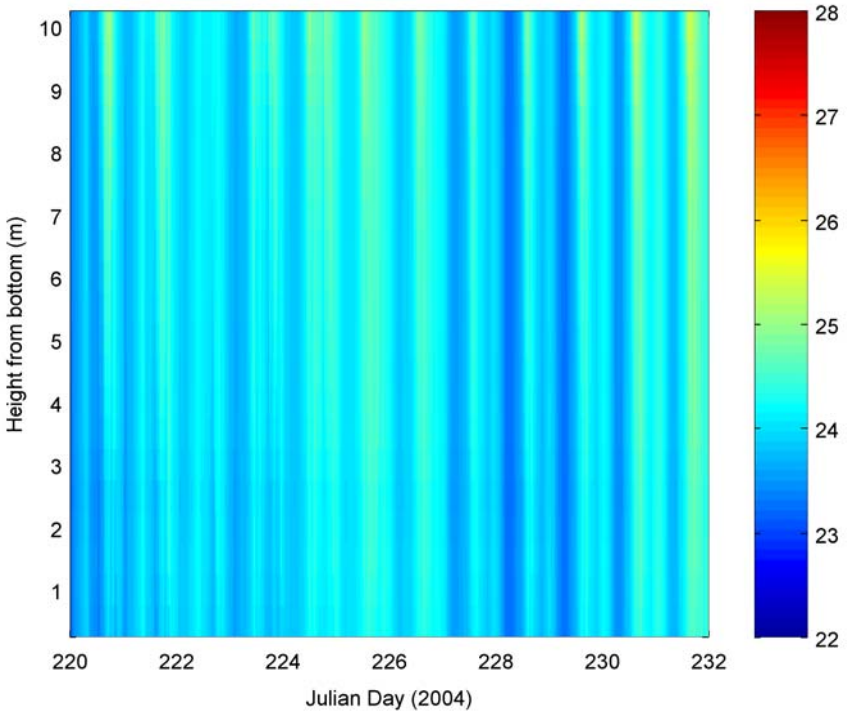

Figure 3-6. Contour plot of water temperature at M5 during model period.

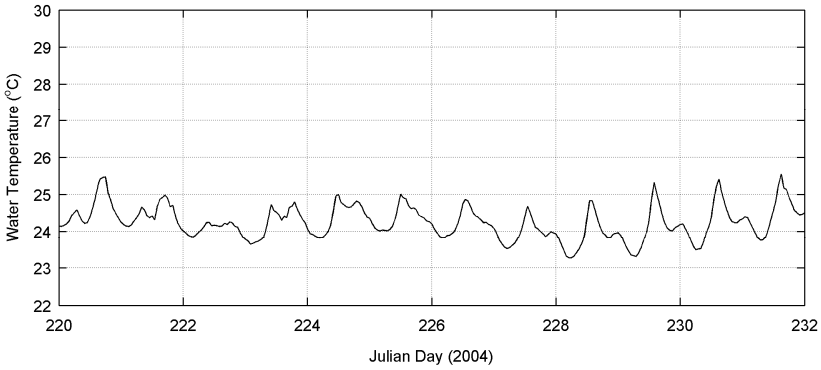

Figure 3-7. Water temperature boundary condition for boundary 1.

3.1.2 Fourteen-Mile Slough Temperature Boundary Condition

Construction of the water temperature boundary condition at Fourteen-Mile Slough follows procedures used by Hydroqual in their model of the Stockton Deep Water Ship Channel. Hydroqual used instream data from the City of Stockton R6 location for Fourteen-Mile Slough. This site provides weekly water temperature measurements. A linear interpolation between measurements is used to construct an hourly boundary condition (Figure 3-8).

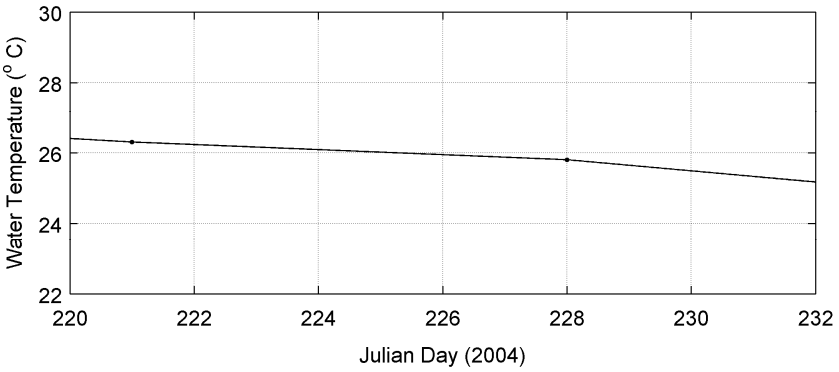

Figure 3-8. Water temperature boundary condition for boundary 2

3.1.3 San Joaquin River below French Camp Slough Boundary Condition

Field data collection did not include collecting data at or near the upstream boundary condition in the San Joaquin River. To construct the water temperature boundary condition at this site, continuous data collected by CDEC at Mossdale were used. As seen in Figure 3-5, between Vernalis and Mossdale, the water temperature in the San Joaquin River increases. Between Mossdale and the start of the Stockton DWSC, there is no additional water temperature information gathered before 2005. Starting in 2005, a water temperature sensor was installed at Brandt Bridge by the USGS. As seen in Figure 3-9, this adds new information between Mossdale and Rough and Ready Island. Brandt Bridge is closer to the most upstream boundary of the model domain. However, one year of data is not sufficient to be considered a trend in water temperature. Because no further information was available, the mean temperatures at Mossdale were be used as the upstream boundary condition in the San Joaquin River below French Camp Slough. This boundary condition is show in Figure 3-10.

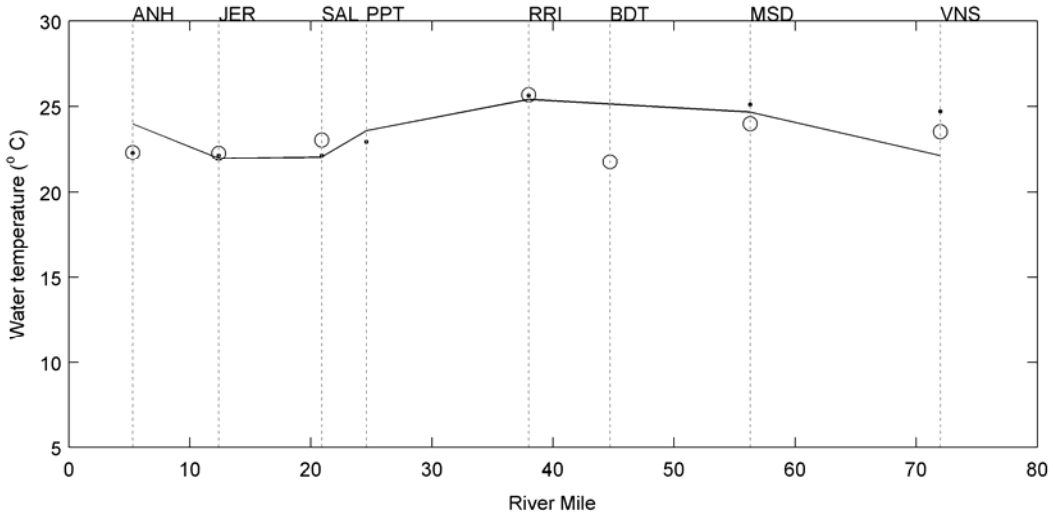

Figure 3-9. Profile of monthly mean water temperature in August for the tidal portion of San Joaquin River. The solid line is the historical average, based on available data from 1984 – 2003, the dots are monthly averages for 2004 and the open circles are monthly averages for 2005. This plot includes the monthly average for Brandt Bridge, which was established in 2005.

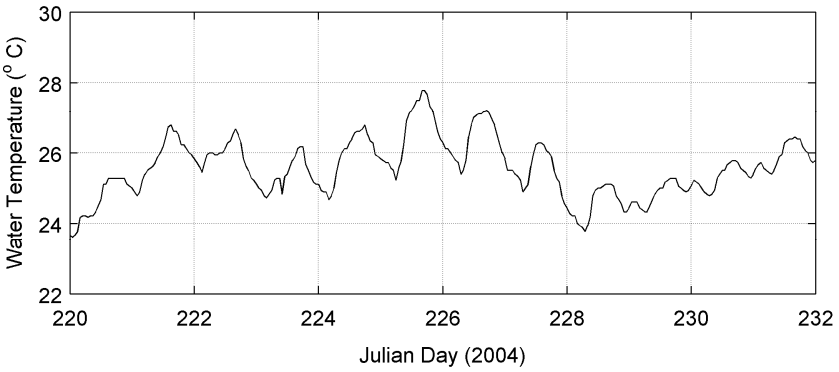

Figure 3-10. Water temperature boundary condition for boundary 3.

3.1.4 Turner Cut Temperature Boundary Condition

Construction of the water temperature boundary condition at Turner Cut follows procedures used by Hydroqual and the boundary condition at Fourteen-Mile Slough. Weekly water temperatures collected at R7 by the City of Stockton are used with a linear interpolation between measurements to construct an hourly boundary condition (Figure 3-11).

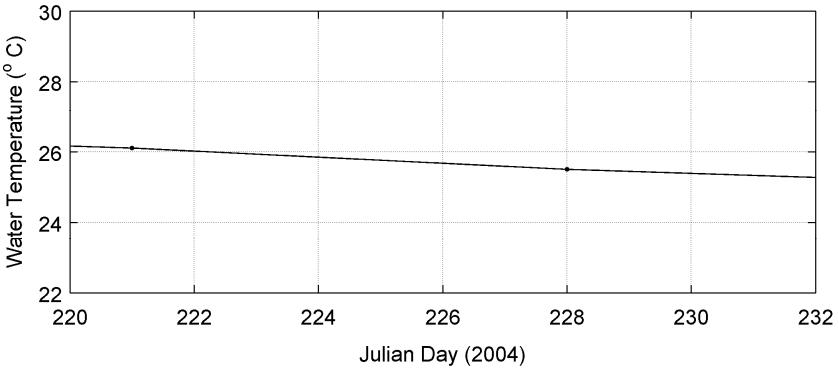

Figure 3-11. Water temperature boundary condition for boundary 4.

3.2 Meteorological Boundary Conditions

In SI3D, the surface heat fluxes that drive the model can be specified directly or computed using model-computed values of surface water temperature, T_s. The latter approach has the advantage of providing negative feedback; if the model predicts temperatures warmer than observations, the heat losses will be greater than actually occur, whereas if the model is tending to be colder, heat losses will be less. The meteorological data necessary to compute heat fluxes, both in pre-processor and in the model include air temperature, shortwave radiation, surface water temperature, relative humidity, wind speed and wind direction. Meteorological data were obtained from the Port of Stockton (wind speed and direction, air temperature and shortwave radiation) and from CIMIS (www.cimis.water.ca.gov) station # 166, Lodi West (relative humidity and wind speed), located 17.4 km from the Port of Stockton station. Figure 3-12 shows the time series of data from the Port and CIMIS stations for the model period.

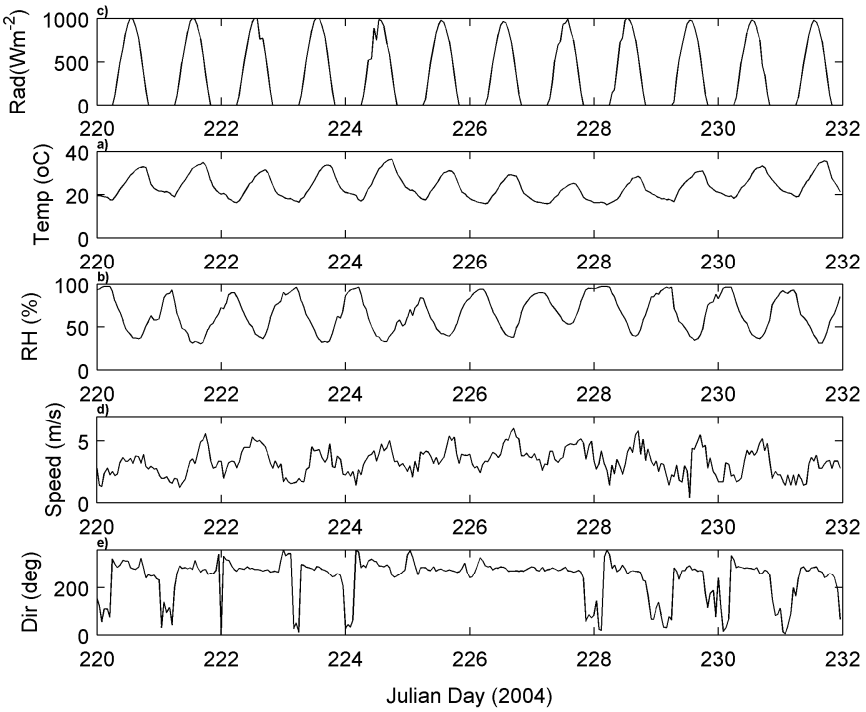

Figure 3-12. Meteorological data for Stockton DWSC: (a) shortwave radiation (POS), (b) air temperature (POS), (c) relative humidity (CIMIS), (d) wind speed (POS), (e) wind direction (CIMIS).

Because the grid used was rotated 34 degrees counter-clockwise, the wind direction was also rotated by the same amount. Figure 3-13 shows the rose plot for the original wind direction and the rotated wind direction.

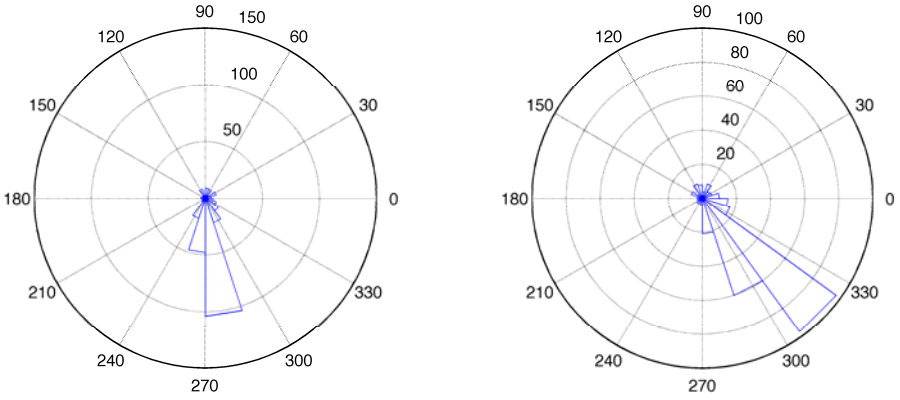

Figure 3-13. Rose plot for (left) original wind direction data and (right) rotated wind direction.

For the Stockton DWSC model application, the data from the Port and CIMIS station were used to calculate the net heat flux and the shortwave heat flux, corrected for albedo, which are then supplied as input to SI3D. There are two types of heat fluxes: penetrative and non-penetrative. The non-penetrative heat fluxes include evaporation or latent heat flux (Q_E), conduction or sensible heat flux (Q_H) and net long-wave radiation flux (Q_B). These fluxes occur only at the surface of the water. The penetrative heat flux include the shortwave radiation (Q_s). Depending on the extinction coefficient, the shortwave radiation distributes heat beyond the surface layer. The net heat flux at the surface includes the contribution from all non-penetrative sources and the shortwave radiation that is absorbed in the surface layer. The net heat flux is:

$$Q_n = Q_s - (Q_B + Q_E + Q_H)$$

The surface water temperature is determined as the average surface water temperature of M1-M5. To determine the shortwave radiation that penetrates the free surface (Q_s), the CIMIS data, which included shortwave radiation that reaches the water surface (Q_G), must be reduced by the albedo of the water surface (A_s). A mean value of 0.06 can be used for albedo. However, the albedo can also be calculated as shown below, equations taken from Rueda (2001).

$$A_s = \frac{a_0}{a_0 + \sin\alpha^*}$$

where α^* is the solar altitude, a_0 is a coefficient and a function of fractional cloud cover, C_1, , and Julian day, J,

$$a_0 = 0.02 + 0.01 \cdot (0.5 - C_1) \cdot \{1 - \sin[\pi \cdot (J - 81)/183]\}$$

The solar altitude α^* is determined using solar altitude to latitude, θ, solar declination, δ, and hour angles as shown below

$$\sin\alpha^* = \sin\theta \cdot \sin\delta + \cos\theta \cdot \cos\delta \cdot \cosh$$

The hour angle *h* is zero at local noon and increases in magnitude by π/12 for each hour before and after noon. The solar declination on the other hand will vary for each Julian day, J, and for the northern hemisphere is given by the expression

$$\delta = 0.4093 \cdot \sin[2\pi \cdot (J * 79.75)/365]$$

To get estimates for cloudiness, the average daily solar radiation data was determined and plotted. The equation

$$y = A\sin[\omega\pi + \mathrm{J}/\alpha] + C \qquad \text{(Equation 3-1)}$$

was fit to encompass all the data. A is the amplitude, ω is the angular frequency, α is the phase shift and C is the vertical offset and J is the Julian day. Equation 3-1 represents expected solar radiation without clouds. The pattern shown in Figure 3-14 follows the expected pattern of maximum solar radiation in the summer. To estimate cloud cover, the observed solar radiation is divided by the theoretical radiation, and that value is subtracted from one. The shortwave radiation at the surface, corrected for albedo is shown in Figure 3-15.

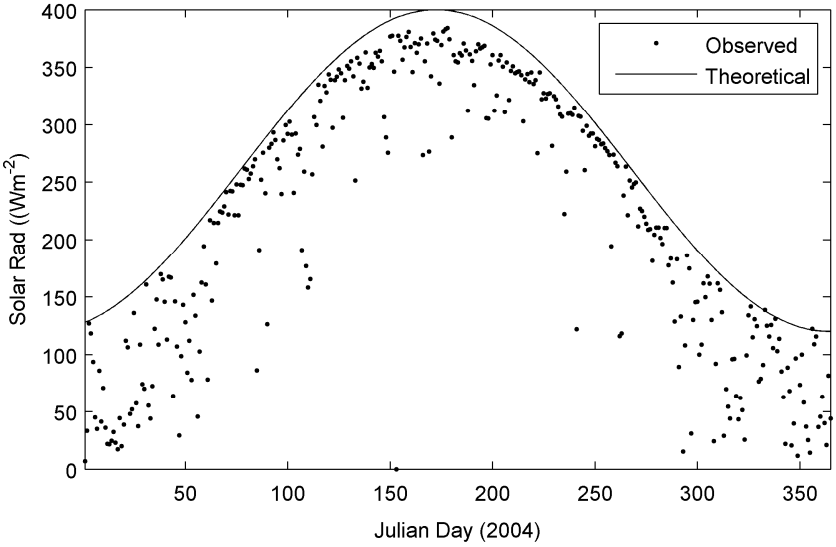

Figure 3-14. Calculation of cloud cover for 2004. The observed data are the daily average solar radiation from CIMIS and the theoretical was calculated from Equation 3-1.

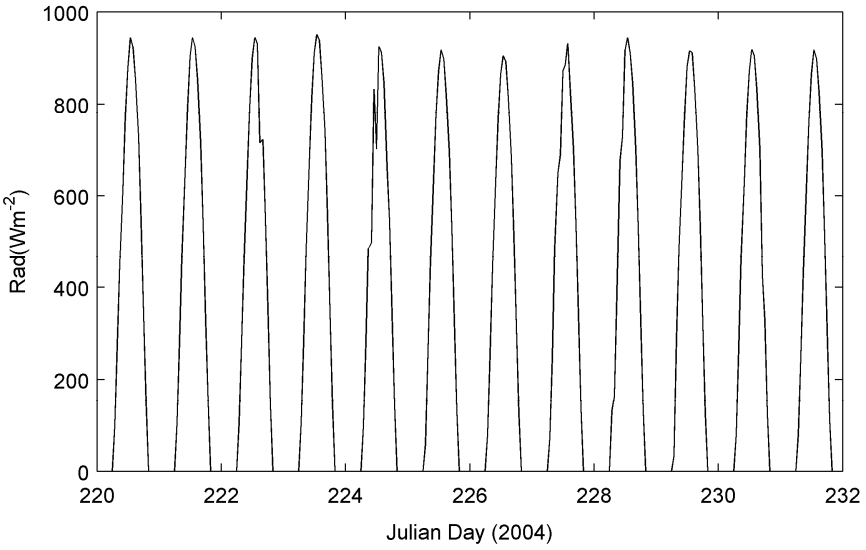

Figure 3-15. Q_G, solar radiation corrected for albedo, for the model period.

The net long wave radiation, Q_B, is composed of two parts, the long-wave radiation emitted by the atmosphere (Q_B^{ro}) and the back-radiation (Q_B^{ra}). The net long wave radiation necessary for model input is calculated as follows:

$$Q_B = Q_B^{ro} + Q_B^{ra}$$
$$Q_B^{ro} = \varepsilon_w T_s^4$$
$$Q_B^{ra} = \varepsilon_s \sigma T_A^4 (1 - A_L)$$

T_s and T_A are surface water and air temperature, in degrees Kelvin, σ is the Stefan-Boltzmann constant and ε_w, ε_s are emissivities of the water and air, respectively. ε_w is a constant and equal to 0.972, but ε_s depends on vapor pressure (e_A), air temperature (T_A) and cloud cover (C_l).

$$\varepsilon_S = 0.642\left(\frac{e_A}{T_A}\right)^{1/7}(1 + 0.17C_l^2)$$

Figure 3-16 shows the emitted long-wave radiation, back-radiation and net long wave radiation.

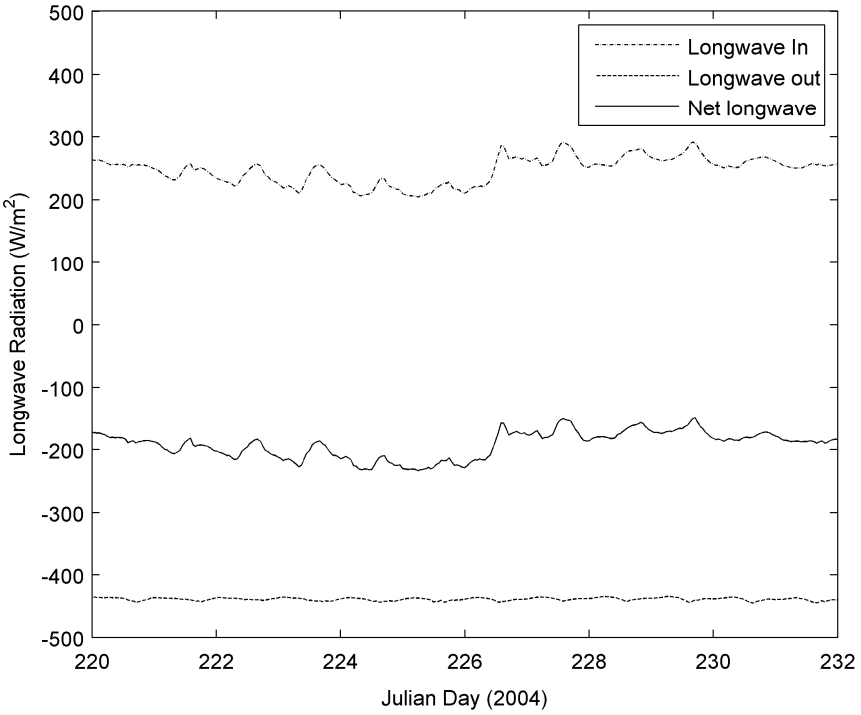

Figure 3-16. Longwave radiation flux for model period.

The evaporative heat flux is calculated in terms of the difference between the saturated vapor pressure at the surface water temperature and the actual vapor pressure at the temperature of the air, following the expression (Henderson-Sellers 1986):

$$Q_E = \rho_w \cdot L_v \cdot 1.15 \cdot 10^{-8} \cdot c_D \cdot u_2 (1 + a_3 c_R)(e_s^{sat} - e_A) = C_E (e_s^{sat} - e_A)$$

where

e_s^{sat} = Saturated vapor pressure at the surface water temperature

e_A = Actual vapor pressure at the temperature of the air

L_v = Latent heat of vaporization

c_D = Aerodynamic drag coefficient

c_R, a_3 = Coefficient that depends on the stability of the atmosphere.

The following figure shows the evaporative heat flux for the period of interest.

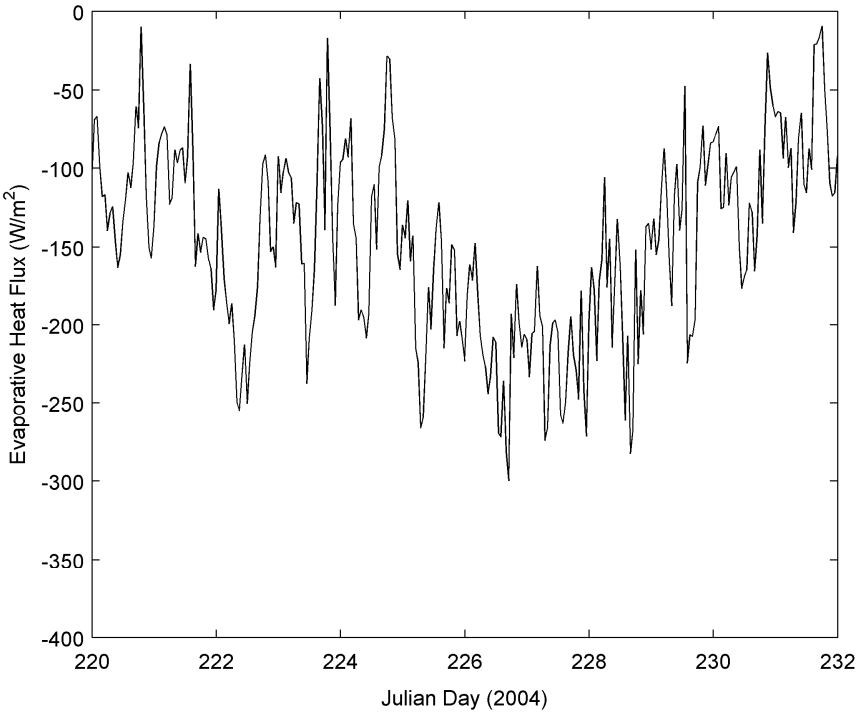

Figure 3-17. Evaporative heat flux during model period.

The sensible heat flux is related to the evaporative heat flux by the Bowen ratio: Q_H/Q_E. For SI3D, the Bowen ratio is assumed to be of the form:

$$Q_H \Big/ Q_E = 0.61 \cdot 10^{-3} \cdot p \cdot \frac{T_s - T_A}{e_s^{sat} - e_A}$$

Therefore, the sensible heat flux is:

$$Q_H = 0.61 \cdot 10^{-3} \cdot C_E \cdot p \cdot (T_s - T_A)$$

Figure 3-18 shows the sensible heat flux for the model period.

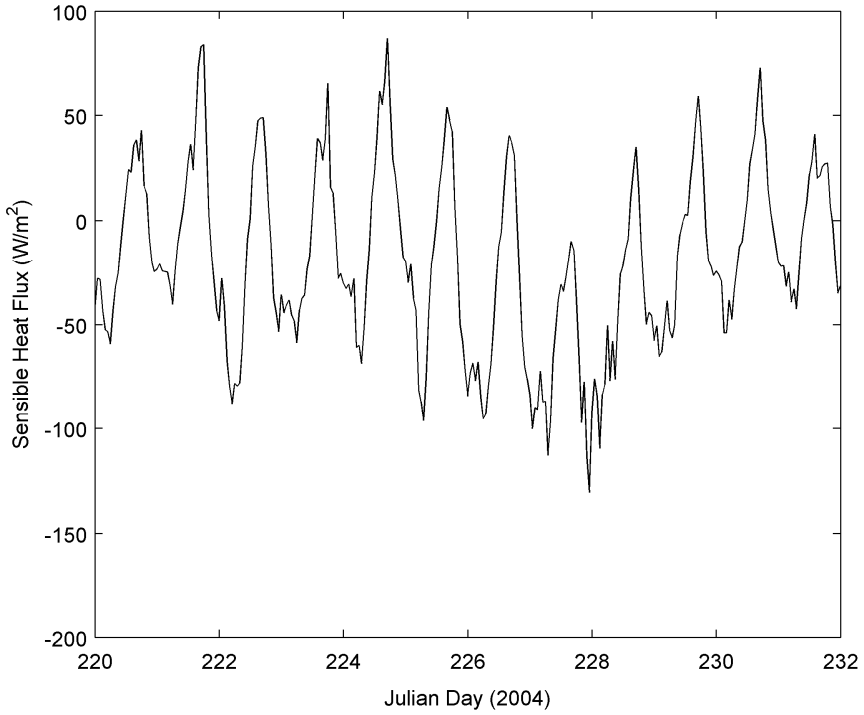

Figure 3-18. Sensible heat flux during model period.

To calculate the fluxes for input into the model, the surface water temperature from the mooring data is used. The meteorological data, together with the surface water temperature data, were used to compute heat fluxes (latent, sensible and net longwave) using the set of Matlab™ routines described by Palowiscz et al. (2001). The net heat flux is shown in Figure 3-19.

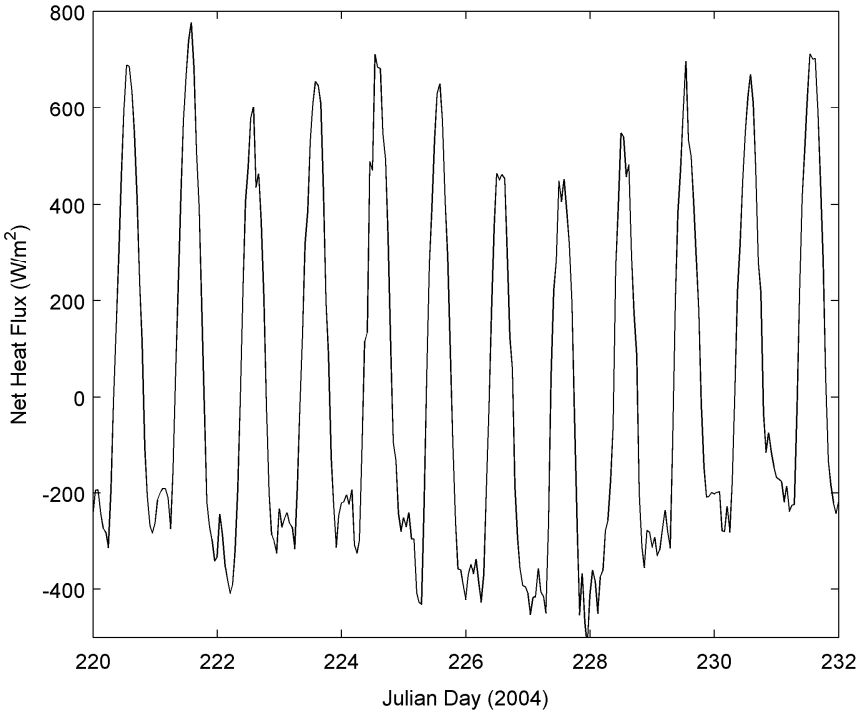

Figure 3-19. Net heat flux during model period.

3.3 Water Quality Boundary Conditions

Water quality boundary conditions were constructed using data collected by the City of Stockton as part of its NPDES permit compliance. Data are available at Vernalis and Mossdale in the San Joaquin River, as well as at eight locations in the San Joaquin River and the Stockton Deep Water Ship Channel, labeled R1 – R8, and shown in Figure 3-20. During 2004, these data were collected once each week beginning in June and ending December 1. The constituents included in the boundary conditions are dissolved oxygen (DO), algae as chlorophyll-a (Chla), particulate organic nitrogen (PON), dissolved organic nitrogen (DON), ammonium (NH_4), nitrate (NO_3), particulate organic phosphorus (POP), dissolved organic phosphorus (DOP), phosphate (PO_4), dissolved organic matter (DOM) and particulate organic matter (POM). The data collected at each site are summarized in Table 3. All necessary model constituents can be estimated from the collected data. Dissolved oxygen, chlorophyll-a, ammonium, nitrate and phosphate are used as presented in the data. If a constituent was reported as <RL, then the reporting limit (RL) was used as an estimate for the constituent at that time period. To determine the dissolved-to-particulate fraction of organic matter, nitrogen and phosphorus, the ratio of dissolved BOD to total BOD was used as the

dissolved fraction and the particulate fraction is 1 – dissolved fraction. The same fractions are applied to each constituent. To calculate total organic nitrogen, ammonia (NH_3) was subtracted from TKN. This was then partitioned into the dissolved and particulate fractions. Similarly, total organic phosphorus was estimated as total phosphorus minus the soluble reactive phosphorus and partitioned the same way. Dissolved organic matter was calculated using dissolved organic carbon. Using the stoichiometric ratios for organic matter presented in Chapra (1997), the DOC was divided by 0.4 to determine dissolved organic matter. The TOC and DOC values in the data were nearly identical, and therefore instead of using DOC – TOC as particulate organic carbon, the VSS was used as POC. The VSS was assumed to represent the particulate organic carbon, and the same stoichiometric ratio for organic matter used for the DOC to DOM conversion.

Table 3. Water quality constituents collected by City of Stockton.

Constituent	Abbreviation	units
Dissolved Oxygen	DO	mg/L
Water temperature	Tw	^oC
pH	pH	SU
Light penetration	PEN	inches
Biological Oxygen Demand	BOD	mg/L
Dissolved Biological Oxygen Demand	DBOD	mg/L
Total Organic Carbon	TOC	mg/L
Dissolved Organic Carbon	DOC	mg/L
Turbidity	Turb	Hach FTU
Total Suspended Solids	TSS	mg/L
Volatile Suspended Solids	VSS	mg/L
Electrical Conductivity	EC	umhos/cm
Ammonia	NH3	mg/L
Nitrate + Nitrite	NO3	mg/L
Total Kjeldahl Nitrogen	TKN	mg/L
Total Phosphorus	TP	mg/L
Soluble Reactive Phosphorus	SRP	mg/L
Chlorine	Cl	mg/L
Chlorophyll-a	Chl-a	ug/L
Pheophytin-a	Phe-a	ug/L

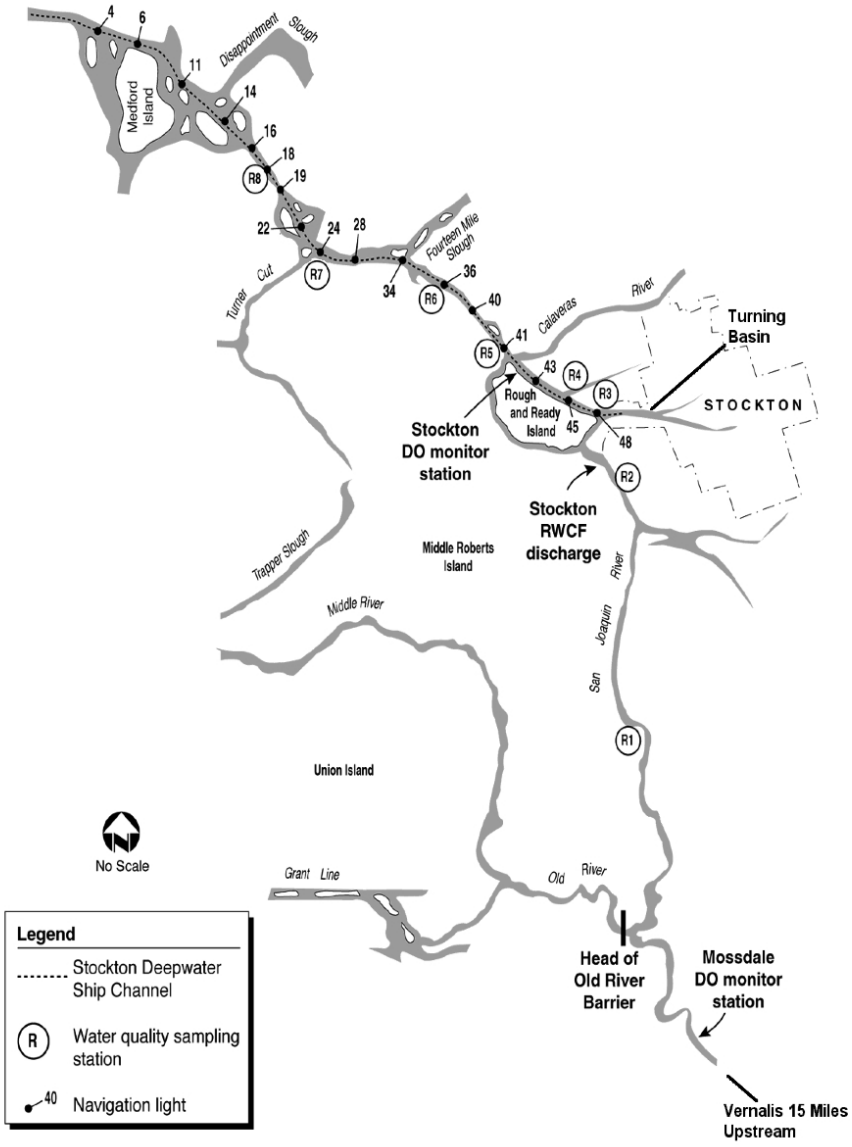

Figure 3-20. San Joaquin River and Stockton Deep Water Ship Channel, showing location of City of Stockton monitoring locations (R1 - R8). Map from Jones & Stokes Data Atlas.

Boundary 1 was created using data from R8, boundary 3 created using data from R1. No data were collected in any other side channels, therefore, R6 was used for boundary 2 and R7 used for boundary 4. A linear interpolation was used to create the boundary condition between sampling points.

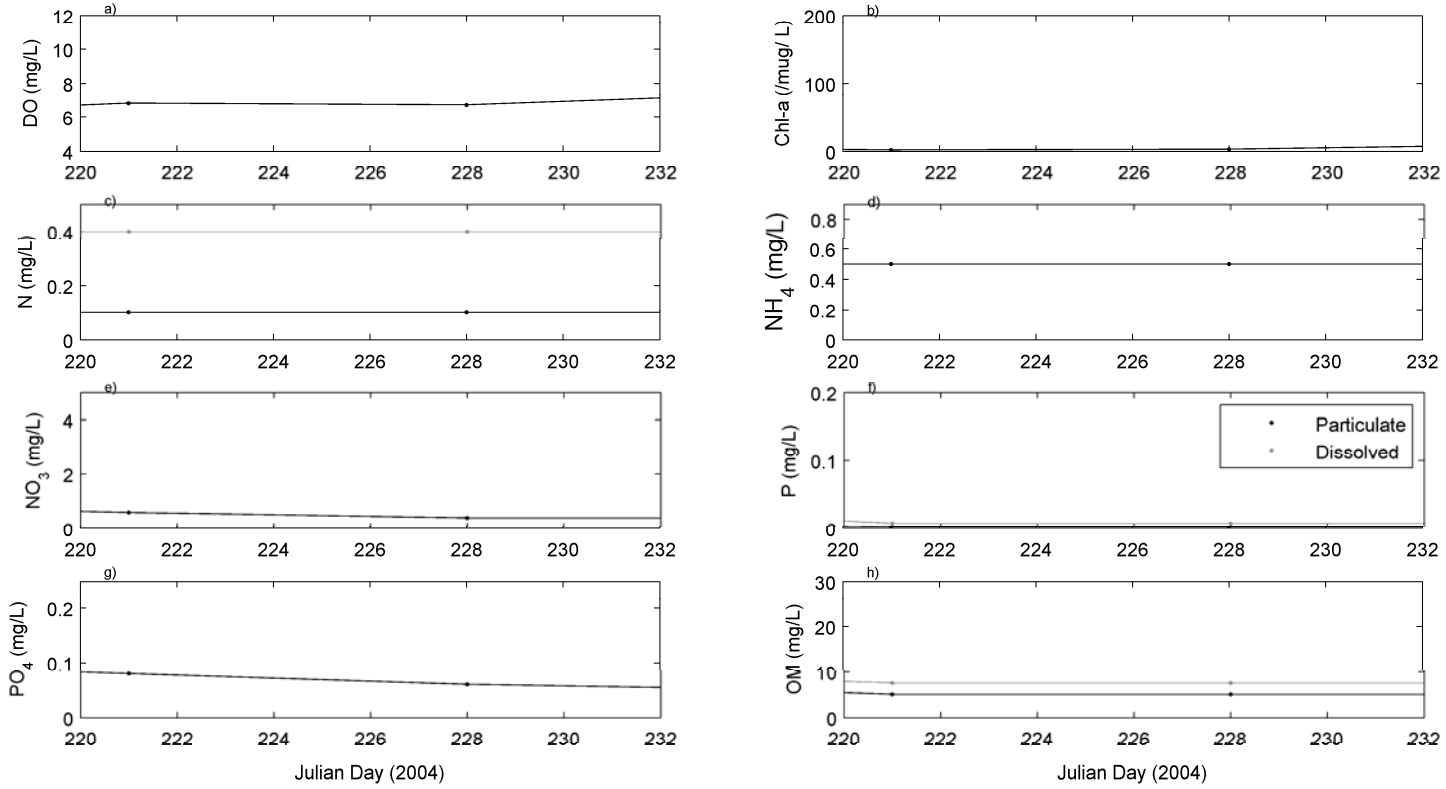

Figure 3-21. Water quality boundary conditions for boundary 1 constructed using data from R8. a) DO, b) Chl-a, c) PON and DON, d) NH_4, e) NO_3, f) POP and DOP, g) PO_4 and h) POM and DOM

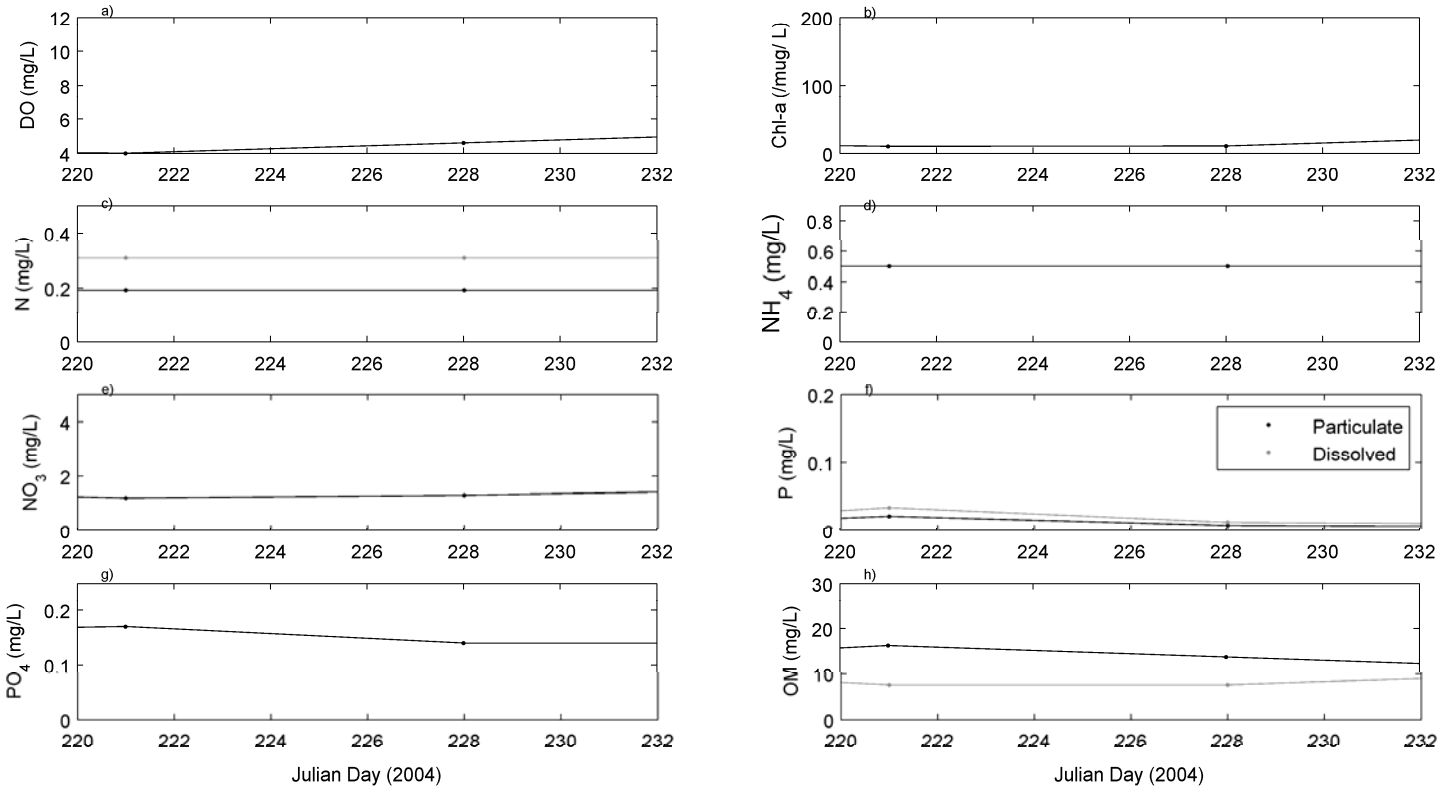

Figure 3-22. Water quality boundary conditions for boundary 2 constructed using R6 data. a) DO, b) Chl-a, c) PON and DON, d) NH_4, e) NO_3, f) POP and DOP, g) PO_4 and h) POM and DOM

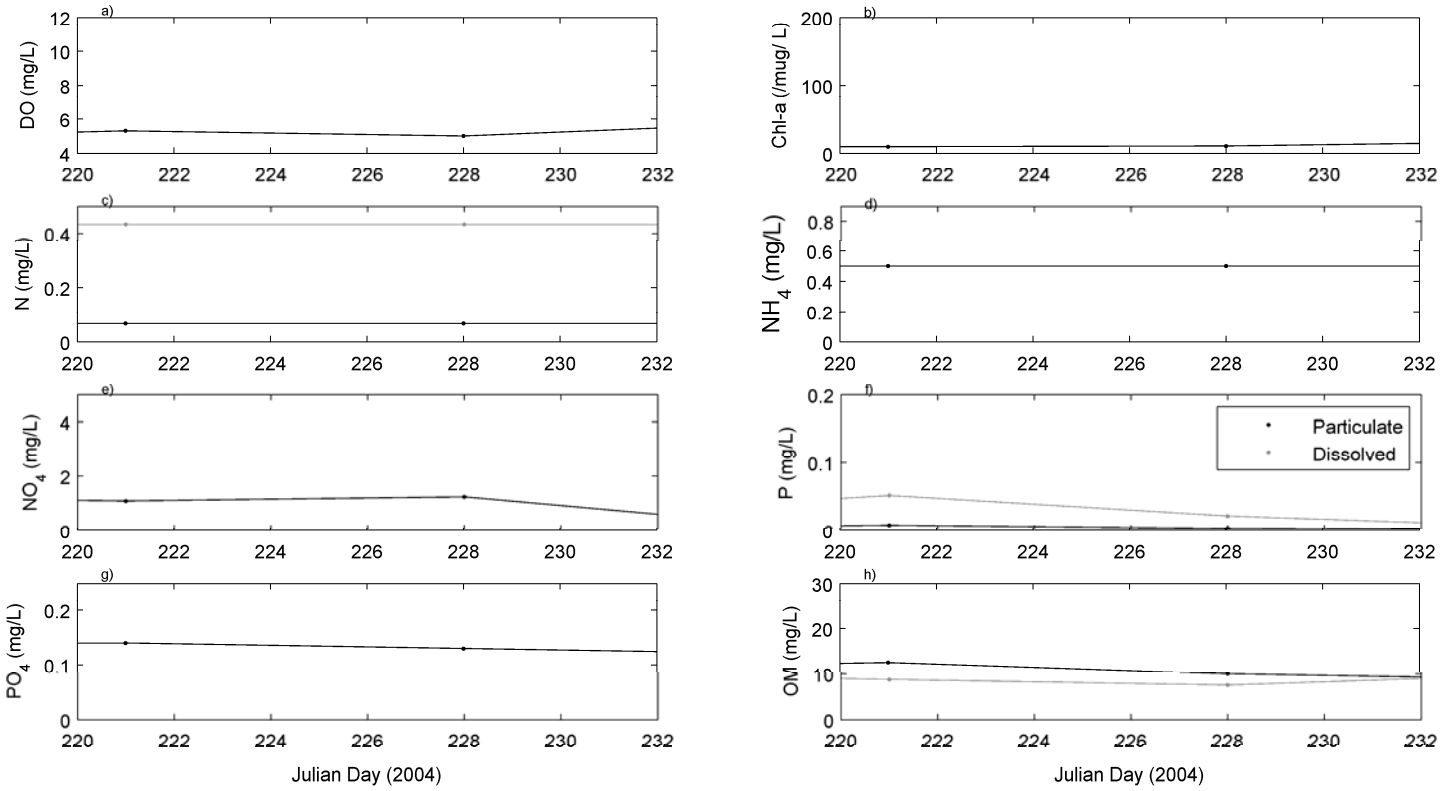

Figure 3-23. Water quality boundary conditions for boundary 3 constructed using R7 data. a) DO, b) Chl-a, c) PON and DON, d) NH_4, e) NO_3, f) POP and DOP, g) PO_4 and h) POM and DOM

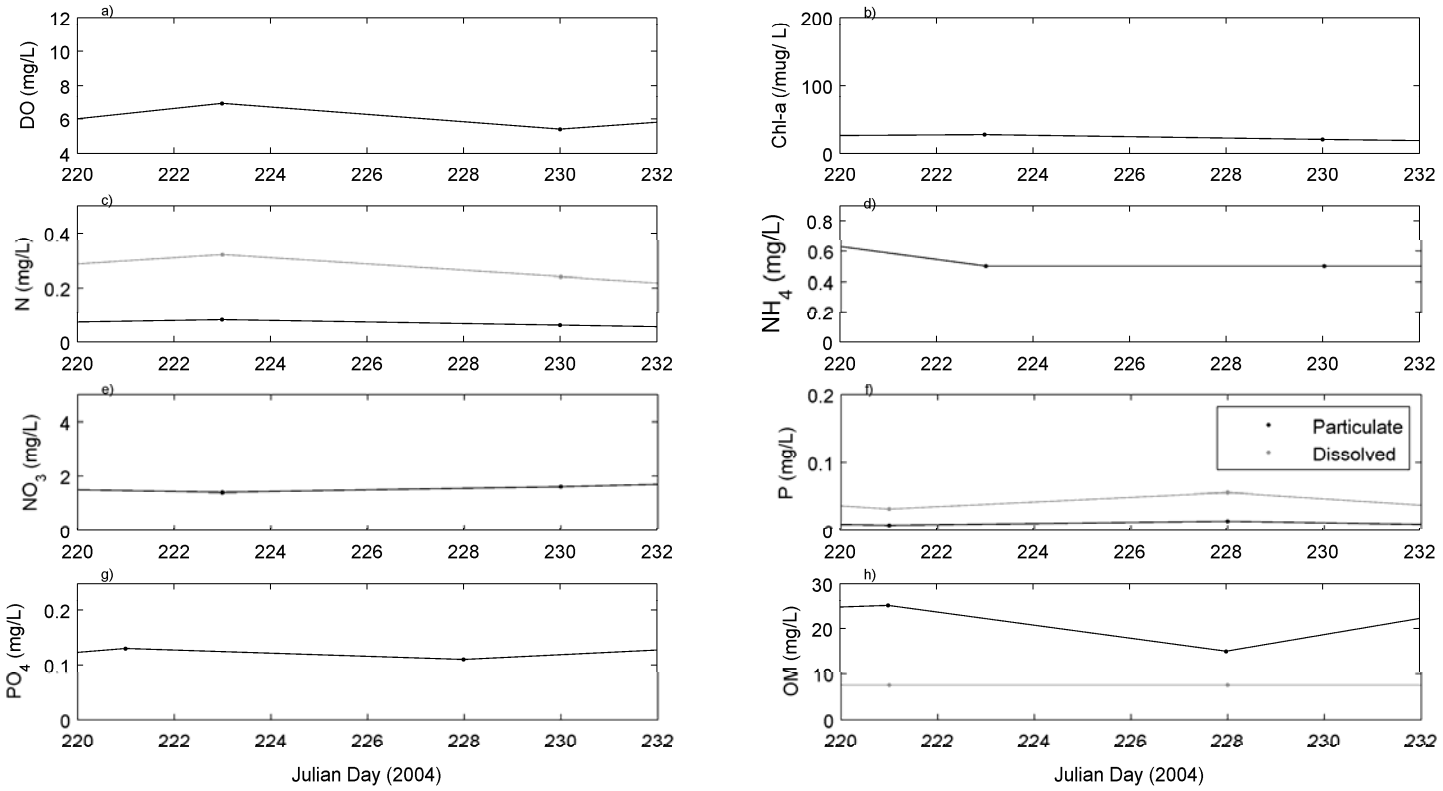

Figure 3-24. Water quality boundary conditions for boundary 4 constructed using R1 data. a) DO, b) Chl-a, c) PON and DON, d) NH_4, e) NO_3, f) POP and DOP, g) PO_4 and h) POM and DOM

3.4 Model Constants

All the water quality model constants are presented in Table 4. Rates were taken from a number of sources. When available, rates for this model application were taken from the Hydroqual modeling effort. Missing variables were estimated from Bowie et al. (1985)

Table 4 Summary of water quality model constants.

Coefficient	Units	Value	Definition
acc	ug-Chla/mgA	40.00	Phytoplankton ratio of C:chl-a
anc	mg-N/ mg-A	8.00	Fraction of algal biomass that is N
apc	mg-P/ mg-S	1.50	Fraction of algal biomass that is P
FNH4	dimensionless	0.50	Algae preference for NH4
k_a	1/day	1.00	Reaeration rate of DO
k_arb	1/day	0.00	Decay rate for arbitrary constituent
k_dn	1/day	0.10	Rate of denitrification
k_DOM	1/day	0.11	Oxidation rate of DOM
k_ex	1/day	0.00	Excretion rate of algae
k_gr	1/day	0.10	Grazing rate of algae
k_hc	1/day	0.05	Hydrolysis rate of POM
k_hn	1/day	0.10	Rate of hydrolysis on PON
k_hp	1/day	0.05	Hydrolysis rate of POP
k_mn	1/day	0.07	Rate of mineralization of DON
k_mor	1/day	0.01	Phytoplankton mortality rate
k_mp	1/day	0.07	Mineralization rate of DOP
k_n	1/day	0.07	Nitrification rate
k_ra	1/day	0.05	Respiration rate of algae
k_rs	1/day	0.00	Resuspension rate
k_set	1/day	0.00	Settling rate
k_setarb	1/day	0.00	Settling rate for arbitrary constituent
k_vn	1/day	0.01	Volatilization rate of NH4
KDOM	mg-DOM/L	0.05	Half-saturation coefficient for DOM oxidation
KNIT	mg-N/L	0.60	Half-saturation coefficient for nitrification
KSN	mg-N/L	0.10	Half-saturation coefficient for nitrogen for algae growth
KSP	mg-P/L	0.01	Half-saturation coefficient for phosphorus for algae growth
mu_max	1/sec	2.20	Maximum growth rate of algae
roc	mg-O/mg-A	2.67	Ratio of O:C in photosynthesis & resp
ron	mg-O/mg-N	4.57	Ratio of O:N in nitrification
Theta_a	dimensionless	1.05	Tw dependence for k_a
Theta_dn	dimensionless	1.045	Tw dependence on denitrification
Theta_DOM	dimensionless	1.045	Tw dependence for DOM oxidation
Theta_gr	dimensionless	1.045	Tw dependence for grazing of algae
Theta_hc	dimensionless	1.045	Tw dependence for hydrolysis of POM
Theta_hp	dimensionless	1.045	Tw dependence for hydrolysis of POP
Theta_mn	dimensionless	1.020	Tw dependence for DON mineralization
Theta_mor	dimensionless	1.080	Tw dependence for phyto mortality
Theta_mp	dimensionless	1.020	Tw dependence for mineralization of Dop

Theta_mu	dimensionless	1.045	Tw dependence for growth of algae
Theta_n	dimensionless	1.045	Tw dependence for nitrification
Theta_PON	dimensionless	1.045	Tw dependence of PON hydrolysis rate
Theta_ra	dimensionless	1.045	Tw dependence for k_ra
Theta_SOD	dimensionless	1.045	Tw dependence for SOD
Theta_vn	dimensionless	1.045	Tw dependence for volatilization of NH4

The boundary conditions and model constituents discussed in this chapter were the best estimate of conditions based on field measurements, previous studies and modeling experience. Through the successful calibration of all constituents, these constants and rates will change so that the model best reflects observed conditions.

4. Hydrodynamic Calibration

After initial calibration of the model for flows and water level only for 2000 (see Monismith et al. 2008), the full model, including the effects of temperature, was applied to the DWSC for the August 2004 experimental period. Calibration of the hydrodynamic sub-model was broken into three parts: water surface elevation, velocity/currents and water temperature. The model discussed in this report is an updated version of the model used by Monismith et al. (2008) for calibration. The original model proved unstable when the effects from water temperature were added, but the revised model did not encounter the same problems.

4.1 Water Depth

Water surface elevation results at the five long-term mooring stations can be seen in Figure 4-25. Results show that there was a temporal lag between the model and the observed data, but very good correlation between SI3D model output and DSM2 output. This was further reflected in Figure 4-26 and Figure 4-27, which show scatter plots of measured and modeled water surface elevation. The correlations (r^2) between modeled and observed data (Figure 4-26) range between 0.649 and 0.714, with increased correlation moving downstream. However, the correlation between SI3D output and DSM2 output is much stronger (Figure 4-27) with all correlations above 0.95. Because the domain was limited, water levels in the interior are largely controlled by the boundary conditions. The model can only be as accurate as the boundary conditions provided from DSM2. This suggests that improvements in calibration of water surface elevation will require a correction to DSM2 output.

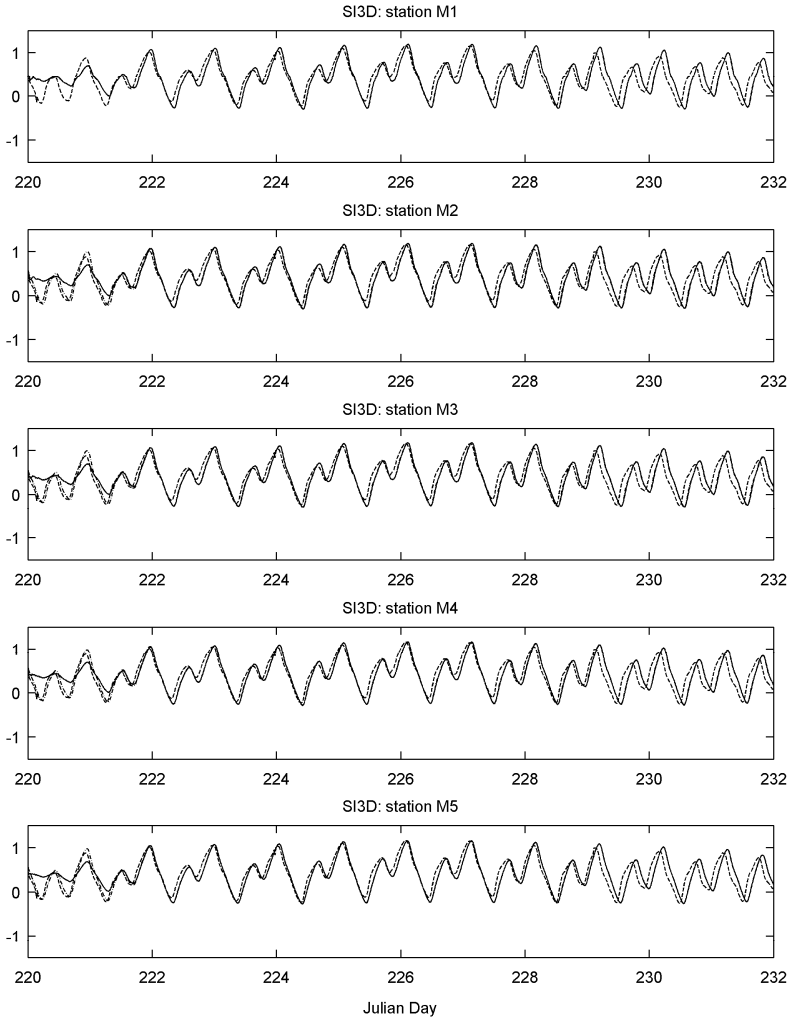

Figure 4-25. Time series comparison of observed (dashed), modeled (solid) and DSM2 output (dash- dot) water surface elevations for August 7 - August 19, 2004.

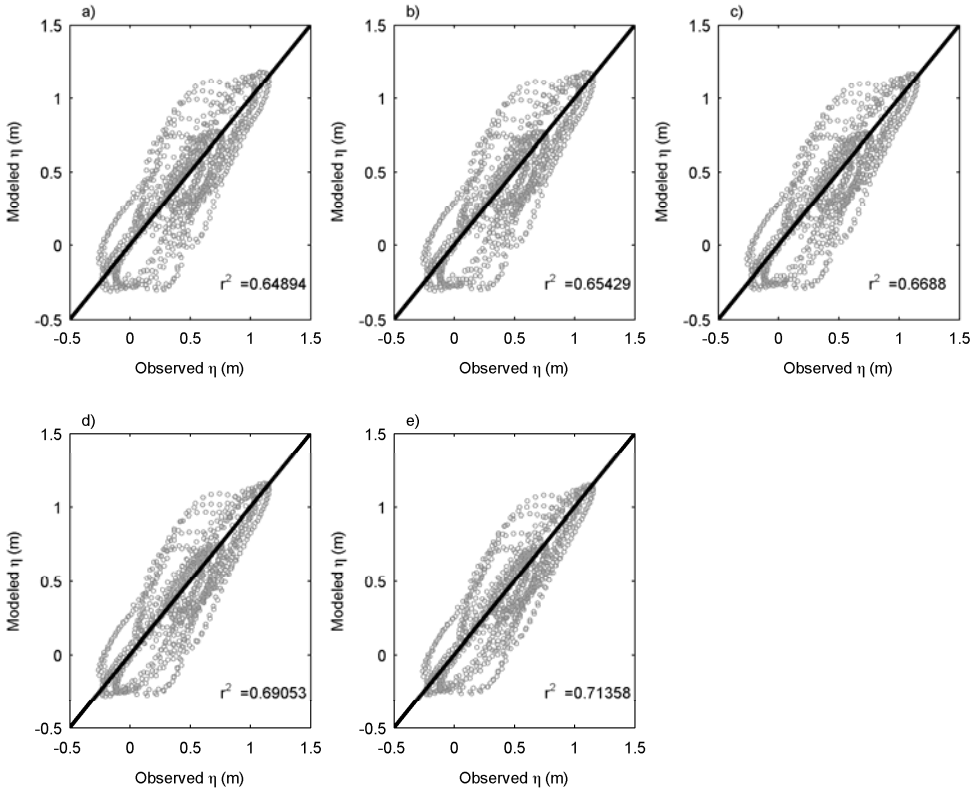

Figure 4-26. Comparison of modeled and observed water levels at selected stations in the San Joaquin River for (a) station M1, (b) station M2, (c) station M3, (d) station M4, (e) station M5.

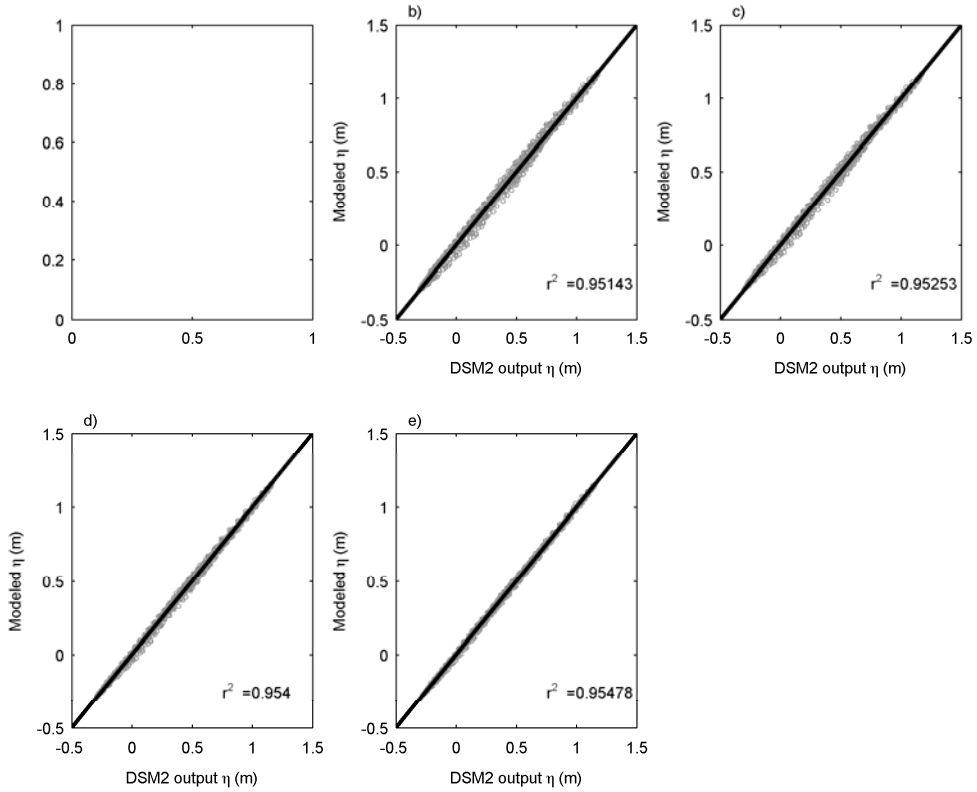

Figure 4-27. Comparison of SI3D model output and DSM2 model output for water levels at selected stations in the San Joaquin River for (a) station M1 (no DSM2 data available), (b) station M2, (c) station M3, (d) station M4, (e) station M5.

4.2 Velocity and Flow

As expected from the water surface elevation, the modeled velocity was out of phase from the observed velocity (Figure 4-28 through Figure 4-32). The model maintained the general observed pattern of flow, which included an influence from the tide. In addition to being out of phase, the model overestimated the range in velocity, at all depths. The peak velocities, in both the positive and negative direction, were greater in the model than the observed conditions. Some of the stations deviated more than others. In particular, station M3, in the middle of the domain, has a better match than the other stations. Station M2 has significant deviations from observed

conditions. This was the station closest the confluence of the San Joaquin River and Deep Water Ship Channel and the location where previous model applications required increasing the mixing coefficient in that region. The amplitude error was similar for a range of horizontal mixing coefficients, ranging from 0.01 m^2/s to 1.0 m^2/s.

Similar to the water surface elevation, the modeled flow did match the DSM2 modeled flow. As discussed in Monismith et al. (2008), the simulated DSM2 and SI3D flows are similar, and both diverge from the observed flow conditions. In 2004, the flow gage in the domain (at RRI) was not functioning properly, so no data exists. However, as shown in Figure 4-33, the flow at this location output by SI3D and DSM2 are similar, further suggesting that SI3D is dependent on the conditions supplied by DSM2.

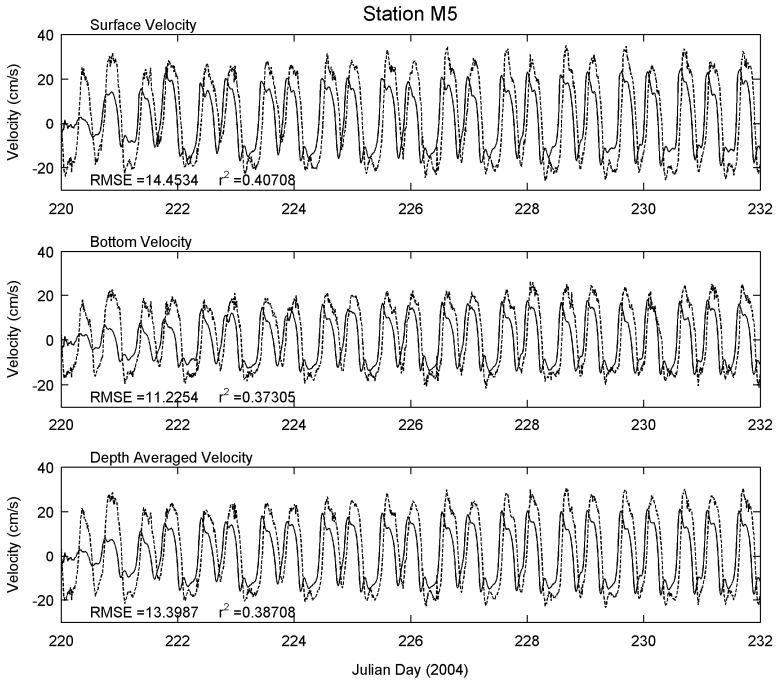

Figure 4-28. Comparison of observed (dashed) and model (solid) velocities at Station M5 in the Stockton DWSC.

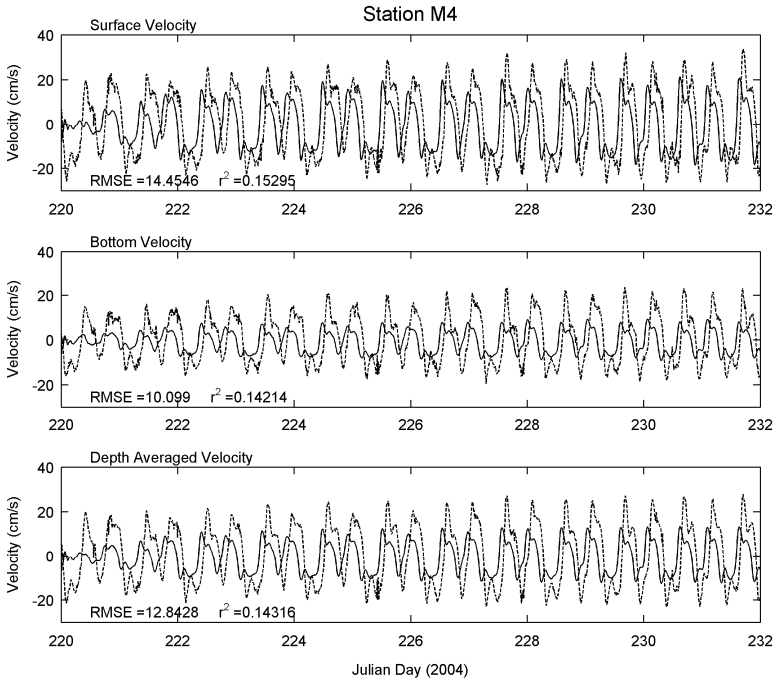

Figure 4-29. Comparison of observed (dashed) and model (solid) velocities at Station M4 in the Stockton DWSC.

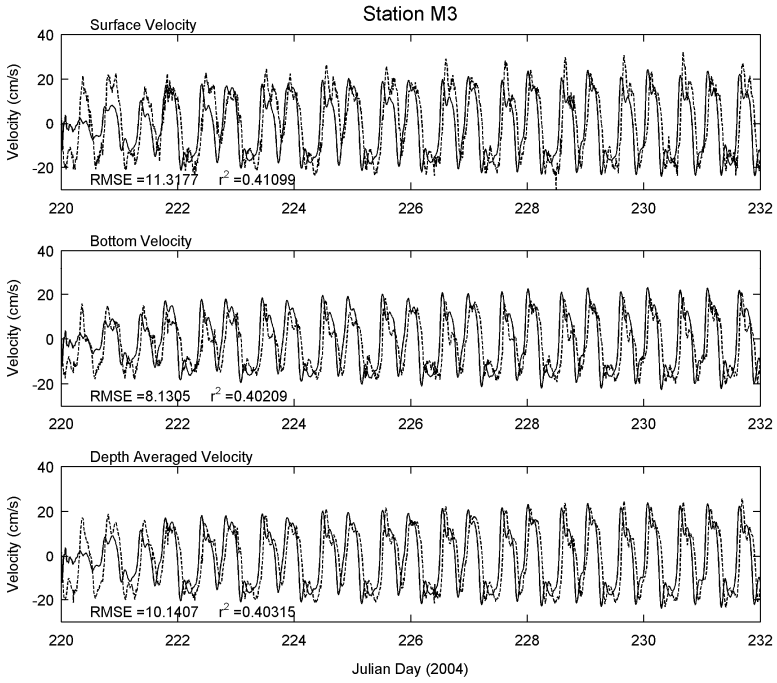

Figure 4-30. Comparison of observed (dashed) and model (solid) velocities at Station M3 in the Stockton DWSC.

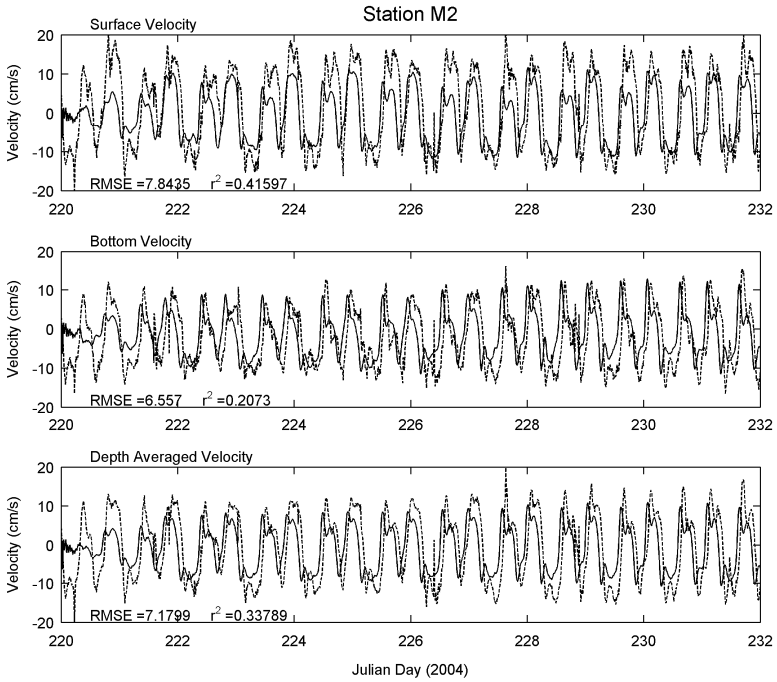

Figure 4-31. Comparison of observed (dashed) and model (solid) velocities at Station M2 in the Stockton DWSC.

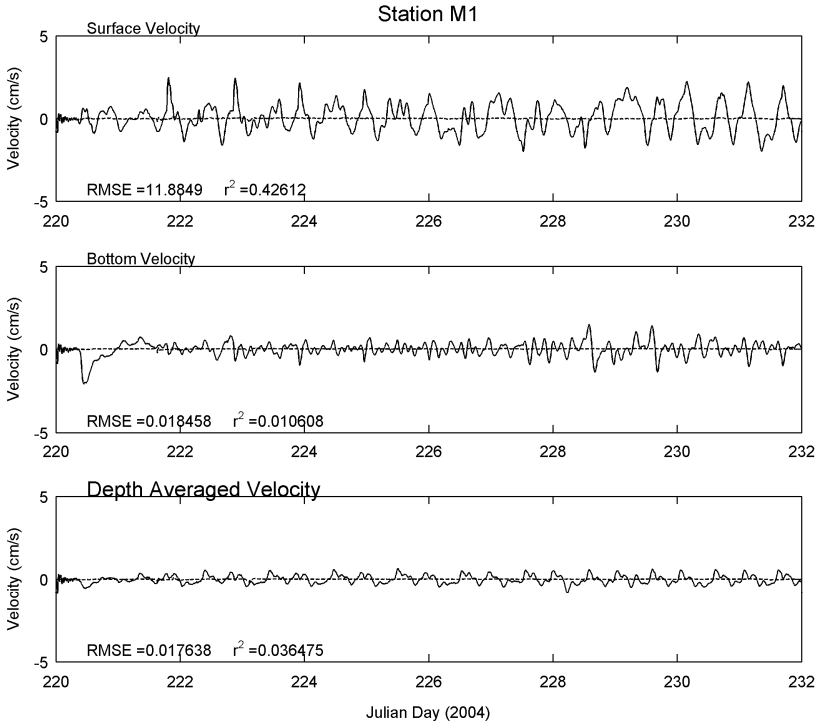

Figure 4-32. Comparison of observed (dashed) and model (solid) velocities at Station M1 in the Stockton DWSC.

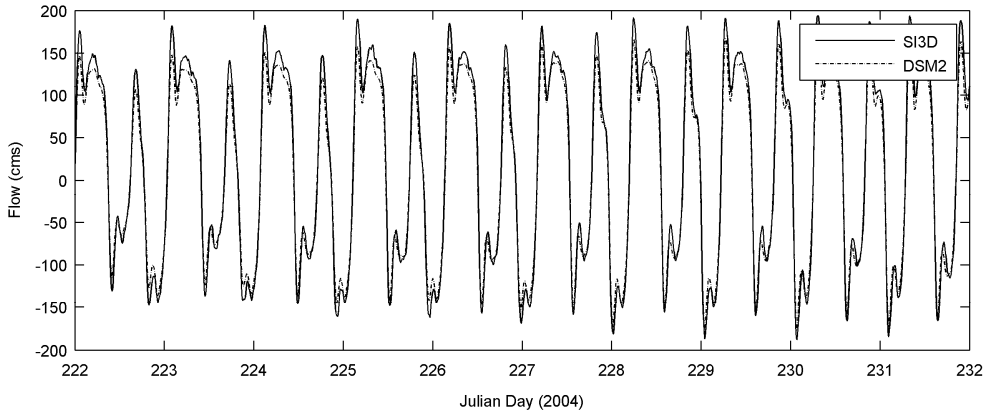

Figure 4-33. Comparison of SI3D (solid) and DSM2 (dashed) flow at RRI in the Stockton DWSC.

4.3 Water Temperature

Water temperature model outputs were compared to two sets of observed data. The first was the month long data set at locations M1 – M5 shown in Figure 3-4. At these locations, fast response thermistors were placed at one-meter intervals. The thermistors collected temperatures every minute during the month of August, providing a complete picture of the thermal pattern over the course of an entire tidal cycle.

The initial model simulation, including water temperature as an active constituent, produced promising results. The model simulation calculated surface boundary conditions in a pre-processed mode, as described in Section 0 of this report. The results are shown in Figure 4-34 through Figure 4-42. The outcome of the model versus observed data was significantly different from location to location. At the location closest to the ocean, station M5, the model was slightly too cool. As expected, the surface water temperatures at M5 were very similar in pattern to the observed temperatures, but the same was not true for the bottom temperatures (Figure 4-35). As previously mentioned, station M5 was close to the downstream boundary, and in fact, the observed surface conditions at M5 were used as the boundary conditions at this location. However, between the boundary and the M5 location, the water warms, suggesting that a correction for the input at boundary condition 1 may be necessary. The results from this location also suggest that assuming constant temperature at the boundary may not be an accurate assumption.

At station M4, the model and observed conditions behave similarly. The pattern of diurnal stratification was reproduced in the model. At the beginning of the period of interest, the peak daily temperatures were similar, but toward the end of the model period, it was the daily low surface temperatures that were similar. The initial temperature used for the model appears to be appropriate for this location.

At station M3, the daily stratification pattern was reproduced by the model, but the model was slightly too cool for the entire period. Even though the pattern of heating and cooling was similar, the predicted temperatures are low. This appeared to be a function of the initial water temperature selected.

At station M2, the model predicted more stratification than was observed in the system. The observed conditions show daily mixing, but the model has long periods where the system remained stratified, with the surface and bottom temperatures remaining separated by half a degree. The peak temperatures predicted do match the observed conditions, but too much cooling occurs. The bottom temperature predicted by the model was much cooler than observed conditions.

At the station furthest upstream, station M1, more stratification was predicted by the model than observed in the system. The bottom temperatures were too cool, by as much as 2 ^{o}C. The surface temperatures, however, were similar, with peak highs and lows matching observed conditions.

Another method used to calibrate and assess the validity of the model predictions was to compare the model and observed data with the theoretical prediction of the longitudinal change in surface temperature. The theory was based on a one-dimensional model of water temperature as described in Monismith et al. (2008). The theory suggests that for weak flows, the temperature approaches equilibrium temperature, whereas for strong flows, the temperature remains close to that of the boundaries. In addition, the maximum temperature is found in the interior of the domain. The observed conditions matched closely to the theory presented, however, the first model simulation exhibited a significantly different pattern (Figure 4-44). The interior of the domain was cooler than the downstream boundary. This model pattern suggests that the water temperature was dominated by the upstream boundary condition. In order to try and fit the model predictions to the theory and observed data, the heat fluxes were altered. After calculating the heat fluxes as described in the

previous section, they were increased by 10%. This was done to try and increase the heat at the surface boundary. The results from this simulation predicted an increase in temperature in the interior section of the domain (Figure 4-45). Looking at the temperature patterns at the moorings for this change in heat fluxes shows an improvement at some stations, but not at others. For example, at Station M1, the bottom temperatures were still too cool, the surface temperatures start out similar to observed conditions, but toward the end of the period, continue to increase (Figure 4-46).

The initial model simulations and calibration results shown were promising, but suggested a number of improvements that should be made to the model. This includes allowing the initial water temperature to vary over the domain. In addition, because the boundary conditions were so close to the area of interest, it will be an improvement if the downstream boundary condition varies over the depth of the channel. Another improvement to the model would be allowing the attenuation coefficient to vary over the domain, allowing some areas to absorb more heat than other sections of the domain. These improvements would go a long way in making the calibration of water temperature to observed conditions a success.

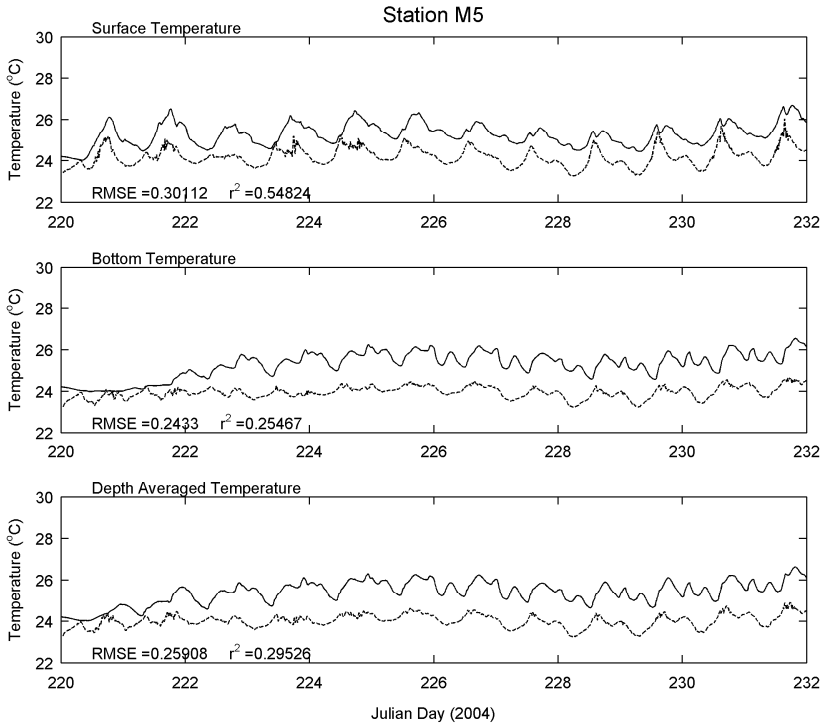

Figure 4-34. Comparison of observed (dashed) and modeled (solid) water temperature at Station M5 in the DWSC.

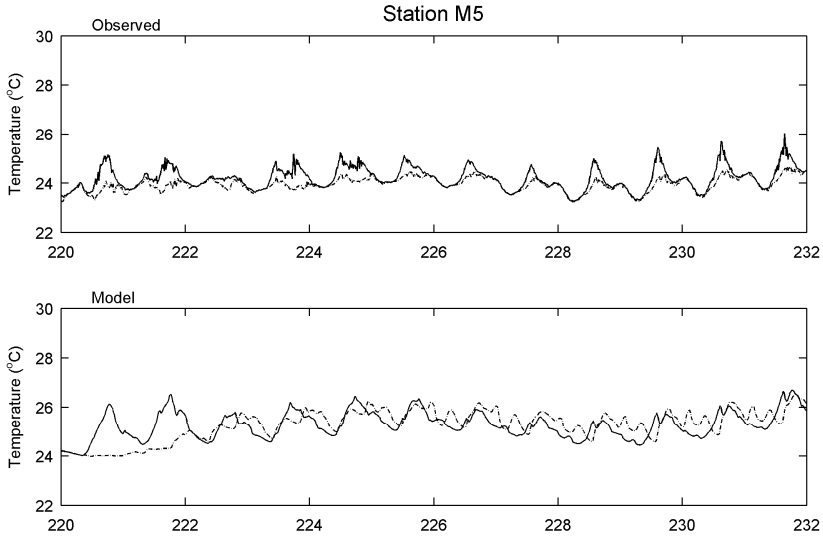

Figure 4-35. Surface (solid) and bottom (dashed) water temperature in the Stockton DWSC.

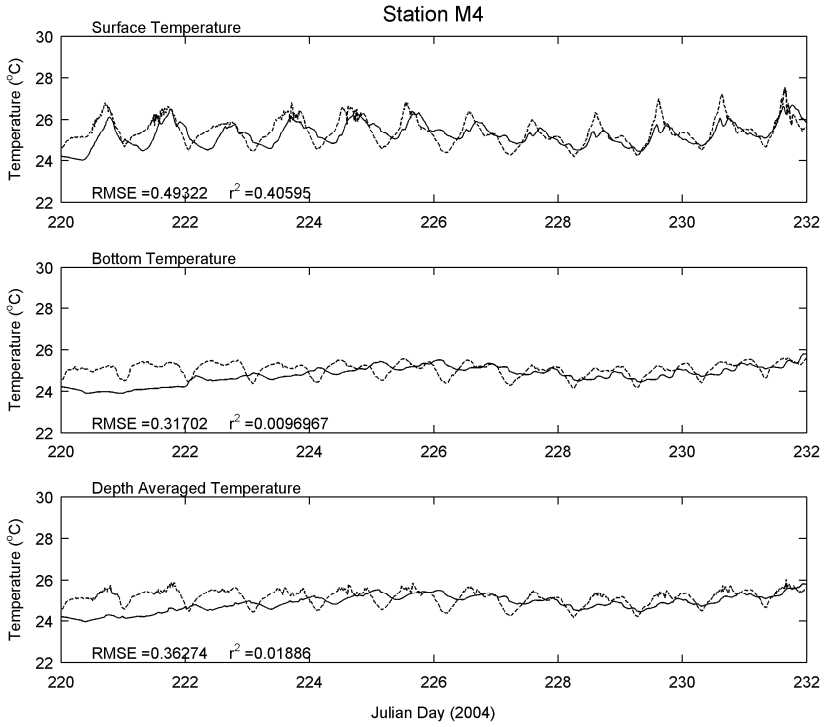

Figure 4-36. Comparison of observed (dashed) and modeled (solid) water temperatures at Station M4 in the DWSC.

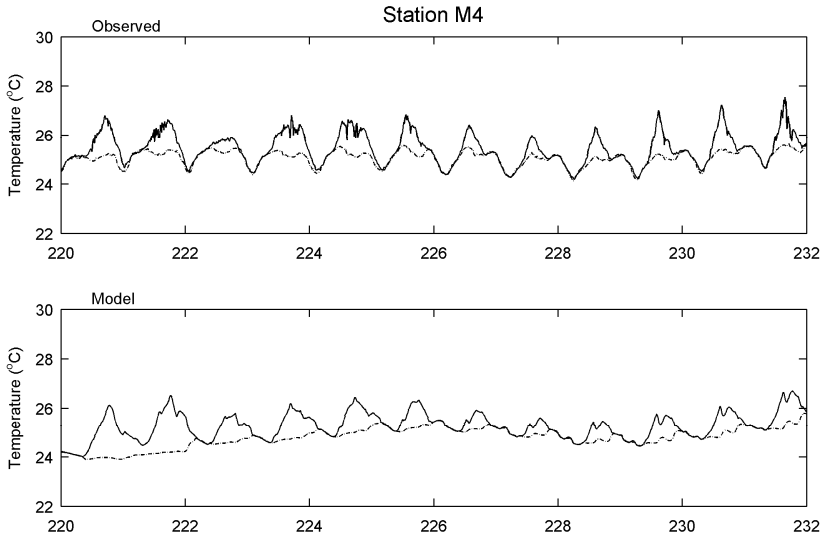

Figure 4-37. Surface (solid) and bottom (dashed) water temperature in the Stockton DWSC.

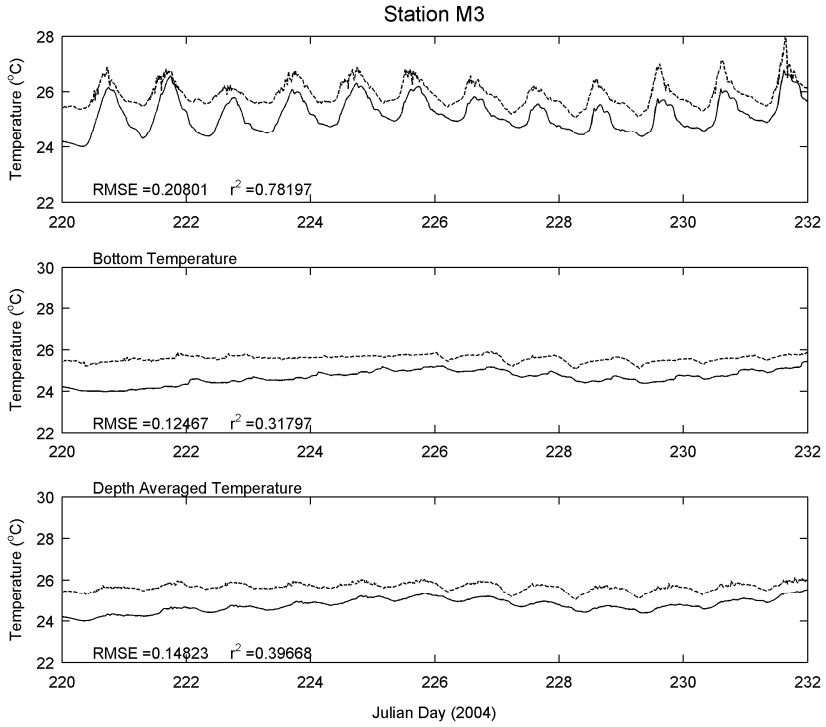

Figure 4-38. Comparison of observed (dashed) and modeled (solid) water temperature at Station M3 in the DWSC.

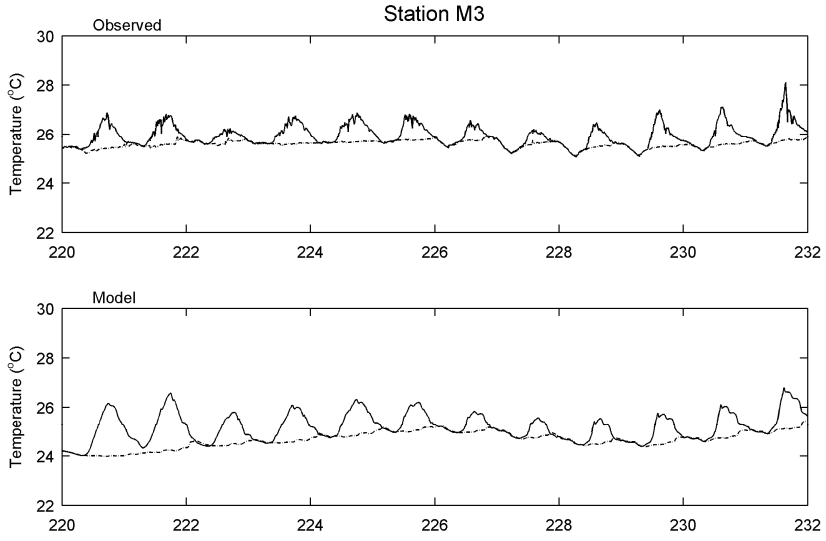

Figure 4-39. Surface (solid) and bottom (dashed) water temperature in the Stockton DWSC

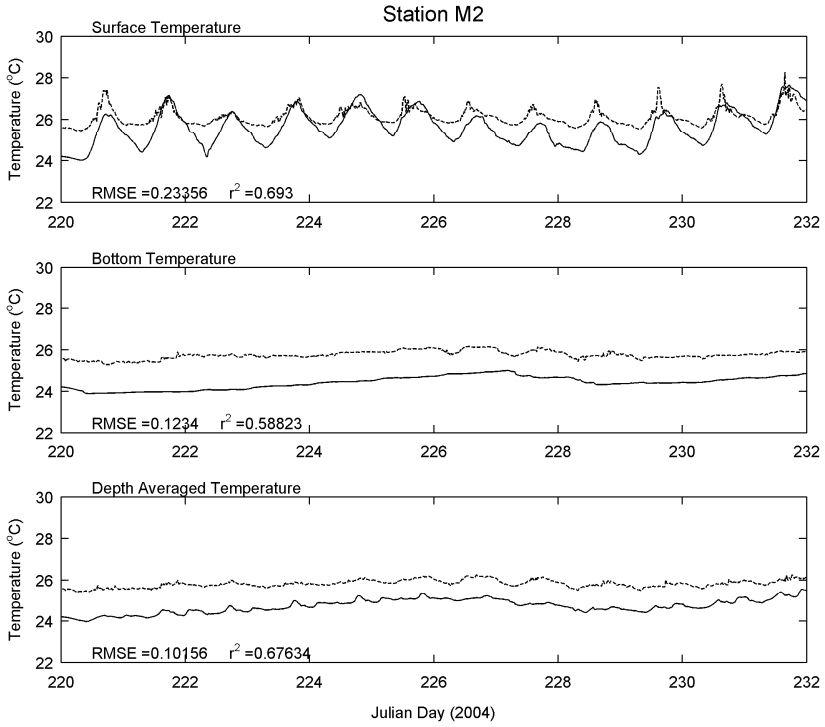

Figure 4-40. Comparison of observed (dashed) and modeled (solid) water temperatures at Station M2 in the DWSC.

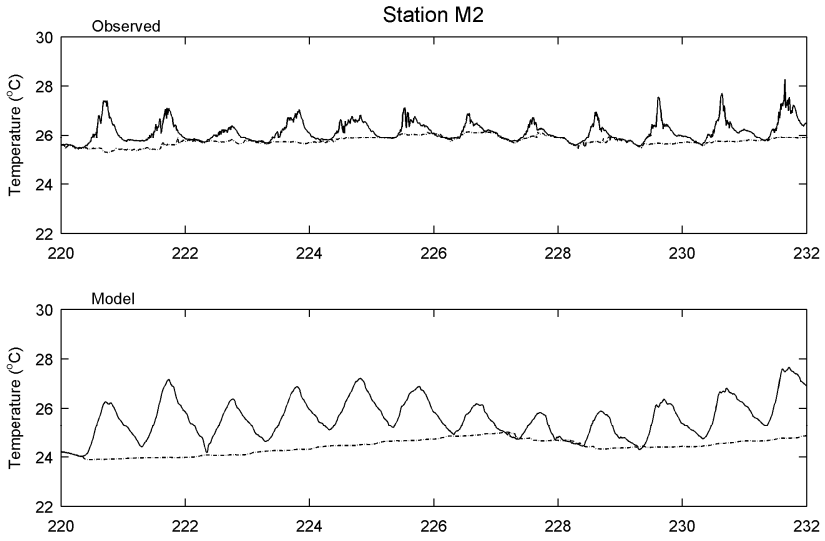

Figure 4-41. Surface (solid) and bottom (dashed) water temperature in the Stockton DWSC

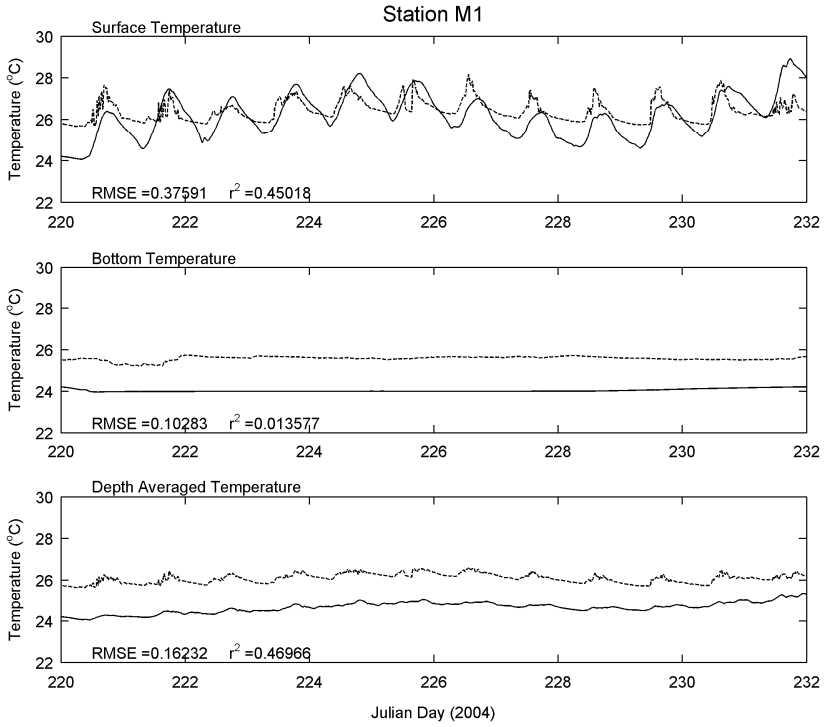

Figure 4-42. Comparison of observed (dashed) and modeled (solid) water temperatures at Station M1 in the DWSC.

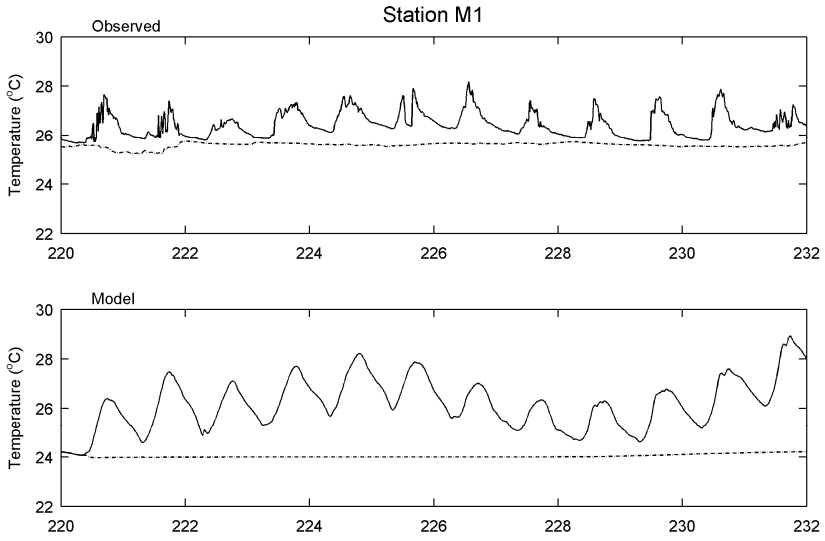

Figure 4-43. Surface (solid) and bottom (dashed) water temperature in the Stockton DWSC

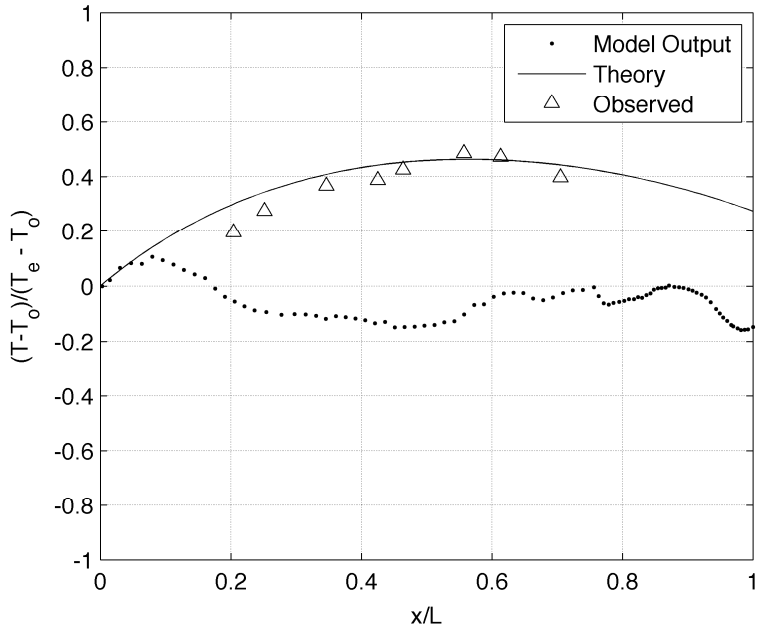

Figure 4-44. Comparison of theory, observed and modeled one-dimensional prediction of longitudinal change in water temperature for original simulation.

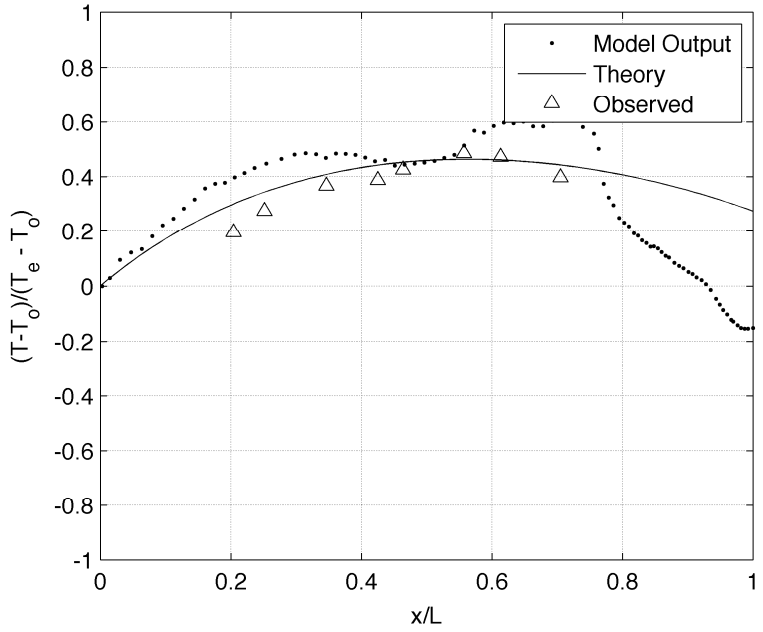

Figure 4-45. Comparison of theory, observation and modeled prediction of longitudinal change in water temperature for an increase in surface heat fluxes of 10%.

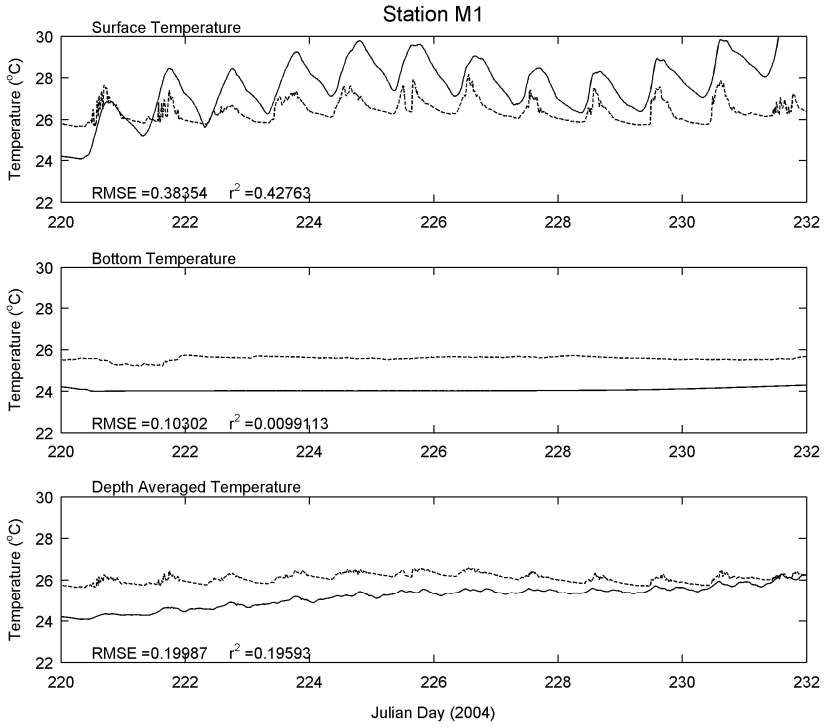

Figure 4-46. Comparison of observed (dashed) and modeled (solid) water temperatures at Station M4 in the DWSC for an increase in fluxes.

5. Conclusion and Recommendations for Further Study

In order to solve the problem of low dissolved oxygen in the Stockton Deep Water Ship Channel, a complete understanding of all processes, physical, biological and chemical, as well as their interactions must be understood. Due to the complex bathymetry of the channel, a detailed three-dimensional model of the system is the best method available for understanding how these processes interact, and, more importantly, what can be done to remedy the poor conditions.

The model selected to represent the hydrodynamics of the system showed promising results, and development and adaptation of the water quality portion of the model suggested that with further model enhancements and improved boundary conditions, a predictive, three-dimensional representation of water quality in the Stockton Deep Water Ship Channel is readily attainable. Some limitation of the current model included the assignment of water temperature boundary conditions and attenuation coefficients. It was obvious from initial model simulations that a constant attenuation coefficient for the entire system was not representative. The model should be updated to allow this constituent to vary over the domain. In addition, assuming well-mixed boundary conditions and a constant initial vertical water temperature are not accurate estimates for this system. Another important improvement to the model would be the assignment of water surface heights at the boundaries. The current model uses DSM2 output. Being able to use the output from another community-supported modeling effort was valuable; however, in this case, DSM2 does not seem to be as accurate as necessary for the section of river under study. With the relatively small model domain, errors introduced at the boundary dominate the entire domain.

Without an accurate model of the hydrodynamics, modeling the water quality will be nearly impossible. There are two ways to improve this downfall. The first would be to extend the model boundaries to locations much further from the section of river of interest. This will decouple the dependence of the area of interest on the boundaries, but would require much more computing power and the further development of the grid. The second would be to move away from the DSM2-derived boundary conditions and derive input from another source. All of the improvements suggested were beyond the scope of this project.

During the course of this project, significant improvements were made to the model. The most notable of these was the development and use of three-dimensional to two-dimensional mapping

functions. This freed up memory used by the model, and allowed the water quality model to be a sub-model of the hydrodynamic model. The original scope of work suggested that the water quality model would be run in a post-processor mode, but the advancement of the hydrodynamic codes allowed the two models to run simultaneously. This will prove to be beneficial in the future use of this model both in the Stockton Deep Water Ship Channel and in other systems. The water quality constituents and hydrodynamic constituents can now interact. For instance, the attenuation coefficient necessary in the temperature sub-model, which drives the hydrodynamics, can be altered with an increased flux of sediment, or as algal biomass increases.

A fully calibrated water quality model of the Stockton Deep Water Ship Channel will be an invaluable tool for stakeholders. Determining the causes and exploring solutions for the dissolved oxygen crisis is essential for the health of the system, and it is the hope of the researchers from this project that the model will be further developed and applied to the system.

6. References

Bain, R. C. and W. H. Pierce (1968). San Joaquin estuary near Stockton, California: An analysis of the dissolved oxygen regimen. San Francisco, California., Department of the Interior, Federal Water Pollution Control Administration, California/Nevada Basins.

Bowie, G.L., Mills, W.B., Porcella, D.B., Campbell, C.L., Pagenkopf, J.R., Rupp, G.L., Johnson, K.M., Chan, P.W.H., Gherini, S.A. and Chamberlin, C.E. (1985). Rates, constants and kinetic formations in surface water quality modeling (Second Addition). U.S. Environmental Protection Agency, ORD, Athens, GA, ERL, *EPA/600/3-85/040*. 455 pp.

Doyle, L, S.G. Schladow and F.J. Rueda (2007). "SI3DWQ User's Manual"

Jassby, A. D. (2005). "Phytoplankton regulation in a eutrophic tidal river (San Joaquin River, California)." San Francisco Estuary and Watershed Science. **3**(1).

Jassby, A. D. and E. Van Nieuwenhuyse (2005). "Low dissolved oxygen in an estuarine channel (San Joaquin River, California): mechanisms and models based on long-term time series." San Francisco Estuary and Watershed Science.

Kantha, L.H. and C.A. Clayson (1994). An improved mixed layer model for geophysical applications. Journal of Geophysical Research, 99(C12), 25235-25266.

King, I.P. (1998). Documentation: RMA-11- A Three Dimensional Finite Element Model for Water Quality in Estuaries and Streams. Version 2.6.

Lee, G.F. and A. Jones-Lee (2000) "Synopsis of Issues in Developing the San Joaquin River Deep Water Ship Channel DO TMDL", unpublished report submitted to San Joaquin River DO TMDL Steering Committee and the CVRWQCB, G. Fred Lee & Associates, El Macero, CA.

Lee, G. F. and A. Jones-Lee (2003). Synthesis and Discussion of Findings on the Causes and Factors Influencing Low DO in the San Joaquin River DWSC near Stockton, CA: Including 2002 Data. El Macero, CA.

Lehman, P. W., J. Sevier, et al. (2004). "Sources of oxygen demand in the lower San Joaquin River, California." Estuaries **27**(3): 405-418.

Monismith, S. G., Hench, J., Smith, P., Fleenor, W. E., Doyle, L. and Schladow, S. G. (2008). An Application of the SI3D Hydrodynamics Model to the Stockton Deep Water Ship Channel: Physics and Model Application. Final Report for CALFED ERP-02D-P51.

Pawlowicz, R., B. Beardlsey, S. Lentz, E. Dever, and A. Anis, (2001) "Software simplifies air-sea data estimates," *EOS Trans. Am. Geophys. Union*, 82, 2.

Rueda, F. J. (2001). "A three-dimensional hydrodynamic and transport model for lake environments." Ph.D. Dissertation, University of California, Davis.

Rueda, F.J. and Schladow, S.G. (2003) The internal dynamics of a large polymictic lake. Part II: three-dimensional numerical simulations. ASCE J. Hydraulic Engineering, 129(2), 92-101.

Rueda, F.J., Schladow, S.G. and Palmarsson, S.O. (2003). Basin-scale internal wave dynamics during a winter cooling period in a large lake. J. Geophysical Research 108 (C3), 3097.

Rueda, F.J. and Cowen, E.A. (2005). Residence time of a freshwater embayment connected to a large lake. Limnology and Oceanography. 50(5), 1683-1653.

Smith, P. E. (1997). "A three-dimensional, finite-difference model for estuarine circulation." Ph.D. Dissertation, University of California, Davis.

Smith, P.E. (2006). "A semi-implicit, three-dimensional model for estuarine circulation", *USGS Open File Report 2006-1004*, 176 pp.

6. SI3DWQ User's Manual

One of the primary objectives of this research project was to develop a three-dimensional hydrodynamic and water quality model, and to use it to better understand processes in the SDWSC. Using three-dimensional models requires familiarity with numerical methods and modeling principles in general. The User's manual, which was completed in December 2007, was written with the assumption that the user will have an appropriate background.

SI3DWQ User's Manual

Laura Doyle, Geoff Schladow, Francisco Rueda

December 29, 2007

1 Introduction

The intent of this manual is to provide guidance to researchers who wish to use the SI3DWQ model created at University of Granada and UC Davis. This water quality model is coupled directly with the SI3D hydrodynamic model. This manual describes the model structure, introduces equations solved by the model and describes in detail the information and input files necessary to run the hydrodynamic and water quality aspects of the model. A general familiarity with hydrodynamic and water quality modeling and Fortran is assumed. Program source code is in Fortran and was developed on the PC platform.

1.1 Summary

SI3DWQ is a semi-implicit, three-dimensional hydrodynamic and water quality model for simulation of lakes and estuaries. The hydrodynamic portion of the model numerically solves the hydrostatic Reynolds-averaged form of the Navier-Stokes equations and includes transport equations for temperature and salinity, and an equation of state relating temperature and salinity to fluid density.

The water quality model uses velocity, water depth and water temperature information solved in the hydrodynamic portion to model the advective and diffusive transport of a number of constituents, described in section 4. This model accounts for the source and sink terms of each constituent.

Water quality constituents that can be represented in this model include:

1. Arbitrary Constituent (ARB)
2. Dissolved Oxygen (DO)
3. Particulate Organic Nitrogen (PON)
4. Dissolved Organic Nitrogen (DON)
5. Ammonium (NH4)
6. Nitrate and Nitrite (NO3)

7. Particulate Organic Phosphorus (POP)
8. Dissolved Organic Phosphorus (DOP)
9. Orthophosphate (PO4)
10. Algae (A)
11. Dissolved Organic Matter (DOM)
12. Particulate Organic Matter (POM)
13. Sediment Oxygen Demand (SOD)

2 Governing Equations for Hydrodynamic Model

The governing equations that form the basis for the hydrodynamic model are the continuity (or mass conservation) equation for incompressible fluids, the Reynolds-averaged from of the Navier-Stokes equation for momentum, and transport equation for active scalar fields (temperature and salinity) (Rueda 2001). These governing equations include some well-known simplifications, including the hydrostatic assumption, the Boussinesq approximations and the Boussinesq eddy viscosity concept. A very detailed analysis and derivation of these governing equations, including simplifying approximations can be found in Smith (2006). The following is the set of governing equations:

$$\frac{\partial u}{\partial x} + \frac{\partial v}{\partial y} + \frac{\partial w}{\partial z} = 0 \tag{2.1}$$

$$\frac{\partial u}{\partial t} + u\frac{\partial u}{\partial x} + v\frac{\partial u}{\partial y} + w\frac{\partial u}{\partial z} - fv$$
$$-\frac{1}{\rho_o}\frac{\partial p}{\partial x} + \frac{\partial}{\partial x}\left(K_H\frac{\partial u}{\partial x}\right) + \frac{\partial}{\partial y}\left(K_H\frac{\partial u}{\partial y}\right) + \frac{\partial}{\partial z}\left(K_V\frac{\partial u}{\partial z}\right) \tag{2.2}$$

$$\frac{\partial v}{\partial t} + u\frac{\partial v}{\partial x} + v\frac{\partial v}{\partial y} + w\frac{\partial v}{\partial z} + fu$$
$$-\frac{1}{\rho_o}\frac{\partial p}{\partial y} + \frac{\partial}{\partial x}\left(K_H\frac{\partial v}{\partial x}\right) + \frac{\partial}{\partial y}\left(K_H\frac{\partial v}{\partial y}\right) + \frac{\partial}{\partial z}\left(K_V\frac{\partial v}{\partial z}\right) \tag{2.3}$$

$$0 = -\frac{\rho}{\rho_o}g - \frac{1}{\rho_o}\frac{\partial p}{\partial z} \tag{2.4}$$

$$\frac{\partial s}{\partial t} + u\frac{\partial s}{\partial x} + v\frac{\partial s}{\partial y} + w\frac{\partial v}{\partial z} \tag{2.5}$$
$$\frac{\partial}{\partial x}\left(K_H\frac{\partial s}{\partial x}\right) + \frac{\partial}{\partial y}\left(K_H\frac{\partial s}{\partial y}\right) + \frac{\partial}{\partial z}\left(K_V\frac{\partial s}{\partial z}\right) + \Delta_s \tag{2.6}$$

$$\rho = \rho(s) \tag{2.7}$$

where

u	=	velocity in the x-direction (m/s)
v	=	velocity in the y-direction (m/s)
w	=	velocity in the z-direction (m/s)
f	=	Coriolis parameter (unit less)
g	=	acceleration of gravity (m^2/sec)
ρ	=	water density variations with respect to ρ_o (kg/m^3)
ρ_o	=	mean reference value for density (kg/m^3)
s	=	active scalar (temperature, salinity)
p	=	pressure (Pa)
K_H	=	horizontal kinematic eddy viscosity (m/sec^2)
K_V	=	vertical kinematic eddy viscosity (m/sec^2)
D_H	=	horizontal eddy diffusivity (m/sec^2)
D_V	=	vertical eddy diffusivity (m/sec^2)
Δ_s	=	source-sink term for scalar (various units)

3 Heat Budget and Thermodynamics

Water temperature is modeled as part of the hydrodynamic portion of the model. The water temperature influences the water density and in part, determines the driving forces of the fluid. To accurately model water temperature, all heat fluxes must be represented. There are two types of heat fluxes: penetrative and non-penetrative heat fluxes. The non-penetrative heat fluxes include evaporation or latent heat flux, conduction or sensible heat flux and long-wave radiation flux. These fluxes occur only at the surface of the water. The penetrative heat flux distributes heat throughout the water column, and comprises shortwave radiation.

The net heat flux at the surface includes the contribution from all non-penetrative sources and the shortwave radiation that is absorbed in the surface layer. The net heat flux is:

$$Q_n = Q_s - (Q_B + Q_E + Q_H) \tag{3.1}$$

where

Q_n	=	Net heat flux (kJ/m^2/hr)
Q_s	=	Net shortwave radiation (kJ/m^2/hr)
Q_B	=	Net long-wave radiation (kJ/m^2/hr)
Q_E	=	Evaporative heat flux (kJ/m^2/hr)
Q_H	=	Conductive heat flux (kJ/m^2/hr)

The following sections describe how each of these heat fluxes is represented in the model. For a complete description of the heat fluxes in the model, the user is directed to Rueda 2001.

3.1 Short-wave radiation

The downward flux of solar radiation penetrating the free surface, Q_s, is given by the amount of radiation reaching the water surface, reduced by the albedo of the water surface.

$$Q_s = Q_G(1 - A_s) \tag{3.2}$$

where

Q_s = Shortwave radiation that penetrates the free surface (kJ/m^2/hr)
Q_G = Shortwave radiation that reaches water surface(kJ/m^2/hr)
A_s = Albedo or shortwave reflectivity (dimensionless)

For a given site, shortwave radiation is a function of the geographical location, time of day and other astronomical data. (TVA 1972). The value must then be corrected for atmospheric attenuation and cloud cover to obtain the shortwave radiation that reaches the water surface. Many weather stations record the shortwave radiation at the surface already corrected for attenuation and cloud cover that can direclty be used in equation 3.2.

SI3DWQ requires shortwave radiation already corrected for albedo as an input. For a description on how to correct shortwave radiation values for albedo, the user is directed to Rudea (2001).

3.1.1 Penetration of shortwave radiation

The shortwave solar radiation that reaches a depth z, $I(z)$ is given by the surface solar radiation multiplied by an attenuation function, $\Phi_A(z)$, that accounts for the attenuation of radiation in the upper layers. $\Phi_A(z)$ is calculated using the Beer-Lambert law (Henderson-Sellers 1986):

$$\Phi_A(z) = (1 - \beta)e^{[-\eta(z - z_a)]} \tag{3.3}$$

where

β = Coefficient that accounts for portion of incoming solar radiation that is absorbed in a thin layer at the top of the water column
z_A = Defines thickness of surface absorption layer $z_A \approx 0.6$ m
η = Extinction coefficient (1/m)

3.2 Long-wave radiation

The long-wave radiation component, Q_B, is composed of two parts, the long-wave radiation emitted by the atmosphere and the back-radiation. Long wave radiation is represented in the model as follows:

$$Q_B = Q_B^{re} + Q_B^{ra} \tag{3.4}$$
$$Q_B^{re} = \varepsilon_w \sigma T_s^4 \tag{3.5}$$
$$Q_B^{ra} = Q_B^{ri}(1 - A_L) = \varepsilon_a \sigma T_A^4 (1 - A_L) \tag{3.6}$$

where

Q_B^{ro} = Emitted long-wave radiation (kJ/m^2/hr)
Q_B^{ra} = Atmospheric radiation after reflection (kJ/m^2/hr)
ε_w = Emissivity of water = 0.972
ε_a = Emissivity of air
A_L = Long-wave reflectivity $\approx$ 0.03
T_s = Water surface temperature (°K)
T_A = Atmospheric temperature (°K)
σ = Stefan-Boltzman constant $\sigma = 2.0412 \cdot 10^{-7}$ (kJ/m^2/hr/°K)

Unlike the emissivity of water which is assumed to be a constant, the emissivity of air depends on a number and variables and can be approximated as follow:

$$\varepsilon_a = 0.642 \left(\frac{e_A}{T_A} \right)^{1/7} (1 + 0.17 C_l^2) \tag{3.7}$$

where

e_A = Vapor pressure (Pascals)
T_A = Air temperature (°C)
C_l = Cloud cover (fraction)

3.3 Latent heat flux

The evaporative heat flux is calculated in terms of the difference between the saturated vapor pressure at the surface water temperature and the actual vapor pressure at the temperature of the air, following the expression (Henderson-Sellers 1986):

$$Q_E = \rho_w \cdot L_v \cdot 1.15 \cdot 10^{-8} \cdot c_D \cdot u_2 (1 + a_3 c_R)(e_s^{sat} - e_A) = C_E (e_s^{sat} - e_A) \tag{3.8}$$

where

e_s^{sat} = Saturated vapor pressure at the surface water temperature (millibars)
e_A = Actual vapor pressure at the temperature of the air (millibars)
L_v = Latent heat of vaporization (J/kg)
c_D = Aerodynamic drag coefficient (dimensionless)
c_R, a_3 = Coefficient that depends on stability of the atmosphere (dimensionless)

The model uses the following expressions for L_v, c_R and a_3:

$$L_v = 1.91846 \cdot 10^{-6} \cdot \left[\frac{T_s}{T_s - 33.91} \right]^2 \tag{3.9}$$

$$c_R = \frac{0.0017 \cdot (T_s - T_A)^{1/3}}{c_D \cdot u_2} \text{ for } T_s < T_A \tag{3.10}$$

$$c_R = 0 \text{ for } T_s > T_a \tag{3.11}$$

$$a_3 = 0.73 \cdot c_R \text{ for } c_R \leq 1.37 \tag{3.12}$$

$$a_3 = 1 \text{ for } c_R > 1.37 \tag{3.13}$$

The following formulation for SI units is adopted to represent the dependence of the saturation vapor pressure on temperature (Henderson-Sellers 1986):

$$e^{sat}(T_A) = 2.1718 \cdot 10^8 \cdot e^{-\frac{4157}{T_A - 33.1}} \tag{3.14}$$

The actual vapor pressure at the air temperature is related to the saturated vapor pressure at that temperature via the relative humidity:

$$e_A = R_h \cdot e_A^{sat} \tag{3.15}$$

3.4 Sensible heat flux

The sensible heat flux is related to the evaporative heat flux by the Bowen ratio: Q_H/Q_E. In the model, the Bowen ratio is assumed to be of the form:

$$Q_H/Q_E = 0.61 \cdot 10^{-3} \cdot p \cdot \frac{T_s - T_A}{e_s^{sat} - e_A} \tag{3.16}$$

Therefore, the latent heat flux is:

$$Q_H = 0.61 \cdot 10^{-3} \cdot C_E \cdot p \cdot (T_s - T_A) \tag{3.17}$$

4 Governing Equations for Water Quality Transport

The water quality model is developed based on the conservation of mass, which accounts for all materials entering and leaving a control volume, including the trasport of material into and out of the control volume and the physical, chemical and biological transformations. The conservation of mass of a constituent, C, in a control volume may be written as:

$$\frac{\partial C}{\partial t} + \underbrace{u\frac{\partial C}{\partial x} + v\frac{\partial C}{\partial y} + w\frac{\partial C}{\partial z}}_{\text{advection}} = \underbrace{\frac{\partial}{\partial x}\left(D_H\frac{\partial C}{\partial x}\right) + \frac{\partial}{\partial y}\left(D_H\frac{\partial C}{\partial y}\right) + \frac{\partial}{\partial z}\left(D_V\frac{\partial C}{\partial z}\right)}_{\text{diffusion}} \pm \underbrace{hS_C}_{\text{source term}} \tag{4.1}$$

where

C	=	concentraion of water quality variable (mg/L^3)
t	=	time (s)
u, v, w	=	velocity (m/s)
D_H, D_V	=	horizontal and vertical turbulent diffusiviity coefficients (m^2/s)
S_c	=	sources and sinks for water quality varaiable C (mg/m^3 - s)

Equation 4.1 is nearly identical to equation 2.6. They are based on the same principles, and in the SI3DWQ model environment, are both solved using the same flux-limiter scheme first developed for the temperature portion of the hydrodynamic model.

5 Governing Equation for Water Quality Source and Sink Terms

5.1 Introduction

The water quality relationships implemented in SI3DWQ are derived from a number of sources, including other water quality models, such as DLM-WQ, RMA-11 and CE-QUAL-W2. The constituents and interactions necessary in an estuary were chosen. In the future, additional water quality constituents and submodels may be necessary. The following sections present the conceptual model for each state variable, as well as the equation for the source sink term. For ease in reading, each section also defines all variables used in the source-sink term, even if they are previously defined in another section. The last section of this section summarizes all variables and defines how they appear in the model environment.

5.2 Temperature dependence of rate coefficients

As will be shown in the following sections, many of the rate coefficients used in SI3DWQ are dependent on water temperature. The rate coefficients are presented in literature and determined in the lab at 20°C, but can be corrected to the water temperature using the following formulation:

$$R_t = R_{20}\theta^{T-20} \tag{5.1}$$

where

R_t = the value of the rate at the modeled water temperature (1/day)
R_{20} = the value of the rate at 20°C
θ = an empirical constant for each reaction coefficient
T = the modeled water temperature

In the following sections, equation 5.1 will appear in many of the source sink equations.

5.3 Arbitrary constituent

At this time, SI3DWQ can model one arbitrary constituent. The model allows this constitutent to decay and to sink or settle. This constituent can also be used as a conservative, neutrally buoyant tracer by setting the decay and settling rates equal to zero.

$$S_{ARB} = \underbrace{k_{ARB}ARB}_{\text{decay}} - \underbrace{k_{set}ARB}_{\text{settling}} \tag{5.2}$$

where

S_{ARB} = concentration of the arbitrary constituent (mg/L)
k_{ARB} = decay rate for arbitrary constituent (1/day)
k_{set} = settling rate for arbitrary constituent (m/day)

5.4 Dissolved oxygen

This model was originally constructed for use in determining the causes for low dissolved oxygen in the Stockton Deep Water Ship Channel. For this reason, special care was taken in the analysis of the source and sink terms for dissolved oxgyen. As seen in Figure 5.1, the source terms for dissolved oxygen include reaeration at the surface and oxygen production during photosynthesis. The sink terms include respiration of algae, nitrification, oxidation of organic matter and sediment oxygen demand. The source-sink term of dissolved oxygen is:

$$\begin{aligned} S_{\mathrm{DO}} &= \underbrace{k_a \theta_a^{T-20}(DO_s - DO)}_{\text{reaeration}} + \underbrace{a_{oc} r_{oc} \mu_A A}_{\text{primary production}} \\ &\quad - \underbrace{a_{oc} r_{oc} k_{ra} \theta_{ra}^{T-20} A}_{\text{respiration}} - \underbrace{k_n r_{on} \theta_n^{T-20} \left(\frac{DO}{K_n + DO} \right) NH_4}_{\text{nitrification}} \\ &\quad - \underbrace{k_{DOM} \theta_{DOM}^{T-20} \left(\frac{DO}{K_{BOD} + DO} \right) DOM}_{\text{oxidation of organic matter}} - \underbrace{h \theta_{SOD}^{T-20} SOD}_{\text{sediment oxygen demand}} \end{aligned} \tag{5.3}$$

where

DO	=	Dissolved oxygen concentration (mgO/L)
A	=	Phytoplankton concentration (mgChl-a/L)
NH_4	=	Ammonium concentration (mgN/L)
DOM	=	Dissolved Organic matter concentration (mgC/L)
SOD	=	Sediment Oxygen Demand (mgO/L)
k_a	=	Reaeration rate (1/day)
DO_s	=	Dissolved oxygen saturation value (mgO/L)
a_{oc}	=	Phytoplankton ratio of C:Chl-a (gC/gChl)
r_{oc}	=	Ratio of O:C in photosynthesis and respiration (mgO/mgC)
μ_A	=	Phytoplankton growth rate (1/day)
k_{ra}	=	Phytoplankton respiration rate (1/day)
k_n	=	Nitrification rate (1/day)
r_{on}	=	Ratio of O:N in nitrification (mgO/mgN)
K_n	=	Half-saturation coefficient for nitrification (mgDO/L)
k_{DOM}	=	Rate of oxidation of organic matter (1/day)
K_{BOD}	=	Half-saturation coefficient for DOM oxidation (mgDO/L)
h	=	Height of computational cell (m)

5.4.1 Dissolved oxygen saturation concentration

Dissolved oxygen saturation concentration is dependent on water temperature, pressure and salinity. Dissolved oxygen saturation can be represented in a model in a number of ways, as summarized in Bowie (1985). SI3DWQ uses the equation describing the concentration of oxygen in water as a function of temperatures and salinity presented by Bowie (1985):

$$\begin{aligned} \ln DO_s &= -139.34410 + 1.575701 \times 10^5/T_k - 6.642308 \times 10^7/T_k^2 \\ &\quad + 1.243800 \times 10^{10}/T_k^3 - 8.621949 \times 10^{11}/T_k^4 \\ &\quad - (1/1.80655) \cdot SAL \cdot [3.1929 \times 10^{-2} - 1.9428E1/T_k + 3.8673 \times 10^3/T_k^2] \end{aligned} \tag{5.4}$$

where

$$\begin{aligned} DO_s &= \text{Equilibrium oxygen conentration at 1.0 atm (mgO/L)} \\ T_k &= \text{Water temperature (°K)} \\ SAL &= \text{Salinity (mg/L)} \end{aligned}$$

To correct the saturation concentration to a pressure other than standard pressure, the following equation is used (Bowie 1985):

$$DO_s = DO_{sn} P \left[\frac{(1 - P_{wv}/P)(1 - \theta P)}{(1 - P_{wv})(1 - \theta)} \right] \tag{5.5}$$

where

$$\begin{aligned} DO_s &= \text{Equilibrium oxygen concentration at non standard pressure (mgO/L)} \\ P &= \text{Atmospheric pressure (atm)} \\ P_{wv} &= \text{Partial pressure of water vapor (atm)} \\ P_{wv} &= 11.8751 - 33840.70/T_k - 216961/T_k \\ \theta &= 0.000975 - 1.426 \times 10^{-5} T + 6.436 \times 10^{-8} T^2 \\ T &= \text{Temperature in ° C} \end{aligned}$$

5.4.2 Reaeration coefficient

Another important process in dissolved oxygen dynamics is reaeration. The reaeration coefficient can be estimated in a number of ways. Currently, the model accepts the reaeration coefficient as a constant input value. However, future improvements to the model will include allowing the user to choose a method for the estimation of the coefficient.

5.5 Particulate organic nitrogen

As Figure 5.2 shows, source terms for particulate organic nitrgoen include mortality of algae and resuspension from the bottom. Sink terms include hydrolysis and settling.

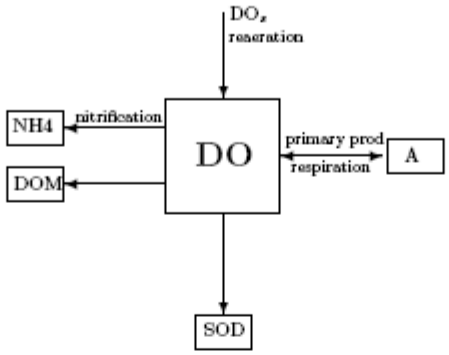

Figure 5.1: Dissolved Oxygen Conceptual Model

$$S_{\text{PON}} = \underbrace{a_{nc}k_{mor}A}_{\text{mortality}} - \underbrace{k_{hn}\theta_{hn}^{T-20}PON}_{\text{hydrolysis}} - \underbrace{k_{set}PON}_{\text{settling}} + \underbrace{k_{rs}PON}_{\text{resuspension}} \tag{5.6}$$

where

PON	=	Particulate Organic Nitrogen Concentration (mgN/L)
A	=	Phytoplankton concentration (mgChla/L)
a_{nc}	=	Phytoplankton ratio of N:Chl-a (mgN/mgChl-a)
k_{mor}	=	Phytoplankton mortality rate (1/day)
k_{hn}	=	Hydrolysis rate of PON (1/day)
k_{set}	=	Particulate matter settling rate (m/day)
k_{rs}	=	Particulate matter resuspension rate (1/day)

5.6 Dissolved organic nitrogen

As Figure 5.3 shows, source terms for dissolved organic nitrogen include respiration and excretion of algae, hydrolysis of PON and atmospheric deposition. Sink terms include mineralization.

$$\begin{aligned} S_{DON} = {} & \underbrace{a_{nc}(k_{ra}-k_{ex})\theta_{ra}^{T-20}A}_{\text{respiration, excretion}} + \underbrace{k_{hn}\theta_{hn}^{T-20}PON}_{\text{hydrolysis}} \\ & - \underbrace{k_{mn}\theta_{mn}^{T-20}DON}_{\text{mineralization}} + \underbrace{hATM_{DON}}_{\text{atmospheric deposition}} \end{aligned} \tag{5.7}$$

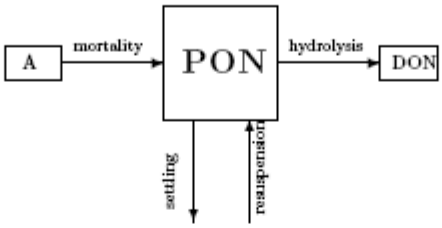

Figure 5.2: Particulate Organic Nitrogen Conceptual Model

where

DON	=	Particulate Organic Nitrogen Concentration (mgN/L)
PON	=	Particulate Organic Nitrogen Concentration (mgN/L)
A	=	Phytoplankton concentration (mgChla/L)
a_{nc}	=	Phytoplankton ratio of N:Chl-a (mgN/mgChl-a)
k_{ra}	=	Phytoplankton respiration rate (1/day)
k_{ex}	=	Phytoplankton excretion rate (1/day)
k_{hn}	=	Hydrolysis rate of PON (1/day)
k_{mn}	=	Mineralization rate of DON (1/day)
h	=	Height of computational cell (m)
ATM_{DON}	=	Atmospheric deposition of DON (mgDON/day)

5.7 Ammonium

As shown in Figure 5.4 Ammonium nitrogen is created by the hydrolysis of organic nitrogen and from benthic release. It can also be added to the system through groundwater flux and atmospheric deposition. The loss of ammonium is through the process of nitrification, algal uptake and volatilization.

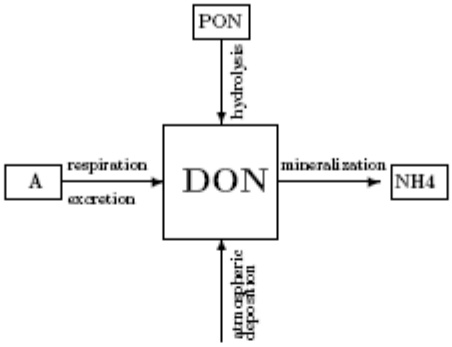

Figure 5.3: Dissolved Organic Nitrogen Conceptual Model

$$
\begin{aligned}
S_{NH4} \;=\; & \underbrace{k_{mn}\theta_{mn}^{T-20}DON}_{\text{mineralization}} - \underbrace{k_n\theta_n^{T-20}\left(\frac{DO}{K_{NIT}+DO}\right)NH4}_{\text{nitrification}} - \underbrace{a_{nc}F_{NH4}\mu A}_{\text{uptake}} \\
& + \underbrace{a_{nc}k_{ra}\theta_{ra}^{T-20}A}_{\text{respiration}} + \underbrace{hJ_{NH4}}_{\text{sediment release}} + \underbrace{hGW_{NH4}}_{\text{groundwater flux}} \\
& + \underbrace{hATM_{NH4}}_{\text{atmospheric deposition}} - \underbrace{k_v\theta_v^{T-20}NH4}_{\text{volatilization}}
\end{aligned}
\tag{5.8}
$$

where

DON	=	Dissolved Organic Nitrogen concenteraiton (mgN/L)
$NH4$	=	Ammonium nitrogen concentration (mgN/L)
A	=	Phytoplankton concentration (mgChla/L)
k_{mn}	=	Mineralization rate of DON (1/day)
k_n	=	Nitrification rate (1/day)
K_{NIT}	=	Half-saturation coefficient for nitrification (mgN/L)
a_{nc}	=	Phytoplankton ratio of N:Chl-a (mgN/mgChl-a)
F_{NH4}	=	Phytoplankton preference factor for NH4 (fraction)
μ	=	Phytoplankton growth rate (1/day)
k_{ra}	=	Phytoplankton respiration rate (1/day)
h	=	Height of computational cell (m)
J_{NH4}	=	Sediment release of NH4 (mgN/day)
GW_{NH4}	=	Groundwater release of NH4 (mgN/day)
ATM_{NH4}	=	Atmospheric depostion of NH4 (mgN/day)
k_v	=	Volatilization rate of ammonium (1/day)

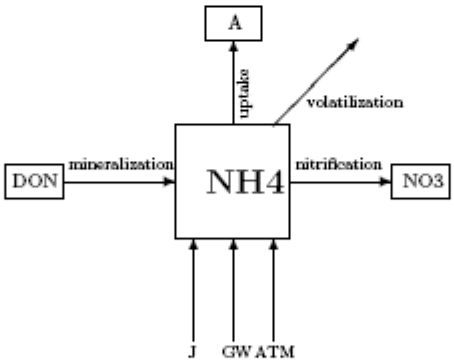

Figure 5.4: Ammonium Conceptual Model

5.8 Nitrate and Nitrite

Because nitrite quickly converts to nitrate, the two are modeled together. Nitrate is added to the system through the nitrification of ammonium, sediment release, groundwater flux and atmospheric depositions. Losses of nitrate include uptake by phytoplankton and denitrification. Figure 5.5 depicts the source and sink terms and the following equaion summarizes the terms:

$$\begin{aligned} S_{NO3} &= \underbrace{k_n \theta_n^{T-20} \left(\frac{DO}{K_n + DO} \right) NH4}_{\text{nitrification}} - \underbrace{a_{nc}(1 - F_{NH4}) \mu A}_{\text{uptake}} - \underbrace{k_{dn} \theta_{dn}^{T-20} NO3}_{\text{denitrification}} \\ &+ \underbrace{hJ_{NO3}}_{\text{sediment release}} + \underbrace{hGW_{NO3}}_{\text{groundwater flux}} + \underbrace{hATM_{NO3}}_{\text{atmospheric deposition}} \end{aligned} \tag{5.9}$$

where

DO	=	Dissolved oxygen concentration (mgO/L)
$NH4$	=	Ammonium concentration (mgN/L)
A	=	Phytoplankton concentration (mgChla/L)
$NO3$	=	Nitrate concentration (mgN/L)
k_n	=	Nitrification rate (1/day)
K_n	=	Half-saturation coefficient for nitrification (mgN/L)
a_{nc}	=	Phytoplankton ratio of N:Chl-a (mgN/mgChl-a)
F_{NH4}	=	Phytoplankton preference factor for NH4 (fraction)
μ	=	Phytoplankton growth rate (1/day)
k_{dn}	=	Denitrification rate (1/day)
h	=	Height of computational cell (m)
J_{NO3}	=	Sediment release of NO3 (mgN/day)
GW_{NO3}	=	Groundwater release of NO3 (mgN/day)
ATM_{NO3}	=	Atmospheric deposition of NO3 (mgN/day)

5.9 Particulate organic phosphorus

Particulate organic phophorus is added to the system through mortality of algae, atmospheric depostion and resuspension and is lost through hydrolysis. Figure 5.6 depicts this relationship.

$$\begin{aligned} S_{\text{POP}} &= \underbrace{a_{pc} k_{mor} A}_{\text{mortality}} - \underbrace{k_{hp} \theta_{hp}^{T-20} POP}_{\text{hydrolysis}} - \underbrace{k_{set} POP}_{\text{settling}} \\ &+ \underbrace{k_{rs} PON}_{\text{resuspension}} + \underbrace{hATM_{POP}}_{\text{atmospheric deposition}} \end{aligned} \tag{5.10}$$

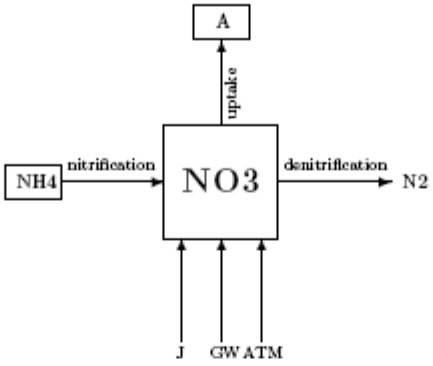

Figure 5.5: Nitrate Conceptual Model

where

POP	=	Particulate Organic Phosphorus Concentration (mgN/L)
A	=	Phytoplankton concentration (mgChla/L)
a_{pc}	=	Phytoplankton ratio of P:Chl-a (mgP/mgChl-a)
k_{mor}	=	Phytoplankton mortality rate (1/day)
k_{hp}	=	Hydrolysis rate of POP (1/day)
k_{set}	=	Particulate matter settling rate (m/day)
k_{rs}	=	Particulate matter resuspension rate (1/day)
h	=	Height of computational cell (m)
ATM_{POP}	=	Atmospheric deposition rate of POP(mgP/day)

5.10 Dissolved organic phosphorus

Dissolved organic phosphorus is added to the system through respiration and excretion of algae and hydrolysis of particulate organic phosphorus. It is lost through mineralization. Figure 5.7 depicts this relationship.

$$S_{PON} = \underbrace{a_{pc}(k_{ra}-k_{ex})\theta_{ra}^{T-20}A}_{\text{respiration, excretion}} + \underbrace{k_{hp}\theta_{hp}^{T-20}POP}_{\text{hydrolysis}} - \underbrace{k_{mp}\theta_{mp}^{T-20}DPN}_{\text{mineralization}} \tag{5.11}$$

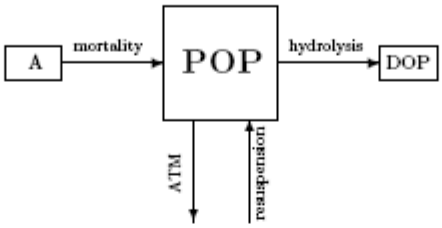

Figure 5.6: Particulate Organic Nitrogen Conceptual Model

where

DOP	=	Particulate Organic Phosphorus Concentration (mgN/L)
POP	=	Particulate Organic Phosphorus Concentration (mgN/L)
A	=	Phytoplankton concentration (mgChla/L)
a_{pc}	=	Phytoplankton ratio of P:Chl-a (mgP/mgChl-a)
k_{ra}	=	Phytoplankton respiration rate (1/day)
k_{ea}	=	Phytoplankton excretion rate (1/day)
k_{hn}	=	Hydrolysis rate of PON (1/day)
k_{mn}	=	Mineralization rate of DOP (1/day)

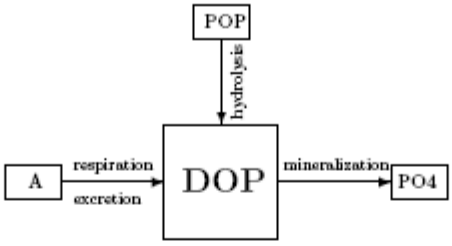

Figure 5.7: Dissolved Organic Phosphorus Conceptual Model

5.11 Orthophosphate

As shown in Figure 5.8, orthophosphate is added to the system through mineraliztion of dissolved organic phosphours, respriation of phytoplankton, sediment release, groundwater flux and atmosphericdepositon and can be lost due to uptake by phytoplankton.

$$S_{PO4} = \underbrace{k_{mp}\theta_{mp}^{T-20}DON}_{\text{mineralization}} - \underbrace{a_{pc}\mu A}_{\text{uptake}} + \underbrace{a_{pc}k_{ra}\theta_{ra}^{T-20}A}_{\text{respiration}} + \underbrace{hJ_{PO4}}_{\text{sediment release}} + \underbrace{hGW_{PO4}}_{\text{groundwater flux}} + \underbrace{hATM_{PO4}}_{\text{atmospheric deposition}} \quad (5.12)$$

where

DOP	=	Dissolved Organic Phosphorus concentration (mgP/L)
$PO4$	=	Orthophosphate concentration (mgP/L)
A	=	Phytoplankton concentration (mgChla/L)
k_{mp}	=	Mineralization rate of DOP (1/day)
a_{pc}	=	Phytoplankton ratio of P:Chla (mgP/mgChla)
μ	=	Phytoplankton growth rate (1/day)
k_{ra}	=	Phytoplankton respiration rate (1/day)
h	=	Height of computational cell (m)
J_{PO4}	=	Sediment release of PO4 (mgN/day)
GW_{PO4}	=	Groundwater release of PO4 (mgN/day)
ATM_{PO4}	=	Atmospheric deposition of PO4 (mgN/day)

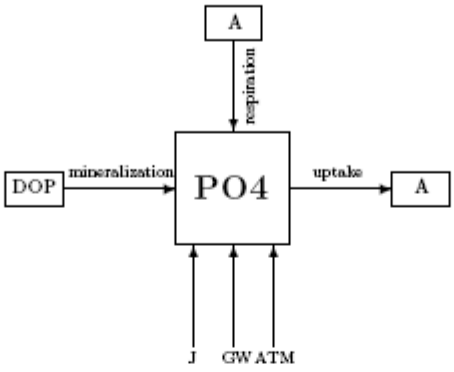

Figure 5.8: Orthophosphate Conceptual Model

5.12 Particulate Organic Matter

The source of particulate organic matter is mortality of phytoplankton and the sinks are hydrolysis and settling. Figure 5.9 depicts the source and sink terms.

$$S_{\text{POM}} = \underbrace{a_{cc} k_{mor} A}_{\text{mortality}} - \underbrace{k_{hp} \theta_{hc}^{T-20} POM}_{\text{hydrolysis}} - \underbrace{k_{set} POP}_{\text{settling}} \tag{5.13}$$

where

POM	=	Particulate Organic Matter Concentration (mgC/L)
A	=	Phytoplankton concentration (mgChla/L)
a_{cc}	=	Phytoplankton ratio of C:Chl-a (mgC/mgChl-a)
k_{mor}	=	Phytoplankton mortality rate (1/day)
k_{hc}	=	Hydrolysis rate of POM (1/day)
k_{set}	=	Particulate matter settling rate (m/day)

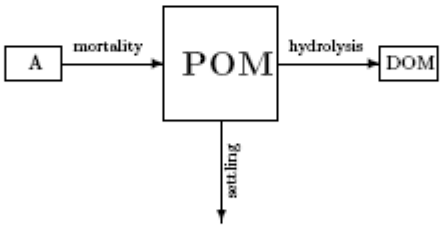

Figure 5.9: Particulate Organic Matter Conceptual Model

5.13 Dissolved Organic Matter

Sources for dissolved organic matter include respiration and excretion of phytoplankton and hydrolysis of particulate organic matter. The sink of DOM from the system is oxidation. Figure 5.10 depicts these source and sink terms.

$$S_{DOM} = \underbrace{a_{cc}(k_{ra}-k_{ex})\theta_{ra}^{T-20}A}_{\text{respiration, excretion}} + \underbrace{k_{hc}\theta_{hc}^{T-20}POM}_{\text{hydrolysis}} - \underbrace{k_{DOM}\theta_{DOM}^{T-20}\left(\frac{DO}{K_{BOD}+DO}\right)DOM}_{\text{oxidation}} \quad (5.14)$$

where

DOM	=	Dissolved Organic Matter concentration (mgC/L)
POM	=	Particulate Organic Matter concentration (mgC/L)
A	=	Phytoplankton concentration (mgChl-a/L)
DO	=	Dissolved oxygen concentration (mgO/L)
a_{cc}	=	Phytoplankton ratio of C:Chl-a (mgC/mgChl-a)
k_{ra}	=	Respiration rate of phytoplankton (1/day)
k_{ex}	=	Excretion rate of phytoplankton (1/day)
k_{hc}	=	Hydrolysis rate of POM (1/day)
k_{DOM}	=	Oxidation rate of DOM (1/day)
K_{BOD}	=	Half-saturation coeff for DOM oxidation (mgO/L)

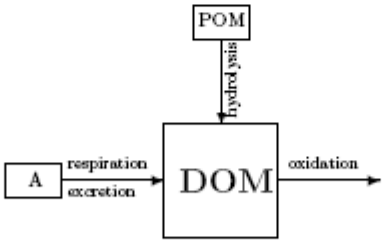

Figure 5.10: Dissolved Organic Matter Conceptual Model

5.14 Chlorophyll-a and Algae

Inclusion of algae and chlorophyll-a in this model was essential. The algae population has a direct influence on the dissolved oxygen concentration. During photosynthesis, the algae population produces oxygen, and during respiration, oxygen is consumed. The death and decay of algae also imposes an oxygen demand on the water body. The algae population also has a direct impact on the concentration of many of the nutrients included in this model. Figure 5.11 depicts the complex interactions included in the algae sub-model. The main source of algae is growth, while the losses include respiration and excretion, mortality, grazing and settling. The equation for the source-sink term of algae is:

$$S_A = \underbrace{\mu_A A}_{\text{growth}} - \underbrace{(k_{ra} + k_{ex})\theta_{ra}^{T-20} A}_{\text{respiration, excretion}} - \underbrace{k_{mor} A}_{\text{mortality}} - \underbrace{k_{gr}\theta_{gr}^{T-20} A}_{\text{grazing}} - \underbrace{k_{set} A}_{\text{settling}} \quad (5.15)$$

where

A = Algae concentration (mgC/L)
μ_A = growth rate of algae (1/day)
k_{ra} = respiration rate of algae (1/day)
k_{ex} = excretion rate of algae (1/day)
k_{mor} = mortality rate of algea (1/day)
k_{gr} = grazing rate of algae (1/day)
k_{set} = settling rate of particulate matter (m/day)

Because most calibration data are available as Chl-a concentrations, SI3DWQ output from the algae submodel is chlorophyll-a concentrations, which are directly proportional to the algal biomass of phytoplankton:

$$Chl-a = \alpha A \quad (5.16)$$

where

$Chl-a$ = chlorophyll-a concentration (μg-Chla/L)
A = algal biomass concentration (mg/L)
α = Chl-a:A conversion factor (μg-Chla/mg A)

5.14.1 Algal growth rate

SI3DWQ includes a number of factors that can limit the growth rate of algae: tempearture, light and nutrient availability. When these factors are considered, the growth rate becomes

$$\mu = \mu_{max} f(I) f(T) f(N) f(P) \quad (5.17)$$

where

μ_{max} = the maximum growth rate of algae (1/day)
μ = the growth rate considering limiting factors (1/day)
$f(x)$ = fuctional relationship that governs how the factor x limits the growth of alage

5.14.2 Temperature as a limiting factor

The temperature effect on the growth rate of alage is treated as all other rates in the water quality model, as described in Section 5.2.

$$f(T) = \theta^{T-20} \tag{5.18}$$

5.14.3 Light as a limiting factor

Sunlight is necessary for phtosynthesis and plant production. The light available for utilization by plant matter is the photsynthestic avaliable radiation (PAR), a component of the incoming shortwave radiation. Although light is necessary for plant growth, toomuch light can be damaging to algal production. This model has adapted Steele's (1965) relationship between shortwave radation and alge growth rate.

$$f(I) = \frac{I}{I_s} e^{-I/I_s+1} \tag{5.19}$$

where

I = incoming shorwave radiation (W/m^2)
I_s = saturating light intensity (W/m^2)

The shortwave radiation is also subject to Beer's Law which describes how much of the radiation that hits the surface reaches each layer in the water column Readers should refer to equation 3.3 to see how the model handles the penetration of light.

5.14.4 Nutrients as limiting factors

The nutrient limitation on growth rate is modeled with a Michaelis-Menten equation which suggests that as the concentration of the nutrient first increases, the algae population increases. However, the growth rate reaches a maximum, even if all other factors are in sufficient supply.

$$f(N) = \frac{NH4 + NO3}{K_N + NH4 + NO3} \tag{5.20}$$

$$f(P) = \frac{PO4}{K_P + PO4} \tag{5.21}$$

where

$NH4$ = Ammonium concentration (mgN/L)
$NO3$ = Nitrate concentration (mgN/L)
K_N = Nitrogen half-saturation concentration for algal growth (mgN/L)
$PO4$ = Orthophosphate concentration (mgP/L)
K_P = Phosphorus half-saturation concentration for algal growth

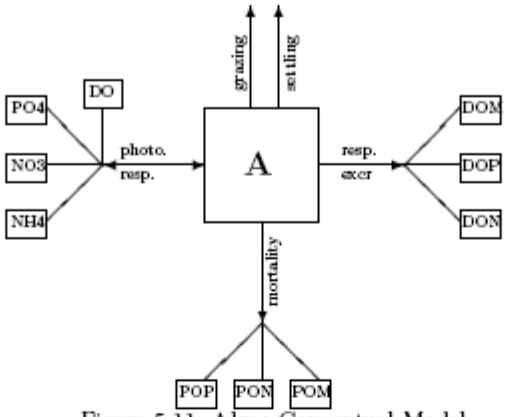

Figure 5.11: Algae Conceptual Model

5.15 Summary of water quality model variables

Table 1: Water Quality State Variables

Symbol	State Variable	Units
ARB	Arbitrary Constituent	mg/L
DO	Dissolved Oxygen	mgO/L
PON	Particulate Organic Nitrogen	mgN/L
DON	Dissolved Organic Nitrogen	mgN/L
NH4	Ammonium Nitrogen	mgN/L
NO3	Nitrate Nitrogen	mgN/L
POP	Particulate Organic Phosphorus	mgP/L
DOP	Dissolved Organic Phosphorus	mgP/L
PO4	Orthophosphate	mgP/L
POM	Particulate Organic Matter	mgC/L
DOM	Dissolved Organic Matter	mgC/L
SOD	Sediment Oxygen Demand	mgO/L
A	Algae/Phytoplankton	μgChl-a/L

Table 2: First order rate constants; units are in 1/sec

Rate Constant	SI3DWQ Appearance	Description
k_a	k_a	Reaeration rate
k_{ra}	k_ra	Phytoplankton respiration rate
k_{ex}	k_ex	Phytoplankton excretion rate
k_{mor}	k_mor	Phytoplankton mortality rate
k_{gr}	k_gr	Grazing rate of zooplankton on phytoplankton
k_{set}	k_set	Settling rate of particulate matter
k_{DOM}	k_DOM	Rate of DOM oxidation
k_{mn}	k_mn	Mineralization rate of DON
k_{mp}	k_mp	Mineralization rate of DOP
k_{vn}	k_vn	Volatilization rate of NH4
k_n	k_n	Nitrification rate
k_{dn}	k_dn	Dentification rate
k_{rs}	k_rs	Resuspension rate of particulate matter
k_{hn}	k_hn	Hydrolysis rate of PON
k_{hp}	k_hp	Hydrolysis rate of POP
k_{hc}	k_hc	Hydrolysis rate of POM
k_{ARB}	k_ARB	Decay rate for ARB
k_{setARB}	k_setARB	Settling rate for ARB

Table 3: Coefficients and variables for water quality model

Coefficient or variable	SI3D Appearance	Description	Units	Model Dependencies
θ_x	theta_x	Temp dependence coeff for process x.	ND	Biological process specific
DO_s	DO_s	DO Saturation coefficient	mgO/L	T_w, P_{atm}
a_{oc}	a_cc	Phytoplankton ratio of C:Chl-a	mgC/μgChl-a	Assumed constant
a_{nc}	a_nc	Phytoplankton ratio of N:Chl-a	mgN/μgChl-a	Assumed constant
a_{pc}	a_pc	Phtoplankton rato of P:Chla-a	mgP/μgChl-a	Assumed constant
r_{oc}	r_oc	Ratio of O:C in phytosynthesis and respiration	mgO/mgC	Assumed constant
r_{on}	r_on	Ratio of O:N in nitrification	mgO/mgN	Assumed constant
K_{DOM}	K_DOM	Oxygen half saturation coeff for DOM oxidation.	mgO/L	Assumed constant
K_{NIT}	K_NIT	Oxygen half saturation coeff for nitrification.	mgO/L	Assumed constant
K_N	K_N	Nitrogen half saturation coeff for phytoplankton growth	mgN/L	Assumed constant
K_P	K_P	Phosphorus half saturation coeff for phytoplankton growth	mgP/L	Assumed constant
GW_x	GW_x	Groundwater flux rate of constituent x	mgX/day	Assumed constant
ATM_x	ATM_x	Atmospheric deposition rate of constituent x	mgX/day	Assumed constant
J_x	J_x	Sediment release of constituent x	mgX/day	Assumed constant.
μ	mu	Phytoplankton growth rate	1/sec	T, $NH4$, $NO3$, $PO4$, μ_{max}, I

6 Using the Model

6.1 Run-time Instructions

To run SI3DWQ, SI3D.exe is executed from the directory containing the input files necessary for the run. This is the same directory where the output files will be placed. The following is a list of input files necessary for the model to run:

1. Main Input file, as described in section 6.2.1. Required input file.
2. Water Quality Input File, as described in section 6.2.3. Required input file if water quality constituents are modeled.
3. Surface Bounday Condition Input File, as described in section 6.2.5. Required input file.
4. Bathymetry file, as described in section 6.2.7. Required input file.
5. Boundary Condition files, as described in section 6.2.9. Required input file.
6. Variable initialization file, as described in section 6.2.11. Required input file.

6.2 Input Files

6.2.1 SI3D Main Input File

The main input file used for the hydrodynamic and water quality model, si3d_inp.txt defines important model parameters and determines how the model will be solved. The file also defines how model output is requested. As described in the following tables, the file is divided into nine separate groups.

The first group includes a title for the run.

The second group defines the start date and time of the model run.

File name	SI3D name	Format	Descrpiton
year	`iyr0`	G20.2	Year for start date of run
month	`imon0`	G20.2	Month for start date of run
day	`iday0`	G20.2	Day for start date of run
hour	`ihr0`	G20.2	Hour for start of run

The third group defines space-time domains, cell size and time steps.

File name	SI3D name	Format	Descrpiton
xl	`xl`	G20.2	Length of domain in EW direction (m)
yl	`yl`	G20.2	Length of domain in NS direction (m)
zl	`zl`	G20.2	Length of domain in vertical direction (m)
tl	`tl`	G20.2	Length of time simulated (s)
idx	`idx`	G20.2	Cell size in EW direction (m)
idy	`idy`	G20.2	Cell size in NS direction (m)
idz	`idz`	G20.2	Cell size in vertical direction (m)
dzmin	`dzmin`	G20.2	Minimum cell size in vertical direction (m)
datadj	`datadj`	G20.2	Adjustment of datum, be default datum = 0.0
zeta0	`zetainit`	G20.2	Initial location of water surface (m)
idt	`idt`	G20.2	Time step (s)
ibathyf	`ibathyf`	G20.2	Defines how bathy file is read. 0 (general) 1(SDWSC) 2(SHR). This depends on how bathy file is created.

The fourth group contains parameters the control the solution algorithm.

File name	SI3D name	Format	Descrpiton
itrap	`itrap`	G20.2	Defines if trapezoidal iteration is used. If itrap = 1, iterations performed, if itrap = 0, single step performed.
niter	`niter`	G20.2	No of trapezoidal iterations performed if itrap = 1.
smooth	`ismooth`	G20.2	Defines how leapfrog solution is smoothed. If ismooth = 1, smoothing performed, if ismooth = 0, NO smoothing.
beta	`beta`	G20.2	Beta parameters for smoothing filter (0.05 - 2.0 recommended)
iturb	`iturb`	G20.2	Defines how vertical eddy viscosity is determined. If iturb = 0, constant eddy viscosity is addumed, if iturb = 1, 2-eq model is used.
az0	`Av0`	G20.2	If iturb = 0, defines vertical eddy viscosity.
dz0	`Dv0`	G20.2	If iturb = 0, defines vertical eddy diffusivity.
iadv	`iadv`	G20.2	Defines if momentum advection is on or off. If iadv = 0, it is off, if iadv = 1, it is on.
itrmom	`itrmom`	G20.2	Algorithm for momentum horizontal advection. If itrmom = 1, centered diff used, if itrmom = 2, upwind is used.
ihd	`ihd`	G20.2	Defines if horizontal diffusion is on or off. If ihd = 0, it is off, if ihd = 1, it is on.
ax0	`Ax0`	G20.2	Horizontal eddy diffusivity/viscosity in EW direction (m^2/s)
ay0	`Ay0`	G20.2	Horizonal eddy diffusivity/viscosity in NS direction (m^2/s)
f	`f`	G20.2	Coriolis parameter.
theta	`theta`	G20.2	Weighting parameter for semi-implict solution. (range is 0.5 - 1.0)

ibc	ibc	G20.2	Defines if baroclinic terms included in momentum solution. If ibc = 1, they are included, if ibc = 0, they are NOT included.
isal	isal	G20.2	Defines if scalar transport equation is solved. If isal = 1, equation is included, if isal = 0, it is not.
itrsch	itrsch	G20.2	Defines algorithm used to solve scalar advection. Itrsch = 1 is centered, 2 is upwind, 3 is centered =U at k = klz+1 and 4 is flux-limiter.
cd	cd	G20.2	Bottom drag coefficient.
ifsbc	ifsurfbc	G20.2	Defines how model determines surface heat flux. Ifsurfbc = 0, no heat flux, = 1, heat fluxes read from file, = 2, heat fluxes calculated in model.
dtsbc	dtsurfbc	G20.2	Time step between records to surfbc.txt
cw	cw	G20.2	Wind drag coefficient, used if ifsurfbc = 0.
ws	wa	G20.2	Wind speed, used if ifsurfbc = 0.
phi	phi	G20.2	Wind direction, used if ifsurfbc = 0.
idbg	idbg	G20.2	Check messages for debugging. If idbg = 0, no messages displayed during run, idbg = 1 displays messages.

The fifth group specifies output information for time files.

File name	SI3D name	Format	Descrpiton
ipt	`ipt`	I20	Number of time steps between consecutive output to time file. The remaining lines in this group are only read and should only be included when ipt > 0
nnodes	`nnodes`	I20	Number of nodes where time file is requested. Maximum number of nodes is 20.
inodes	`inodes`	I4	Lists the i-location of nodes where time file is requested. The number of entries on this line should match nnodes.
jnodes	`jnodes`	I4	Lists the j-location of nodes where time file is requested. The number of entries on this line should match nnodes.

The sixth group specifies information for model output to H-plane files.

File name	SI3D name	Format	Descrpiton
iht	`iop`	I20	Number of time steps between consecutive output to plane file. Remaining lines in this group are only read and should only be included if iop > 0.
nplanes	`n_planes`	I20	The number of planes where solution is output. The maximum number of planes the model will accept is 10.
plane1	`pout(j)`	I20	The k-value for the plane at which a plane file is requested. This line is repeated for j = 1 to j = n_planes.

The seventh group specifies the information necessary for the model to create cross-section files.

File name	SI3D name	Format	Descrpiton
ixt	`iox`	I20	Number of time steps between consecutive writes to cross-section file. Remaining lines in this group are only read and should only be included if iox >0
nsections	`n_sections`	I20	The number of sections requested. The max number of sections is 10.
Section ID			This line is ignored by the model and is for user reference.
n_cells	`n_sectioncells(j)`	I20	The number of cells for the first section. This line and the following two sets of lines are repeated for j = 1 to j = n_sections.
xinodes	`xinode(j,nn)`	I4	The i location values for the first cross-section. The model reads 10 nodes per line. If more than 10 nodes are included in the cross-section, they are placed on the next line. The model will read the node values for nn=1,n_sectioncells.
xjnodes	`xjnode(j.nn)`	I4	The j location values for the first cross-section. The model reads 10 nodes per line. If more than 10 nodes are included in the cross-section, they are placed on the next line. The model will read the node values for nn=1,n_sectioncells.

The eighth group defines information regarding the open boundaries for the model.

File name	SI3D name	Format	Descrpiton
nopen	nopen	I20	The number of open boundaries in the model.
dts	dtsecopenbc	G20.2	The number of seconds between records in the openbc files.
OpenBdry 1			Comment line, ignored by model. This line and the following six lines are repeated for each of the open boundaries (nn = 1 to nn = nopen).
iside	iside(nn)	I20	Determines the side of the domain the boundary lies on. 1 = West; 2 = North; 3 = East; 4 = South boundary
itype	itype(nn)	I20	Determines type of boundary:1 = wse ; 2 = surface flow; 3 = sub-surface flow
isbc	isbc(nn)	I20	i-location for first cell along open boundary
jsbc	jsbc(nn)	I20	j-location for first cell along open boundary
iebc	iebc(nn)	I20	i-location for last cell along open boundary
jebc	jebc(nn)	I20	j-location for last cell along open boundary

The ninth group in si3d_inp.txt defines the number of water quality constituents modeled.

File name	SI3D name	Format	Descrpiton
ntr	ntr	I20	The number of water quality constituents modeled. If ntr>0, the following line is also read.
iotr	iotr	I20	The nubmer of time steps between consecutive output to tracer file.

6.2.2 Example file: si3d_inp.txt

```
*****************************************************
PRELIMINARY SIMULATIONS FOR Stockton DWSC
=====================================================
Start date and time for simulations
-----------------------------------------------------
year          !    2004            !
month         !       7            !
day           !       1            !
hour          !    0000            !
-----------------------------------------------------
Space-time domains, cell size & time steps
-----------------------------------------------------
xl            !    17340.          ! Length of domain (m) in EW direction
yl            !     5550.          !   "    "    "    (m) in NS       "
zl            !       12.6         !   "    "    "    (m) in vertical
tl            !  1036800.          ! Length of time (s) simulated
idx           !       30           ! Cell size (m) in EW direction
idy           !       30           ! Cell size (m) in NS direction
idz           !      0.5           ! Cell size (m) in vertical
dzmin         !      0.1           ! Min. cell size (m) in vertical
datadj        !      0.0           ! Adjustment of datum by default datum = 0.0
zeta0         !       .4736        ! Initial location of water surface
idt           !       20           ! Time step (s)
ibathf        !        1           ! How bathy file is read
-----------------------------------------------------
Parameters controlling solution algorithm
-----------------------------------------------------
itrap         !        1           ! 1 = trapezoidal iteration is used
niter         !        1           ! No. of trapezoidal iterations
smooth        !        1           ! Smoothing of LF solution
beta          !     0.05           ! Beta parameter for smoothing filter
iturb         !        1           ! How turbulence is solved
az0           !    1.E-4           ! Constant vert. eddy viscosity
dz0           !    1.E-4           ! Constant vert. eddy diffusivity
iadv          !        1           ! Is mom adv on?
itrmom        !        2           ! Algorithm for mom. horizontal advection
ihd           !        1           ! Horiz diffusion on?
ax0           !    1.E-1           ! EW Horizontal eddy diffusivity/viscosity
ay0           !    1.E-1           ! NS Horizontal eddy diffusivity/viscosity
f             !    1.e-4           ! f Coriolis parameter (s-1)
theta         !      0.5           ! Weighting parameter for semi-implicit soln
ibc           !        1           ! 1 = Baroclinic terms is included in mom. soln
isal          !        1           ! Solve scalar transport?
```

```
itrsch       !        4           ! Algorithm for scalar advection
cd           !    .0025           ! Bottom drag coefficient (adimensional)
ifsbc        !        1           ! How mom heat fluxes read.
dtsbc        !    3600.           ! Time step (s) between records in surbc.txt
cw           !   1.5E-3           ! Wind drag coefficient (only if ifsbc = 0)
ws           !    1.E-1           ! Wind speed (constant in m/s) when ifsbc = 0
phi          !     90.0           ! Wind direction (const in degress) when ifsbc = 0
idbg         !        0           ! debug - check messages?
-----------------------------------------------------
Output specifications for time files (individual nodes)
-----------------------------------------------------
 ipt         !       20           ! No. of time step between output to time file
 nnodes      !       13           ! No. of nodes where time file is requested
 inodes      ! 520 414 376 313 287 234 170 138  66   2 579 106 231
 jnodes      ! 120  69  74  88  93  90  65  43  60  86  19   2 186
-----------------------------------------------------
Output specifications for H-plane files
-----------------------------------------------------
 iht         !      180           ! No. of time step between output to plane file
 nplanes     !        5           ! No. of planes where solution is output
 plane 1     !        2           ! Repeat as many lines as nplanes
 plane 2     !        4
 plane 3     !        6
 plane 4     !        8
 plane 5     !       10
-----------------------------------------------------
Output specifications for X-section files
-----------------------------------------------------
 ixt         !      180           ! No. of time step between output to section file
 nsections   !        1           ! No of sections
 ###### SECTION ID :  1 (EW section)
 n_cells     !       53           ! No of cells in the section
 xinodes     !   2  10  20  30  40  50  60  70  80  90
             ! 100 110 120 130 140 150 160 170 180 190
             ! 200 210 220 230 240 250 260 270 280 290
             ! 300 310 320 330 340 350 360 370 380 390
             ! 400 410 420 430 440 450 460 470 480 490
             ! 500 510 520
 xjnodes     !  85  84  81  76  71  67  63  58  54  49
             !  45  42  41  41  43  46  53  65  74  80
             !  84  85  87  89  91  93  94  96  95  93
             !  90  88  86  84  81  79  77  75  73  71
             !  69  69  70  73  75  78  80  83  88  96
             ! 104 113 119
-----------------------------------------------------
```

```
Open boundary conditions specifications
-------------------------------------------------------
 nopen       !        4           ! No. of open boundaries
 dts         !     900.           ! Time (s) between consecutive records in files
 OpenBdry 1  !   ##########       ! Comment line
 iside       !        1           ! 1 = W; 2 = N; 3 = E; 4 = S boundary
 itype       !        1           ! 1 = wse ; 2 = surf flow; 3 = subsurf flow
 isbc        !        2           ! i- location for first cell along open bc
 jsbc        !       84           ! j- location for first cell along open bc
 iebc        !        2           ! i- location for last cell along open  bc
 jebc        !       91           ! j- location ofr last cell along open bc
 OpenBdry 2  !   ##########       ! Comment line
 iside       !        2           ! 1 = W; 2 = N; 3 = E; 4 = S boundary
 itype       !        1           ! 1 = wse ; 2 = surf flow; 3 = subsurf flow
 isbc        !      230           ! i- location for first cell along open bc
 jsbc        !      186           ! j- location for first cell along open bc
 iebc        !      231           ! i- location for last cell along open bc
 jebc        !      186           ! j- location for last cell alont open bc
 OpenBdry 3  !   ##########       ! Comment line
 iside       !        3           ! 1 = W; 2 = N; 3 = E; 4 = S boundary
 itype       !        1           ! 1 = wse ; 2 = surf flow; 3 = subsurf flow
 isbc        !      579           ! i- location for first cell along open bc
 jsbc        !       18           ! j- location for first cell along open bc
 iebc        !      579           ! i- location for last cell along open bc
 jebc        !       19           ! j- location ofr last cell alont open bc
 OpenBdry 4  !   ##########       ! Comment line
 iside       !        4           ! 1 = W; 2 = N; 3 = E; 4 = S boundary
 itype       !        1           !  1 = wse ; 2 = surf flow; 3 = subsurf flow
 isbc        !      105           ! i- location for first cell along open bc
 jsbc        !        2           ! j- location for first cell along open bc
 iebc        !      107           ! i- location for last cell along open bc
 jebc        !        2           ! j- location ofr last cell alont open bc
-------------------------------------------------------
Specification for tracer (not oxygen) simulations
-------------------------------------------------------
 ntr         !        0           ! No. of tracers sim
-------------------------------------------------------
Output specifications for 3D space files
-------------------------------------------------------
 ipxml       !        0           ! No. of time step between output to 3D-space file
 itspf       !        0           ! No. of time steps before first output to file
```

6.2.3 WQ Input File

The water quality input file is needed if any water quality constituents besides temperature are to be included in the model. wq_inp.txt defines which water quality constituents are to be modeled and also defines the rates and constants necessary for the model. As described below, the file is divided into five groups.

The first group defines which water quality constituents are modeled. If the value of each of these variables is 1, the corresponding constituent is modeled and if the value is zero, the constituent is not modeled.

File name	SI3D name	Format	Description
iARB	`iARB`	I20	Defines if arbitrary constituent is modeled.
iDO	`iDO`	I20	Defines if dissolved oxygen is modeled.
iPON	`iPON`	I20	Defines if particulate organic nitrogen is modeled.
iDON	`iDON`	I20	Defines if dissolved organic nitrogen is modeled.
iNH4	`iNH4`	I20	Defines if ammonium is modeled.
iNO3	`iNO3`	I20	Defines if nitrate is modeled.
iPOP	`iPOP`	I20	Defines if particulate organic phosphorus is modeled.
iDOP	`iDOP`	I20	Defines if dissolved organic phosphorus is modeled.
iPO4	`iPO4`	I20	Defines if orthophosphate is modeled.
iALG	`iALG`	I20	Defines if algae is modeled.
iDOM	`iDOM`	I20	Defines if dissolved organic matter is modeled.
iPOM	`iPOM`	I20	Defines if particulate organic matter is modeled.
iSOD	`iSOD`	I20	Defines if sediment oxygen demand is modeled.

The second group defines model constants.

File name	SI3D name	Format	Description
a_{cc}	acc	G20.2	Phytoplankton ratio of carbon to chlorophyll-*a*.
a_{nc}	anc	G20.2	Fraction of algal biomass that is nitrogen.
a_{pc}	apc	G20.2	Fraction of algal biomass that is phophorus.
r_{oc}	roc	G20.2	Ratio of oxygen produced or consumed to carbon consumed or produced in photosynthesis and respiration.
r_{on}	ron	G20.2	Ratio of oxygen consumed to ammonium nitrified during nitrification.
K_{DOM}	KDOM	G20.2	Half-saturation coefficient of oxygen for oxidation of dissolved organic matter.
K_{NIT}	KNIT	G20.2	Half-saturation coefficient of oxygen for nitrification.
K_{SN}	KSN	G20.2	Half-saturation coefficient of nitrogen for algal growth rate.
K_{SP}	KSP	G20.2	Half-saturation coefficient of phosphorus for algal growth rate.
F_{NH4}	FNH4	G20.2	Algae preference factor for NH4.

The third group defines model rates.

File name	SI3D name	Format	Description
k_a	k_a	G20.2	Reaeration rate.
k_{arb}	k_arb	G20.2	Decay rate for arbitrary constituent.
k_{dn}	k_dn	G20.2	Denitrification rate.
k_{DOM}	k_DOM	G20.2	Rate of oxidation of dissolved organic matter.
k_{ex}	k_ex	G20.2	Excretion rate of algae.
k_{gr}	k_gr	G20.2	Rate of algae grazing.
k_{hc}	k_hc	G20.2	Rate of hydrolysis of particulate organic matter.
k_{hn}	k_hn	G20.2	Rate of hydrolysis of particulate organic nitrogen.
k_{hp}	k_hp	G20.2	Rate of hydrolysis of particulate organic phosphorus.
k_{mn}	k_mn	G20.2	Rate of mineralization of dissolved organic nitrogen.
k_{mor}	k_mor	G20.2	Rate of algae mortality.
k_{mp}	k_mp	G20.2	Rate of mineralization of dissolved organic phosphorus.
k_n	k_n	G20.2	Rate of nitrification.
k_{ra}	k_ra	G20.2	Rate of algal respiration.
k_{rs}	k_rs	G20.2	Rate of resuspension.
k_{set}	k_set	G20.2	Settling rate of particulate matter.
k_{setarb}	k_setarb	G20.2	Settling rate for arbitrary constituent.
k_{vn}	k_vn	G20.2	Volatilization rate of ammonium.
μ_{max}	mu_max	G20.2	Maximum growth rate for algae.

The fourth group defines the temperature factors.

File name	SI3D name	Format	Description
θ_{a}	Theta_a	G20.2	Temperature dependence for reaeration.
θ_{dn}	Theta_dn	G20.2	Temperature dependence for denitrification.
θ_{DOM}	Theta_DOM	G20.2	Temperature dependence for dissolved organic matter oxidation.
θ_{gr}	Theta_gr	G20.2	Temperature dependence for grazing of algae.
θ_{hc}	Theta_hc	G20.2	Temperature dependence for hydrolysis of particulate organic matter.
θ_{hn}	Theta_hn	G20.2	Temperature dependence for hydrolysis of particulate organic nitrogen.
θ_{hp}	Theta_hp	G20.2	Temperature dependence for hydrolysis of particulate organic phosphorus.
θ_{mn}	Theta_mn	G20.2	Temperature dependence for mineralization of dissolved organic nitrogen.
θ_{mor}	Theta_mor	G20.2	Temperature dependence for mortality of algae.
θ_{mp}	Theta_mp	G20.2	Temperature dependence for mineralization of dissolved organic phosphorus.
θ_{mu}	Theta_mu	G20.2	Temperature dependence for growth of algae.
θ_{n}	Theta_n	G20.2	Temperature dependence for nitrification.
θ_{PON}	Theta_PON	G20.2	Temperature dependence for hydrolysis of particulate organic nitrogen.
θ_{ra}	Theta_ra	G20.2	Temperature dependence for algal respiration.
θ_{SOD}	Theta_SOD	G20.2	Temperature dependence for sediment oxygen demand consumption.
θ_{vn}	Theta_vn	G20.2	Temperature dependence for volatilization of ammonium.

The fifth group defines miscellaneous coefficients and rates.

File name	SI3D name	Format	Description
ATM_{DON}	ATM_DON	G20.2	Atmospheric deposition of dissolved organic nitrogen.
ATM_{NH4}	ATM_NH4	G20.2	Atmospheric deposition of ammonium.
ATM_{NO3}	ATM_NO3	G20.2	Atmospheric deposition of nitrate.
ATM_{PO4}	ATM_PO4	G20.2	Atmospheric deposition of orthophosphate.
ATM_{POP}	ATM_POP	G20.2	Atmospheric deposition of particulate organic phosphorus.
GW_{NH4}	GW_NH4	G20.2	Groundwater flux of ammonium.
GW_{NO3}	GW_NO3	G20.2	Groundwater flux of nitrate.
GW_{PO4}	GW_PO4	G20.2	Groundwater flux of phosphorus.
J_{NH4}	J_NH4	G20.2	Sediment release of ammonium.
J_{NO3}	J_NO3	G20.2	Sediment release of nitrate.
J_{PO4}	J_PO4	G20.2	Sediment release of phosphorus.

6.2.4 Example file: wq_inp.txt

```
**************************************************
TITLE
==================================================
List of tracers simulated (if value at stpot 22 =1 , tracer simulated)
--------------------------------------------------
iARB          !       1            ! Arbitrary Constituent
iDO           !       1            ! Dissolved Oxygen
iPON          !       1            ! Particulate Organic Nitrogen
iDON          !       1            ! Dissolved Organic Nitrogen
iNH4          !       1            ! Ammonium
iNO3          !       1            ! Nitrate and Nitrite
iPOP          !       1            ! Particulate Organic Phosphours
iDOP          !       1            ! Dissolved Organic Phosphorus
iPO4          !       1            ! Orthophospate
iALG          !       1            ! Algae
iDOM          !       1            ! Dissolved Organic Matter
iPOM          !       1            ! Particulate Organic Matter
iSOD          !       1            ! Sediment Oxygen demand
------------------------------------------------------------------
Model Constants
------------------------------------------------------------------
acc           !      1.0           ! Phytoplankton ratio of C:Chla
anc           !      1.0           ! Fraction of algal biomass that is N
apc           !      1.0           ! Fraction of algal biomass that is P
roc           !      1.0           ! Ratio of O:C in photo and resp
ron           !      1.0           ! Ratio of O:N in nitrification
KDOM          !      1.0           ! Half-saturation coeff for N for DOM oxid
KNIT          !      1.0           ! Half-saturation coeff for nitrification
KSN           !      1.0           ! Half-saturation coeff for N
KSP           !      1.0           ! Half-saturation coeff for P
FNH4          !      1.0           ! Algae preference factor for NH4
------------------------------------------------------------------------
Model rates
------------------------------------------------------------------------
k_a         !       1.0           ! Reaeration rate
k_arb       !       1.0           ! Decay rate for ARB
k_dn        !       1.0           ! Rate of denitrification
k_DOM       !       1.0           ! Oxidation rate of DOM
k_ex        !       1.0           ! Excretion rate of algae
k_gr        !       1.0           ! Grazing rate of algae
k_hc        !       1.0           ! Rate of hydrolysis of POM
k_hn        !       1.0           ! Rate of hydrolysis of PON
k_hp        !       1.0           ! Rate of hydrolysis of POP
```

```
k_mn        !       1.0          ! Rate of mineralization of DON
k_mor       !       1.0          ! Phytoplankton mortality rate
k_mp        !       1.0          ! Mineralization rate of DOP
k_n         !       1.0          ! Rate of Nitrification
k_ra        !       1.0          ! Rate of algal respiration
k_rs        !       1.0          ! Rate of resuspension
k_set       !       1.0          ! Rate of settling ARB
k_vn        !       1.0          ! Volitilization rate of NH4
mu_max      !       1.0          ! Maximum growth rate for algae
-------------------------------------------------------------------------------
Temperature Correction Factors
-------------------------------------------------------------------------------
Theta_a     !       1.0          ! Tw dependence for k_a
Theta_dn    !       1.0          ! Tw dependence for denitrification
Theta_DOM   !       1.0          ! Tw dependence for DOM oxidation
Theta_gr    !       1.0          ! Tw dependence for phyto grazing
Theta_hc    !       1.0          ! Tw dependence for hyrolysis of POM
Theta_hn    !       1.0          ! Tw dependence for hyrolysis of PON
Theta_hp    !       1.0          ! Tw dependence for hydrolysi of POP
Theta_mn    !       1.0          ! Tw dependence for DON mineralization
Theta_mor   !       1.0          ! Tw dependence for phytoplankton mortality
Theta_mp    !       1.0          ! Tw dependence for mineralization of DOP
Theta_mu    !       1.0          ! Tw dependence for growth of algae
Theta_n     !       1.0          ! Tw dependence for nitrification
Theta_PON   !       1.0          ! Tw dependence for PON hydrolysis
Theta_ra    !       1.0          ! Tw dependence for k_ra
Theta_SOD   !       1.0          ! Tw dependence for SOD consumption
Theta_vn    !       1.0          ! Tw dependence for volitilization of NH4
-------------------------------------------------------------------------------
Miscillaneous coefficients and rates
-------------------------------------------------------------------------------
ATM_DON     !       0.0          ! Atmospheric deposition of DON
ATM_NH4     !       0.0          ! Atmospheric deposition of NH4
ATM_NO3     !       0.0          ! Atmospheric deposition of NO3
ATM_PO4     !       0.0          ! Atmospheric deposition of PO4
ATM_POP     !       0.0          ! Atmospheric deposition of POP
GW_NH4      !       0.0          ! Groundwater flux of NH4
GW_NO3      !       0.0          ! Groundwater flux of NO3
GW_PO4      !       0.0          ! Groundwater flux of PO4
J_NH4       !       0.0          ! Sediment release of NH4
J_NO3       !       0.0          ! Sediment release of NO3
J_PO4       !       0.0          ! Sediment release of PO4
-------------------------------------------------------------------------
```

6.2.5 Surface Boundary Condition File

There are three options available for the surface boundary condition file, and the form is specified by variable ifsbc in si3d_inp.txt. The options for ifsbc are 0, 1 and 2. When ifsbc = 0, no heat flux is modeled and the surface boundary conditions are set to a constant value. A surface boundary condition file is not necessary in this condition.

For ifsbc = 1 or ifsbc = 2, a surface boundary condition file is necessary. The first seven lines of the surface boundary condition file are the same for either case. Lines 1 - 6 are header lines that are ignored by the model. Line seven contains the number of points in the file. The remainder of the file contains the time series of data necessary for the model. If ifsbc = 1, the model reads surface heat fluxes from the surface boundary condition file and if ifsbc = 2, the model calculates the surface heat fluxes and reads meteorological conditions from the surface boundary condition file. The following tables summarize the information necessary for either condition.

Table 4: Surface boundary condition file for ifsbc = 1

Column	SI3D name	Variable	Units
1	ignored	time	hr
2	`eta`	extinction coefficinet	(1/m)
3	`Qsw`	shortwave radiation, corrected for albedo	(kJ/m^2/s)
4	`Qn`	net radiation, includes shortwave radiation	(kJ/m^2/s)
5	`cdw`	wind drag coefficient	(NDL)
6	`uair`	u-direction wind speed	(m/s)
7	`vair`	v-direction wind speed	(m/s)

Table 5: Surface boundary condition file for ifsbc = 2

Column	SI3D name	Variable	Units
1	ignored	time	hr
2	`eta`	extinction coefficinet	(1/m)
3	`Qsw`	shortwave radiation, corrected for albedo	(kJ/m^2/s)
4	`Ta`	air temperature	(^{o}C)
5	`Pa`	atmospheric pressure	(Pascals)
6	`Rh`	relative humidity	(fraction)
7	`cdw`	cloud cover	(fraction)
8	`cdw`	wind drag coefficient	(NDL)
9	`uair`	u-direction wind speed	(m/s)
10	`vair`	v-direction wind speed	(m/s)

6.2.6 Example file: surfbc.txt

Example file for option ifsbc = 1 (enter in heat flux terms)

```
Surface boundary condition file for si3d model
Stockton Deep Water Ship Channel
Time is in given in hours from 00:00 hrs on August 7, 2004)
   Time in    // Data format is (10X,G11.2,...) Time attc Hsw Hnet cw ua va
   60-min     // SOURCE = Laura DiPalermo (UCDAVIS)
 intervals  (Note : file prepared on Sept. 21, 2007)
   npts = 575
    0.0000     1.8500     0.0000  -247.3100     0.0010     0.2220    -0.4480
   24.0000     1.8500     0.0000  -268.2805     0.0010     0.4290    -0.2580
   48.0000     1.8500     0.0000  -284.5609     0.0010     0.3250     0.2330
   72.0000     1.8500     0.0000  -293.4444     0.0010     0.3800    -0.1260
   96.0000     1.8500     0.0000  -299.6795     0.0010     0.3800    -0.1240
  120.0000     1.8500    19.6272  -275.1215     0.0010     0.4810     0.1360
  144.0000     1.8500   125.2080   -97.9907     0.0010    -0.4970     0.6270
  168.0000     1.8500   245.0016    40.2230     0.0010    -0.8790     0.4770
  192.0000     1.8500   366.8256   189.9819     0.0010    -1.0600     0.2940
  216.0000     1.8500   474.4368   324.7348     0.0010    -1.1880     0.5290
  240.0000     1.8500   558.3600   469.2558     0.0010    -0.7780     0.7780
  264.0000     1.8500   608.4432   515.2086     0.0010    -0.9680     0.8680
  288.0000     1.8500   619.2720   526.2715     0.0010    -0.9630     0.8730
  312.0000     1.8500   586.7856   494.1380     0.0010    -1.2590     0.3250
  336.0000     1.8500   522.4896   425.6823     0.0010    -1.3790     0.2430
  360.0000     1.8500   423.0000   329.7340     0.0010    -1.2890     0.1650
  384.0000     1.8500   309.2976   214.3754     0.0010    -1.1540     0.3310
  408.0000     1.8500   184.0896    90.4145     0.0010    -0.5250     0.7310
  432.0000     1.8500    62.9424   -25.4863     0.0010    -0.4870     0.1120
  456.0000     1.8500     1.3536  -133.7499     0.0010    -0.8600    -0.5110
  480.0000     1.8500     0.0000  -176.1501     0.0010    -0.8640    -0.2530
```

Example for ifsbc = 2

```
Surface boundary condition file for si3d model
Stockton Deep Water Ship Channel
Time is in given in hours from 00:00 hrs on August 7, 2004)
   Time in   // Data format is (10X,G11.2,...) Time attc Hsw Ta Pa Rh Cc cw ua va
   60-min    // SOURCE = Laura DiPalermo (UCDAVIS)
 intervals  (Note : file prepared on Sept. 21, 2007)
   npts = 575
    0.0000     1.8500     0.0000    15.3000 101300.000     0.9300     0.2620     0.0010     0.2220    -0.4480
   24.0000     1.8500     0.0000    14.2000 101300.000     0.9400     0.2620     0.0010     0.4290    -0.2580
   48.0000     1.8500     0.0000    13.1000 101300.000     0.9600     0.2620     0.0010     0.3250     0.2330
   72.0000     1.8500     0.0000    12.6000 101300.000     0.9700     0.2620     0.0010     0.3800    -0.1260
   96.0000     1.8500     0.0000    12.3000 101300.000     0.9700     0.2620     0.0010     0.3800    -0.1240
  120.0000     1.8500    27.2600    12.7000 101300.000     0.9700     0.2620     0.0010     0.4810     0.1360
  144.0000     1.8500   173.9000    17.2000 101300.000     0.9100     0.2620     0.0010    -0.4970     0.6270
  168.0000     1.8500   340.2800    19.6000 101300.000     0.8000     0.2620     0.0010    -0.8790     0.4770
  192.0000     1.8500   509.4800    22.0000 101300.000     0.7300     0.2620     0.0010    -1.0600     0.2940
  216.0000     1.8500   658.9400    24.5000 101300.000     0.6700     0.2620     0.0010    -1.1880     0.5290
  240.0000     1.8500   775.5000    27.1000 101300.000     0.5700     0.2620     0.0010    -0.7780     0.7780
  264.0000     1.8500   845.0600    28.9000 101300.000     0.4800     0.2620     0.0010    -0.9680     0.8680
  288.0000     1.8500   860.1000    30.2000 101300.000     0.4400     0.2620     0.0010    -0.9630     0.8730
  312.0000     1.8500   814.9800    31.3000 101300.000     0.4100     0.2620     0.0010    -1.2590     0.3250
  336.0000     1.8500   725.6800    32.0000 101300.000     0.3700     0.2620     0.0010    -1.3790     0.2430
  360.0000     1.8500   587.5000    32.7000 101300.000     0.3700     0.2620     0.0010    -1.2890     0.1650
  384.0000     1.8500   429.5800    32.8000 101300.000     0.3600     0.2620     0.0010    -1.1540     0.3310
  408.0000     1.8500   255.6800    32.7000 101300.000     0.3700     0.2620     0.0010    -0.5250     0.7310
  432.0000     1.8500    87.4200    31.5000 101300.000     0.4300     0.2620     0.0010    -0.4870     0.1120
  456.0000     1.8500     1.8800    26.5000 101300.000     0.5100     0.2620     0.0010    -0.8600    -0.5110
  480.0000     1.8500     0.0000    23.9000 101300.000     0.5600     0.2620     0.0010    -0.8640    -0.2530
```

6.2.7 Bathymetery file

The bathymetery file, called h by the model, contains the information regarding the geometry of the domain. The bathymetery file is read in the subroutine bathy. The depths from the h file are assumed to be defined at the corners of each computational cell and are stored in the array 'h4'. The first line is the header line and contains imx, the number of cells in the i-direction, jmx, the number of cells in the j-direction and ncols which defines how many columns are in each row. In the h file, there is an entry for each cell corner. If the cell is dry, a value of -90 is entered.

6.2.8 Example file: h

```
DWSC rotated 30 m depth grid,   imx =  579,jmx =  186,ncols =  18  (11/23/04)
HV       V   V   V   V   V   V   V   V   V   V   V   V   V   V   V   V   V
HU     U z U z U z U z U z U z U z U z U z U z U z U z U z U z U z U z U z U
  91    5   5   5   5   5   5   9   9   9   9   8   8   5   5 -90 -90 -90 -90
  90   16  19  22  21  21  20  24  24  23  19  16  16  16  19  14   5 -90 -90
  89   40  40  44  45  44  40  40  37  31  27  23  20  23  28  25  15   5 -90
  88   71  70  69  67  69  70  69  64  52  43  37  32  31  33  33  31  20   5
  87   99  99 102 100 100 105  99  86  77  71  63  51  44  45  42  46  45  20
  86  112 112 113 113 113 121 124 112 103  98  91  82  70  65  49  32  36  35
  85  107 107 111 112 112 112 113 115 116 110 108 107 101  92  73  46  37  43
  84   72  72  76  84  84  86  96 103 108 109 111 112 112 109 103  93  74  66
  83   33  32  29  29  31  38  51  53  60  77  92 104 109 110 110 109 102  93
  82  -90 -90 -90 -90 -90 -90 -90   5  10  24  43  62  80  98 106 109 110 110
  81  -90 -90 -90 -90 -90 -90 -90 -90 -90 -90 -90  16  35  54  74  94 104 111
  80  -90 -90 -90 -90 -90 -90 -90 -90 -90 -90 -90 -90  10  24  39  63  80  92
  79  -90 -90 -90 -90 -90 -90 -90 -90 -90 -90 -90 -90 -90 -90  20  37  46  51
  78  -90 -90 -90 -90 -90 -90 -90 -90 -90 -90 -90 -90 -90 -90 -90  14  29  41
  77  -90 -90 -90 -90 -90 -90 -90 -90 -90 -90 -90 -90 -90 -90 -90 -90  11  30
```

6.2.9 Open Boundary Condition file

The open boundary conditions are defined in si3d_inp.txt. There will be an OpenBC file for each open boundary defined in the input file. The boundary condition files contain time series data that defines flow and water quality conditions for each boundary. The first five lines of the file are header lines and are ignored by the model. The sixth line contains Table 6.2.9 summarizes the data in the open boundary condition file.

Table 6: Surface boundary condition file for ifsbc = 2

Column	Variable
1	time
2	flow boundary condtion*
3	water temperature
4	tracer 1
5	tracer 2
3 + ntr	tracer ntr **

Notes: There are three options for how column 2, the flow boundary condition is defined. If itype, defined in si3d-inp.txt is equal to 1, then water surface elevations are defined. If itype is eqaul to 2, the free surface flow is defined and if itype is equal to 3, submerged flow is defined. The number of columns in the open boundary files should be equal to the number of water quality constituents being modeled plus three, time, flow and temperature. The order of the boundary conditions is also important and should follow the list of constituents listed in the water quality input file. For example, if the following five constituents are modeled: arbitrary constituent, dissolved oxygen, algae, particulate organic matter and dissolved organic matter, it is important that the order of columns in the boundary condition files is: arbitrary constituent, dissolved oxygen, algae, dissolved organic matter and particulate organic matter. If the order is not correct, the model will misinterprret the boundary conditions as the wrong constituent. Also note that all constituents must be input at the same time frequency. The model will interpolate between entries to the time series.

6.2.10 Example file: openbc01.txt

```
Open boundary condition file for Stockton
Time is in hours from day 220 in 2004
Data - (2) wse (m); (3) Temp. (oC); (4) - (3+ntr) Consituents
Data from USGS (Peter Smith)
*****************************************************
   npts =  2016
   0.0000    0.4312   24.1513    0.0000    7.0000    0.2000    3.6300    0.3300
   0.2500    0.4314   24.1483    0.0000    7.0000    0.2000    3.6300    0.3300
   0.5000    0.4313   24.1454    0.0000    7.0000    0.2000    3.6300    0.3300
   0.7500    0.4306   24.1425    0.0000    7.0000    0.2000    3.6300    0.3300
   1.0000    0.4297   24.1396    0.0000    7.0000    0.2000    3.6300    0.3300
   1.2500    0.4283   24.1456    0.0000    7.0000    0.2000    3.6300    0.3300
   1.5000    0.4264   24.1518    0.0000    7.0000    0.2000    3.6300    0.3300
   1.7500    0.4243   24.1580    0.0000    7.0000    0.2000    3.6300    0.3300
   2.0000    0.4218   24.1643    0.0000    7.0000    0.2000    3.6300    0.3300
   2.2500    0.4191   24.1759    0.0000    7.0000    0.2000    3.6300    0.3300
   2.5000    0.4157   24.1875    0.0000    7.0000    0.2000    3.6300    0.3300
   2.7500    0.4121   24.1991    0.0000    7.0000    0.2000    3.6300    0.3300
   3.0000    0.4079   24.2107    0.0000    7.0000    0.2000    3.6300    0.3300
   3.2500    0.4035   24.2309    0.0000    7.0000    0.2000    3.6300    0.3300
   3.5000    0.3984   24.2511    0.0000    7.0000    0.2000    3.6300    0.3300
   3.7500    0.3935   24.2714    0.0000    7.0000    0.2000    3.6300    0.3300
   4.0000    0.3882   24.2916    0.0000    7.0000    0.2000    3.6300    0.3300
   4.2500    0.3826   24.3276    0.0000    7.0000    0.2000    3.6300    0.3300
   4.5000    0.3775   24.3635    0.0000    7.0000    0.2000    3.6300    0.3300
   4.7500    0.3722   24.3991    0.0000    7.0000    0.2000    3.6300    0.3300
   5.0000    0.3670   24.4346    0.0000    7.0000    0.2000    3.6300    0.3300
   5.2500    0.3625   24.4550    0.0000    7.0000    0.2000    3.6300    0.3300
   5.5000    0.3591   24.4754    0.0000    7.0000    0.2000    3.6300    0.3300
   5.7500    0.3568   24.4958    0.0000    7.0000    0.2000    3.6300    0.3300
   6.0000    0.3561   24.5162    0.0000    7.0000    0.2000    3.6300    0.3300
```

6.2.11 Variable Initialization file

The last file necessary for SI3DWQ is the variable initialization file. This file contains a profile for temperature and all constituents modeled. The values from this file set the initial condition for the entire model domain. Similar to the open boundary files, care must be taken in the order the water quality constituents are written to the file. The order should match that found in the open boundary condition files.

6.2.12 Example file: si3d_init.txt

```
%Stockton DWSC - Profiles
%# Profile
%kmm1=   12
%
%
%
                24.15       0.00       6.625      0.6975     3.6775     0.3875
                24.15       0.00       6.625      0.6975     3.6775     0.3875
                24.15       0.00       6.625      0.6975     3.6775     0.3875
                24.15       0.00       6.625      0.6975     3.6775     0.3875
                24.15       0.00       6.625      0.6975     3.6775     0.3875
                24.15       0.00       6.625      0.6975     3.6775     0.3875
                24.15       0.00       6.625      0.6975     3.6775     0.3875
                24.15       0.00       6.625      0.6975     3.6775     0.3875
                24.15       0.00       6.625      0.6975     3.6775     0.3875
                24.15       0.00       6.625      0.6975     3.6775     0.3875
                24.15       0.00       6.625      0.6975     3.6775     0.3875
```

Appendix I

Estuaries and Coasts
DOI 10.1007/s12237-008-9109-9

ORIGINAL PAPER

Thermal Variability in a Tidal River

Stephen G. Monismith · James L. Hench · Derek A. Fong · Nicholas J. Nidzieko · William E. Fleenor · Laura P. Doyle · S. Geoffrey Schladow

Received: 14 February 2008 / Revised: 10 September 2008 / Accepted: 6 October 2008

Abstract In this paper, we discuss observations of temperature variability in the tidal portion of the San Joaquin River in California. The San Joaquin River makes up the southern portion of the Sacramento San Joaquin Delta, the eastern end of San Francisco Bay. Observations made in August 2004 and August 2005 show significant diurnal variations in temperature in response to surface heat exchange. However, to account for observed changes in heat content a sizeable downstream heat flux (approximately 100 W m^{-2}) must be added to the surface heat flux. To account for this flux via Fickian dispersion, a flow-dependent dispersion coefficient varying from 500 to 4,000 m^2 s^{-1} is needed. These values are much larger than would be predicted for a river of this size, suggesting that the complex topology of the Delta greatly enhances longitudinal dispersion. Building on these observations, we present a simple theory that explores how the subtidal temperature field varies in response to changes in flow rate, dispersion, and heat exchange.

Keywords Estuaries · Tides · Water temperature · Dispersion · Surface heat exchange

S. G. Monismith (✉) · J. L. Hench · D. A. Fong · N. J. Nidzieko
Environmental Fluid Mechanics Laboratory, Stanford University, Stanford, CA 94305-4020, USA
e-mail: monismith@stanford.edu

W. E. Fleenor · L. P. Doyle · S. G. Schladow
Department of Civil and Environmental Engineering, University of California, Davis, CA 95616, USA

Introduction

Models to predict temperatures in rivers and lakes are in common use (see e.g., Bohrmans and Webster 1998). For example, models of river and stream temperatures have been used to develop standards for waste heat discharge, to design reservoir release strategies, and to understand annual variations in a variety of biogeochemical processes such as nutrient cycling or the development of harmful algal blooms. In lakes, variability in temperature stratification plays a central role in mixing and transport, thus determining the rates and paths by which different portions of the lake are connected to each other (Romero et al. 2004).

Predictions of temperatures in estuaries are less commonly reported (see Uncles and Stephens 2001 for a notable exception), at least partially, because temperature is generally assumed to have little effect on flow dynamics in most estuaries. Nonetheless, in many cases, knowledge of temperature is important because it is important biologically. For example, in the complex of interconnected channels where the Sacramento and San Joaquin rivers come together (hereinafter referred to as "the Delta"), water temperature standards have been developed to protect outmigrating chinook salmon smolts. Additionally, it is known that temperature strongly influences when Delta Smelt, an endangered native fish resident in the Delta, spawn (Bennett 2005). Predictions of water temperatures are thus important to understanding when spawning will take place and thus when larval Delta Smelt are likely to be present in the system, information that is important in operating in-Delta diversions so as to minimize entrainment losses (Bennett 2005).

In this paper, we report observations of temperature variation gathered as part of a project studying the effects of thermal stratification on low dissolved oxygen in the Deep

Water Ship Channel (DWSC) of the San Joaquin River (SJR). The original motivation for this work was the hypothesis that stratification played an important role in the development of hypoxia in this system (Jassby 2005; Jassby and Van Nieuwenhuyse 2005).

Overall, the variation in temperature can be described by the Reynolds averaged heat conservation equation (see e.g., Tennekes and Lumley 1972),

$$\frac{\partial \overline{\theta}}{\partial t} + \overline{U} \cdot \nabla \overline{\theta} \cong -\frac{\partial}{\partial z}\left(\overline{w'\theta'}\right) \tag{1}$$

where $\overline{\theta}$ and $\overline{U}$ are the tidally varying Reynolds averaged temperature and velocities, θ' and w' are the turbulent fluctuating temperature and vertical velocity, and z is vertical position.

If Eq. 1 is integrated over the cross-sectional area and is filtered to remove tidal variations, a one-dimensional advection diffusion equation results (see e.g., Edinger et al. 1974; Fischer et al. 1979; Uncles and Stephens 2001)

$$A(x)\frac{\partial T}{\partial t} - Q_f \frac{\partial T}{\partial x} = \frac{\partial}{\partial x}\left(K(x)A(x)\frac{\partial T}{\partial x}\right) - \frac{WH_f}{\rho c_p} \tag{2}$$

In this equation, A is the cross-sectional area, Q_f is the river flow, T is the cross-sectionally averaged and subtidally filtered temperature, K is the dispersion coefficient, W is the local width, and H_f is the surface heat flux in W m^2. The usual sign convention is that H_f is negative for heating of the water column and positive for cooling. (see Fig. 1). The x-axis points upstream. Such 1D models have a long history in the theory and modeling of salinity in estuaries (see e.g., Savenije 2005; Monismith et al. 2002). As discussed in Fischer (1976), the sub-tidal representation of tidally averaged sheared advection is usually assumed to take the form of Fickian diffusion, although as discussed by Ridderinkhof and Zimmerman (1992), such advection need not lead to pure Fickian diffusion, instead, depending on the mechanism causing the shear, can lead to scale-dependent dispersion.

In this paper, we discuss what shapes the along-channel variation of temperature observed in the tidal San Joaquin River, emphasizing how the processes described in Eq. 2, namely advection, surface heat fluxes, and most notably, dispersion, all play an important roles in determining the temperature field we observe.

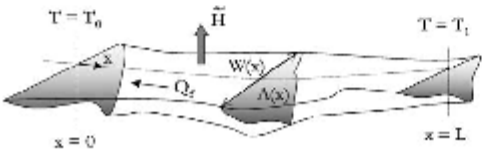

Fig. 1 Sketch of tidal river for one-dimensional analysis

Field Site and Data Collection

The San Joaquin River flows west from the Sierra Nevada mountains into the southern San Joaquin valley and then north into the Delta formed by the confluence of the San Joaquin and Sacramento Rivers. The Delta itself consists of a matrix of hundreds of levee-bordered islands of different sizes created in the nineteenth century by "reclamation" of the tidal marsh through which the Sacramento and San Joaquin Rivers flowed in San Francisco Bay. For approximately 30 km starting near the city of Stockton, the San Joaquin has been dredged to create the Deep Water Ship Channel, a channel that facilitates passage of shipping to the port of Stockton (Fig. 2). Near the junction of the San Joaquin River with the DWSC, there is a dead-end section of channel used for turning around ships visiting the port. Except for peak runoff events, most of the natural flow in the river is diverted for use by irrigated agriculture, such that in summer, non-tidal flows of freshwater into the Delta might only amount to O(10) m^3 s^{-1}. Tidal flows in the Delta are stronger, with tidal velocities in the DWSC ranging from 0.1 to 0.3 m s^{-1}, with stronger velocities found at seaward end of the river. Nonetheless, the flows remain primarily tidal until at least 20 km upstream of the start of the DWSC. In this portion of the Delta, salinities are close to zero and are not dynamically significant. For further information, the reader is referred to Jassby (2005).

In August 2004 and 2005, we deployed, for several weeks at a time, a series of moorings including temperature loggers and current meters at a series of stations arranged as shown in Fig. 1. Our set of temperature loggers included Richard Brancker Research TR1000, Oregon Environmental 9311, and Seabird 39 units. When newly calibrated, these all have accuracies approaching 0.002°C, although for our data sets, comparison of data from instruments of different types and ages on the same mooring suggested typical calibration offsets of as much as 0.2°C. Velocity measurements were made using 1,200 kHz RD Instruments workhorse ADCPs, deployed on the bottom looking up through the water column and measuring velocities from about 0.6 mab (meters above bottom) and covering about 90% of the total water column depth in 0.25-m bins.

In addition to our instruments, we also obtained other data from several local, state, and federal agencies, notably flow in the San Joaquin River measured ultrasonically by the USGS approximately 4 km upstream of the junction of the DWSC and the SJR, and temperatures measured by the California Dept of Water Resources[1] at various stations along the SJR both upstream and downstream of our moorings.

[1] http://cdec.water.ca.gov/

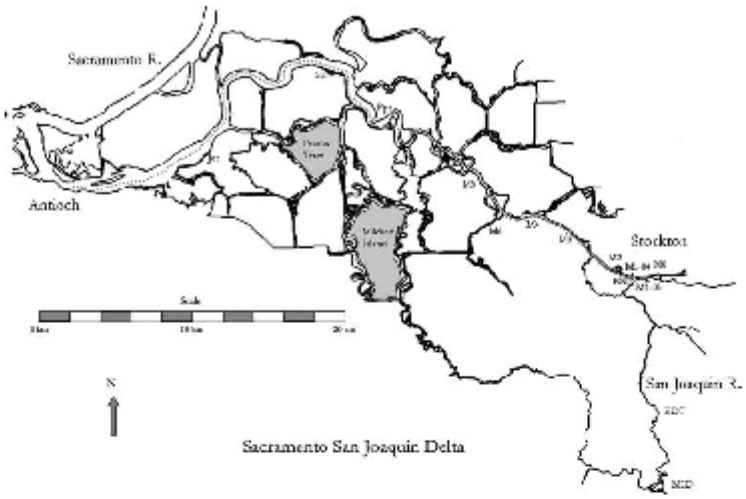

Fig. 2 Overview of the Sacramento San Joaquin Delta. Along with instrument locations for 2004 and 2005 experiments (*M0 to M6*), positions of selected California Dept. of Water Resources continuous monitoring (e.g., *MSD* Mossdale) stations are also shown. One DWR station on the San Joaquin River, Vernalis (VER), is not shown; it is approximately 45 km south of MSD

As discussed in detail in Edinger et al. (1974) (see also Pawlowicz et al. 2001), heat fluxes through the air–water interface are due to shortwave radiation (Q_w), net longwave radiation (Q_{lw}), latent heat transfer (H_l), and sensible heat transfer (H_s). The total surface heat exchange can be written as

$$H_f = Q_{sw} + Q_{lw} + H_l + H_s \quad (3)$$

The first term on the right of Eq. 3 is usually measured, whereas the other three terms are computed using empirical formulae based on measured surface water temperature, air temperature, relative humidity and wind speed, and cloud cover (see Fischer et al. 1979).

Meteorological data were obtained from the Port of Stockton (wind speed and direction, air temperature ,and relative humidity) and for the CIMIS[2] weather station in Manteca (incident shortwave radiation), closest to, but approximately 20 km NNW from our M2 mooring. Examination of other CIMIS stations in this part of California (e.g., one 20 km WSW of Manetca) showed a high degree of correlation ($R^2 \approx 0.99$) with nearly identical shortwave radiation values such that mean shortwave radiation values were different by less than 8 W/m^2. Combined with our surface temperature data, these sets of meteorological data were used to compute heat fluxes (latent, sensible, and net longwave) using the set of Matlab™ routines describe by Palowiscz et al. (2001). Because we did not have any data on cloud fraction, i.e., the portion of the sky covered by clouds, we assumed a "cloudiness" of 0.9 (cloudiness=1 corresponds to a clear sky) of for all our calculations.

[2] http://wwwcimis.water.ca.gov/cimis/

Exploration of diurnal stratification dynamics using the 3D circulation model Si3D (Rueda and Schladow 2003) and the 2004 data set suggested that the measured shortwave radiation should be reduced by 10% and that latent and sensible heat fluxes should be increased by 10% to best model the stratification that developed diurnally. The albedo chosen is the same as what Cole et al. (1992) used to model photosynthesis in the tidal freshwater region of the Hudson estuary, and is within the range of values given by Mohseni and Stefan (1999). These increases in surface heat exchanges are reasonable given uncertainty in the applicability of bulk meteorological formulae developed for open ocean conditions to limited fetch waterbodies like the DWSC and the extent to which winds measured at the Port of Stockton represent winds over the domain of interest. These changes were used for both the 2004 and 2005 data sets.

Observations

Tides, depth-averaged velocities, heat fluxes, and depth-averaged temperatures for August 2004 for our mooring stations are shown in Fig. 3. As observed, diurnal variations dominate variations in temperature, with little direct effect of tides. These diurnal variations included diurnally varying vertical stratification of 2 to 4°C that developed through the day due to heating and broke down at night due to cooling. Results from our study pertaining to stratification dynamics will be reported elsewhere.

Spatial variations in temperature are also clear, with the warmest temperatures generally seen at the upstream end of

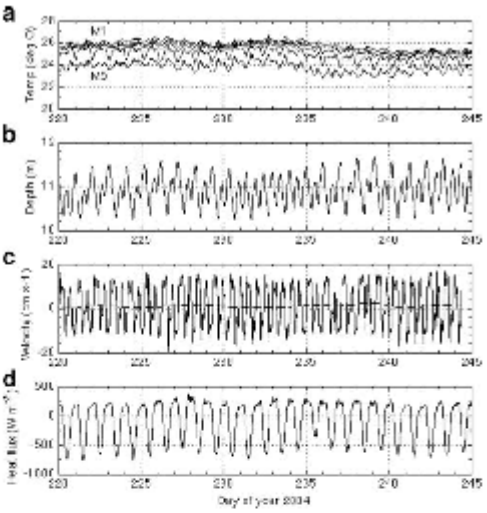

Fig. 3 a Temperature; b depth at M2; c depth-averaged velocities at M2; and d heat fluxes; all for August 2004

the DWSC (M1) and the coldest at the downstream end (M3). The small tidal variation in temperature can be explained by noting that the temperature change over one tidal cycle due to advection by a sinusoidally varying tidal velocity is

$$\Delta T_{\text{tidal}} \approx \frac{U_{\text{tide}}}{\omega_{\text{tide}}} \frac{\partial T}{\partial x} \tag{4}$$

where U_{tide} is the peak velocity of tide with frequency ω_{tide}. For the DWSC, $U_{\text{tide}} \approx 0.1$ m/s, $\omega_{\text{tide}} \approx 1.5 \times 10^{-4}\ s^{-1}$, and $\partial T/\partial x \approx 10^{-4}$°C s^{-1}. Thus, $\Delta T_{\text{tidal}} \approx 0.1$°C, in contrast with diurnal variations of approximately 1°C. Note that subtidal variations in the longitudinal temperature gradient mean that harmonic analysis of temporal temperature variations would not be especially useful.

The combination of spatial and temporal variations in temperature for the entire San Joaquin system (river to estuary) are shown for 2004 (Fig. 4) and 2005 (Fig. 5), with the x-axis in each image representing time and the y-axis in the upper panel of each figure showing stations, arrayed with downstream (Antioch) at the top of the figure and upstream (Vernalis) at the bottom. In addition to diurnal variations, both 2004 and 2005 show significant longer period variations that may either be associated with changes in meteorological forcing (especially the latter half of 2005, which was a period of significant cooling) or in spring-neap variations in upstream (negative) heat flux.

Interestingly, the 2004 data show two different temperature patterns, one in which the temperatures monotonically

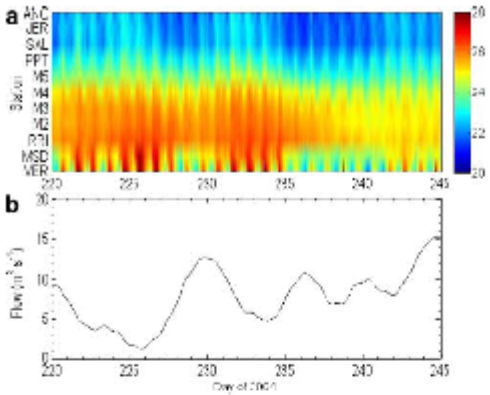

Fig. 4 San Joaquin River July/Aug 2004: a Temperatures—Stations are Vernalis (*VER*), Mossdale (*MSD*), Brandt bridge (*BDT*), M0, Rough and Ready Island (*RRI*), M1, M2, M5, Prisoners Point (*PPT*), San Andreas Landing (*SAL*), Jersey point (*JER*), and Antioch (*ANC*). All are given in °C; b subtidal flows measured upstream of the DWSC

increase up into the river and one in which the DWSC near Stockton [i.e., near Rough and Ready Island (RRI)] is the warmest part of the San Joaquin. The 2005 data only show the latter pattern, a likely effect of larger flows in August 2005 than in August 2004 (Fig. 5b). Nonetheless, the overall mean spatial structure of the temperature field for both years are (Figs. 6 and 7) similar. Most importantly, both data sets show the importance of heat fluxes from both the Bay and from the San Joaquin River in setting temperatures in the DWSC. For example, at a tidally

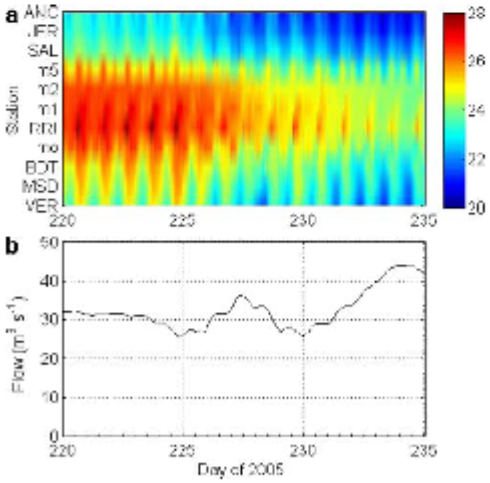

Fig. 5 Same as Fig. 4 except for July/Aug 2005. Labels as above

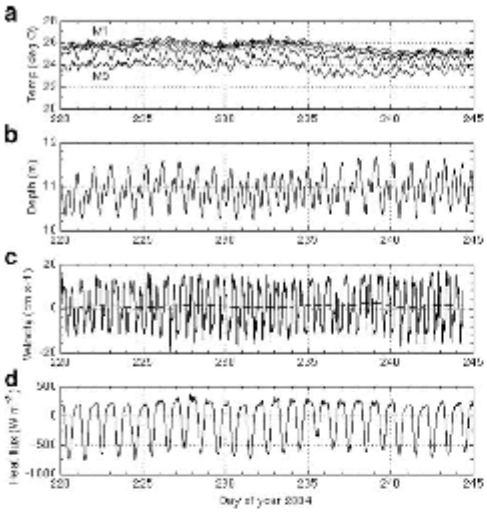

Fig. 3 a Temperature; b depth at M2; c depth-averaged velocities at M2; and d heat fluxes; all for August 2004

the DWSC (M1) and the coldest at the downstream end (M3). The small tidal variation in temperature can be explained by noting that the temperature change over one tidal cycle due to advection by a sinusoidally varying tidal velocity is

$$\Delta T_{\text{tidal}} \approx \frac{U_{\text{tide}}}{\omega_{\text{tide}}} \frac{\partial T}{\partial x} \tag{4}$$

where U_{tide} is the peak velocity of tide with frequency ω_{tide}. For the DWSC, $U_{\text{tide}} \approx 0.1$ m/s, $\omega_{\text{tide}} \approx 1.5 \times 10^{-4}\ s^{-1}$, and $\partial T/\partial x \approx 10^{-4}$°C s^{-1}. Thus, $\Delta T_{\text{tidal}} \approx 0.1$°C, in contrast with diurnal variations of approximately 1°C. Note that subtidal variations in the longitudinal temperature gradient mean that harmonic analysis of temporal temperature variations would not be especially useful.

The combination of spatial and temporal variations in temperature for the entire San Joaquin system (river to estuary) are shown for 2004 (Fig. 4) and 2005 (Fig. 5), with the x-axis in each image representing time and the y-axis in the upper panel of each figure showing stations, arrayed with downstream (Antioch) at the top of the figure and upstream (Vernalis) at the bottom. In addition to diurnal variations, both 2004 and 2005 show significant longer period variations that may either be associated with changes in meteorological forcing (especially the latter half of 2005, which was a period of significant cooling) or in spring-neap variations in upstream (negative) heat flux.

Interestingly, the 2004 data show two different temperature patterns, one in which the temperatures monotonically

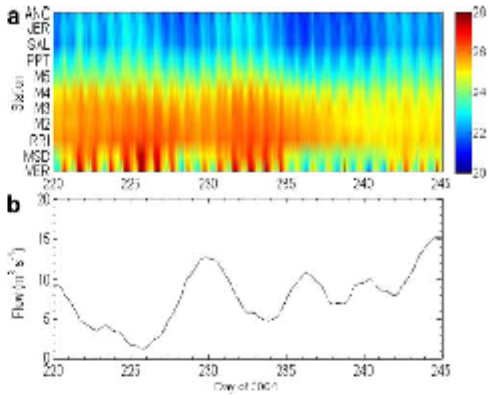

Fig. 4 San Joaquin River July/Aug 2004: a Temperatures—Stations are Vernalis (*VER*), Mossdale (*MSD*), Brandt bridge (*BDT*), M0, Rough and Ready Island (*RRI*), M1, M2, M5, Prisoners Point (*PPT*), San Andreas Landing (*SAL*), Jersey point (*JER*), and Antioch (*ANC*). All are given in °C; b subtidal flows measured upstream of the DWSC

increase up into the river and one in which the DWSC near Stockton [i.e., near Rough and Ready Island (RRI)] is the warmest part of the San Joaquin. The 2005 data only show the latter pattern, a likely effect of larger flows in August 2005 than in August 2004 (Fig. 5b). Nonetheless, the overall mean spatial structure of the temperature field for both years are (Figs. 6 and 7) similar. Most importantly, both data sets show the importance of heat fluxes from both the Bay and from the San Joaquin River in setting temperatures in the DWSC. For example, at a tidally

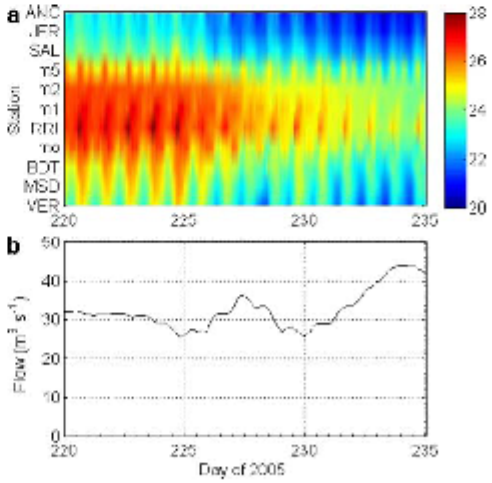

Fig. 5 Same as Fig. 4 except for July/Aug 2005. Labels as above

and neglect advection, the rate of change of heat content due to surface fluxes is

$$\rho c_p \frac{d}{dt} \int_{-D}^{0} \overline{\theta} dz = -H_s \tag{5}$$

where D is the local depth. In both cases, the computed fluxes show net heating, whereas the observations in general do not. There is also a tidal variation that spectral analysis (not shown) revealed is primarily semidiurnal, although other periods (24, 8, 6, 4.8, and 4 h) are also present. These frequencies reflect the spectral energy content of the velocity record shown in Fig. 3c.

For 2004, the imbalance amounts to an average heat loss of over 100 W m^{-2}, a number that is far larger than potential errors in computing the heat flux. For example, uncertainty in the net longwave radiation due to uncertainty about cloud cover and uncertainty in shortwave radiation due to uncertainty in albedo are each less than 10 W/m^2. This imbalance can be used to estimate the net horizontal heat transport as the subtidal difference between the rate of change of heat content and the incoming heat fluxes. Calculating this way (Fig. 9c) reveals a downriver heat flux of approximately 50 to 150 W/m^2, with the sign of the flux correct for Fickian diffusion-like process.

We can evaluate the relative importance of subtidal advection and dispersion by integrating Eq. 2 from $x=x_0$, the downstream end of DWSC to the upstream end at Stockton, $x=x_1$ and assuming that the surface heat flux is uniform (in the absence of any other data). This gives

$$\rho c_p \overline{D} \frac{\partial \overline{T}}{\partial t} + H_f \approx -\frac{\rho c_p K(x_0) A(x_0) \frac{\partial \overline{T}}{\partial x}(x_0)}{\overline{W}(x_1 - x_0)} + \rho c_p Q_f \frac{(T(x_1) - T(x_0))}{\overline{W}(x_1 - x_0)} \tag{6}$$

where quantities with overbars are averages between $x=x_0$ and $x=x_1$, so that K can be determined from the heat balance. To carry out this calculation, the heat content, flows, etc. were low-pass filtered using a fourth order Butterworth filter with a cutoff frequency of 0.25 cpd. Based on the data shown in Figs. 6 and 7, $\partial T/\partial x$ was calculated from the difference in temperature between M2 and Prisoner Point (PPT) for 2004, whereas for 2005, we used RRI and Antioch.

The results of this calculation for the 2004 data are shown in Fig. 10, where it can be seen that values of K range from 500 to 900 m^2 s^{-1}. The same calculation for 2005 is shown in Fig. 11, where even larger values of K (up to 4000 m^2 s^{-1}) are evident. Note that since these values of K come from a requirement to lose heat from the DWSC, they cannot be an effect of error in the measured flow rate, since the overall contribution to the needed heat flux is small and has the wrong sign. Somewhat surprisingly,

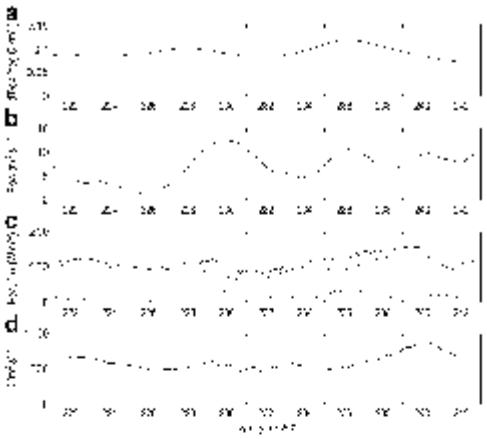

Fig. 10 Inferred dispersion coefficients from heat balance for 2004: a horizontal temperature gradient; b subtidal flow in San Joaquin River; c advective heat flux (*dotted line*), inferred correction to 1D balance (*broken line*), and total dispersive heat flux (*solid line*); d inferred longitudinal dispersion coefficient

combining the two data sets (Fig. 12) reveals a substantial and unexpected dependence on flow.

These values of K are at the large end of what is typically found for rivers and estuaries (see Fischer et al. 1979). For example, the dispersion coefficient associated with an oscillating shear flow can be approximated by

$$K \approx 0.2 \frac{W^2 U^2}{D u_*} f\left(\frac{\omega W^2}{D u_*}\right) \tag{7}$$

where u_* is the average shear velocity and the function f is given in Fischer et al. (1979). Using values of W, etc., appropriate to the DWSC, we find that a value of $K \approx 30$ m^2 s^{-1} would be predicted.

Thus, it seems likely that the large value of K required for the thermal energy balance reflects the dispersive effects of the numerous channel junctions and bifurcations along the SJR. Indeed, 2D calculations by Monsen (2001) showed that in-channel sub-tidal fluxes of scalars are largely due to advection. Thus, the observed dispersion must be associated almost exclusively with the channel junctions. The dependence on mean flow may be associated with an increase in the tendency for fluid particles in the DWSC to "sample" several geometrically complex features, e.g., the divided channels near M5.

From the practical standpoint of predicting temperatures in a complex system like the tidal San Joaquin River, the fact that subtidal dispersive heat fluxes are comparable to net surface heat exchanges means that hydrodynamic

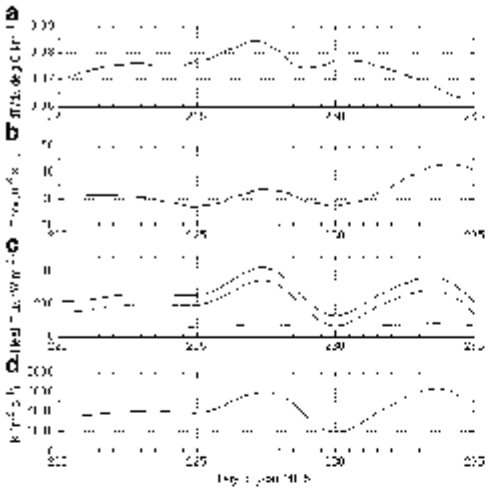

Fig. 11 Inferred dispersion coefficients from heat balance for 2005: a Horizontal temperature gradient; b subtidal flow in San Joaquin River; c advective heat flux (*dotted line*), inferred correction to 1D balance (*broken line*), and total dispersive heat flux (*solid line*); d inferred longitudinal dispersion coefficient

models like that used by Monsen (2001) or DeGeorge (1996) must do a reasonable job at predicting dispersive heat fluxes and making use of accurate surface heat fluxes if it is to accurately predict temperature. In the next section, we discuss, in an idealized fashion, this balance of dispersion and surface heating.

Theory

We focus in this paper on a simple analytical model of subtidal variations in temperature. Consequently, we also assume the heat flux to be constant or at least not vary diurnally. We also assume that the temperature is, to first order, uniform across the cross-section and thus varies only in the longitudinal direction. Thus, our starting point is the 1D advection dispersion equation for heat, including surface heating through an imposed surface heat that depends on wind speed, air-water temperature difference, etc. given above.

For the sake of developing analytical solutions that describe the main features of the temperature distributions reported above, we further neglect time variations, assume that K and A do not depend on x, and that the surface heat exchange can be represented by the form

$$\frac{H_f}{\rho c_p} = -\alpha(T_e - T) \tag{8}$$

where α is the heat transfer velocity and T_e is the equilibrium temperature in the water, both of which are functions of the given the meteorological conditions and the incident shortwave radiation (Mohseni and Stefan 1999). With these drastic simplifications, it becomes

$$-\frac{Q_f}{A}\frac{\partial T}{\partial x} = K\frac{\partial^2 T}{\partial x^2} + \alpha\frac{(T_e - T)}{D} \tag{9}$$

where $D=A/W$ is the effective depth. We suppose that the temperature at the riverine and ocean ends of this tidal river are specified. Without loss of generality, these can be assumed to be the same, so that

$$T = T_0 \quad x = 0, L \tag{10}$$

To proceed, we look at the deviation of the temperature from T_0, i.e.

$$T' = T - T_0 \tag{11}$$

and then construct dimensionless variables from the temperature difference $\Delta T = T_e - T_0$:

$$\begin{aligned} T^* &= T'/\Delta T \\ x^* &= x/L \end{aligned} \tag{12}$$

In terms of these dimensionless variables, Eq. 9 becomes

$$\frac{\partial^2 T^*}{\partial x^{*2}} + \frac{Q_f L}{KA}\frac{\partial T^*}{\partial x^*} = -\frac{\alpha L^2}{KD}\left(1 - T^*\right) \tag{13}$$

or

$$\frac{\partial^2 T^*}{\partial x^{*2}} + P_1\frac{\partial T^*}{\partial x^*} = -P_2\left(1 - T^*\right) \tag{14}$$

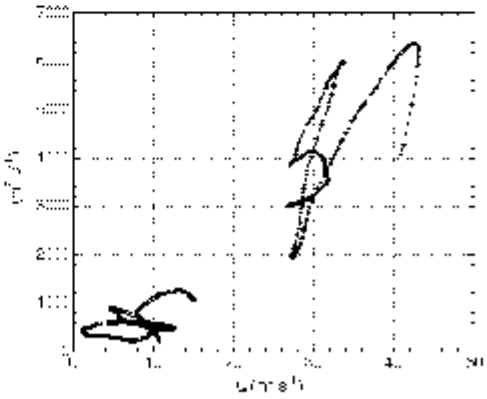

Fig. 12 Inferred dispersion coefficients as a function of flow for 2004 (*circle*) and 2005 (*plus*)

The parameter $P_1=Q_f L/KA$ reflects the relative importance of advection and dispersion; this term will be important when L is comparable to or larger than intrusion length KA/Q_f that plays a fundamental role in salinity intrusion when salinity variations are present (which is not the case in the DWSC). $P_2=\alpha L^2/KD$ reflects the relative importance of diffusion to heat exchange. In this case, heat transfer will be important when L is comparable to or larger than the diffusion scale $(KD/\alpha)^{1/2}$.

The solution to Eq. 14, given the imposed conditions, is easily found to be

$$T^* = 1 + A_+ \exp\left(\lambda_+ x^*\right) + A_- \exp\left(\lambda_- x^*\right) \tag{15}$$

where

$$\lambda_\pm = -\frac{P_1}{2} \pm \frac{\sqrt{P_1^2 + 4P_2}}{2}$$

$$A_+ = \frac{-1 + \exp(\lambda_-)}{\exp(\lambda_+)} \left(1 - \frac{\exp(\lambda_-)}{\exp(\lambda_+)}\right)^{-1}$$

$$A_- = -1 - A_+$$

As expected, the nature of the temperature field in the river depends on both advection and heat exchange, i.e., for systems like the San Joaquin River, on both water project operations (which determine flows in summer) and on weather. The solution given by Eq. 15 can easily be modified to choose $T^*(1)=\delta$, i.e., to specify an upstream temperature that is $T_0+\delta\Delta T$. For this case, A_- remains as given above (in terms of A_+) but A_+ becomes

$$A_+ = \frac{\delta - 1 + \exp(\lambda_-)}{\exp(\lambda_+) - \exp(\lambda_-)} \tag{16}$$

In Figs. 13 and 14, we have plotted sample solutions for different values of P_1 and P_2. The basic behavior that emerges is that for weak flows, the temperature approaches

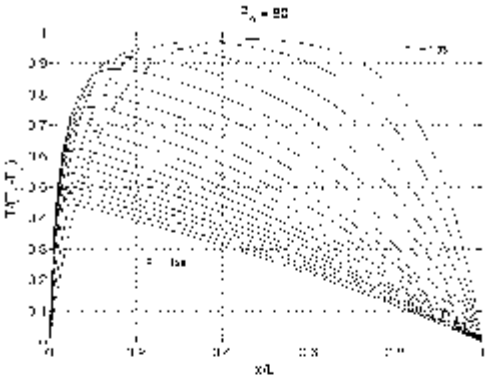

Fig. 14 Dimensionless temperature as computed by theory for $P_2=80$ and $1.33\le P_1\le 128$

the equilibrium temperature, whereas for strong flows, the temperature remains close to that of the boundaries, in all cases, because the maximum temperature is found in the interior of the domain, exactly as seen in the observations. This simple theory shows that as the flow rate drops, upstream diffusion of "coldness" from the downstream boundary becomes increasingly important. For the case with asymmetrical boundary conditions, as the flow (Fig. 15) increases, the maximum temperature in the interior rises as the flow carries heat from the upstream boundary further into the domain.

For the case of an asymmetrical temperature distributions, the effects of the upstream boundary condition seem to be stronger than the direct effects of flow (Fig. 16). However, the inflow temperature itself is also an effect of flow in that the water that enters the tidal portion of the system often comes from an upstream reservoir that is

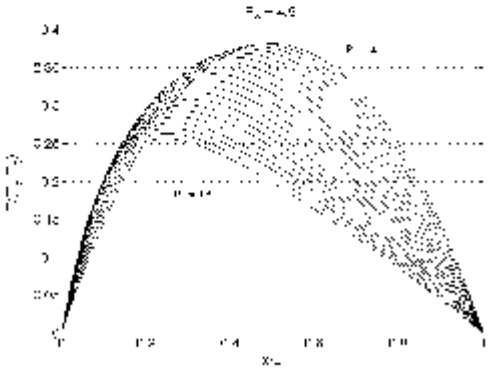

Fig. 13 Dimensionless temperature as computed by theory for $P_2=4.5$ and $0.1\le P_1\le 9.6$

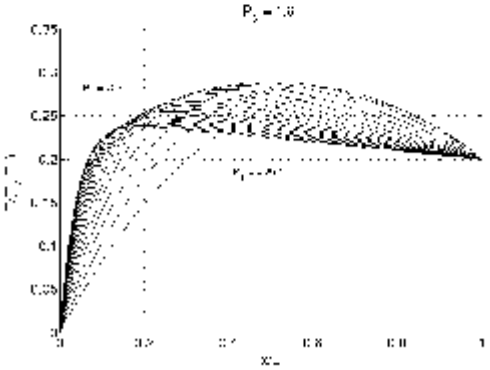

Fig. 15 The effects of flow for a case with asymmetrical boundary conditions: $\delta=0.2$, $P_2=1.6$, and $0.26\le P_1\le 25.6$

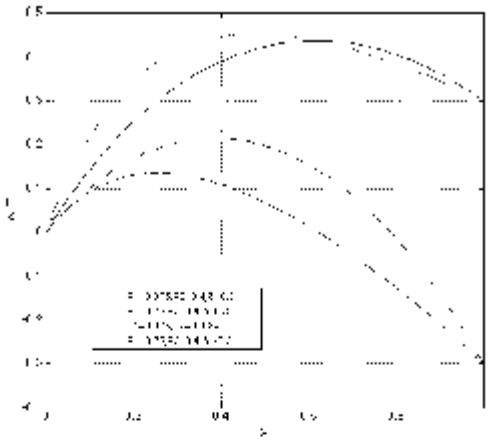

Fig. 16 Effect of upstream temperature condition and flow on temperature distributions

relatively cold; this should particularly be the case where selective withdrawal structure permits releases of cold hypolimnetic water (see e.g., Fischer et al. 1979). If we consider discharge from a reservoir, a distance L_{res} upstream of the tidal portion of the river at temperature T_{res}, and assume that dispersion is negligible in the river, then we find that the temperature rise coming from the reservoir to tidal river is

$$\Delta T_{res-riv} = (T_e - T_{res})\left(1 - \exp\left(\frac{-\alpha W L_{res}}{Q_f}\right)\right) \quad (17)$$

According to Eq. 17, the effect of increasing Q_f is most pronounced when Q_f is small. For example, for conditions typical of the San Joaquin, L_{res} (100 km), the change in temperature rise going from 5 to 20 $m^3 s^{-1}$ is three times as large as the change for the same flow increment in going from 20 to 35 $m^3 s^{-1}$. Likewise, the closer the reservoir is to the tidal river, the more closely the upstream temperature in the tidal river will reflect the reservoir release temperature.

Application of theory to observations

To apply this theory to the DWSC, it is necessary to estimate α, the heat transfer parameter. This can be done using the observations to compute T_e and then to use the observed surface heat transfer to compute α

$$\alpha = \frac{H_s}{\rho c_p (T_e - T_s)} \quad (18)$$

T_e itself is calculated iteratively by computing heat flux as a function of water surface temperature (using the algorithms discussed above) and then finding the temperature at which the heat flux is zero. Calculated values of T_e for 2004 are shown in Fig. 17.

Using the value of α calculated from the data along with mean values of K (=600 m^2/s) and Q (=7.6 m^3/s) also calculated from the data, we find that $(P_1, P_2, \delta) = (0.49, 1.53, 0.37)$. Using these parameters, the predicted and measured dimensionless temperature distribution for 2004 are shown in Fig. 18. This comparison is quite encouraging, with the simple model representing both the spatial scale of the temperature variation and some rise in temperature in the DWSC. Alternatively, since α and Q are known, the theory can be used to estimate K and δ via non-linear fitting of the data to theory. Doing so using a non-linear, least squares regression method-based Gauss–Newton iteration (see e.g., Seber and Wild 2003), we find that the best fit values are K=607 m^2/s giving and δ=0.44. These give (P_1,P_2)=(0.49,1.53); the resulting distribution is also shown in Fig. 18.

The simple theory does not work nearly as well for 2005. As shown in Fig. 19, there is a significant difference between observations and theory. Most notably, the theory fails completely at predicting the elevated temperature in the interior. This is arguably an effect of unsteadiness in temperature during the 2005 experiment, a period of substantial cooling for which T_e dropped by 3°C over 2 weeks. Indeed, the interior dimensionless temperature initially appears to rise during the initial cooling phase, an effect of the fact that ΔT dropped much faster than the temperature field could actually adjust and then relaxes back to the steady solution, although given that the

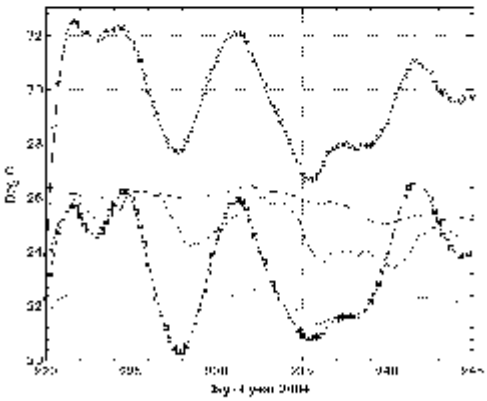

Fig. 17 Temperatures in San Joaquin DWSC in 2004: T_e (*circle*), T_s (*square*), and water temperatures at VER (*solid line*), M2 (*broken line*), and ANC (*dotted line*). All have been low pass filtered to remove diurnal variations

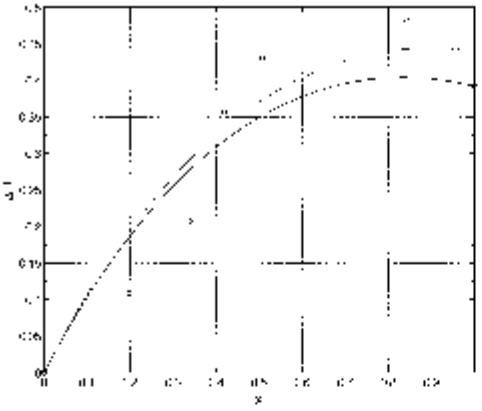

Fig. 18 Comparison of theory (*solid line*) with observations (*circle*) for 2004 conditions. Downstream boundary is set to PPT and upstream is set to MSD. Mean values from data are used for Q_f, K, and α. Observations are averages of temperatures between days 220 and 245. Theoretical curve based on best fit values of K and δ are also shown (*dotted line*)

adjustment time, which is O(LA/Q) (MacCready 1999), is approximately 30 days, this adjustment has not been completed by the end of the experiment. Thus, the 2005 data show that applicability of the simple theory is limited to times when the surface heat fluxes, or other forcing, are not rapidly changing, i.e., when $LA/Q \ll T_F$, where T_F is the timescale over which the forcing changes.

Discussion and Conclusions

Our observations and simple analytical model show that a balance of advection, dispersion, and surface forcing determines subtidal temperature variations in the DWSC, the tidal portion of the San Joaquin River. Notably, dispersion plays a significant role such that temperatures are elevated in the middle of the DWSC relative to both upstream riverine and downstream estuarine temperatures.

In examining the thermal energy balance for the DWSC, we used a very limited set of meteorological data, i.e., standard wind data (speed, direction, air temperature, and humidity) from one location and shortwave radiation data from another. This is likely appropriate for the domain that was the focus of our study. However, it may not be so for the larger issue of temperature prediction to meet temperature standards in the Delta. The reason is that the topography of the Delta leads to substantial variations in wind speeds along the length of the San Joaquin River and thus to variations in latent heat flux. In a like fashion, because of the diurnal movement of the marine cumulus layer (the fog)—significant variations in incident shortwave radiation, i.e., O(100 W m^2), might also be expected.

The thermal energy balance suggests a longitudinal dispersion coefficient, $K \approx 1{,}000$ m^2 s^{-1}, a value far in excess of what might be expected from existing descriptions of shear flow dispersion in rivers and estuaries, i.e., $K \approx 100$ m^2 s^{-1} or less (Fischer et al. 1979). Dispersion in the DWSC appears to result from a combination of how water parcels navigate the array of junctions and how flows in different connected channels are phased. In effect, this combination of processes may be considered to be a form of tidal pumping as described by Fischer et al. (1979), although given that multiple channels are involved also means that the dispersion may also have similarities to the chaotic dispersion model discussed by Ridderinkhof and Zimmerman (1992). Indeed, scale dependence should be expected since particle clouds that remain in a given channel only experience the kind of shear flow dispersion described by Eq. 7, whereas particle clouds that span a significant portion of the Delta effectively feel the dispersive effects of a number of channel junctions (Monsen 2001), leading (hypothetically) to the large dispersion coefficients we infer in this study.

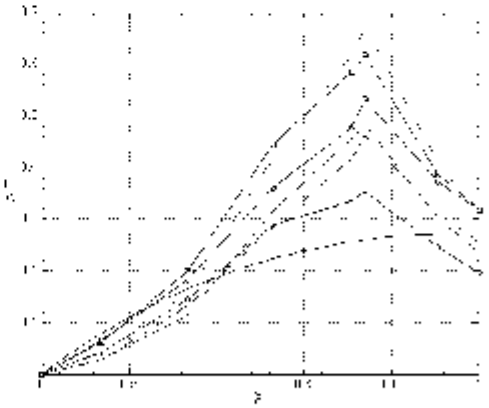

Fig. 19 Comparison of theory (*solid line*) with observations for 2005 conditions. For the theory, mean values from data are used for Q_f, K, and α. Longitudinal profiles at day 222.25 (broken wave tracings), day 224.75 (*dotted dashed line*), day 227.25 (*dotted line*), day 229.75 (*circle*), day 232.25 (*square*), and day 234.75 (*diamond*) have all been made dimensionless using values of T_e and T_0 appropriate to the time the profile represents. A single value is shown for the theory, since there was little variation in the dimensionless theoretical profile for this period

Acknowledgments The authors wish to thank the large group of students from Stanford and UC Davis as well as Jay Cuetara, John Yokimizo and their colleagues from the USGS California District, all of whom participated in the field work. This work was supported by CALFED Ecosystem Restoration Program contract ERP-02D-P51. SGM also is grateful for support from the Singapore Stanford Partnership.

Conflict of interest statement The authors have no financial relationship with the organization that sponsored the research. They also have no financial relationship with the publisher of *Estuaries and Coasts*. Finally, the authors have full control of all primary, data and they agree to allow the journal to review their data if requested.

References

Bennett, W.A. 2005. Critical assessment of the Delta Smelt population. *San Francisco Estuary and Watershed Science* 3(2), Article 1.

Bohrmans, M., and I.T. Webster. 1998. Dynamics of temperature stratification in lowland rivers. *ASCE Journal of Hydraulic Engineering* 12410: 1059–1063. doi:10.1061/(ASCE)0733-9429(1998)124:10(1059).

Cole, J.J., N.F. Caraco, and B.L. Peierls. 1992. Can phytoplankton maintain a positve carbon balance in a turbid, freshwater, tidal estuary? *Limnology and Oceanography* 37(8): 1608–1617.

DeGeorge, J.F. 1996. A multi-dimensional finite element transport model utilizing a characteristic-galetkin algorithm. Ph. D. Dissertation, University Of California, Davis.

Edinger, J.E., D.K. Brady, and J.C. Geyer. 1974. *Heat exchange and transport in the environment*. Electric Power Research Institute Report 14, 125 pp.

Fischer, H.B., E.J. List, R.C.Y. Koh, J. Imberger, and N.H. Brooks. 1979. *Mixing in Inland and coastal waters*. New York: Academic.

Fischer, H.B. 1976. Mixing and dispersion in estuaries. *Annual Review of Fluid Mechanics* 8: 107–133.

Jassby, A.D. 2005. Phytoplankton regulation in a eutrophic tidal river (San Joaquin River, California). *San Francisco Estuary and Watershed Science* 3(1), Article 3.

Jassby, A.D. and E.E. Van Nieuwenhuyse. 2005. Low dissolved oxygen in an estuarine channel (San Joaquin River, California): mechanisms and models based on long-term time series. *San Francisco Estuary and Watershed Science* 3(2), Article 2.

MacCready, P. 1999. Estuarine adjustment to changes in river flow and tidal mixing. *Journal of Physical Oceanography* 294: 708–726. doi:10.1175/1520-0485(1999)029<0708:EATCIR>2.0.CO;2.

Mohseni, O., and H.G. Stefan. 1999. Stream temperature/air temperature relationship: a physical interpretation. *Journal of Hydrology* 218: 128–141. doi:10.1016/S0022-1694(99)00034-7.

Monismith, S.G., W. Kimmerer, M.T. Stacey, and J.R. Burau. 2002. Structure and flow-induced variability of the subtidal salinity field in Northern San Francisco Bay. *Journal of Physical Oceanography* 32(11): 3003–3019.

Monsen, N.E. 2001. A study of sub-tidal transport in Suisun Bay and the Sacramento–San Joaquin Delta, California. PhD thesis. Stanford Univ.

Pawlowicz, R., B. Beardsley, S. Lentz, E. Dever, and A. Anis. 2001. Software simplifies air–sea data estimates. *EOS Transactions of the American Geophysics Union* 82: 2. doi:10.1029/01EO00004.

Ridderinkhof, H., and J.T.F. Zimmerman. 1992. Chaotic stirring in a tidal system. *Science* 258085: 1107–1109. doi:10.1126/science.258.5085.1107.

Romero, J.R., J.P. Antenucci, and J. Imberger. 2004. One- and three-dimensional biogeochemical simulations of two differing reservoirs. *Ecological Modeling* 174: 143–160. doi:10.1016/j.ecolmodel.2004.01.005.

Rueda, F.J., and S.G. Schladow. 2003. Dynamics of a large polymictic lake. II Numerical simulations. *Journal of Hydrologic Engineering* 1292: 92–101. doi:10.1061/(ASCE)0733-9429(2003)129:2(92).

Savenije, H.H.G. 2005. *Salinity and tides in alluvial estuaries*. Amsterdam: Elsevier.

Seber, G.A.F., and C.J. Wild. 2003. *Nonlinear regression*. New York: Wiley.

Tennekes, H., and J.L. Lumley. 1972. *A first course in turbulence*. Cambridge: MIT Press.

Uncles, R.J., and J.A. Stephens. 2001. The annual cycle of temperature in a temperate estuary and associated heat fluxes to the coastal zone. *Journal of Sea Research* 46: 143–159. doi:10.1016/S1385-1101(01)00078-8.

Appendix II

Estuaries and Coasts (2008) 31:1038–1051
DOI 10.1007/s12237-008-9093-0

An SF_6 Tracer Study of the Flow Dynamics in the Stockton Deep Water Ship Channel: Implications for Dissolved Oxygen Dynamics

Paul J. Schmieder · David T. Ho · Peter Schlosser · Jordan F. Clark · S. Geoffrey Schladow

Received: 23 February 2008 / Revised: 22 August 2008 / Accepted: 29 August 2008 / Published online: 23 September 2008

Abstract A sulfur hexafluoride (SF_6) tracer release experiment was conducted in the Stockton Deep Water Ship Channel (DWSC) to quantify mixing and transport rates. SF_6 was injected in the San Joaquin River upstream of the DWSC and mapped for 8 days. From the temporal change in SF_6 distributions, the longitudinal dispersion coefficient (K_x) was determined to be 32.7±3.6 $m^2 s^{-1}$ and the net velocity was 1.75±0.03 km day^{-1}. Based on the decrease in SF_6 inventory during the experiment, the pulsed residence time for waters in the DWSC was estimated at ~17 days. Within the DWSC from Stockton downstream to Turner Cut, dissolved oxygen concentrations maintained a steady state value of 4 mg l^{-1}. These values are below water quality objectives for the time of year. The low flow rates observed in the DWSC and the inability of oxygen-rich waters from downstream to mix into the DWSC upstream of Turner Cut contribute to the low dissolved oxygen concentration.

Keywords Dissolved oxygen · Sacramento–San Joaquin delta · Stockton deep water ship channel · SF_6 · Tracer · Mixing

P. J. Schmieder · D. T. Ho · P. Schlosser
Lamont-Doherty Earth Observatory, Columbia University,
61 Route 9W,
Palisades, NY 10964, USA

P. J. Schmieder (✉) · P. Schlosser
Department of Earth and Environmental Sciences,
Columbia University,
New York, NY 10027, USA
e-mail: schmied@ldeo.columbia.edu

D. T. Ho
Department of Oceanography, University of Hawaii,
Honolulu, HI 96822, USA

P. Schlosser
Department of Earth and Environmental Engineering,
Columbia University,
500 West 120th Street,
New York, NY 10027, USA

J. F. Clark
Department of Earth Science,
University of California at Santa Barbara,
Santa Barbara, CA 93106, USA

S. G. Schladow
Department of Civil and Environmental Engineering,
University of California at Davis,
Davis, CA 95616, USA

Introduction

The Stockton Deep Water Ship Channel (DWSC) is a segment of the lower San Joaquin River (SJR), located in the eastern portion of the Sacramento–San Joaquin River inland delta. The delta is comprised of a complex network of river channels and diversion canals. The natural river flows are altered by export pumping for industrial, agricultural, and drinking water demands. Waters from the SJR alone provide drinking water for 22 million California residents (Jassby and Van Nieuwenhuyse 2005). Flows are further altered within the delta by the use of temporary barriers and gates, which are used in part to protect endangered species and oppose the salt water intrusion upstream (Kimmerer 2002). For instance, a temporary barrier is installed at the junction of the SJR and Old River, ~22 km upstream from the DWSC, twice a year. The timing of the installation is associated with spring and fall salmon runs and helps keep the salmon within the SJR. The fall installation also helps maintain higher water flows through the DWSC by reducing flows towards pumps in

Old River. The higher flows aid in reducing the seasonal hypoxia that often develops this time of year.

Seasonal hypoxia is characteristic of many estuaries, including the DWSC portion of the SJR. The 11.5 km stretch of channel, from the confluence of the upstream SJR (USJR) with the DWSC in Stockton, CA, USA downstream to Turner Cut, routinely experiences low dissolved oxygen (DO) concentrations (Fig. 1). Although low DO concentrations can be observed for all months of the year, depressed values primarily occur between summer and fall (June to October). DO values typically range between 2–2.5 mg l^{-1} during this time period (Foe et al. 2002). Historically, the depressed DO values have existed within the DWSC since the 1960s (Bain and Pierce 1968; Lehman et al. 2004).

Low DO concentrations can have adverse impacts on aquatic life, including fish kills during times of severe hypoxia, fish egg and larvae mortality and growth rate reductions (Breitburg 2002). More directly, the SJR has traditionally served as a spawning ground for the endangered Chinook salmon. Low DO concentrations can prevent the upstream Fall migration of these fish which limits their ability to reach the spawning grounds (CRWQCB 2005). Consequently, the California Regional Water Quality Control Board (CRWQCB) has defined DO limits for the Sacramento–San Joaquin Delta. During the months of September through November, DO concentrations within the channel between the city of Stockton and downstream to Turner Cut must remain above 6 mg l^{-1}. During all other times of the year, DO concentrations must remain above 5 mg l^{-1} (CRWQCB 2005). Violations of these regulations frequently occur. Over the span of the past three decades, the frequency of observing DO concentrations below 5 mg l^{-1} has not decreased (Lehman et al. 2004).

Many factors can contribute to low DO concentrations in estuary systems, but a few have been identified as most important for the DWSC. First, both point source and nonpoint source nutrient loading upstream of the DWSC contribute to increased algae growth, which subsequently is a source of oxygen demand for the DWSC. A very significant point source for nutrient loading is the Stockton Regional Wastewater Control Facility, which supplies a direct source of dissolved ammonia to the SJR system (Lehman et al. 2004). In natural unpolluted river systems, ammonia concentrations range between 0.005 and 0.04 mg l^{-1} (Meybeck 1993). The average ammonia concentration in the effluent discharge from the wastewater facility was 12.5 and 13.6 mg l^{-1} for the years 2000 and 2001, respectively, and the average ammonia concentration within the DWSC during the summer months in the years 2000 and 2001 was 0.40 mg l^{-1} with a maximum observed value of 1.10 mg l^{-1} (Lehman et al. 2004). Nitrate and phosphate also contribute significantly to the nutrient loading and furthermore contribute to significant

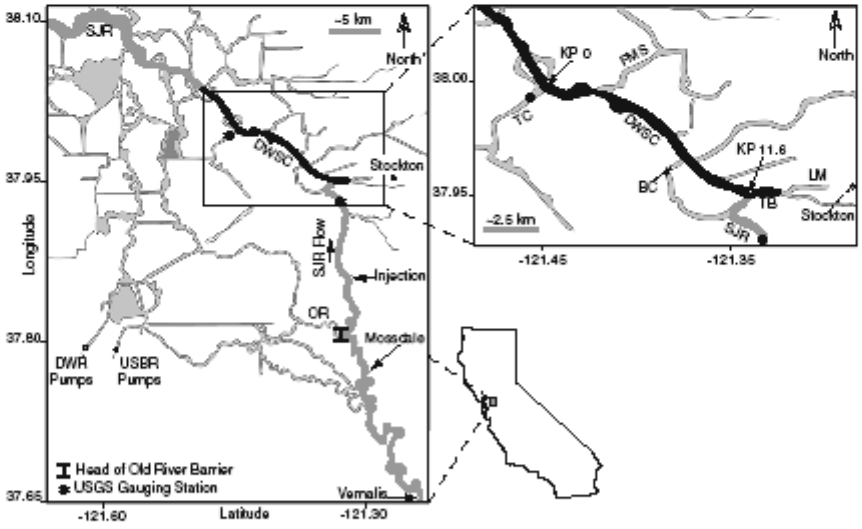

Fig. 1 Map depicting the study region within the Sacramento–San Joaquin Delta. The San Joaquin River (*SJR*) is shaded *dark gray*, the Deep Water Ship Channel (*DWSC*) portion of the SJR is highlighted in *black*, and the surrounding delta channels are shaded *light gray*. The locations along the DWSC are defined as the distance away from Turner Cut, with distance increasing upstream. The confluence of the DWSC with the upstream SJR is 11.6 km upstream of Turner Cut. *BC* Burns Cutoff at Rough and Ready Island, *DWR Pumps* Department of Water Resources pumping station, *FMS* Fourteen Mile Slough, *KP* kilometer point, *LM* Lake McLeod, *OR* Old River, *SJR* San Joaquin River, *TB* turning basin, *TC* Turner Cut, *USBR Pumps* United States Bureau of Reclamation pumping station

algae growth (Diaz 2001). In natural river systems, nitrate concentrations range from 0.05 to 0.2 mg l^{-1}, while phosphate concentrations range from 0.002 to 0.025 mg l^{-1} (Meybeck 1993). Nitrate concentrations in the SJR at Vernalis have ranged from 2.3 to 23.6 mg l^{-1} during the summer of 2001, and phosphate concentrations ranged from 0.063 to 0.104 mg l^{-1} during the same time period (Foe et al. 2002). For the years of 2000 and 2001, nitrification was identified as the largest contributor to oxygen demand (Lehman et al. 2004).

The second factor contributing to the low DO concentrations is the geometry of the DWSC. The DWSC is a dredged portion of the SJR, downstream of the city of Stockton. The increase in water depth moving from the USJR into the DWSC strengthens the influence of the biochemical oxygen demand (BOD) exerted on the system. The greater depth increases the time required to aerate the water column via gas exchange and increases the fraction of the water column removed from the photic zone, thereby increasing the portion of the water column that experiences net respiration. Finally, reduced net flows down the SJR during periods of the year increase the residence time of waters in the DWSC which consequently strengthens the influence of the BOD exerted on the system (CRWQCB 2005). Modeling results conducted for periods when the barrier at the head of Old River is in place and when there is no export pumping down Old River for agricultural and drinking water usage also suggest that substantial reductions in DO depletion can occur by maintaining flow down the SJR (Fig. 1; Jassby and Van Nieuwenhuyse 2005).

The goal of this study was to investigate the mixing dynamics in the DWSC portion of the SJR through the use of an sulfur hexafluoride (SF_6) tracer release experiment. This method allows the quantification of mixing and residence times (e.g., Clark et al. 1996; Ho et al. 2002), as well as the examination of the connectivity of the different hydrological components in the DWSC system by determining the net velocity, the dispersion coefficient, and gas exchange rates from changes in tracer distribution and concentrations with time. Knowledge of the connectivity, transport, and mixing rates will enhance our understanding of the development and persistence of the low DO zone within the DWSC.

Study Location

The SJR, at 530 km long, is the second largest river in California and drains an area of 19,153 km^2. Its headwaters are in the Sierra Nevada Mountain Range, and the river passes through the dense agricultural region of the San Joaquin Valley. It ultimately flows west and combines with the Sacramento River to form the Sacramento–San Joaquin Delta (Kratzer et al. 2004), which drains into San Francisco Bay.

The DWSC (Fig. 1) is located 125 km due east of the Golden Gate Bridge, which is located at the entrance to San Francisco Bay. Dredging of the DWSC to a depth of 9.25 m commenced in the 1930s, and between 1984 and 1987, the channel was deepened to 10.75 m (Bowersox 2002). The SJR is tidally influenced up to Vernalis, CA, located 48 km upstream of the confluence between the USJR and the DWSC at the Port of Stockton. Upstream of the confluence in Stockton, the mean width of the SJR is 60 m and the mean depth is ~3.3 m with a tidal range of 1.2 m. The DWSC downstream of Stockton has tidal flows that range between 55 and 115 $m^3 s^{-1}$ and a tidal range of 1 m. The mean annual rainfall recorded in Stockton for the past 49 years is 354 mm per year, of which 89% falls between November and April. The mean SJR discharge recorded at Vernalis peaks at 236 $m^3 s^{-1}$ at the beginning of June and rapidly decreases to a minimum of 40 $m^3 s^{-1}$ during the month of August. Typically, flows slowly increase from August to December but remain below 75 $m^3 s^{-1}$ during this period.

Materials and Methods

Past studies have successfully utilized SF_6 as a tracer in both river and estuarine environments (e.g., Clark et al. 1996; Ho et al. 2002, 2006b; Caplow et al. 2003, 2004a, b). SF_6 is primarily of anthropogenic origin, and its atmospheric mixing ratio has been increasing since the 1950s (Maiss and Brenninkmeijer 1998). The primary use of SF_6 is in high voltage switching gears as an electrical insulator. For tracer studies, SF_6 is considered conservative when losses due to air–water gas exchange are accounted for in mass inventories. This loss can be quantified directly by injecting a second volatile tracer (e.g., ^3He; Clark et al. 1994, 1996) or indirectly by using wind speed-based gas exchange parameterizations. SF_6 also works well as a tracer for long-term (days to weeks) and large spatial scale (tens of kilometers) studies, whereas dyes like fluorescein are better suited for smaller time and length scales (Ho et al. 2006b).

For 9 days starting on August 14, 2005 (day 0), an SF_6 tracer release experiment was conducted within the USJR and the DWSC portion of the SJR. On day 0, approximately 1.6 mol of SF_6 were injected into the USJR over a period of 10 min at a mean depth of 3.3 m, while the boat traversed the width of the river channel. The injection was located 13 km upstream of the confluence between the USJR and the DWSC and occurred at slack before ebb tide (SBE). Based on the decay of the total SF_6 mass inventory between days 2 and 8, $\sim 6.5 \times 10^{-2}$ mol of SF_6 (~4% of the amount released) actually dissolved during tracer injection. This value is significantly lower than those achieved in previous experiments (e.g., Ho et al. 2002; Caplow et al.

2003) and is most likely due to the shallower depth of the tracer injection. As the gas was injected at shallower depths, the bubbles have less time to equilibrate with the surrounding water, and the decreased hydrostatic pressure reduces the equilibrium concentration.

SF_6 samples were analyzed using an automated, high-resolution, measurement system that continuously measured the SF_6 concentration in the water at approximately 1-min intervals (Ho et al. 2002; Caplow et al. 2004a). This system included a membrane contactor (Liqui-Cel) to extract gases from the water sample, dual analytical columns to separate SF_6 from other gases, and a gas chromatograph with an electron capture detector to measure SF_6. For this experiment, modifications were made to the original system to use a peristaltic pump in place of the submersible pump for water sampling.

While sampling, the gas stripping efficiency of the membrane contactor decreased due to particles (<40 μm) clogging the contactor pores, and water flow rates varied since the flow is controlled manually. Final data calibrations account for the variability of these parameters, and SF_6 concentrations are expressed in femtomoles (10^{-15}) per liter of water (fmol l^{-1}).

Following the tracer release (days 1–8), two longitudinal surveys were conducted each day in the DWSC and the USJR to define the vertical and horizontal distribution of the tracer patch. Locations along the channel are defined as the distance from Turner Cut in kilometers, with positive kilometer point (KP) values being located upstream of Turner Cut. Surveys commenced and ended when background SF_6 concentrations were observed. At the time of the study, the predicted background SF_6 concentration was 1.5 fmol l^{-1} based on a northern hemisphere background atmospheric ratio of 5.9 parts per trillion (NOAA/CMDL 2007) and solubility equilibrium for the conditions in the DWSC. The average conditions observed during the survey include a water temperature of 24.7°C and a salinity of 0.263, where salinity values have no units as defined by the use of the Practical Salinity Scale (Lewis 1980). For solubility calculations, the low salinity value is negligible. Background concentration values were determined from surveys conducted outside of the tracer patch. The mean background concentration was 4.8 fmol l^{-1}, a value approximately three times greater than that calculated from northern hemisphere background values. This result is not surprising, as previous studies have observed elevated atmospheric SF_6 mixing ratios near urban areas (Ho and Schlosser 2000). The SF_6 concentrations in the tracer patch were typically two–three orders of magnitude greater than background values and masked any elevated background signature.

Past experiments utilizing SF_6 as a tracer in tidally influenced rivers have performed a tidal correction on the locations of the SF_6 measurements in order to yield a synoptic distribution of the data (Clark et al. 1996; Ho et al. 2002, 2006b). As the DWSC is closed at the far eastern end of the turning basin (TB) at Lake McLeod, a standing wave persists within the study region, and the traditional correction following Ho et al. (2002) cannot be applied (Bowersox 2002). The standing wave is a result of a reflection of the tidal wave that progresses upstream at the end of the channel at Lake McLeod. The longitudinal transects for depicting the evolution of the tracer for this study are plotted at the time of sample collection rather than the time of slack before ebb tide (Figs. 2 and 3).

During the replicate surveys on days 5, 6, and 8, a conductivity–temperature–depth (CTD) sonde (Sea-Bird SBE 19*plus* SEACAT Profiler) was lowered every 1 to 2 km to establish the temperature, salinity, and DO concentration gradients with depth. On days 3, 5, 6 and 8, in order to define the vertical SF_6 concentration gradients, water samples from depth were pumped through the continuous system and analyzed aboard the boat. Discrete samples from depth were also collected, stored in evacuated glass containers (Vacutainers) and later analyzed in the laboratory at The University of California, Santa Barbara following the experiment using the procedure outlined by Clark et al. (2004). A total of three stations were sampled on these transects and samples were collected from three to five depths at each station. The calibrations for the continuous SF_6 measurements and the Vacutainers are different, and the values are not directly comparable. The vertical SF_6 profile data presented within depicts the ratio of surface to bottom concentrations and not the absolute concentration. The use of the ratio allows for a relative comparison between data collected in Vacutainers and the data collected via the continuous system.

SF_6 mass inventories for each day were calculated from measured SF_6 concentrations and channel volume. The SF_6 mass inventory for days following the tracer injection was conducted to determine the mass of SF_6 dissolved into the system upon injection and to determine the e-folding loss rate for tracer within the system. Volumes for the portions of the DWSC sampled during the study were determined using electronic NOAA navigational chart 18663 in ArcGIS. Depth measurements provided in the charts are sparse, and caution was used when interpolating depth measurement. As the volumes of side channels and embayments are much less than the volume of the main channel, they are excluded from the inventory calculations. Also, the measured vertical and horizontal SF_6 gradients were generally small, so the concentration in the center of the channel was applied in all directions.

Since SF_6 is a gas, air–water gas exchange must be included in the mass balance, utilizing the parameterization of gas exchange based on wind speed from (Ho et al. 2006a):

$$k_{600} = (0.266 \pm 0.019)u_{10}^2 \quad (1)$$

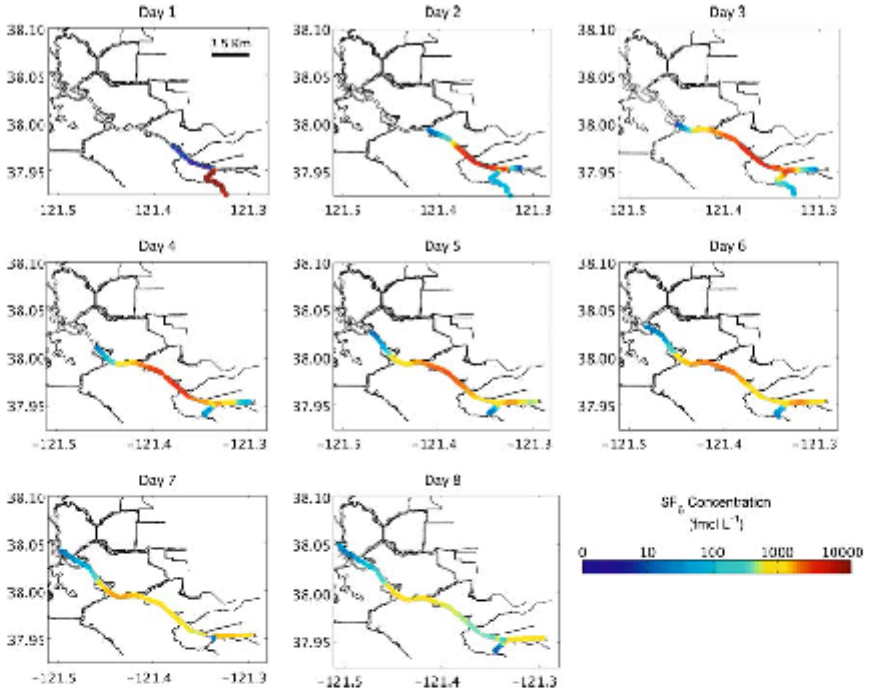

Fig. 2 Temporal evolution of the SF_6 tracer patch from the SJR through the DWSC for eight consecutive daily surveys following the tracer release in the upstream SJR. SF_6 concentrations are in units of fmol l^{-1}

where k_{600} (cm h^{-1}) is the gas transfer velocity normalized to a Schmidt number, Sc, of 600, corresponding to CO_2 in freshwater at 20°C, a common reference condition (Sc = the kinematic viscosity of water divided by the molecular diffusivity of the gas in water). u_{10} is the wind speed at 10 m height, and measurements were obtained from the National Weather Service Station located at the Stockton Municipal Airport, where the mean hourly u_{10} wind speed was 3.6 m s^{-1} during the course of the study. Hourly u_{10} values were applied to the wind speed parameterization and a daily average k_{600} was determined. Because the wind speed parameterization is nonlinear, an enhancement correction $\left(\varepsilon = \overline{u_{10}^2}/\overline{u_{10}}^2\right)$ was made following the methods of Wanninkhof et al. (2004) and Ho et al. (2006a).

Results

Sulfur Hexafluoride

For 8 days following the tracer release, longitudinal transects were carried out in the DWSC and the USJR to define the evolution of the tracer. On day 1, the peak tracer concentration was located 11.5 km downstream of the tracer injection line and 1.5 km upstream of the confluence between the DWSC and the USJR. Small quantities of tracer entered the DWSC, and the maximum SF_6 concentration detected on day 1 was 103,230 fmol l^{-1}. The distribution of SF_6 concentrations was highly skewed upstream of the peak location, and tracer concentrations decreased rapidly to background values within 2 km downstream of the peak location (Fig. 2).

The transect performed on day 2 revealed that only small quantities of tracer remained within the USJR and that the majority of tracer mass had entered the TB and was being advected and dispersed downstream in the DWSC. At this time, the tracer patch had spread to a width of 8 km and was defined by multiple peaks in tracer concentration (Fig. 3). A peak concentration of 9,465 fmol l^{-1} was observed on day 2. By day 3, the longitudinal tracer profile had grown to a width of 15 km, and the peak tracer concentration had decreased by roughly one half to 5,002 fmol l^{-1}. By the last day of surveys, day 8, the tracer was detectable for nearly 23 km, stretching from the eastern end of the TB downstream past Turner Cut and the peak concentration had decreased to 1,132 fmol l^{-1}.

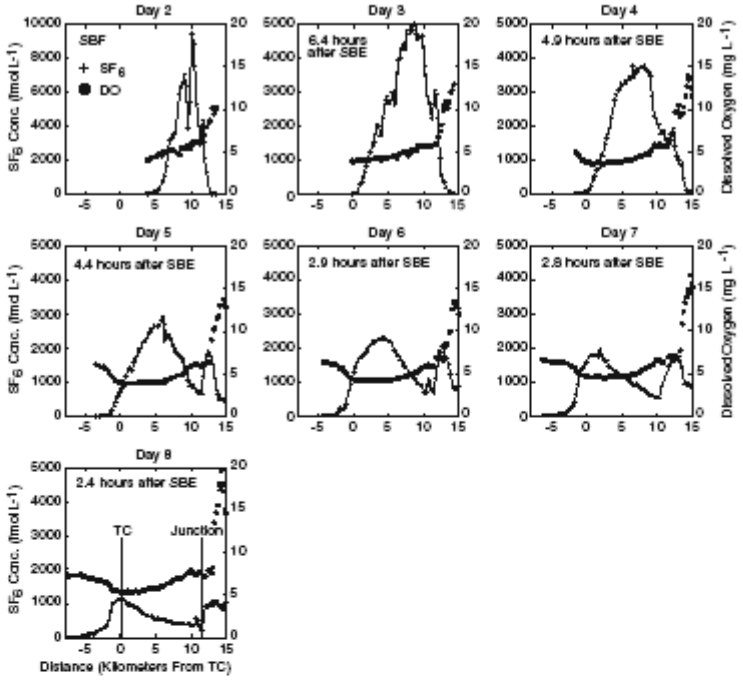

Fig. 3 Temporal evolution of the longitudinal SF_6 and dissolved oxygen profiles in the DWSC and the turning basin for days 2–8 following the tracer injection. Locations upstream of the kilometer point 11.6 define the section of the channel leading to the TB and Lake McLeod, and Turner Cut is located at kilometer point 0. Note that the concentration scale changes following day 2. *SBF* slack before flood tide, *SBE* slack before ebb tide

During the course of the repeated surveys, two distinct regions of high SF_6 concentrations emerged. These two regions were separated at KP 11.6, which corresponds to the confluence between the DWSC and the USJR. The evolution of these water masses was noted from very early on in the surveys (day 2) and was very distinct by day 5. The tracer peak along the DWSC stretch downstream of the confluence decayed more rapidly than the peak located within the TB, with SF_6 concentrations decreasing from 9,465 fmol l^{-1} on day 2 to 1,132 fmol l^{-1} on day 8. For days 4 through 7, peak concentrations in the TB remained relatively stable near 2,000 fmol l^{-1}. By day 8, the SF_6 concentrations were homogeneous in the TB with a concentration of ~1,000 fmol l^{-1}.

Starting on day 5, when tracer tagged waters reached the confluence between Turner Cut and the DWSC (KP 0), tracer concentrations decreased rapidly. The furthest extent of tracer migration downstream of Turner Cut was 6 km on day 8. During this same time period, the portion of the SF_6 profile between the peak location and the TB developed a very linear concentration gradient, thus skewing the profiles upstream. The minimum SF_6 concentration at the confluence of the DWSC, USJR and the TB was relatively constant between days 5 and 8 at 700 fmol l^{-1}.

Dissolved Oxygen

Along the length of the surveyed channel, the surface water (~1 m in depth) DO concentrations were variable in space but temporally stable (Fig. 3). Upstream of the confluence between the DWSC and the USJR in the TB, DO concentrations in the upper ~8 m of the water column remained above solubility equilibrium with the atmosphere for the duration of the study and reached values as high as 216% of solubility equilibrium (19.7 mg l^{-1}) on day 8. The values at a depth of ~10 m ranged from 5.0–5.5 mg l^{-1} within the TB. The elevated oxygen values were attributed to the presence of visible algae blooms near the surface of the water. Downstream in the DWSC, surface DO concentrations repeatedly decreased from 6 to ~4 mg l^{-1} over a distance of approximately 4 km. Relatively constant surface DO concentrations of 4 mg l^{-1} were observed for 7 km from KP 7 to KP 0. The lowest DO concentration of 3.6 mg l^{-1} was observed on day 4 at KP 0.9. Concentrations increased downstream of KP 0, where surface DO values increased up to 6.5 mg l^{-1}. The rise in DO values in this portion of the channel occurred over a shorter distance than the DO decrease that occurred upstream.

CTD profiles revealed that there exists little vertical stratification in DO except in the TB region where the

highest DO concentrations were observed (Fig. 4). The DO signature of ~7 mg l^{-1} from USJR water is clearly noted at depths below 6 m at KP 11.6 in the DWSC. The lowest surface DO concentrations were observed around Turner Cut and concentrations increased linearly moving downstream from KP −2 to end of the CTD profiles (KP −8).

Salinity

The salinity of the SJR has doubled during the past 60 years. The change in salinity is primarily attributed to upstream reservoir development, the use of higher salinity water for agriculture, and drainage from preexisting saline soils (CRWQCB 2004). Based on CTD profiles within the TB and the DWSC, the salinity structure from KP 13.2 downstream to KP −2.1 was fairly homogeneous with values ranging between 0.25 and 0.30 and averaging 0.28 (Fig. 4).

The USJR water imparted a characteristic salinity signal of 0.27 just downstream of KP 11.6. Upstream of this location in the TB, there was a slight increase in salinity that most likely developed from evaporation. Downstream in the DWSC, salinity concentrations were generally vertically homogeneous and tended to increase with distance downstream to Turner Cut. An exception to this trend occurred at KP 2.4. This location corresponds to the junction with Fourteen Mile Slough. The slight freshening documented at KP 2.4 could be attributed to this tributary, but no corresponding distinct signature was noticed in the

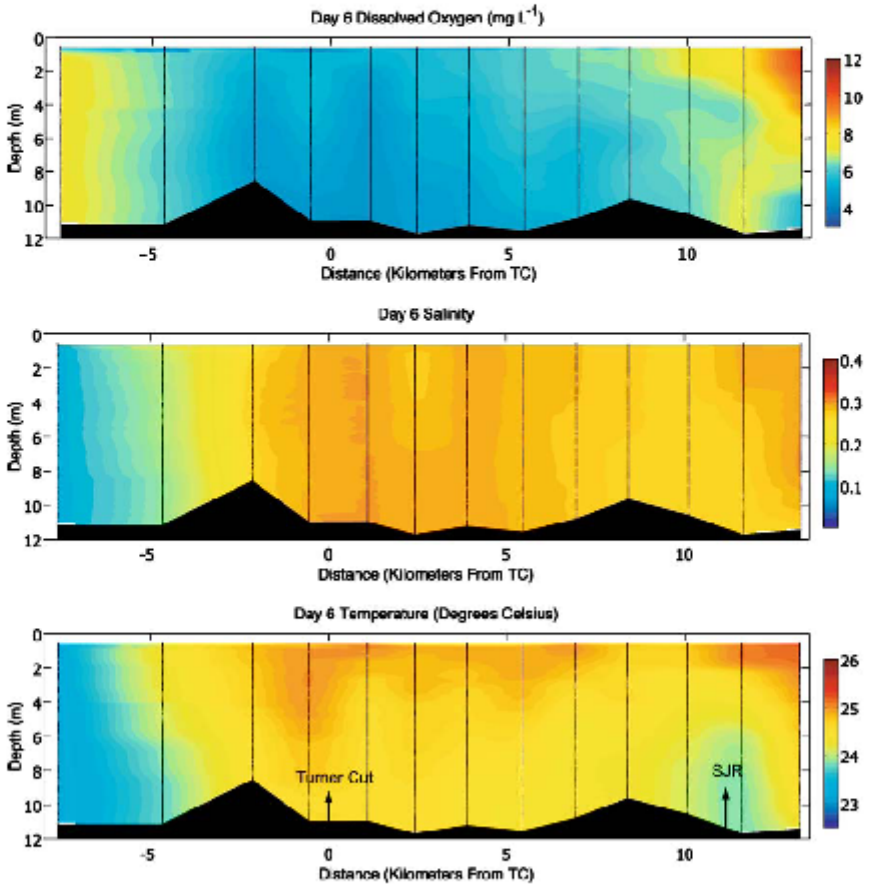

Fig. 4 Dissolved oxygen concentrations, salinity, and temperature measurements from CTD casts on day 6 of the longitudinal surveys. The survey commenced in the TB and progressed downstream to kilometer point −7.5. The last CTD cast in the survey was conducted 30 min following slack before flood tide. The profiles conducted on this day of survey are representative of the study period

DO and temperature profiles. Downstream of Turner Cut, waters freshened to 0.15 by KP −2.7, and continued to freshen to 0.1 by KP −7.6. The freshening downstream was associated with Sacramento River waters mixing upstream into the DWSC. In the vicinity of TC, significant mixing of Sacramento River waters and SJR waters has been documented (Brown 2002). Slight increases in surface salinity are most likely due to evaporation.

Temperature

Each water mass that composes the DWSC system displayed a characteristic signal in the temperature profile (Fig. 4). Slight thermal stratification was documented in the TB (KP 13.2) where surface water temperatures were 25.7°C and decreased to 24.1°C near the channel bed. The USJR waters that flowed into the DWSC at KP 11.6 displayed a distinct temperature signal of 23.5°C from the channel bed up to 4 m depth. At this location, temperatures rose quickly up to 24.5°C for waters shallower than 4 m. The cool water signal of the USJR had diminished by the time waters were advected to KP 4.5 downstream. Thermal stratification was slight but evident down to KP −2.1. It was here that the cooler signature of the Sacramento River water (23.3°C) was imprinted onto the system.

Discussion

San Joaquin River

The hydrology of the DWSC and SJR system is highly dynamic. The system is best described by separating it into three components: (1) the USJR waters, (2) the TB, and (3) the DWSC section of the SJR down to Turner Cut. In the USJR, net velocities are greater in comparison to those in the DWSC due to a smaller cross-sectional area and, hence, faster net velocity for a given volumetric flow rate (Q). Although advection should rapidly flush the USJR of all tracer tagged waters, tidal movement allows for exchange between the USJR and the DWSC sections. Each consecutive survey documented tracer tagged water within the USJR up to 2.2 km from the confluence. Provided that the peak concentration migrated 11.5 km from the injection line between the time of injection and the time of the first survey, the net velocity for the sampled portion of the USJR during the time of study was 13.2 km day^{-1}.

Turning Basin

From the longitudinal SF_6 profiles in the DWSC and the TB beginning on day 2, two peaks emerged on the upstream edge of the profile and persisted throughout the study. The peak furthest upstream corresponded to waters located within the TB. The existence of this peak was most likely derived by the tidal trapping mechanism characterized by Fisher et al. (1979). First, as water is advected out of the USJR, some tracer tagged waters may be entrained into the TB, while the majority flows downstream in the DWSC. As waters flow upstream during flood tide, tracer tagged water will enter both the TB and the USJR from the DWSC. Upon ebb tide, tracer-free water from the USJR separates the TB water from DWSC and two peaks are formed. It is possible that tidal waves in the DWSC and USJR are out of phase with the tidal wave in the TB embayment. Provided this is true, then the migration of tracer tagged waters from the TB will be separated from the bulk of the tracer mass since the currents within the TB and those in the DWSC will be out of phase.

Net velocity within the TB was very small, and dispersivity due to tidal motion determined the evolution of the tracer concentrations in the TB. By day 8, this tidal movement uniformly mixed the SF_6 in the surface waters of the TB. Surveys on this day revealed that surface tracer concentrations were nearly homogenous from the confluence with the SJR up to Lake McLeod, which suggests that mixing processes acted on shorter timescales than the processes that created heterogeneity within the water mass. Within the TB though, the water column never fully mixes, and surface concentrations remain greater than at depth (Fig. 5).

The TB also influenced tracer concentrations downstream of KP 11.6. As the effluent from the USJR entered the DWSC, water from the TB was entrained and served as a continuous source of SF_6 to the downstream system. This concept was supported by the fact that for days 6–8 (Fig. 3), there appeared to be mixing between two end members: mixing between the peak concentration in the DWSC and waters entering from the TB. The upstream limb of the SF_6 tracer profile had a linear rather than the expected Gaussian shape, consistent with rapid mixing of waters from two end members. As the peak tracer concentrations within the TB decreased more slowly than the peak downstream, the e-folding flushing time for waters in the TB appears to be longer than that for the downstream system.

Deep Water Ship Channel

From days 2–8, the tracer mass advected in the DWSC in a fashion similar to that of standard tidal river systems. The net velocity of 1.75± 0.03 km day^{-1} was determined by plotting the location of the peak tracer concentration against the time since tracer injection and fitting a linear least-squares regression (R^2=0.98; Fig. 6). A flushing time of ~7 days was then determined for the section of the channel from KP 11.6 downstream to KP 0 simply by length of the channel/net velocity. This is a first order analysis of the hydraulic

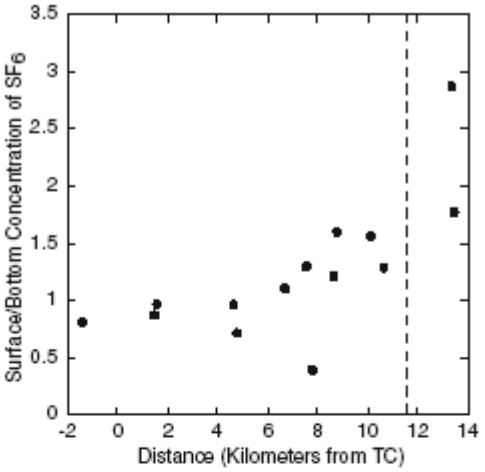

Fig. 5 Ratios of surface to bottom SF_6 concentration compiled from all of the vertical concentration profiles. For locations upstream of KP 8, waters are not vertically well mixed with respect to SF_6 concentrations

timescales in the channel and assumes a constant cross-sectional area. Also, given an average cross-sectional area of 1,500 m^2 for the DWSC between KP 11.6 and KP 0, the net volumetric flow rate was about 30.4 $m^3\ s^{-1}$ through this section of the channel. The mean measured flow exiting the USJR for the duration of the study was 34.1 $m^3\ s^{-1}$ (US Geological Survey (USGS) gauging station 11304810, below Garwood Bridge), which is in good agreement with the flow determined from the SF_6 tracer release experiment.

Below KP 0, tracer concentrations eroded rapidly as a result of mixing with SF_6-free Sacramento River waters from downstream, as well as loss of DWSC water into Turner Cut. Mixing with Sacramento River water has been documented at this location as well as the diversions down Turner Cut (Brown 2002). In this study, losses down Turner Cut are simply deduced from USGS gauging measurements, as sampling did not occur in the Turner Cut channel. Mean flows out of the DWSC into Turner Cut were 50.9 $m^3\ s^{-1}$ during this study (USGS gauging station 11311300, Turner Cut Near Holt, CA). The increase in mean flow into Turner Cut above the measured SJR flow of 34.1 $m^3\ s^{-1}$ is attributed to contributions from the Sacramento River downstream.

Dispersion Coefficient

To assess the dispersion in the system, we first use a simple one-dimensional (1-D) estimation. We assume that the transverse and the vertical are well mixed with regard to the SF_6 tracer. The advection and the dispersion coefficient can be described by the 1-D advection diffusion equation (Fischer et al. 1979; Rutherford 1994):

$$\frac{\partial c}{\partial t} + u\frac{\partial c}{\partial x} = K_x\frac{\partial^2 c}{\partial x^2} - \lambda c \tag{2}$$

where c is averaged cross-sectional concentration, t is time, u is the net downstream velocity, x is distance along the length of the channel, K_x is the dispersion coefficient, and λ is the first order loss rate for processes such as gas exchange.

In order to calculate the dispersion coefficient, we apply the change in moment method that tracks changes in the variance of a Gaussian curve fitted through the data, using the following equation (Fischer et al. 1979; Rutherford 1994):

$$K_x = \frac{1}{2}\left(\frac{d\sigma_x^2}{dt}\right) \approx \frac{1}{2}\frac{\sigma_x^2(t_2) - \sigma_x^2(t_1)}{t_2 - t_1} \tag{3}$$

where $\sigma_x^2(t_1)$ and $\sigma_x^2(t_2)$ are the variance of the Gaussian curve fit for times 1 and 2, respectively. The times that are used in the calculation correspond to the time that the peak SF_6 concentration was encountered during the daily surveys (Fig. 7). Only days 2–6 were used to determine the dispersion coefficient because the errors of the Gaussian fits were too large for days 7 and 8. For these days, the longitudinal SF_6 concentration profiles were highly skewed toward the upstream portion of the profile and were no longer Gaussian in shape. For the stretch of the DWSC from KP 11.6 to KP 0, the longitudinal dispersion coefficient was determined to be 32.7±3.6 $m^2\ s^{-1}$, with an R^2 value for the fit of 0.89 (Fig. 8).

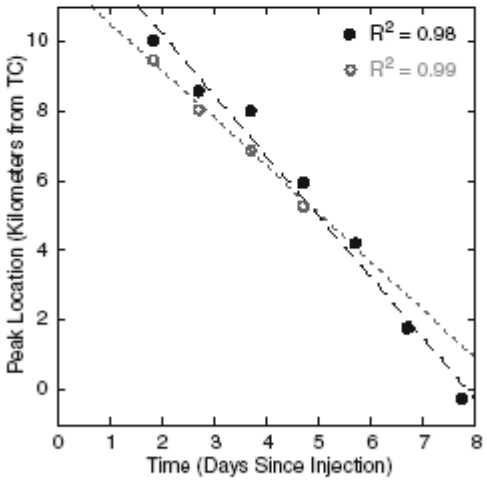

Fig. 6 Net velocity of the SF_6 tagged water in the Stockton Deep Water Channel. The *full dots* represent the location of the measured SF_6 maxima, and the *open circles* depict the location of the maxima of the fitted Gaussian distributions (Fig. 7). The net velocity of 1.75 km day^{-1} is derived from location of the measured maxima

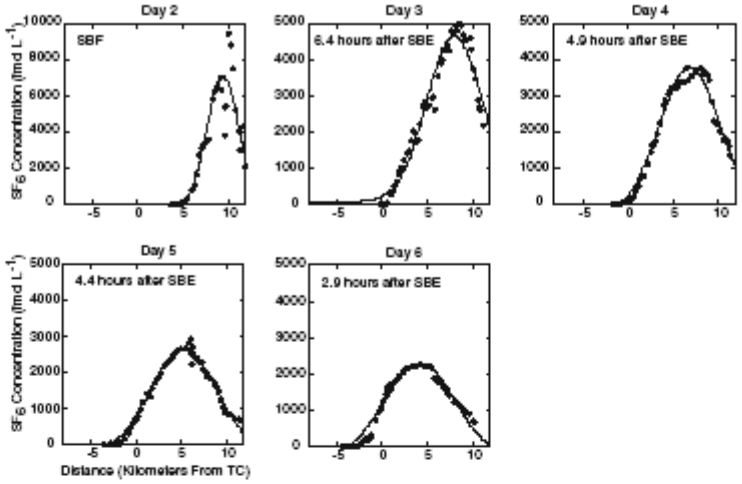

Fig. 7 Gaussian distributions fitted to the observed longitudinal SF_6 concentration profiles used to determine the dispersion within the DWSC for days 2–6

Downstream of this point, tracer tagged waters are diluted due to mixing with Sacramento River water and are removed from the DWSC via Turner Cut. Due to the complex nature of this process dispersion coefficients for this portion of the channel cannot be calculated using this method.

To better understand the relative importance of advection versus dispersion in the system, an estimate for the time scale of each process is computed. For advection within the DWSC down to Turner Cut, the time scale is defined as length/net velocity and yields an advective time scale of ~7 days. The dispersive time scale can be estimated by length$^2/K_x$, and yields a timescale of ~48 days. Therefore, net advection should dominate as the removal mechanism for this stretch of the channel under the observed flow conditions.

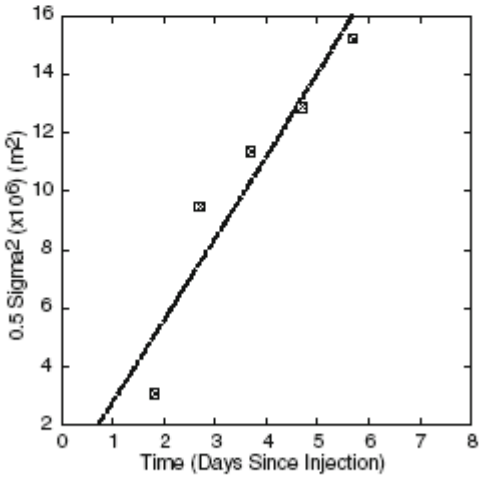

Fig. 8 Values of $1/2\sigma^2$ used for the calculation of the dispersion coefficient plotted versus the time when the peak concentration was reached in the longitudinal surveys. The slope of the linear regression defines K_x=32.7 m^2 s^{-1} (R^2=0.89)

SF_6 Mass Inventory

The SF_6 mass inventory was utilized to determine the pulse residence time (PRT) for waters within the DWSC and the TB (Miller and McPherson 1991; Sheldon and Alber 2002). This method is used to describe the time required to remove a portion of dissolved substance given that it was introduced to the system and one location as a pulse. Here, we present an e-folding PRT for waters in the DWSC, thus describing the time required to remove 63% of the tracer mass. The PRT is explicitly determined as 1/loss rate. The SF_6 mass inventory followed an exponential decay and yielded a first order loss rate (λ) of 0.14 day^{-1} (R^2=0.86) for combined flushing from the DWSC due to all loses such as advection, dispersion, and gas exchange (Fig. 9). This translated into a PRT of 7.1 days for the combined losses due to flushing from the system and gas exchange.

The decay in SF_6 mass as predicted by gas exchange alone was also exponential. Application of the above gas exchange parameterization (Eq. 1) yielded a first order loss rate due to gas exchange (λ_{GasEx}=re-aeration coefficient) alone of 0.08 day^{-1} (R^2=0.99). Therefore, the first order loss rate of tracer due to flushing or dilution out of the system was calculated as follows:

$$\lambda_{Flushing} = \lambda - \lambda_{GasEx} \quad (4)$$

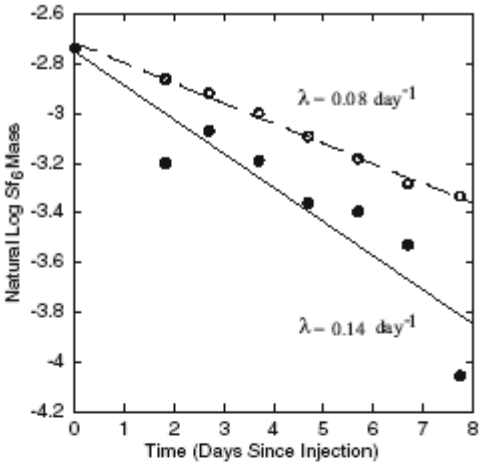

Fig. 9 SF_6 mass inventories based on loss due to predicted gas exchange alone (*open grey circles*) and the measured SF_6 concentrations (*closed black circles*). The measured SF_6 concentrations account for combined losses due to gas exchange and removal from the DWSC system via flushing

where $\lambda_{Flushing}$=0.06 day^{-1}, which translates to a PRT of 17 days if gas exchange was not included in the loss calculations. The 17-day PRT is much larger than the flushing time determined via the advection of the SF_6 peak through the DWSC. This is attributed to the fact that the PRT derived from the mass inventory includes the tracer tagged waters in the TB, whereas the flushing time derived for the DWSC only includes waters downstream of the TB. On the last day of survey, the TB waters contained 26% of the tracer mass in the system.

For comparison, the air–water gas exchange versus wind speed parameterizations from Wanninkhof (1992), Clark et al. (1995), and Nightingale et al. (2000) were also applied to the data. Using these parameterizations, the first order loss rates due to gas exchange alone range from 0.076–0.12 day^{-1}, with the Nightingale parameterization yielding the lowest value and the Clark parameterization yielding the highest value. The variability of the determined loss rate due to gas exchange suggests that the PRT of 17 days for DWSC and TB portions of the system might serve as a lower bound under the observed flow conditions.

Dissolved Oxygen

During the course of the study, the longitudinal DO distributions remained more or less in steady state. This steady state was defined by DO concentrations of ~6 mg l^{-1} at the confluence of the USJR and the DWSC, and a minimum DO concentration of ~4 mg l^{-1} that was persistent from KP 7 to KP 0.

There are four factors that determine the DO steady state balance within the DWSC system: (1) the biochemical oxygen demand and nitrogenous oxygen demand (NOD) contributed from upstream sources such as the Stockton Regional Wastewater Control Facility, agricultural runoff in the SJR watershed, and algal biomass; (2) the BOD from sediments along the length of the DWSC; (3) DO added by air–water oxygen exchange; and (4) water discharge rates through the system. The BOD and NOD added from upstream sources and from the sediments within the channel continually caused the DO to decrease moving downstream of the USJR to KP 7 in a nearly linear fashion. From this location downstream to KP 0, the influence of the BOD exerted from the water column and the sediments must match the addition of DO from atmospheric gas exchange.

Dissolved Oxygen Mass Balance

Based on the net velocity in the DWSC calculated in this study, a first order mass balance was used to estimate the apparent biochemical oxygen demand (BOD_A) value for the DWSC during the study:

$$BOD_A = DO\,Flux_{SJR} + DO\,Flux_{GasEx} - DO\,Flux_{TC} \quad (5)$$

where BOD_A (kg day^{-1}) is the rate of oxygen consumption through the combined oxidation processes in the sediments, as well as the organic and inorganic oxidation reactions within the water column; DO_{SJR} (kg day^{-1}) is the DO flux associated with the supply of DO from the SJR to the DWSC; DO_{GasEx} (kg day^{-1}) is the DO flux added via air–water gas exchange and was derived from the k_{600} value determined in this study; and DO_{TC} is the DO flux associated with the removal of waters from the system via exports to Turner Cut and the downstream SJR. The difference in DO fluxes from inputs and removals is attributed to BOD_A.

To calculate the oxygen flux from the SJR, the average observed surface DO concentration at the junction of the SJR and the DWSC, 7.1 mg l^{-1}, was multiplied by an average SJR discharge rate of 35.3 m^3 s^{-1}, yielding a dissolved oxygen flux of 2.16×10^4 kg day^{-1}. The discharge rate includes additions of treated sewage effluent from the municipal sewage facility of ~1.2 m^3 s^{-1}. The net oxygen flux into the channel due to predicted air–water gas exchange was calculated to be approximately 1.25×10^4 kg day^{-1}. For the oxygen exports at Turner Cut, we used the same flow rate as the input multiplied with a DO value of 4.0 mg l^{-1}, yielding a value of 1.22×10^4 kg day^{-1}. To close the mass balance, any oxygen load deficit was attributed to BOD exerted on the system. Therefore, the BOD_A estimate was determined to be 2.19×10^4 kg day^{-1}.

The first order estimate for BOD_A loading rates compares well with the BOD_{10} loading rates presented by Volkmar and Dahlgren (2006), which were calculated under flow conditions (32 $m^3 s^{-1}$) very similar to this study. That study presented a loading rate of ~2.7×10^4 kg day^{-1} for samples collected in the SJR at Mossdale, 26 km upstream of the DWSC. One factor that contributes to this study's lower value is that dispersive fluxes are not included in the mass balance. As net advection appears to dominate over dispersion under the observed flows, only advective fluxes were included in the mass balance. The BOD_A loading rate is associated solely with the flushing time scale of 7 days calculated from the net velocity of the peak tracer concentration. A more complete mass balance based on a PRT of 17 days, which incorporates the effects dispersion, would increase the estimated BOD_A loading rate.

The 17-day PRT determined from the exponential decay of the SF_6 mass inventory is comparable to flushing rates presented in other studies. Monsen et al. (2007) performed a modeling investigation to determine the impact of flow diversions on water quality and flushing times within the Sacramento–San Joaquin delta. The modeled flushing time for the DWSC was determined by counting the number of neutrally buoyant particles that remain in the DWSC domain over time, after being released evenly throughout the domain. The PRT calculation in this study is determined very similarly, except the initial release of particles is a pulse at one location and not spread evenly through the domain. For net flows slightly higher (40–60 $m^3 s^{-1}$) than observed in this study, the model flushing time was 16 days. For net flows near 0 $m^3 s^{-1}$, the flushing time increased to 31 days. The Monsen et al. (2007) modeling results indicate that DO depletions in the DWSC develop on flushing time scales of one to several weeks and also find that these results agree well with the BOD half-life of 12–15 days determined by Volkmar and Dahlgren (2006), a time-scale that leads to depleted DO concentrations. At the beginning of this study, the low DO conditions were already established, as flow rates similar to those observed were already occurring for a month prior to the investigation. The results presented within suggest DO depletions persist over the determined flushing and residence times.

The DO concentrations observed over the majority of the DWSC during this study fall below the CRWQCB regulations for DO of 6 mg l^{-1}. The CRWQCB identified nutrient and algal loading, geometry of the DWSC, and low volumetric flow rates as potential factors contributing to the low dissolved oxygen concentrations. Out of the factors that can contribute to BOD such as nitrification of ammonium, oxidation of dissolved organic carbon and nitrogen, and respiration of algal biomass, nitrification has been identified as the principle contributor to BOD for waters in the DWSC (Lehman et al. 2004). For waters upstream of Mossdale, algal biomass was the principle source of BOD in the SJR (Volkmar and Dahlgren 2006). One way to alleviate the observed DO deficit is to decrease algal loads delivered from the USJR waters to the DWSC by reducing nutrient concentrations, but the high nutrient concentrations in the SJR suggest that nutrient reductions may not work alone (Volkmar and Dahlgren 2006).

The impacts of geometry and flow on the low DO are inversely correlated, as the net velocity decreases when the channel area increases stepping from the USJR into the DWSC. Modifications to the shipping channel geometry as a solution to DO depletions are highly unlikely, since shipping traffic will continue through the DWSC and water depths must be maintained.

For the duration of the tracer study and for the entire year of 2005, the water flow barrier at the head of Old River was removed. The Monsen et al. (2007) modeling results were for the same operational state of the barrier, and for comparison, with the barrier in place, model flushing times decreased by a factor greater than 5. It has also been shown that on monthly time scales, net river flows provide the greatest impact on DO concentrations and exert more influence on changes in DO concentrations than ammonium and chlorophyll concentrations (Jassby and Van Nieuwenhuyse 2005). The Jassby and Van Nieuwenhuyse (2005) modeling results suggest that minor increases in net river flow can significantly decrease the DO deficit. The flow diverted down Old River was small in this study. By computing the difference in discharge rates at Vernalis, upstream of the SJR junction with Old River, and the Garwood Bridge gauging station, the flow diverted to Old River was only 6.7 $m^3 s^{-1}$. Depending on the level of export pumping down Old River, the entire SJR flow can be diverted down Old River thus reducing the net flow in the DWSC to zero and even reversing the direction of flow. This extreme case will certainly create a low DO problem and increase the flushing and residence times observed in this study.

Conclusions

The observed low DO concentrations suggest that the 17-day PRT determined for a net flow of 34.1 $m^3 s^{-1}$ is of a long enough timescale for DO depletions to persist and that the BOD within the DWSC has sufficient time to decrease oxygen concentrations. In order to comply with regulations, flushing and residence times would need to decrease so that the BOD from the SJR has less time to exert its full potential on the system. Shipping traffic through the DWSC will not be eliminated so modification to the channel geometry by reducing the volume of the channel is not a viable solution for decreasing the flushing and residence times in the DWSC. Reductions could partly be achieved by reducing water diversion and export flows from the

USJR into Old River, so that net flows through the USJR into the DWSC increase. Reduced diversions at Turner Cut could also potentially allow more oxygen rich Sacramento River water to mix upstream into the DWSC. Most likely, a combination of reducing BOD sources and increasing flows down the USJR into the DWC is necessary to achieve the DO standards set by the CRWQCB.

Acknowledgements We thank J. McDermott and A. Sharma for their dedicated support in the field study, D. Hurst for lending us his miniature ECD, and L. Doyle for the post processing of the CTD profile data. Funding was provided by CALFED. This is LDEO contribution 7193.

References

Bain, R.C., and W.H. Pierce. 1968. San Joaquin estuary near Stockton, California: an analysis of the dissolved oxygen regimen. San Francisco, California: Department of the Interior, Federal Water Pollution Control Administration.

Bowersox, R.P. 2002. Design of a destratification system to control algae in a tidal channel. B.S. Thesis, University of California, Davis, California.

Breitburg, D. 2002. Effects of hypoxia, and the balance between hypoxia and enrichment, on coastal fishes and fisheries. *Estuaries* 25: 767–781.

Brown, R.T. 2002. Stockton deep water ship channel tidal hydraulics and downstream exchange. Available at: http://www.sjrtmdl.org/technical/2001_studies/reports/final/brown_tidal2.htm. Part of Jones & Stokes. Accessed 05 May 2007.

California Regional Water Quality Control Board, Central Valley Region. 2004. Amendments to the water quality control plan for the Sacramento River and San Joaquin River Basins for the control of salt and boron discharges into the lower San Joaquin River. Available at: http://www.waterboards.ca.gov/centralvalley/water_issues/tmdl/central_valley_projects/vernalis_salt_boron/index.html. Accessed 03 May 2007.

California Regional Water Quality Control Board, Central Valley Region. 2005. Amendments to the water quality control plan for the Sacramento River and San Joaquin River Basins. Available at: http://www.waterboards.ca.gov/centralvalley/available_documents/basin_plans/SacSJR.pdf. Accessed 03 May 2007.

Caplow, T., P. Schlosser, D.T. Ho, and N. Santella. 2003. Transport dynamics in sheltered estuary and connecting tidal straits: SF_6 tracer study in New York Harbor. *Environmental Science & Technology* 37: 5116–5125. doi:10.1021/es034198+.

Caplow, T., P. Schlosser, D.T. Ho, and R.C. Enriquez. 2004a. Effect of tides on solute flushing from a strait: imaging flow and transport in the East River with SF_6. *Environmental Science & Technology* 38: 4562–4571. doi:10.1021/es035248d.

Caplow, T., P. Schlosser, and D.T. Ho. 2004b. Tracer study of mixing and transport in the upper Hudson River with multiple dams. *Journal of Environmental Engineering-ASCE* 130: 1498–1506. doi:10.1061/(ASCE)0733-9372(2004)130:12(1498).

Clark, J.F., R. Wanninkhof, P. Schlosser, and H.J. Simpson. 1994. Gas exchange rates in the tidal Hudson River using a dual tracer technique. *Tellus* 46B: 274–285.

Clark, J.F., P. Schlosser, R. Weppernig, M. Stute, R. Wanninkhof, and D.T. Ho. 1995. Relationship between gas transfer velocities and wind speeds in the tidal Hudson River determined by the dual tracer technique. In *Air-water gas transfer*, eds. Jähne, B. and E. Monahan. 783–800. Hanau, Germany: AEON.

Clark, J.F., P. Schlosser, M. Stute, and H.J. Simpson. 1996. SF_6–^{3}He tracer release experiment: a new method of determining longitudinal dispersion coefficients in large rivers. *Environmental Science and Technology* 30: 1527–1532. doi:10.1021/es9504606.

Clark, J.F., G.B. Hudson, M.L. Davisson, G. Woodside, and R. Herndon. 2004. Geochemical imaging of flow near an artificial recharge facility, Orange County, CA. *Ground Water* 42: 167–174. doi:10.1111/j.1745-6584.2004.tb02665.x.

Diaz, R.J. 2001. Overview of hypoxia around the world. *Journal of Environmental Quality* 30: 275–281.

Fischer, H.B., E.J. List, R.C.Y. Koh, J. Imberger, and N.H. Brooks. 1979. *Mixing in inland and coastal waters*. New York: Academic.

Foe, C., M. Gowdy, and M. McCarthy. 2002. Draft Strawman allocation of responsibility. California Regional Water Quality Control Board Central Valley Region. http://www.sjrtmdl.org/load_allocation/strawman.htm. Accessed 20 January 2007.

Ho, D.T., and P. Schlosser. 2000. Atmospheric SF_6 near a large urban area. *Geophysical Research Letters* 2711: 1679–1682. doi:10.1029/1999GL006095.

Ho, D.T., P. Schlosser, and T. Caplow. 2002. Determination of longitudinal dispersion coefficient and net advection in the tidal Hudson River with a large-scale, high resolution SF_6 tracer release experiment. *Environmental Science & Technology* 36: 3234–3241. doi:10.1021/es015814+.

Ho, D.T., C.S. Law, M.J. Smith, P. Schlosser, M. Harvey, and P. Hill. 2006a. Measurements of air–sea gas exchange at high wind speeds in the Southern Ocean: implications for global parameterizations. *Geophysical Research Letters* 33: L16611. doi:10.1029/2006GL028295.

Ho, D.T., P. Schlosser, R.W. Houghton, and T. Caplow. 2006b. Comparison of SF_6 and fluorescein as tracers for measuring transport processes in a large tidal river. *Journal of Environmental Engineering-ASCE* 132: 1664–1669. doi:10.1061/(ASCE)0733-9372(2006)132:12(1664).

Jassby, A.D. and E.E. Van Nieuwenhuyse. 2005. Low dissolved oxygen in an estuarine channel (San Joaquin River, California): Mechanisms and models based on long-term time series. *San Francisco Estuary & Watershed Science* 3(2): Article 2.

Kimmerer, W.J. 2002. Physical, biological, and management responses to variable freshwater flow in the San Francisco Estuary. *Estuaries* 256B: 1275–1290.

Kratzer, C.R., P.D. Dileanis, C. Zamora, S.R. Silva, C. Kendall, B.A. Bergamaschi, and R.A. Dahlgren. 2004. Sources and transport of nutrients, organic carbon, and Chlorophyll-a in the San Joaquin River upstream of Vernalis, California, during summer and fall, 2000 and 2001. United States Geological Survey, Water-Resources Investigations Report 03-4127. Sacramento, California.

Lehman, P.W., J. Sevier, J. Giulianotti, and M. Johnson. 2004. Sources of oxygen demand in the lower San Joaquin River, California. *Estuaries* 27: 405–418.

Lewis, E.L. 1980. The practical salinity scale 1978 and its antecedents. *IEEE Journal of Oceanic Engineering* OE-5: 3–8. doi:10.1109/JOE.1980.1145448.

Maiss, M., and C.A.M. Brenninkmeijer. 1998. Atmospheric SF_6: trends, sources, and prospects. *Environmental Science and Technology* 32: 3077–3086.

Meybeck, M. 1993. C, N, P and S in rivers: from sources to global inputs. In *Interactions of C, N, P and S in biogeochemical cycles and global change*, eds. R. Wollast, , F.T. Mackenzie, and L. Chou, 163–193. Berlin, Heidelberg, Germany: Springer.

Miller, R.L., and B.F. McPherson. 1991. Estimating estuarine flushing and residence times in Charlotte Harbor, Florida, via salt balance and a box model. *Limnology and Oceanography* 36: 602–612.

Monsen, N.E., J.E. Cloren, and J.R. Burau. 2007. Effects of flow diversions on water and habitat quality: examples from California's highly manipulated Sacramento–San Joaquin Delta. *San Francisco Estuary & Watershed Science* 5(3): Article 2.

National Oceanic and Atmospheric Administration–Climate Monitoring and Diagnostics Laboratory (NOAA/CMDL). 2007. Atmospheric sulfur hexafluoride concentrations. http://www.esrl.noaa.gov/gmd/. Accessed 15 March 2007.

Nightingale, P.D., P.S. Liss, and P. Schlosser. 2000. Measurements of air–sea gas transfer during an open ocean algal bloom. *Geophysical Research Letters* 27: 2117–2120. doi:10.1029/2000GL011541.

Rutherford, J.C. 1994. *River mixing*. New York: Wiley.

Sheldon, J.E., and M. Alber. 2002. A comparison of residence time calculations using simple compartment models of the Altamaha River Estuary, Georgia. *Estuaries* 25(6B): 1304–1317.

Volkmar, E.C., and R.A. Dahlgren. 2006. Biological oxygen demand dynamics in the lower San Joaquin River, California. *Environmental Science & Technology* 40: 5653–5660. doi:10.1021/es0525399.

Wanninkhof, R. 1992. Relationship between wind speed and gas exchange over the ocean. *Journal of Geophysical Research* 97: 7373–7382. doi:10.1029/92JC00188.

Wanninkhof, R., K.F. Sullivan, and Z. Top. 2004. Air–sea gas transfer in the Southern Ocean. *Journal of Geophysical Research* 109: C08S19. doi:10.1029/2003JC001767.